Magnetic Resonance Imaging of the Placenta in Fetal Growth and Placenta Accreta Spectrum

Hiba Alessa

A thesis submitted in partial fulfilment of the requirements for the degree of Doctor of Philosophy

The University of Sheffield Faculty of Medicine Dentistry and Health Department of Oncology and Metabolism

30 November 2023

Acknowledgements

I could not be more thankful to my wonderful supervisor; her big heart and patience was the reason to write this thesis from scratch. I could never imagine finding better support than that.

I am thankful for:

The University of Sheffield for giving me this opportunity

The Iraqi ministry of higher education and the University of Jabir Ibn Hayan for funding the whole journey.

All women involved in this study, believed in research and wanted to make an impact in health science.

The consultants and midwives in the day-care and FMU clinics at Jessop wing hospital for helping me in the recruitment.

The team in the MRI unit for being supportive and accepting to make this happen.

Pathology consultants and team who worked on my samples to get them reported for my research.

301 team for assisting in the statistical analysis.

I would like to award this work to my only beloved parents, my mother who used to follow up on my day-to-day work passionately and give me confidence throughout the whole journey while staying on distance. My dad, RIP… passed away due to the COVID pandemic. He sacrificed and supported me to see me pursue my dream. This work is dedicated to you.

Finally, I am especially thankful to my family; husband, brother and sisters who gave me the support to complete this journey.

Abbreviations

ADC	Apparent diffusion coefficient
AC	Abdominal circumference
AGA	Appropriate for gestational age
ART	Assisted reproductive techniques
APS	Anti-phospholipid syndrome
ASL	Arterial spin labelling
BMI	Body mass index
CRL	Crown-rump length
CS	Caesarean section
DM	Diabetes mellitus
DCE	Dynamic contrast-enhanced
EPI	Echo planar imaging
EFW	Estimated fetal weight
FAIR	Flow-sensitive alternating invasion recovery
FGR	Fetal growth restriction
FDA	Food and drug administration
FMU	Feto-maternal unit
fMRI	Functional MRI
GCAs	Gadolinium contrast agents
GLRLM	Grey-level run-length matrix
GLCM	Grey-level cooccurrence matrix
GLZLM	Grey level zone length matrix
GLZLM ZP	Grey-level zone length matrix-zone percentage
GDM	Gestational diabetes mellitus
GLNU	Grey-level non uniformity
GA	Gestational age
GDM	Gestational diabetes
HBA1c	Haemoglobin A1c
HTN	Hypertension
HOG	Histogram-oriented gradients
IVIM	Intra-voxel incoherent motion

ICSI	Intracytoplasmic sperm injection
IFV	Intra-placental fetal vessel
IVF	In vitro fertilisation
IUI	Intra ureteric insemination (IUI)
LGA	Large for gestational age
LRE	Long run emphasis
LRHGE	Long run high grey emphasis
MRI	Magnetic resonance imaging
MPT	Midpoint thickness
ms	Millisecond
Min	Minimum
Max	Maximum
NVD	Normal vaginal delivery
Mm	Millimetre
NICU	Newborn intensive care unit
NGLDM	Neighbourhood grey-level difference matrix
PI	Pulsatility index
PPROM	Preterm premature rupture of membranes
PQ	Placental quotient
SGA	Small for gestation age
SSFSE	Single-shot fast spin-echo
SSFP	Steady-state free precession
SAA	Surface attachment axial section
SAS	Surface attachment sagittal section
Sec	Second
SI	Signal intensity
SRE	Short run emphasis
SRHGE	Short run high grey emphasis
US	Ultrasound
RBCs	Red blood cells
ROI	Region of interest
TTTS	Twin-to-twin transfusion syndrome
TFs	Textural features
TA	Textural analysis

TE	Time to echo
VS	Volume sagittal section
VEGF	Vascular endothelial growth factor
VA	Axial volume section
3D US	Three-dimensional ultrasound

List of Figures

List of Tables

Table of Contents

Introduction to the thesis

Year 1

I started my PhD in January 2019. In my first year, I undertook the required modules and several additional modules whilst also reading and understanding the area of my work.

I wrote my literature review and commenced the complicated ethics application, registering the project with the trust and also completing and submitting an IRAS form. During this time, I was developing the project from the original idea into a research proposal. As part of this, I was able to undertake a retrospective review of cases that had been scanned for clinical need. I undertook the GCP training, and I applied to the trust for both a letter of access and a research passport to allow me to become part of the clinical care team as an observer and to consent patients within the clinical setting.

The retrospective work allowed me to:

- Practice recognising the placenta on the MRI images and manually segmenting it with the propriety software.
- Collect normative data on placental growth.
- Assess the hypothesis on a small number of cases where the patient had an FGR baby (Section 2.3).

Year 2

Full registration and ethics approval was obtained in February 2020 and suspended by the local trust in March 2020 due to COVID.

As the trust deemed the research high risk as 1) Pregnant women and 2) The hospital visits for the scan were deemed non-essential.

COVID mitigation: I was left as an international student in the UK, specially isolated and unable to return home without huge Visa complications and unsure that if I did go home whether I would be allowed to return.

A study was ongoing (based on placenta accrete spectrum cases) in which images of the placenta had already been obtained and I was able to be provided with anonymised studies on a CD to evaluate at home.
I was also provided with a database of outcomes on these cases.
For my part I would add in 2 new aspects to the database and assess their role in aiding the diagnosis of placenta accrete spectrum (PAS) and its differing degrees.
These were:

1. Does the ADC value of the placenta either as a whole organ or the area over the previous caesarean section scar predict PAS? (section 1.3).
2. Does textural analysis of either the whole placenta or a region of interest above the previous C-section scar predict PAS? (section 1.3).

Year 3
The ethics was suspended for 18 months so the initial part of this year also involved work from Year 2 and the case report from a clinical case that occurred at the time.
The case report is essential to my future work as it became clear that in some cases the placenta was involved and infected by COVID causing stillbirths. Initially, no one knew if this could be predicted and there remain few publications of recognising placenta failure due to COVID-19 infection whilst the pregnancy is ongoing as the majority of the work has been on the placenta after delivery and the histological changes.
As the case report demonstrated the placenta shows changes in utero on the MRI scan and this led me to add in COVID not only as part of the demographic data collected in the prospective study but also to request a substantial amendment to the study and add in a group of patients that had had COVID infection during the pregnancy.
August 2021 Finally the ethics was activated, and the trust were happy with recruitment commencing.

Years 3 and 4
Prospective study and write up.
Unfortunately, due to COVID affecting the placenta the pathology departments throughout the UK were accepting all placentas from women that had had COVID at

any stage of their pregnancy in a desperate attempt to try and find out the impact of COVID and hence hopefully protect pregnant women in the future. This meant a large backlog of work that had to take priority over the research cases and many of the placentas in this study remain stored awaiting analysis. In the final part of the prospective work (section 2.4) I have listed the most common features we saw in the FGR cases and not in the control cases but formal assessment alongside the pathology team remains to be done.

Overall:

This is a story of the difficulties due to COVID and how I tried to overcome them, how the research changed direction to one of what was available and broadly linked to my proposed work and keeping the work linked to the placenta. My personal life was also deeply affected by the COVID pandemic as were the lives of many others worldwide.

I hope I have overcome the barriers this produced and remain pleased with the work I managed to do and my own resilience during difficult times.

I believe the body of work here contains new data and novel concepts that need further investigation before they can be used in clinical practice but provides important pilot data and the foundations for further work.

Placenta development

For animals to grow normally in pregnancy, the placenta is necessary. Pre-eclampsia and fetal growth restriction are two frequent pregnancy illnesses in humans that are caused by faulty placental development. There is a huge variation of placenta types between mammals hence it is difficult to comprehend human placental development using animal models. Nonetheless, new methods for researching human placental development—such as single-cell RNA sequencing, stem cell culture techniques, and three-dimensional organoids—have expanded our understanding of this area.

Type of placentation

Animals display a vast array of placental approaches, especially with the extent of trophoblast penetration into uterine tissues and the number of cell layers separating the fetal and maternal circulations (Roberts, Green et al. 2016). A hemochororial placenta is found in both laboratory mice and primates, in which the trophoblast directly contacts the mother's blood by invading through the uterine epithelium, stroma, and maternal artery walls (Georgiades, Ferguson-Smith et al. 2002). In predators with an endotheliochorial placenta, where trophoblast cells come into touch with maternal endothelium cells, there is a lower degree of invasion seen. According to Carter and Enders (2013), the trophoblast stays superimposed on the uterine epithelium in the least invasive type, known as an epitheliochorial placenta, which is found in ruminants and ungulates (Carter and Enders 2013).

Even among animals having hemochorid placentas, such as laboratory mice and non-human primates, there is no ideal experimental model to study human placentation(Carter and Pijnenborg 2011). Another issue is that, from the perspective of an obstetrician, only humans and probably great apes are known to have conditions like pre-eclampsia, in which failure of placentation is the main abnormality (Carter 2011). There are significant distinctions between placentation in mice and humans.

The blastocyst is superficially implanted in the majority of primates. For instance, in macaques and baboons, the trophoblast enters the endometrium to form a placenta,

but the growing embryo stays within the uterus. The human blastocyst, on the other hand, is drawn into the endometrium, which closes above it and entirely embeds it by the twelfth day (James, Carter et al. 2012). The growing embryo is protected by the capsular decidua, whereas the basal decidua lie underneath the placental bed. Both gibbons and large apes share the trait of interstitial implantation (Hill 1932). Although it does happen in rodents, the mechanism is different and has developed on its own.

Syncytiotrophoblast is the first to penetrate the endometrium (Carter, Enders et al. 2015). This is created when cellular trophoblasts fuse together to create a multicellular syncytium. Syncytins, which are proteins expressed by endogenous retroviral envelope genes that have been integrated into the genome and evolved to stimulate cell fusion in the placenta, are mostly responsible for the process (Dupressoir, Lavialle et al. 2012). Two distinct syncytin genes were acquired by humans at distinct times. Syncytin-1 is exclusive to apes, but Syncytin-2 is present in all haplorrhine primates (Dupressoir, Lavialle et al. 2012). Numerous mammals possess syncytin genes, each of which is a unique gene capture (Dupressoir, Lavialle et al. 2012). On the other hand, it has been suggested that the emergence of invasive placentation in mammals requires the acquisition of retroviral envelope genes (Dupressoir, Lavialle et al. 2012).

Parts of the placenta and how related to the fetus inside the uterus

Both fetal tissue from the chorionic sac and maternal tissue from the endometrium make up the utero-placental unit. The term "chorionic plate" refers to the fetal portion of the mature placenta. The fetal chorionic blood vessels originate from the umbilical vessels and branch radially in this area. The term "basal plate" refers to the placenta's maternal portion. The placenta's major functional units, densely packed, highly branching villous structures that house fetal blood arteries, are located in the intervillous area, which lies between these two zones. A significant portion of maternal—fetal exchange takes place in the terminal portions of these chorionic villi (Benirschke, Baergen et al. 2022). A multinucleated syncytium known as the syncytiotrophoblast entirely lines the intervillous region.

Maternal blood circulates through spiral endometrial arteries, bathes the villi, and returns through endometrial veins to this region. Fetal blood lacking oxygen travels via

the branching chorionic arteries and two umbilical arteries to reach the vast arteriocapillary—venous system located inside the chorionic villi. Through the many chorionic veins and the one umbilical vein, the well-oxygenated fetal blood in the capillaries is returned to the fetus (Blackburn 2007).

Placental membranes

The layers of cells that divide the fetal blood in the vasculature at the centre of the villi from the mother blood in the intervillous gap are referred to as the placental membrane, also known as the placental barrier (Moore, Persaud et al. 2008). The placental membrane is initially composed of four layers: the endothelium lining the fetal capillaries, the connective tissue of the villus, a layer of cytotrophoblast cells, and the maternal facing syncytiotrophoblast. However, the cytotrophoblast cell layer of many villi attenuates and vanishes by about 20 weeks. The membrane then has three layers in the majority of chorionic villi and thins out in certain places to the point where the syncytiotrophoblast touches the fetal capillary endothelium directly.

Fetal membranes

Throughout the pregnancy, the fetus is contained by the fetal membranes, which finally burst during the first stage of labour. They are made up of the mother-facing chorion and the fetal-facing amnion (Bryant-Greenwood 1998). There are five separate levels in an amnion. The amniotic epithelium, the deepest layer, is directly in touch with the amniotic fluid on one side and a basement membrane on the other. The fibroblast layer, the spongy or intermediate layer, and the compact layer make up the remaining layers. The reticular layer, the basement membrane, and the trophoblast cell region—which, at term, clings securely to the maternal decidual tissue—make up the chorion. The fetal membranes are essential to the development of the fetus and the course of pregnancy, just like the placenta is.

Apart from their autocrine regulatory functions, the membranes release chemicals into the amniotic fluid, which in turn affects the homeostasis of the fluid, and into the uterus, where they might potentially impact the cellular physiology of the mother. The fetus's membranes also shield it against infections that might climb the reproductive canal.

Types of villi

The migration of cytotrophoblasts into trabeculae generated by the primitive syncytium to form 'basic villi' occurs approximately 13 days following conception. At roughly 21-day post conception, mesenchymal cells infiltrate the main villi, changing them into "secondary villi." The initial creation of fetal blood vessels occurs in the mesenchymal core within a few days by a process known as vasculogenesis, forming the 'tertiary villi' (Demir, Seval et al. 2007, James, Carter et al. 2012).

Subtypes of villi are categorised according to their position in the villous tree, calibre, and architectural features. The primary structural support of the villous tree is provided by the stem villi, which also include the 10 generations of more slender villi that extend into the periphery villous tree and are located closest to the chorionic plate, which is more proximal to the fetus. The primary location of maternal-fetal interaction, terminal villi are densely capillaried and connect stem and intermediate villi. Eventually, columns of invasive EVTs link the placenta to the maternal decidua and basal plate. These anchoring villi are a subgroup of terminal villi. Additionally, during the first phases of pregnancy, these EVTs shift laterally at the decidual surface forming the trophoblast shell (Knöfler, Haider et al. 2019).

Normal implantation

Uterine receptivity for implantation lasts for a brief amount of time. Progesterone and 17h-estradiol are secreted cyclically, which regulates the endometrium's physiological readiness. The implantation window is opened, and the uterine surface is modified by these hormones through the regulation of growth factors, cytokines, and adhesion molecules (Blackburn 2007). After a few days, other substances like fibronectin close the window. The zona pellucida around the blastocyst disappears before it attaches to the uterine epithelium. Following attachment, the blastocyst's trophoblast cell layer proliferates quickly and divides into an outer multi-nucleated syncytiotrophoblastic mass and an interior cytotrophoblastic layer. Synthetic trophoblasts penetrate the connective tissue and expand into the endometrial epithelium (Boyd and Hamilton 1970). The endometrial surface progressively heals as the blastocyst descends underneath it (Fig. 1a).

Lacunar networks arise inside the syncytiotrophoblast, and nourishment is received from the eroded maternal tissues (Fig. 1b) (Aplin 2000). The uteroplacental circulation is established by the flow of maternal blood into and out of these networks. The syncytiotrophoblast is invaded by extensions of growing cytotrophoblast cells in a variety of locations. The placenta's chorionic villi are developing, with these extensions marking the beginning of this process (Moore, Persaud et al. 2008).

By the end of the first three months of pregnancy, placental development is completed, and then continues to grow parallel to the uterus (Herrick EJ [2023 May 1]).

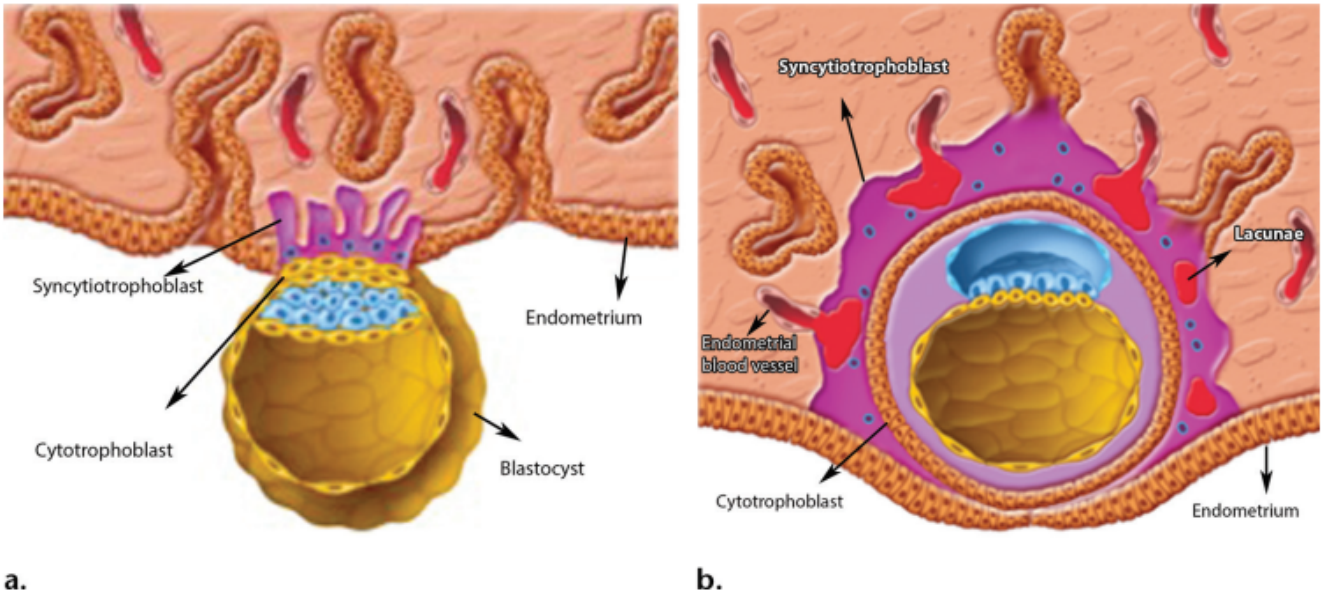

Figure 1 Implanted blastocyst into the uterine wall showing the process of placenta development. (12). Copyright permission was obtained from RSNA journal https://www.rsna.org/.

Functions of the placenta

The placenta has a significant role in fetal and maternal health. In the early days of embryonic life, the placenta plays essential physical and functional roles in the development and protection of the fetus. It is a unique organ with multisystemic functions, which acts as a respiratory, gastrointestinal, renal, cardiovascular,

endocrine, and immune system (Guttmacher, Maddox et al. 2014). Oxygen, nutrients, carbon dioxide and other waste products are transported through the placenta between the maternal and fetal circulations. The placenta secretes certain hormones and metabolites into maternal and fetal circulations that regulate pregnancy, fetal growth, and metabolism. In addition to that, defending against infections, xenobiotic molecules, and maternal diseases means the placenta has an immune function. The placenta is programmed to accommodate the functional needs of the growing fetus (Gude, Roberts et al. 2004).

Placental malfunction may cause severe early abnormalities related to growth restriction, neurodevelopmental abnormalities, preterm delivery as well as preeclampsia (Stables D 2010). Impaired delivery of sufficient nutrients to the fetus can result in abnormal fetal tissue development (Sehgal, Dahlstrom et al. 2019). More importantly, later complications have been linked to placental problems (Grigsby 2016). For example, a deficiency of elastin development in fetal vessels may lead to stiffer arteries and long-term cardiovascular complications (Martyn and Greenwald 1997). As an adult stroke, hypertension and myocardial infarction rates have been linked to low birth weight (Guttmacher, Maddox et al. 2014). Fetal growth abnormalities have been linked to defects in normal placental invasion due to many pathological reasons. When the placenta trophoblast fails to invade the uterine tissue properly, for instance, the defective transformation of the spiral arterioles during the first trimester may result in placental insufficiency and subsequently fetal growth restriction (FGR) (Ness and Sibai 2006, Pijnenborg, Vercruysse et al. 2006).

MRI of the placenta

How MRI works

Magnetic resonance imaging, otherwise, known as MRI, is a technique developed in the 1970s to produce diagnostic images of the body or part of it. It makes use of the naturally existent magnetic properties in the body and in particular, the hydrogen atom, which is abundant in water and fat. The hydrogen protons are like a spinning magnet, with north-south poles, randomly aligned. As the body enters the MRI machine, which is essentially a much stronger magnetic field, usually ranging between 0.5 and 1.5 Tesla, these protons line up. With the addition of a radio wave, certain slices of the body will resonate at specific frequencies. When the radio frequency is turned off, these protons return to rest at their initial state, thus, emitting a detectable signal at a certain frequency. It is these signals that make up the MRI image. Receiving coils enhances the detection of the intensity of these signals which are plotted. The time for the magnetic vector to be back at its resting state is called T1 relaxation time. The time it takes for the magnetic spin to return to its original state is called T2 relaxation time. These can be stored as sequences of information and then plotted as a grey scale. MRI is unlike x-rays in the sense that it doesn't harm tissues as it is operating in the radio frequency range, however, any metal contained in the body such as pacemakers can be affected under the magnetic field so precautions are warranted (Berger 2002). Magnets that operate MRI machines are of three types (Carr and Grey 2002).

The primary magnet (static magnet)

This magnet is the strongest one, the units used to measure the magnetic field strength are called Tesla (T) which are inspired by Nikola Tesla. MRI machine work using magnetic fields of various strength ranges (i.e., 0.5 T, 1T. 1.5T, etc).FDA has limited the magnetic field strength to up to 4T (FDA. Feb.1997) as this is mandatory to ensure the safety of clinical usage. One Tesla is equal to 20.000 times the magnetic strength of the earth. Currently, 1.5 T is commonly used in MRI.

The source of this magnet is often a superconductive magnet. This magnet is synthesized from coils of wires in liquid helium that operate at very low temperatures (-269 C$^{\circ}$) to reduce the use of electricity and so make it cheaper for daily clinical practice. When any body part is exposed to a magnetic field, hydrogen atoms spin in one of two directions, either with or opposite the direction of the field. Making them in unstable condition, soon after the magnetic field goes off, these atoms return to their

original state releasing signals of different intensities according to their body composition.

Gradient magnet

This is another magnet that comprises the MRI machine. It is weak in comparison to the static magnet and consists of 3 small magnets. This creates another magnetic field in addition to the main field explained earlier. The advantage of this field is spatial localization which enables the localization of the signals coming from the area of interest and from other body parts. This enables a view of MR images with different orientations and sequences without turning the patient (axial, sagittal, coronal, and oblique).

Radiofrequency (RF) pulses

This is another part of the MRI machine. It sends and receives signals of different intensities necessary to make hydrogen atoms enter an unsteady state (Larmor frequency). The Larmor frequency varies according to the magnetic field strength. It has 2 parts which send and receive signals, and then process these signals into images that can be read by the computer system (Carr and Grey 2002).

Fetal MRI of the placenta

40 years ago the first use of magnetic resonance imaging (MRI) in pregnancy was reported, (Smith, Adam et al. 1983), MRI is becoming more common in pregnancy, particularly in women of advanced gestation or who are obese (Millischer, Sonigo et al. 2013). Contrast agents were introduced to improve imaging quality and visualize delicate soft tissue structures and blood vessels. But due to the controversial risk of gadolinium chelating agents on the fetus, their use in pregnancy is restricted (Avni, Neeman et al. 2015). Brunelli et al. used gadoterate melamine administration a few hours before caesarean section delivery to demonstrate perfusion in the placenta. Normal placentas appeared homogeneous, whereas, in pregnancies with severe IUGR, the circulation was severely compromised, displaying many patchy non-perfused areas (Brunelli, Masselli et al. 2010). Fetal MRI has been utilized in pregnancy as it showed great value in the assessment of soft tissues and organs such as the brain and tumours. MRI can also be used to assess perfusion (e.g., DCE, ASL), microstructure (DWI and ADC, IVIM), oxygenation (BOLD and T2*) and metabolism (spectroscopy).

1. Diffusion MRI DWI

This is a sensitive method for imaging the incoherent movements of water molecules, offering information into tissue microstructure. DWI experiments often yield measurements of apparent diffusion coefficients (ADCs). DW-MRI investigates the mobility and diffusion of water molecules inside tissues. The faster the movement, the higher the diffusion and the lower the SI (Siauve, Chalouhi et al. 2015). ADC is the most common parameter used to measure the diffusion between two different tissues that required two different b values (Avni, Neeman et al. 2015). Placental mean ADC values may indicate a variety of movements other than free water diffusivity, such as blood microcapillary flow, morphological restrictions acting on molecular diffusion, and exchange, and conventional DW MRI cannot discriminate between these motions (Siauve, Chalouhi et al. 2015). This sequence was used in our study protocol as it also used in our clinical practice but was not studied in detail in the project itself as we concentrated on placenta morphology not blood flow.

2. BOLD and T2*

The oxygen condition of the blood provides an endogenous MRI contrast mechanism because of the paramagnetic characteristics of deoxyhaemoglobin; therefore, it reflects oxygenation status. BOLD-MRI examines tissue oxygenation using T2 and T2* weighted images. T2 is the transverse relaxation period of water protons following a radiofrequency pulse. The fluctuation of signal intensity (SI) on T2 and T2* weighted images is affected by the amount of deoxyhaemoglobin. Increasing tissue oxygenation reduces the amount of deoxyhaemoglobin, which raises SI because deoxyhaemoglobin has paramagnetic characteristics with high magnetic susceptibility. Magnetic susceptibility discrepancies between red blood cells and blood plasma result from the dispersion of deoxygenated haemoglobin molecules, which raises the relaxation rates (R*2). Changes in T*2-weighted BOLD signal intensity during a respiratory challenge are primarily impacted by changes in haemoglobin saturation and may thus be utilised to imaging changes in tissue oxygenation (Avni, Neeman et al. 2015, Siauve, Chalouhi et al. 2015). BOLD would involve time consuming imaging techniques and the participant breathing in pure oxygen for several minutes. BOLD was not included in our study protocol due to the complexities and time taken to obtain

the data and again is not related to morphology but to blood flow. However BOLD maybe worth considering in future work depending on the T2* data obtained.

T2* MRI

The time it takes for the detected signal to decay is described by the MRI transverse relaxation time, or T2*. These sequences use gradient echoes and relatively long TE (time to echo) values. They are used to enhance local magnetic homogeneity effects to identify bleeding or calcifications. T2*-sensitive sequences are also used in functional MRI (fMRI) employing the BOLD (Blood Oxygen Level Dependent) approach(Wright, Morris et al. 2011). BOLD imaging contrast suggests a challenge to T2* imaging optimization because the former is dependent on deoxygenated haemoglobin found in maternal and fetal blood. The effects have been classified as paramagnetic (positive) or diamagnetic (negative) (Sorensen, Hutter et al. 2019).

T2* depends on a range of biological and structural features. These factors include oxygenation of the blood and state of placental tissue (i.e., presence of infarction, fibrosis) which reduce the level of T2*. Changes in the magnetic field and maternal respiration can also cause variations in the level of T2* (Sorensen, Hutter et al. 2019). T2 can be used to measure placental oxygenation since it can give an indication of placental vascularization and sufficiency. The former was used in placental MRI measurements in order to first get a normal T2 * background in the developing fetus and then to assess the impact of insufficiency on the image obtained. T2* signal diminishes as deoxygenated haemoglobin content rises (Hutter, Jackson et al. 2019). T2* is faster than T2 and offers a distinctive value for visualising tissue inhomogeneities. This sequence's main function is to identify magnetic changes in tissue lesions that include hemosiderin, methaemoglobin, or deoxyhaemoglobin (Chavhan, Babyn et al. 2009). We included this in our study protocol as it was quick to perform, did not rely on the patient breathing oxygen and gave an indication of abnormal structure e.g. fibrosis, infarction etc that we could relate to the visual appearance, the morphology and the histology.

The following techniques provide useful information on the blood flow in the placenta but were not used in our study as we were concentrating on

morphology and needed to keep the protocol simple to avoid excess time on the scanner. Additional reasons for exclusion are included in each section below.

3. DCE (dynamic contrast-enhanced)

This modality involves the use of gadolinium chelate intravenous injection to assess the perfusion function. DCE-MRI has been used to study perfusion in the heart, brain, and different malignancies (Gordon, Partovi et al. 2014). Although DCE-MRI is not recommended for regular clinical prenatal follow-up in normal pregnancy, it is a reliable approach for evaluating placental perfusion and may provide significant information about placental disorders (Avni, Neeman et al. 2015, Siauve, Chalouhi et al. 2015). DCE-MRI necessitates the capture of serial images before, during, and after the intravenous injection of the contrast agent, allowing for a comprehensive description of the wash-in and wash-out contrast dynamics inside tissues (Siauve, Chalouhi et al. 2015). There have been no human placental DCE-MRI investigations published. All research was conducted on animals (Salomon, Siauve et al. 2006).

Gadolinium chelates should not be utilised on a regular basis in pregnant women, this is the reason it has not been used in our studies. Even though no teratogenic or harmful consequences have been documented in animal studies (Wang, Chong et al. 2012, Kanal, Barkovich et al. 2013). Transplacental passage of gadolinium still has a questionable risk and for that reason its utilisation is limited to life-threatening conditions such as in placenta accreta spectrum (Wong 2014). Furthermore, data analysis and interpretation are difficult and require intensive computing skills (Gordon, Partovi et al. 2014).

4. ASL (arterial spin labelling)

ASL MRI examines the protons of water molecules in arterial blood that have been magnetically tagged (Siauve, Chalouhi et al. 2015). It is the first MRI technology that was used to analyse the human placenta (Gowland, Francis et al. 1998). The signal is acquired by counting the difference between two sets of images, the first is generated by labelling the water molecules with a specific radio frequency and

allowing some time to reach into body organs. According to the method used, the second image set is generated by tagging the investigated organs or not (Ferré, Bannier et al. 2013, Wong 2014). This technique has many limitations which include low signal-to-noise ratios (SNR) due to minor detectable changes between tagged and untagged images, delay in transit time and high sensitivity to motion (Wong 2014) and we chose not to use this in the current study.

5. IVIM

An IVIM-MRI is a more advanced technique for evaluating diffusion; It is a subtype of the DWI MRI (LeBihan 1990). IVIM acquisition yields three parameters to quantify diffusion and perfusion. The diffusion coefficient reflects the placenta's cellular and interstitial properties (Moore, Issa et al. 2000). Perfusion fraction (f) represents the moving blood volume fraction when compared with the pseudo diffusion coefficient which represents blood circulation in the intervillous gaps and fetal capillaries within the villi (Moore, Strachan et al. 2000). This is a time-consuming technique that may be worth investigating if the standard ADC and DWI show potentially interesting results. This was not included in our study protocol.

6. Spectroscopy

The biochemical characteristics of the placenta can be retrieved non-invasively by magnetic resonance spectroscopy to form an image that gives knowledge about the metabolism of the placenta (McKelvey and Kay 2007).

The chemicals of visible nuclei (hydrogen, carbon, and phosphorus) are detected by MRS which uses them to create a graph or spectrum to arrange these nuclei in their region of interest (Siauve, Chalouhi et al. 2015). This technique has many limitations including low signal sensitivity and low resolutions, and sensitivity to motion. Also, it is costly and needs special software to form the specified spectra. The clinical scanner available for use in this project did not have the capabilities to perform spectroscopy of the placenta.

MRI safety

Although the safety of MRI in pregnancy has been determined for magnetic fields of up to 3 tesla (T) in the second and third trimesters, long-term effects are still being investigated (Bulas and Egloff 2013, Siauve, Chalouhi et al. 2015). When assessing the safety of fetal MRI, two important parameters need to be considered: teratogenic effects and acoustic damage (Mevissen, Buntenkötter et al. 1994, Yip, Capriotti et al. 1995) if performed early in gestation (i.e., before 18 weeks) (Bulas and Egloff 2013).

Teratogenic effects

The teratogenic effects may result from either thermal damage or electromagnetic field effect (Heinrichs, Fong et al. 1988, Saunders 2005). Static magnetic fields expose patients to short-term effects of high field (0.2-3T) and MR staff to long-term effects of low fields (0.5–200 mT). Investigations which involved animals have revealed effects such as ocular abnormalities in genetically susceptible mice (Tyndall and Sulik 1991), a reduction in crown-rump length in mice exposed to MRI during the second trimester(Heinrichs, Fong et al. 1988), and death of chick embryo when exposed to intense magnetic fields (Yip, Capriotti et al. 1994). These findings are not relevant to humans, but they do raise issues.

Infants that were exposed to MRI during pregnancy demonstrated no increased risk of teratogenesis in small observational studies (Baker, Johnson et al. 1994, Myers, Duncan et al. 1998, Clements, Duncan et al. 2000, Kok, de Vries et al. 2004). Perinatal mortality rate and birth weight have not been affected in fetuses exposed to MRI when observed in a few larger retrospective studies (Strizek, Jani et al. 2015, Ray, Vermeulen et al. 2016). A comprehensive, large retrospective Canadian study looked at MRI risk during pregnancy. A database of 1737 infants exposed to MRI in the first trimester was compared with 1.4 million controls. There was no increase in the rate of congenital abnormalities, malignancy, and fetal mortality. This was the largest population-based study although Its limitation was the exclusion of early pregnancy loss as it didn't predict the risk of abortion (Ray, Vermeulen et al. 2016).

Kanal et al. conducted a low-field exposure survey on female MR technicians (Kanal, Gillen et al. 1993). There were approximately 1900 answers, but no statistically

significant relationships were discovered. Radiofrequency fields produce heat and are governed by the Specific Absorption Rate (SAR). RF values that are tolerated by humans have been established using mathematical models based on simulations; nevertheless, fetal dosimetry is just now being developed (Levine, Zuo et al. 2001, Dimbylow 2006, Hand, Li et al. 2010). High-specification magnetic field gradients are used in fast sequences.

The ratio between the amount of change in amplitude of the magnetic field (decibel) and the time it takes to make that change within a period of time has to be further explored not just in adults but in the fetus as well. Long-period imaging sessions and higher magnetic strength exposure may have biological impacts if used at critical phases of development. The Medical Device Agency (MDA) rules in the UK demand SAR to be no more than 10 W/kg (Mevissen, Buntenkötter et al. 1994, Yip, Capriotti et al. 1995).

Effect on fetal hearing

Hearing impairment is a possible side effect of fetal MRI. When coils are subjected to fast fluctuating electromagnetic currents, MRI makes a loud tapping noise. Initially, there was concern about potential acoustic harm to the developing ear. The noise generated by MRI could be more than 110 dB depending on the sequence and setup (Heismann, Ott et al. 2015). The attenuation of sound by maternal tissues and amniotic fluid happens in different degrees according to sound frequency. In fact, low-frequency sounds might be enhanced by them (Selander, Albin et al. 2016). Therefore, a possible danger to the fetal hearing system is expected.

Conflicting results were yielded following several pieces of research on animal models. Studies in sheep and guinea pigs revealed the possibility of hearing loss following MRI exposure (Cook, Konishi et al. 1982, Griffiths, Pierson et al. 1994, Gerhardt, Pierson et al. 1999). Human studies including the retrospective Canadian data found no difference in hearing between MRI-exposed and non-exposed neonates which followed up children to preschool age (Reeves, Brandreth et al. 2010, Strizek, Jani et al. 2015, Ray, Vermeulen et al. 2016).

Baker et al. found that hearing was intact in their investigation, however, the sample size was small (Baker, Johnson et al. 1994). Another research in 1995 mimicked the auditory environment of the gravid uterus by inserting a microphone through the

oesophagus of a volunteer. This exhibited adequate sound attenuation to a tolerable level that was not detrimental to the developing fetal ear (Glover, Hykin et al. 1995).
The only prospective approach to address hearing damage was conducted by Bouyssi et al. who followed-up 72 children exposed to MRI during pregnancy in the 2nd and third trimesters till 2 years of age. The results showed no hearing impairment, but it was also limited by the lack of a control group and its observational nature (Bouyssi-Kobar, du Plessis et al. 2015).

Long term effects

No negative long-term effects of fetal MRI have been identified, although the studies that assessed those risks consisted of a small sample and did not assess higher intensity signals of up to 3T (Myers, Duncan et al. 1998, Clements, Duncan et al. 2000, Kok, de Vries et al. 2004).
Practice guidelines issued by the American College of Radiologists (ACR) in 2017 stated that although there are no known risks to performing an MRI scan during pregnancy, the indication should be based on clinical background. For various reasons, ACR endorses the use of non-contrast MRI (ACR 2014). Also, the radiological society of north America in their recent updated statement stated that fetal MRI is a safe procedure when it's used within normal limits (i.e. up to 3T) (RSNA 2022).

Gadolinium contrast agents (GCAs) in pregnancy

There is evidence supporting the passage of GCAs to the fetus from the maternal circulation (Dean, Niemi et al. 1988, Panigel, Wolf et al. 1988, Novak, Thurmond et al. 1993, Okazaki, Murayama et al. 1996). But all studies were on animal cohorts. A recent study has found a small amount of GCAs in the fetal tissues at 24-48 hrs (Mühler, Clément et al. 2011). The risk of GCAs exposure has been classified by the FDA as category C. Unfavourable side effects on the fetus were found in animal studies and have not been well-tested in humans. They advised avoiding their usage unless there is a potential danger.
It is still unknown as to what the teratogenic consequences of GCAs exposure are. Spontaneous abortion, congenital defects, and lower birth weight have been explored in animal studies using daily supra-clinical doses although some have shown no abnormal changes (Soltys 1992, Rofsky, Pizzarello et al. 1994). Human studies included numerous case reports of gadolinium administration either inadvertently or

for maternal purposes showed no reported fetal damage. However, these studies were restricted to a small sample size and their observation nature (Barkhof, Heijboer et al. 1992, Tanaka, Sohda et al. 2001, De Santis, Straface et al. 2007, Millischer, Deloison et al. 2017).

Furthermore, exposure to GCAs has been linked to increased fetal death. In a Canadian retrospective study involving a large cohort. Rey et al. compared 397 children exposed to GCAs during pregnancy to 1.4 million controls with no MRI exposure. There was a 1% increase in the incidence of infant mortality in the exposed group. The risk of congenital abnormality was not significantly different among exposed groups. This study, however, has major drawbacks which were the unknown clinical indications of MRI and poor follow-up rate (Ray, Vermeulen et al. 2016).

Long-term and repeated exposure has been linked to severe consequences. As gadolinium changes into a de-chelated form with time, it turns up into a toxic substance that accumulates in various body organs, especially the brain and bones. The fetuses' continuous fast growth and gadolinium extended exposure with time due to recirculation make fetal imaging of particular concern (Rozenfeld and Podberesky 2018). Regardless of these observations, no illness has been linked to GCAs except for nephrogenic systemic fibrosis (Tanaka, Sohda et al. 2001). Most of the studies to measure postnatal gadolinium exposure are on animals. There are no studies on humans that measure the concentration of gadolinium in utero. The ACR states in their most recent Contrast Manual, which was updated in 2018, that since the impact of GCAs on the fetus is unknown, they should be used with caution in pregnant or potentially pregnant patients and their use should be confined to cases when it is likely to change maternal or fetal treatment (ACR2010).

Eligible patients to undergo the MRI scan

Metal objects

Research looked at the effect of MRI on medical implants with metal components (Shellock 2001, Shellock 2002). For instance, cardiac pacemakers, neurostimulators, pumps for drug infusion and other tools that electromagnetic field could influence them. As scanning patients will put them at risks such as the dislodgment of these implants that could have a disastrous effect on nearby organs such as vessels, nerves, and sensitive ocular implants. Brain clips used to fix intracranial anurysms could be

dislodged and result in a fatal outcome (Shellock and Crues 1988, Teitelbaum, Bradley et al. 1988, Klucznik, Carrier et al. 1993). Devices with magnetic parts such as dental and ocular and dental implants should be taken off, if possible, prior to conveying MRI. Regarding heart defibrillators, careful screening should be done ahead of the scan to look at their compatibility to such scan. Patients having tattoos have to get information regarding the adverse effects of MR scan (Kreidstein, Giguere et al. 1997). These could be local heating, swelling and redness, however they are not contraindications for the scan. Other objects such as jewellery and body piercing should be removed prior to the scan to reduce the risk of images artifacts.

Claustrophobia

Panic episodes occur in 20% of persons who get an MRI, which can be caused by claustrophobia (Gollub 2000).

The reasons for this include: the relatively small space in which the patient is contained, the limitation of mobility, the length of the process, the noise created by the machinery, and the elevated body temperature caused by the RF pulses.

Adverse reactions can be minimised by carefully conveying to the patient what to expect. Additional methods for reducing stress in MRI patients include keeping verbal contact through an intercom, allowing a screened family member to enter the room, playing relaxing music through headphones and providing a fan to circulate air and decrease RF pulse-induced warmth.

As a distraction, some MRI rooms now incorporate video applications. Some patients may also respond favourably to strong illumination, which illuminates the otherwise dark recesses of the bore. Some modern MRI scanners contain open magnets, which do not form entire circles like normal magnets and may cause less distress in people suffering from claustrophobia or anxiety. Open scanners, on the other hand, may necessitate lengthier scanning periods due to their lower magnetic field intensity, which may be unsatisfactory to patients or clinicians.

If a patient is uncomfortable or claustrophobic, a sedative may be administered. To prevent burns from equipment or cables that may cause warmth or electric current, careful preparation and constant monitoring of the sedated patient should be used.

Section 1
Placenta accreta spectrum (PAS)

Overview

Placenta accreta spectrum (PAS) is a serious pregnancy condition that occurs when the placenta grows too deeply into the uterine wall. Typically, the placenta detaches from the uterine wall after childbirth, but with placenta accreta spectrum, the placenta remains attached due to the deep growth, which can cause severe blood loss after delivery. It is a spectrum of conditions, of differing severity, collectively called placenta accreta spectrum disorders, which includes placenta increta (where the placenta invades into the muscle of the uterus) and placenta percreta (where the placenta penetrates through the entire uterine wall and can attach to other organs).

PAS causes 7% of maternal mortality (Chen, Mar et al. 2019). It is an obstetric emergency and a leading cause of life-threatening bleeding (Maurea, Romeo et al. 2018). Diagnosis is still not definitive and relies on identifying invasion signs on MRI, such as heterogeneity and dark bands, which depends on the experience of the radiologist, and therefore developing an objective approach is warranted. Effective antenatal diagnosis may significantly help in reducing maternal morbidity and mortality (Zhang, Xu et al. 2020). This raises the need for a complementary approach to assess placental invasion. Diffusion and textural analysis have shown a correlation with some types of tumours (Sarioglu, Sarioglu et al. 2020) and given that the placenta itself is abnormal in cases with PAS we hypothesise that the ADC values and the texture will both be different between PAS cases and normal placentas. The use of radiomics can give an indication into the microstructural features, for example increased texture is thought to reflect the invasion of vessels and pools of blood disrupting the normal placental architecture. A small study has shown significant results with differences in texture between normal and abnormal placentas (Chen, Mar et al. 2019). The objective of this research is to evaluate the utilization of ADC and texture analysis in PAS diagnosis in a large cohort with known outcome based on either pathology if available and if not based on the surgical findings.

1.1 Background

PAS was first described in 1937, nearly 80 years ago by Irving and Hertig who defined it as the failure of the placenta to separate at the time of delivery (Irving 1937). The primary reason behind the development of PAS is due to a defect in the myometrium. It was first thought that trophoblastic defect in the placenta leads to hyper-invasion of the placenta beyond the normal uterine linings. It is now thought that the development of placenta percreta is not due to a deeper invasion of the trophoblastic tissue into the adjacent organs, rather the presence of an extended CS scar makes it easier for the trophoblastic tissue to extend out of the normally confined uterine tissue. The increase in the rate of caesarean deliveries over the last decades led to a higher incidence of PAS which supports the latest theory.

Both adherent and invasive placentas are included in the term placenta accreta spectrum (Jauniaux, Chantraine et al. 2018). The wide variation in terms of describing abnormal placentation was the reason why less reporting of the prevalence of PAS happened. Different terms are used to describe placental invasion, for example (placenta vera, placenta creta, placenta accreta disorders (PAD) and morbidly adherent placenta). Generalising the term under the umbrella of PAS is essential to increase the accuracy of reporting abnormal placenta cases.

Prenatal diagnosis of PAS cannot be based on the histopathological assessment of placental tissue which is the standard way to diagnose PAS. About half to two-thirds of PAS cases remain undiagnosed until delivery (Bailit, Grobman et al. 2015, Thurn, Lindqvist et al. 2016). As with advanced gestation, the decidua (basal placental layer) becomes discontinued, and the presence of myometrial fibres in the placenta layers makes the diagnosis more challenging (Jauniaux, Collins et al. 2018). The histological diagnosis sometimes is not definitive, so making a clinical diagnosis at the site of surgery is necessary. Diagnosis of PAS and planned management involving a multidisciplinary team and highly specialised centres have been found to reduce maternal mortality and morbidity (Eller, Bennett et al. 2011, Shamshirsaz, Fox et al. 2015).

Based on the visual appearance of placental invasion and destruction of the adjacent structures, PAS has been classified according to FIGO guidelines into 3 grades (Fig.2) (Hecht, Baergen et al. 2020, Jauniaux E1 and Panel. 2020). Grade 1 is the placenta which is difficult to detach from the uterine wall (accreta), which is non-invasive. Grade 2 or increta, is where the placenta invades the uterine wall but keeps more than 25%

of the wall thickness intact. Grade 3 represents placenta percreta, it has 3 subcategories: A, D and E. PAS grade 3A is invaded placenta with involvement of most of the myometrium (less than 25% of the wall left intact). 3D and 3E invasion reaches the adjacent organs. Grade 3D (D is for Deep invasion) represents the placental invasion of the uterine wall and serosa. Grade 3E (E is for Extra uterine invasion) is the involvement of extrauterine structures especially the bladder or parametrial tissues.

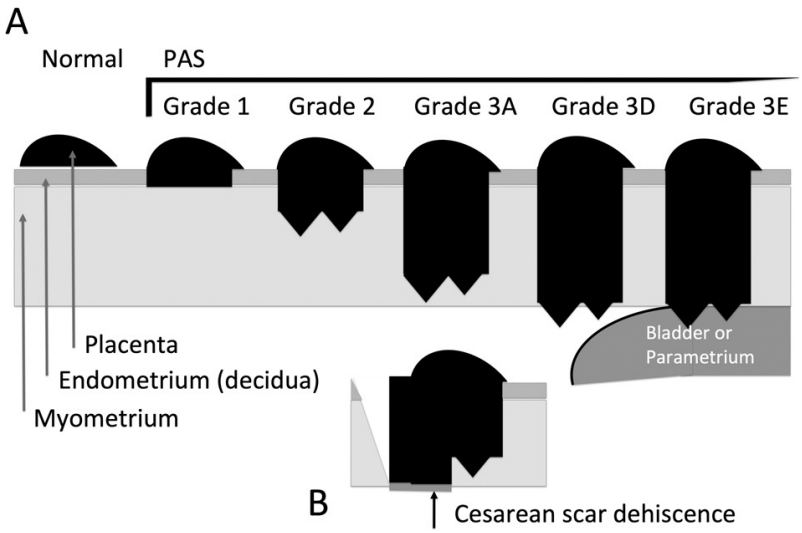

Figure 2 Classification of PAS grading system (Figure adapted from (Hecht, Baergen et al. 2020).

This classification is clinically relevant as it guides the management strategies. For instance, a higher grade (like placenta percreta) typically requires more extensive surgical intervention and poses a higher risk for severe postpartum haemorrhage.

Prenatal identification and appropriate grading of PAS allow for detailed planning including assembling expert multidisciplinary teams, planning the surgical approach, blood product availability, and considering the patient's wishes (like future fertility). It's important to note that definitive diagnosis and grading often require both high-quality imaging and clinical judgment.

Placenta accreta accounts for about 60% of PAS and 16% and 22% represents the percentage of increta and percreta respectively (Abuhamad 2013, Jauniaux, Bunce et al. 2019). The incidence of PAS has been rising with time, observational studies

reported an increased rate of 1 in 2510 in 1970 to 1 in 533 in 2002. In the United States, the incidence reached 1 in 272 in 2016 (Obstetric Care Consensus2018). In the UK a systematic review and meta-analysis in 2019 reported 0.5% of accreta cases and 0.3/1000 births for invaded cases. It's hard to give a single number for the incidence as over years there have been heterogeneous studies and different terminologies were used to describe PAS. Depending on the number of previous caesarean sections with placenta previa the incidence range was from 3% with one CS (Silver, Landon et al. 2006) to 67% for the fifth CS (Silver, Landon et al. 2006, Jauniaux, Grønbeck et al. 2019).

Causes of PAS

Although non-surgical risk factors of PAS for example uterine pathologies such as adenomyosis, bicornuate uterus and submucous fibroids were reported (Benirschke 1967, Jauniaux and Jurkovic 2012). Uterine surgeries particularly CS comprise the main risk factor for PAS. Surgical scars don't heal completely leaving a scar area with the absence of re-epithelialization. As a result, in the next pregnancy, the trophoblast and villi invade the endometrial layer and get attached and or pierce the myometrial layer and adjacent structures (Jauniaux, Collins et al. 2018). Some have suggested that over invasion of the trophoblasts might be the reason behind the deep anchoring villa in accreta and destruction of the smooth muscle in the increta which is an old theory (Cramer and Heller 2016). Placenta previa is commonly recognised as a risk factor for placenta accreta (Lam, Kuller et al. 2002). Multiparity, advanced maternal age, prior uterine surgeries and Asherman syndrome are all risk factors for PAS (Jauniaux, Grønbeck et al. 2019). However, CS constitutes the primary cause in developed countries (Silver, Landon et al. 2006).

Diagnosis of PAS

Prenatal assessment of PAS is now commonly performed using ultrasound scans and MRI (D'Antonio, Iacovella et al. 2013, Meng, Xie et al. 2013, D'Antonio, Iacovella et al. 2014, Jauniaux, Collins et al. 2016). Ultrasound is the main tool used for the screening and diagnosis of PAS (Jauniaux and Ayres-de-Campos 2018). MRI is an adjuvant

technique that is used in cases of challenging diagnosis (Berkley and Abuhamad 2013, Hershey 2014) and to aid surgical planning. Although effective diagnosis can be made using prenatal US, it is still uncertain whether MRI enhances the diagnosis (Jauniaux, Hussein et al. 2019) and different studies give conflicting results. Half (Fitzpatrick, Sellers et al. 2014, Bailit, Grobman et al. 2015) to two-thirds (Thurn, Lindqvist et al. 2016) of PAS cases might remain undiagnosed as shown in recent studies. MRI is not a practical screening tool due to its cost and limited access which makes ultrasound a convenient tool to identify pregnancies at high risk of developing PAS.

Accurate diagnosis of PAS often relies on a combination of clinical history, imaging studies, and intraoperative findings. While histologic examination is considered the gold standard for diagnosis, it's typically not used as the primary method of diagnosis due to limitations, such as sampling errors and difficulty in obtaining an adequate specimen, especially in cases of conservative management where the placenta might be left in situ. Clinical history and risk factors are essential in suspecting PAS. They include conditions like a previous caesarean section, placenta previa, prior uterine surgery, advanced maternal age and in-vitro fertilization. Imaging methods such as ultrasound and MRI are the most commonly used tools for the prenatal diagnosis of PAS disorders. Ultrasound, in the hands of an experienced operator, can be highly sensitive and specific. Certain ultrasound features are suggestive of PAS, including loss of the normal 'clear zone', the presence of multiple vascular lacunae (areas of swirling blood flow within the placenta) and abnormal placental lacunae. When ultrasound findings are unclear, MRI can be used for further assessment. Intraoperatively, a placenta that does not detach spontaneously or that requires excessive traction for removal may be consistent with an abnormally adherent placenta. Superficially adherent/accreta placenta indeed might pose a challenge because it could be hard to differentiate from severe adhesion due to previous caesarean sections. Pathologists could also miss these areas due to their superficial nature and thus lead to negative histology. In conclusion, the diagnosis of PAS disorders relies heavily on a combination of clinical history, imaging studies and intraoperative findings. The role of histologic examination while being the gold standard is limited by several factors.

PAS signs on ultrasound

In 1967, Sadovsky et al. first diagnosed PAS using radioisotope placentagraphy (Sadovsky, Palti et al. 1967) and Tabsh et al. first defined PAS on US in 1982 (Tabsh, Brinkman et al. 1982). PAS features on ultrasound were essentially described by Finberg and Williams for grey-scale (Finberg and Williams 1992). 9 features were identified but the disappearance of the normal uteroplacental clear zone, hypervascularity of the placenta (lacunae) and myometrium thinning are the primary features recognized in the US.

a) Clear zone disappearance

In a normal placenta, the hypoechoic retroplacental area is visible on ultrasound. Abnormal extension of the placental villi into the myometrium results in the disappearance of the clear zone (Jauniaux, Collins et al. 2016). This was one of the first signs identified by ultrasound in cases of PAS (Kerr de Mendonça 1988, Jauniaux, Collins et al. 2016) and was stated in 70% of cases (Jauniaux, Collins et al. 2016). Limitations of this sign are its change with advanced GA, placental location and the presence of scar tissues which make it less accurate (Comstock, Love et al. 2004, Hamada, Hasegawa et al. 2011). In addition, it is operator dependent as bladder filling and pressure on the ultrasound probe will also change the appearance of the clear zone.

b) Placental lakes (lacunae)

The most documented sign in PAS is placental lacunae with around 80% (Jauniaux, Collins et al. 2016). It was also referred to as the “Swiss cheese" sign (Japaraj, Mimin et al. 2007). This feature is frequently seen in ultrasound as lucent intraplacental, irregular wide gaps that resemble the moth-eaten appearance (Kerr de Mendonça 1988, Finberg and Williams 1992, Jauniaux and Jurkovic 2012). The benefit of this sign is its independence on the degree of placental invasion (Jauniaux, Collins et al. 2016) but the location of the placenta, direct probe pressure and gestational age influence the number and form of lakes. These lakes can be seen also in the normal placenta, but there are a few differences. They tend to be less in number, smaller, and narrower (Finberg and Williams 1992).

c) Thinning of the myometrium

This sign has been recognized in 50% of studies (Jauniaux, Collins et al. 2016). It forms due to thinning of the myometrial layer to 1 mm or absence on the ultrasound (Hoffman-Tretin, Koenigsberg et al. 1992, Twickler, Lucas et al. 2000, Wong, Cheung et al. 2008). Several factors could affect the accuracy of this sign. Gestational age normally causes thinning of the myometrium, especially at age >32-34 weeks. False-positive signs could be present in severe myometrial thinning and could be misdiagnosed as an abnormal invasion. The cause of that is the physiologic uterine stretching by the action of fetal presentation and Braxton-Hick's contractions. In addition, direct pressure by the ultrasound probe and the bladder fullness influences the myometrial thickness and the clear zone. It is challenging to differentiate these features in some situations, however, in cases with combined PAS and placenta previa, the myometrium looks very thin or invisible. Other signs could also present like the disappearance of the clear zone and placental hypervascularity.

d) Bladder wall interruption

This sign is only present in advanced placental invasion and so this limits its utilization. It is caused by the villous passage into the bladder posterior wall from the placental anterior wall. It manifests as bladder wall loss or irregularity, or as a hyperechoic line between the bladder lumen and the uterus (Finberg and Williams 1992, Shih, Palacios Jaraquemada et al. 2009).

e) Placental bulge

This sign is found during laparotomy and could be identified by both US and MRI, it is also known as the snowman sign (Matsuo, Conturie et al. 2014). This happens due to the expansion of the uterus housing the placenta out from its usual plane and into the surrounding tissue, notably the bladder. It most likely suggests deep myometrial invasion, which causes changes in uterine tension characteristics.

f) Exophytic mass

When the infiltration of villous tissue occurs as a localised exophytic mass outside the uterine serosa, it forms an exophytic structure. This should only exist in situations of placenta previa and is seen by US, it has only been observed in 30% of PAS cases (Jauniaux, Collins et al. 2016).

g) Sub placental and/or utero-vesical hypervascularity

This is a characteristic hallmark of PAS on prenatal ultrasonography and occurs when the uteroplacental circulation dilates beyond the spiral arteries (Chou, Ho et al. 1992, Chou and Ho 1997, Levine, Hulka et al. 1997, Shih, Palacios Jaraquemada et al. 2009, Chantraine, Blacher et al. 2012, Collins, Stevenson et al. 2015, Jauniaux, Collins et al. 2016). Neovascularization inside the peritoneum, particularly between the uterine anterior wall and the bladder posterior wall is often present as well. This vascular pattern may present in 75% of cases with placenta previa and 81% of invaded placentas (Jauniaux, Collins et al. 2016). But the abnormal pattern tends to be more variable in size and spatial organisation (Chantraine, Blacher et al. 2012).
Placental location relevant to the main uterine main arteries does affect the distribution of vessels. Furthermore, the myometrial thickness, lacunae, and vascular features under and around the accreta area change with advancing gestation.

h) Feeder vessels of placenta lacunae

This feature signifies large aberrant high-velocity vasculature that emerges from deep myometrial arteries and supplies the placental lacunae. These vessels could also be present in normal placentas but can be differentiated from abnormal ones as they tend to be fewer and larger in size. Also, they are usually accompanied by the placental lakes (Chantraine, Blacher et al. 2012).

i) Bridging vessels

These are caused by dilatation of the big and deeper myometrial arteries below the junction zone of normal implantation and have been found in 66% of instances with abnormally invasive placenta identified prenatally (Jauniaux, Collins et al. 2016). In situations of placenta previa accreta, they have been referred to as "bladder varicosities." (Jauniaux, Collins et al. 2018).

Role of MRI in the diagnosis of PAS

Ultrasound is the main modality used to detect placental invasion because of its immediate availability, ease of use, established efficacy and safety for the mother and the fetus. However, MRI is needed in cases of indecisive ultrasound results such as posterior placenta and maternal habitus (Thorp, Councell et al. 1992, Fejgin, Rosen et al. 1993). MRI is regarded as an additional technique to obtain further information about the degree of placental involvement in suspected cases of invasion as MRI provides higher tissue resolution and a larger field of view. In terms of diagnostic capability, it is unknown if MRI is superior to ultrasound. Currently, there are few agreed diagnostic criteria on MRI for PAS (Lax, Prince et al. 2007) and there are contradicting outcomes in the literature. MRI has been shown to have little sensitivity in a few studies (Lam, Kuller et al. 2002). Other studies have shown its usefulness particularly when the placenta is difficult to assess using an ultrasound scan (Thorp, Councell et al. 1992, Fejgin, Rosen et al. 1993). Guidelines for MRI utilization in doubtful situations were issued by the royal college of obstetrics and gynaecology and the national institute of clinical excellence in 2011 (NICE 2011, RCOG 2011).
Establishing the MRI characteristic features of PAS has been difficult. A study used ultrasound features to explore the corresponding features on MRI for 18 participants with PAS suspicion (Levine, Hulka et al. 1997). One of the patients was diagnosed with normal placenta previa but developed a haemorrhage at the time of CS which ended in a hysterectomy. MRI has shown to diagnose placenta accreta in posterior placenta that ultrasound is unable to detect due to the placental location. In one such case MRI revealed a 4 cm region of the placenta with loss of myometrium. Overall, US displayed a sensitivity of 86% and a specificity of 92% for the diagnosis of PAS. MRI adjuvant role to US increased the sensitivity to 100%; US was only 100% sensitive for identifying the anterior placenta cases in the study of 18 cases (Levine, Hulka et al. 1997).

Maldijan et al. utilized MRI to evaluate two patients with placenta accreta and two patients with placenta percreta (Maldjian, Adam et al. 1999). They assessed myometrium thinning and/or the presence of abnormal myometrial signals, invasion of

adjacent structures and bladder wall irregularity. In both cases of placenta accreta, the myometrium close to the site of the defect presented with lower signal intensity with a localized thinning in the myometrium and fuzziness at the anomaly site. The placenta was close to the area of relative thinning. Whilst in percreta cases, there was focal destruction of the uterine wall with tissue crossed and merged with it. This made it appears as isointense to the intrauterine placenta on the MRI. In comparison with accreta cases, the appearance of the anomaly was more clearly visible on MRI. In one of these two cases, MRI revealed placental tissue close to the bladder wall, which seemed ill-defined.

Thorp et al. looked at the obliteration of the uterine lower segment and myometrium thinning or loss in a single patient with a suspicion of placenta percreta (Thorp, Councell et al. 1992). There was a complete destruction of the lower uterine section with placenta previa inserted right on the base of the bladder. The myometrium was lost in the lower uterine segment. Transabdominal sonography revealed full placenta previa but invasion into the bladder was not detected.

Furthermore, 9 patients diagnosed with PAS were evaluated by Lam et al. to assess the efficacy of MRI (Lam, Kuller et al. 2002). The features used were interruption, attenuation, and non-visualization of the uterine wall, the presence of irregular masses, myometrium invasion, and attenuation of the space separating the uterine and bladder wall. US sensitivity was 33% whereas sensitivity in MRI was 38%.

Gadolinium-enhanced MRI has also been proposed in the diagnosis of placenta accreta. A study claimed it can aid in the differentiation of placenta accreta from placenta percreta (Palacios Jaraquemada and Bruno 2000). The use of contrast in 6 participants has shown good differentiation between the uterine wall and the placenta (Tanaka, Sohda et al. 2001). Nevertheless, the use of gadolinium contrast agents in prenatal MRI is not recommended since its safety has not been clearly understood.

Lax et al. have thoroughly assessed 17 MRI features but only 7 features were reported to have high diagnostic accuracy and reliability. (Lax, Prince et al. 2007). These included placenta previa, abnormal uterine bulging, intraplacental haemorrhage, dark intraplacental bands, placenta signal intensity, myometrium seen beneath the

placenta and increased placental thickness. Excellent reliability was observed for 3 features to be different between normal and invaded placentas. Abnormal uterine bulge, heterogeneous placenta, and dark placental bands were the most credible MR imaging results (Lax, Prince et al. 2007, Baughman, Corteville et al. 2008).

Abnormal uterine bulge

The mechanism behind this abnormality is unknown but it could be due to the stiffness of the uterine wall and /or the bleeding and the thickness due to placental invasion into the myometrial layer. This sign was more predominant in cases with PAS however there have been few normal cases that appeared with uterine bulging (Lax, Prince et al. 2007). It is important to note that uterine bulge only appears in percreta instances so it's specific but not sensitive (Rahaim and Whitby 2015). In some instances, this sign might be misleading and result in a false positive diagnosis such as in cases where there are bladder varices which is why diffusion sequences are needed to distinguish between these pitfalls (Cuthbert, Teixidor Vinas et al. 2016). Furthermore, uterine dehiscence could also present in a similar picture of PAS on MRI which is in fact a part of the placenta occupying an abnormally formed gap in the myometrium (Cuthbert, Teixidor Vinas et al. 2016).

Heterogeneity

Haemorrhage products and/or distortions of blood flow might cause the heterogeneous pattern of the placenta in PAS. It was reported that all patients with placental invasion have a substantial heterogeneity (Lax, Prince et al. 2007, Rahaim and Whitby 2015). Similarly, normal placentas were homogenous on T2W images. Nevertheless, mild heterogenous signal intensity might be of minimal help as this is common in both normal and invasive placentas (Lax, Prince et al. 2007).

Dark bands

The presence of fibrous tissue in placentas with invasion might be the reason why they have dark bands. This could be confirmed with the histology which reveals an excess of basal fibrin (Frank 2000). Normally the uterine septa are smooth thin like extensions, these must be distinguished from the abnormally present dark bands. The latter tends

to be hypoechoic on T2 W images, finger-like or nodular structures that originate from the maternal surface. They are of variable locations and thickness (Cuthbert, Teixidor Vinas et al. 2016). The presence of these bands should raise the suspicion of placental invasion. Clinically, high-risk pregnancies whose placentas show dark bands, have to be treated as PAS, and PAS could be excluded when there are no dark bands (Lax, Prince et al. 2007).

Placental and uterine vascular malformations

Abnormal dilated and tortious intraplacental vessels of 0.6 mm are another characteristics of invaded placentas which are correlated with the degree of invasion and are found in areas of dark bands (Derman, Nikac et al. 2011). It is essential to compare different sequences during the assessment of vascular malformations. i.e., T2 single-shot fast spin-echo (SSFSE) and balanced gradient echo (BGE) sequences are used. These vessels demonstrate low signal intensity on T2 SSFSE and high signal on BGE which are equivalent to lacunae on ultrasound scan (Cuthbert, Teixidor Vinas et al. 2016).

Increased peri uterine vascularity and noticeable placental lacunae were of particular importance on ultrasound to predict placental invasion (Hoffman-Tretin, Koenigsberg et al. 1992). However, matching MRI findings were not discovered (Lax, Prince et al. 2007). Also, the presence of abnormal peri uterine and intraplacental vascularity on sonography was observed, they were also not consistently seen on MRI. Possibly this was because current MRI sequences do not detect aberrant vascularity as flow voids (Lax, Prince et al. 2007). MRI helps to detect the extrauterine extension in high-risk pregnancies. The serosal vascular sign referring to MRI visible uterine serosal vessels was the most reliable MRI characteristic (Bourgioti, Zafeiropoulou et al. 2018). In addition to that, these vessels might extend and narrows the space between the uterus and the bladder (i.e., bladder vessel sign) and or the parametrial space (i.e., parametrial vessel sign). These were the most accurate characteristic of MRI for identifying placental growth into the urinary bladder and parametrial tissues (Bourgioti, Zafeiropoulou et al. 2018).

Interestingly the two main features used to diagnose and assess the extent of PAS on the MRI images are not specific to the area of attachment of the placenta to the uterine

wall but are changes that affect the bulk of the placental tissue either as a full thickness focal area usually at the site of the previous caesarean section or the entire placenta.

Other features

It was unexpected to see that some sonographic markers used to indicate placental invasion had not been demonstrated to be meaningful in MRI evaluation (Lax, Prince et al. 2007). While sonography has used thinned or absent myometrial zones to identify placenta accreta (Finberg and Williams 1992), these features have no diagnostic importance on MRI. Furthermore, the presence of exophytic masses and irregularity of the linear hyperechoic uterine serosa bladder wall complex are two other crucial findings in the ultrasonography diagnosis of placental invasion. MRI was also not correlated with the abnormalities detected in the invaded placentas. Similarly, the ultrasonographic literature shows that rupture of the uterine serosa-bladder line may be a good marker with high specificity but low sensitivity (Comstock, Love et al. 2004).

ADC in the diagnosis of PAS

To increase the diagnostic accuracy of MRI, new techniques have involved functional MRI as a biomarker for the placenta accreta spectrum. DWI is a method that can describe the microstructural features antenatally without the need for invasive procedures as it targets the movement of water molecules by measuring ADC (Lu, Wang et al. 2022, Lu, Li et al. 2023).

Multiple techniques have been used to measure the diffusion and perfusion functions of the placenta. For example, IVIM is an advanced form of DWI which was utilized to measure placental function. Bao et al. discovered perfusion and diffusion markers in placentas with accreta lesions were considerably greater (Bao, Pang et al. 2021). Another modality of DWI is DKI which measures tissue cellularity and was used in only one study to look at the differences between normal and PAS. Its measures an index that is equivalent to corrected ADC (Lu, Li et al. 2023).

ADC biomarkers were used for the assessment of placental invasion in one study. Their results showed that ADC was higher in increta and percreta than in normal cases (Lu, Li et al. 2023).

This was a retrospective project that included 53 individuals with invasive placentas and 47 with non-invasive placentas who underwent standard diffusion-weighted imaging (DWI), intravoxel incoherent motion (IVIM), and diffusion kurtosis imaging (DKI).
Both IVIM and DKI models had poor signal to noise ratio owing to the imaging with free breathing technique. Breath- hold imaging was hard to obtain from pregnant ladies.

Pathology of PAS

Irreversible damage to the uterine wall up to the serosa, with placental tissue reaching the deep uterine circulation, is the hallmark of PAS histopathology (Jauniaux, Collins et al. 2018). When examining cases with placenta accreta, placental villi tend to be in direct contact with the myometrium. Whereas cases of increta and percreta proliferated interstitial trophoblasts were noticed in the placental-myometrial junction. Also, infiltration of inflammatory cells especially mononuclear cells and remains of endometrial glands were seen in between muscle fibres and surrounding arteries. In some cases, the myometrial muscle is pushed into the placental septa, which are usually made up of maternal decidua and trophoblastic parts. (Khong and Robertson 1987). Accurate pathological assessment requires skill and expertise that is not available in all centres.
There is a large number of placentas delivered that are hard to diagnose by histopathology even in some cases of hysterectomy (Hecht, Baergen et al. 2020). Eller et al. couldn’t find the definitive histopathological confirmation of 18-20% of cases even with the examination (Eller, Bennett et al. 2011).

The placentas in PAS are delivered by either evacuation with part of the myometrium in case of adherent placenta or by hysterectomy in case of invasive ones. To diagnose PAS, there are specific gross and microscopic features. Placental tissue alone or placental bed biopsies cannot be used to make the pathologic diagnosis of PAS; instead, specimens from hysterectomy or partial myometrial excision are the only sources of information.

Microscopically, the placental bed is the basis for the diagnosis of PAS following excision (Fig. 3). The sections between the myometrium and villous tissue must exhibit broad regions of missing decidua. This can involve regions where the placental villi adhere to the superficial myometrium directly or aberrant implantation where a fibrinoid and intermediate trophoblast layer is present between the villi and the muscle (Hecht, Baergen et al. 2020).

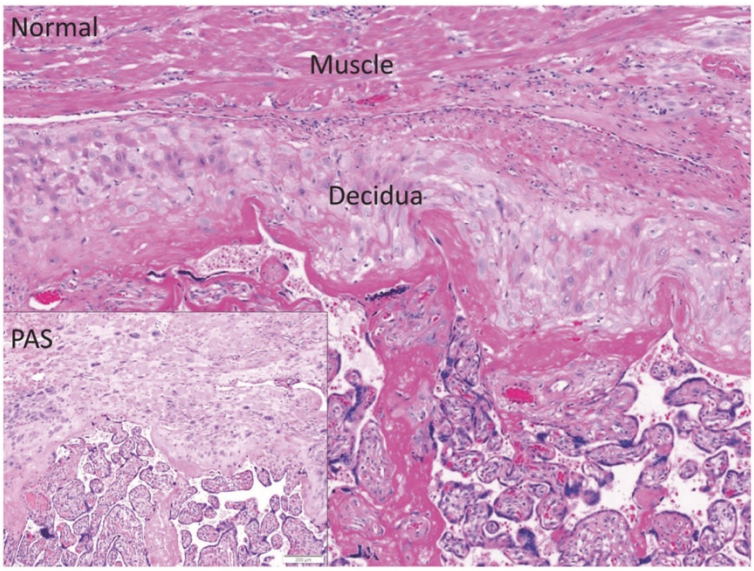

Figure 3 Normal implantation and PAS. PAS is characterized by the loss of the decidua layer. H & E-stained section at x100 original magnification. Adapted from (Hecht, Baergen et al. 2020).

Macroscopic features

The uterus shows areas of infiltrative nodules with wide boundaries with uneven thinning of the underlying uterine wall in locations where the myometrium has been intact. Typically, in situations of placenta previa, there is also a lower uterine segment bulging and elongation, with accompanying uterine wall remodelling during pregnancy or as a result of dehiscence of the caesarean scar. This region is frequently quite thin and may exhibit iatrogenic surgical disruption sites (Jauniaux, Hussein et al. 2020). To note, uterine dehiscence of CS scar has been approved by the FIGO panel to be a

uterine issue rather than placental implantation issue (Hecht, Baergen et al. 2020) (Fig. 4).

Furthermore, mechanical separation of the placenta tissue should be attempted in cases where there is no visual invasion sites to roll out accreta cases (Dannheim, Shainker et al. 2016, Jauniaux, Hussein et al. 2020). Following that, the junction between the placental bed and the myometrium should be assessed thoroughly to confirm the grade of the PAS.

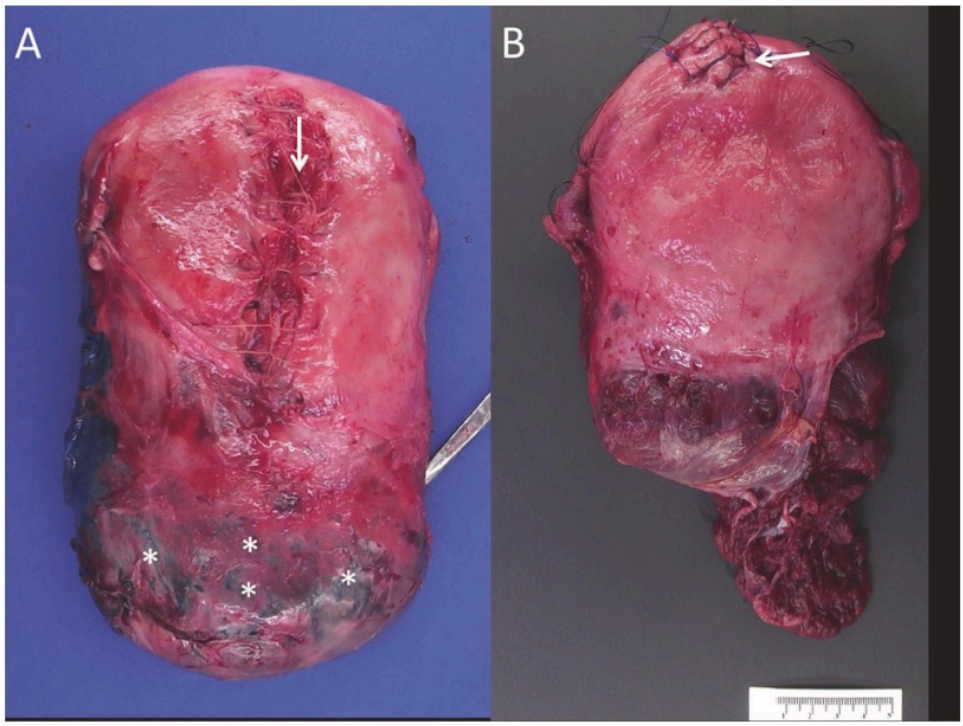

*Figure 4 Remodelling of the uterus. Bulging and distension of the lower uterine segment with prominent serosal vasculature in a case of placenta previa (2, *). B Thin areas of the uterine wall are prone to distension either due to invasion beyond the serosa or to manipulation of the specimen during and after surgery. Adapted from (Hecht, Baergen et al. 2020).*

Microscopic features

Chorionic villi implanted abnormally on the surface myometrium without a decidual layer in between is the typical feature under the microscope. These villi are often covered by extravillous trophoblast (EVT) and fibrin layer over the myometrial layer.

Unlike EVT, which has more amphophilic cytoplasm, decidual cells have pale, eosinophilic to gray cytoplasm. They also usually form sheets as opposed to infiltrating patterns.

The majority of PAS cases may exhibit interstitial oedema, chronic inflammation, degenerated myofibers, and tissue injury (Cramer and Heller 2016, Ernst, Linn et al. 2017). Additionally, remodelling of the outer myometrial vessels will be present in most cases, with some exhibiting intimal thickening or hemosiderin-laden macrophages (Fig. 5).

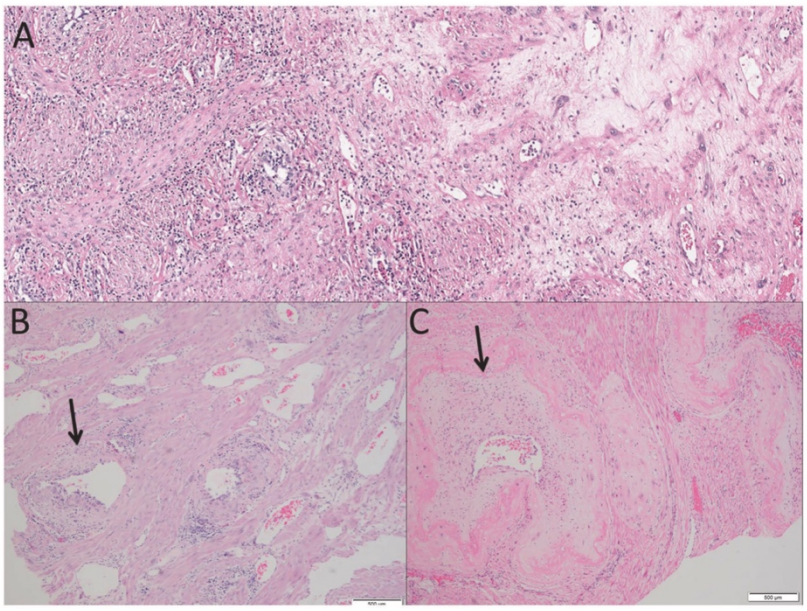

Figure 5 PAS with invasion. a. A case of PAS showing infiltrative invasion with fibrosis replacing myofibers accompanied by increased chronic inflammation (left) with oedema (right). b. Deeper sections show trophoblast remodelling of outer myometrial vessels (arrows). Adapted from (Hecht, Baergen et al. 2020).

Throughout all phases of PAS, intact villous tissue intrusion into enormously dilated arteries at the placenta-myometrial interface is quite prevalent (Fig. 6).

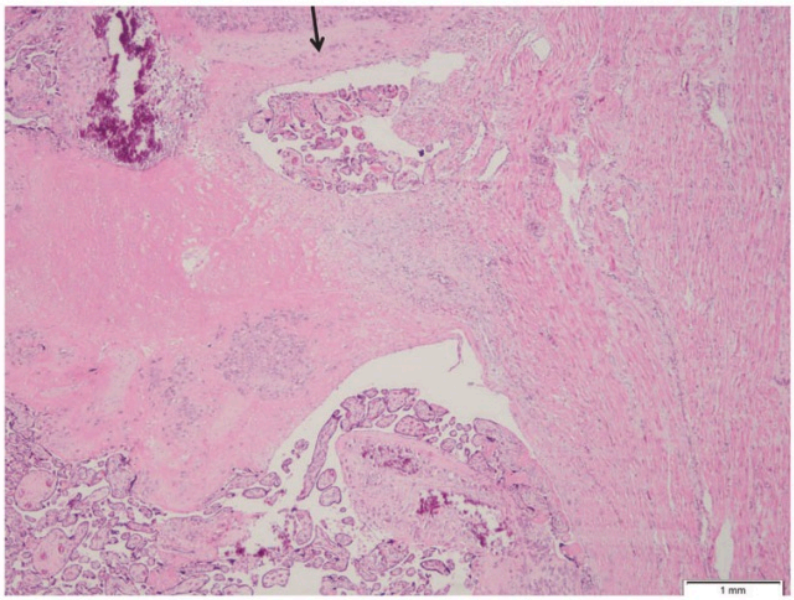

Figure 6 Villous tissue in dilated myometrial vessels at the invasive front (arrow). This, along with remodelled arteries, may give the appearance of vascular continuity between the placenta and uterus, but the dilated vessels are uterine, not placental. Adapted from (Hecht, Baergen et al. 2020).

In PAS, an altered EVT pattern has been reported. While EVT is often seen in the decidua, inner myometrium, and basal plate, PAS is characterised by deeper uterine wall penetration (Fig. 7).

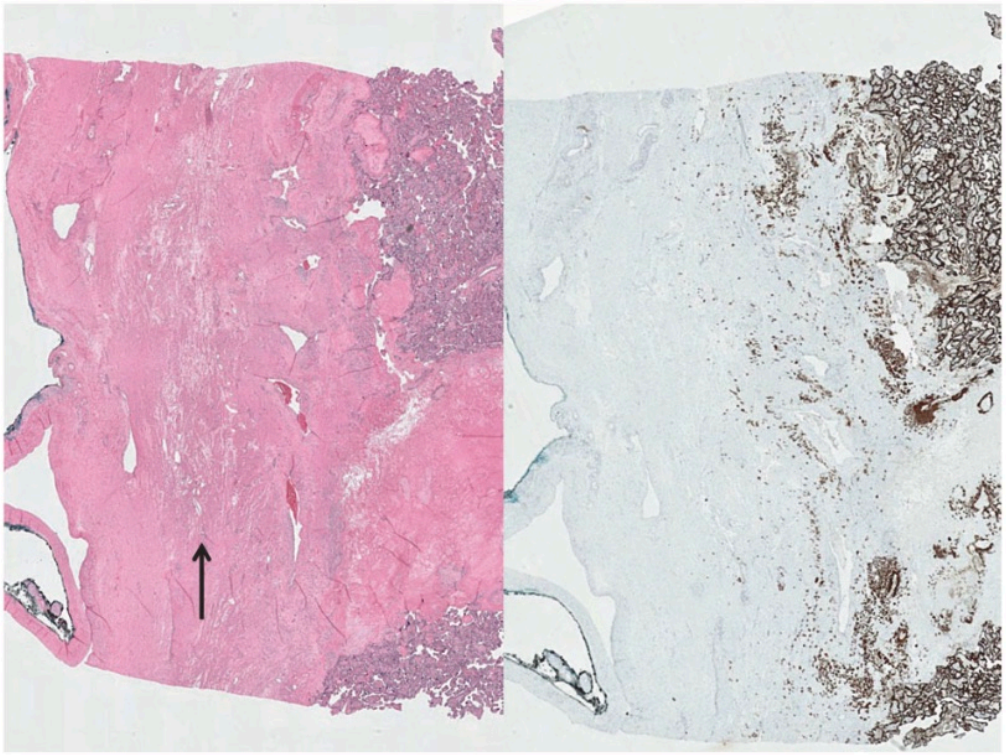

Figure 7 A case of PAS demonstrating an altered pattern of extra villous trophoblast, extending well beyond the decidua and inner myometrium. H & E and cytokeratin stain. Adapted from (Hecht, Baergen et al. 2020).

PAS management

If the diagnosis of PAS is missed or the management is not efficient, massive bleeding at the time of placental delivery (PPH) could happen. For that reason, proper management is mandatory. Following an antenatal diagnosis of PAS, the decision of the time of delivery, and the availability of experienced surgical, anaesthetists and interventional radiologist team is required. An elective caesarean section is planned at 36 weeks and matched blood products should be ready at the time of delivery (Cuthbert, Teixidor Vinas et al. 2016). There is a high risk of massive bleeding at the time of CS which could lead to a hysterectomy. The current surgical management of PAS has included other options, depending on the imaging findings, the obstetrician might decide to avoid placental separation to reduce the risk of morbidity. This is either by hysterectomy without placental separation or CS followed by methotrexate injection

and the use of B-Lynch suture. When fertility needs to be preserved, interventional radiologists play a crucial role. This includes the use of prophylactic use of balloon tamponade placed in the internal iliac arteries (Panici, Anceschi et al. 2012, Clausen, Stensballe et al. 2013, Teixidor Viñas, Chandraharan et al. 2014) or embolization of the uterine artery in emergency cases (Hansch, Chitkara et al. 1999, Sivan, Spira et al. 2010).

1.2
MRI placental texture analysis to diagnose placenta accreta spectrum: a systematic review and meta-analysis

Introduction

Placenta accreta spectrum is a range of abnormal placental invasion into the uterine wall and adjacent structures. Placenta previa and previous C-sections are the most important risk factors. The most common adverse effects of delivering invaded placenta are uterine, urethral and bladder injury and a higher risk of maternal death (Oyelese and Smulian 2006).

Diagnosis of placenta accreta spectrum (PAS) comprises a challenge in clinical practice. Identification of magnetic resonance imaging (MRI) invasion signs require specialized experience. It is important to determine the degree of invasion since the deeper the invasion is, the higher possibility of a catastrophic outcome (Oyelese and Smulian 2006). Studies have found a significant reduction in mortality rates when there was a planned multidisciplinary approach (Jauniaux, Chantraine et al. 2018). The need for an objective approach arises to aid in the evaluation and assessment of placental diseases thus improving maternal and fetal outcomes. Textural analysis (TA) can help measure the degree of heterogeneity of tissue by analysing the degree of grey level and pixel intensity, which in turn, may aid in PAS diagnosis. Placenta texture develops physiologically with advanced gestation. Changes in vascularisation, lobulation and deposition of fibrin are all reasons behind this (Fadl, Moshiri et al. 2017). Radiomics is a recently advanced imaging analysis technique, the benefits of which can help to localise structural changes in a specific region of interest, by tracking the pixels' distinct changes (Castellano, Bonilha et al. 2004). The first published work on texture was published by Haralick et al. in 1973 (Haralick, Shanmugam et al. 1973). The analysis techniques used are still valid and have profound evidence-based support for the currently followed texture analysis. Haralick textural features are composed of grey tone values which aim to define pictorial characteristics from a block of resolution cells in a specific image. The purpose of textural features is to describe the characteristics of resolution cells. Each image is composed of a different tone of grey levels and their spatial statistical distribution can be examined using textural analysis (TA). Both texture and tone have been described as characteristics of gry level resolution of an image. According to Haralick, there is a paradoxical relationship of texture and tone, i.e., when there is less variation in grey levels, the tone will be dominant, and vice versa when the grey level variations is wide the texture characteristics will be dominant. Each single texture feature describes the relation of

grey-level resolution cells within a spatial matrix. Since almost 50 years ago, 28 textural features have been described such as contrast, coarseness, and entropy (Haralick, Shanmugam et al. 1973).

Magnetic resonance imaging (MRI) offers advanced tissue visualisation to help distinguish diseased and normal tissue structures. MRI can detect PAS with a diagnostic accuracy of 92% (Valentini, Gui et al. 2017, Maurea, Romeo et al. 2018) but sometimes there is a need for expertise (Siauve 2019). Some tissue changes cannot be picked by the human eye which has been a serious issue for changes in metastatic brain tumours and necrosis that alters the plan of the treatment (Larroza 2016). Histopathology is the only available procedure that gives a definitive diagnosis, but it is late for the prevention of life-threatening delivery complications.

Therefore, the need for a quantitative machine-based analysis has emerged. Utilizing MRI conventional sequences and the use of computer software may help to predict advanced texture assessment (TA) (Castellano, Bonilha et al. 2004). Texture analysis can help in measuring the degree of heterogeneity of specific tissue by analysing the degree of grey level and pixel intensity and that may aid in PAS diagnosis. Different forms were reported to measure TA, first-order statistics such as histogram and second-order statistics such as grey level cooccurrence matrix (GLCM) which evaluate the spatial resolution of tissue intensity at a certain value of grey level (Lubner, Smith et al. 2017).

Rational

The need for an objective approach to assessing MR images and the high professional expertise to detect placental invasion necessitates the use of machine learning applications for TA (Romeo and Maurea 2020).

Objective

To give an overview of the available knowledge about placental texture measurement and evaluate their diagnostic accuracy.

Detection of PAS

MRI has been used to assess placental invasion, especially in cases of inconclusive ultrasound and inaccessible placental locations such as posterior and laterally located placentas. MRI specialists depend on specific signs to evaluate the degree of invasion (Elsayes, Trout et al. 2009). There is an urgent need for a quantitative diagnostic tool, which can aid in confirming the diagnosis.

The diagnostic performance of radiomics to assess the placenta images qualitatively has been proposed in a few studies (Chen, Mar et al. 2019, Do, Lewis et al. 2019, Romeo, Ricciardi et al. 2019, Sun, Qu et al. 2019, Do, Lewis et al. 2020). Analysis of placental texture has been found to give statistical differences between normal and abnormal placentas (Chen, Mar et al. 2019). The degree of invasion is another aspect to consider, as the higher the degree of invasion the higher the possibility of a catastrophic outcome (Do, Lewis et al. 2020).

There have been trials conducted to evaluate the texture of hypothesized abnormal placental areas such as those over caesarean section scars. Results show a significant difference from those of non-scar tissues as there were 22 out of 39 significant differences between normal and invaded cases(Do, Lewis et al. 2020). High-level statistics such as grey level cooccurrence matrix were linked to the degree of placenta heterogeneity and ageing (Romeo, Ricciardi et al. 2019). Textural features can be used to describe the characterisation of grey levels in a specific region of interest, for example, the entropy feature evaluates the degree of randomness of a specific area in a spatial matrix. Textural methods analysis of placental invasion has been reported to be effective in several research papers; however, the diagnosis accuracy was inconsistent. It was as high as 98.1 % (Romeo, Ricciardi et al. 2019), 96% (Sun, Qu et al. 2019) and as low as 80% (Do, Lewis et al. 2020).

Methods of textual analysis (TA)

With the introduction of machine learning and algorithms, several software programs are now freely available to conduct texture analysis. The software used by the reviewed papers was heterogenous, such as pyradiomics (Romeo, Ricciardi et al. 2019) and customised Mat-Lab (Chen, Mar et al. 2019). IT-Ksnap was used by Sun et al. to perform an automatic machine learning segmentation and create 3D images. Images then undergo normalization, and discretisation through the implementation of

a fixed bin size of 5 and correction of the gestational ages effect (Sun, Qu et al. 2019). Do, Q. N. et al. in their first published paper, Haralick textural features were used to assess placental heterogeneity and textural changes throughout gestation. They also obtained ADC values and their correlation with gestation (Do, Lewis et al. 2019). Later, they conducted another study where 13 textural features were generated using software (OsiriX, pyOsiriX, Mahotas). These were counted from GLCM after intensity normalisation and histogram equalization (Do, Lewis et al. 2020). Image segmentation was performed using Python software.

Segmentation process

The site, dimensions and the number of segmented regions can affect the results of TA and yield differences in the reported results. The region of interest was either the whole placenta or a small area. Sun et al. used automated machine learning performed through It-Ksnap software to segment the whole placenta. Do Q. N. et al. included the entire placenta in the segmentation (Do, Lewis et al. 2019). While in their second study, another approach was used, where they drew 4 ROIs, two above the CS scar and two below (Do, Lewis et al. 2020). Chen et al. placental segmentation was performed manually, and the ROI included the whole placenta. Romeo et al. drew multiple regions, around 3 in each patient, rounded in shape, 13 pixels each located in the posterior 1/3 of the bladder's superior surface (Romeo, Ricciardi et al. 2019).

Reporting texture features

Results reporting texture cover a wide range of statistical analyses where first and second-order statistics had been used. Histograms can describe the standard distribution of first-order statistics and give an idea about the overall texture. In the context of placental texture, a wider distribution histogram reflects a heterogenous invaded placenta (Chen, Mar et al. 2019). Fractal dimension and standard deviation of pixel/signal intensity were higher in cases with PAS than in normal (Chen, Mar et al. 2019).

Chen et al. reported texture in form of histograms, coefficient of variation, grey-level cooccurrence matrix (GLCM) and fractal dimension of box sizes from 2 to 512 to report tissue texture. These represent the mathematical measurements of structure dimensions that can be reported in algorithms and box-counting methods. According

to their study, GLCM, histogram-oriented gradients (HOG) and coefficient of variation had a non-significant correlation with PAS (Chen, Mar et al. 2019). Histograms and standard deviations were analysed. Interestingly, cases with PAS were presented with a wide distribution of pixel intensity which reflected a more heterogenous structure, while a more homogenous histogram was in the normal group. Standard deviation outputs were also higher in the abnormal group. Textural features were able to differentiate the severity of PAS that requires hysterectomy versus the ones that do not. 13 second-order textural features were assessed in three MRI sequences. 22 features out of 39 were significantly different in those who required hysterectomy (Do, Lewis et al. 2020). Second-order statistics were also found to be significantly correlated with gestational age. Out of 13 Haralick features, five were significant (Do, Lewis et al. 2019). Machine learning models were used to analyse placental texture; the optimal model was the gradient-boosting classifier with 584 features. 10 features were significantly different in invasive placentas with high sensitivity and specificity(Sun, Qu et al. 2019). Romeo et al. study reported first, second and high-order statistics which were processed in special machine learning models to test their link to PAS. K- nearest neighbour was the best model tested with the highest accuracy. In that model, 26 textural features were significantly different in PAS (Linduska, Dekan et al. 2009).

How placenta texture across GA could change

The placenta structure changes with the growing fetus as the vessels and trophoblast undergo maturation (Linduska, Dekan et al. 2009). The effect of gestational age due to the growing placenta and lobulation changes texture. Several statistical models have been applied to exclude the effect of GA in a way to have a solid textural level related to normal and abnormal invasion (Do, Lewis et al. 2019, Sun, Qu et al. 2019, Do, Lewis et al. 2020). Placental images of T1 and T2 images across different gestational ages had 5 out of 13 textural features which were correlated with the gestational age (Do, Lewis et al. 2019). In a following study conducted by the same group, multiple linear regression and subgroup analysis were implemented to evaluate the effect of GA on the placental texture (Chen, Mar et al. 2019). Gestational age had no effect on textural results. In two groups of TA, stratified analysis was conducted where cases were classified according to their trimester and the results of the

difference between invasion versus normal along with gestational age were compared with the overall group. Multiple linear regression was applied to evaluate the significant changes caused by gestation on texture then a next step to remove the effect of gestation on texture was performed (Sun, Qu et al. 2019).

Materials and Methods

The review was conducted in January 2021, the keywords used were (MRI), (Placenta accreta spectrum) and (texture). PubMed, web of science and google scholar were searched.

Inclusion criteria was original articles in the English language. Reviews, editorials, and case-control studies were eliminated. Following the search process, all the resulting studies were imported into Covidence. Duplicates were removed automatically by Covidence. In the search process, two independent reviewers (HA and Supervisor) screened the studies using the online Covidence site. Four stages were addressed in the Prisma diagram (Fig.8).

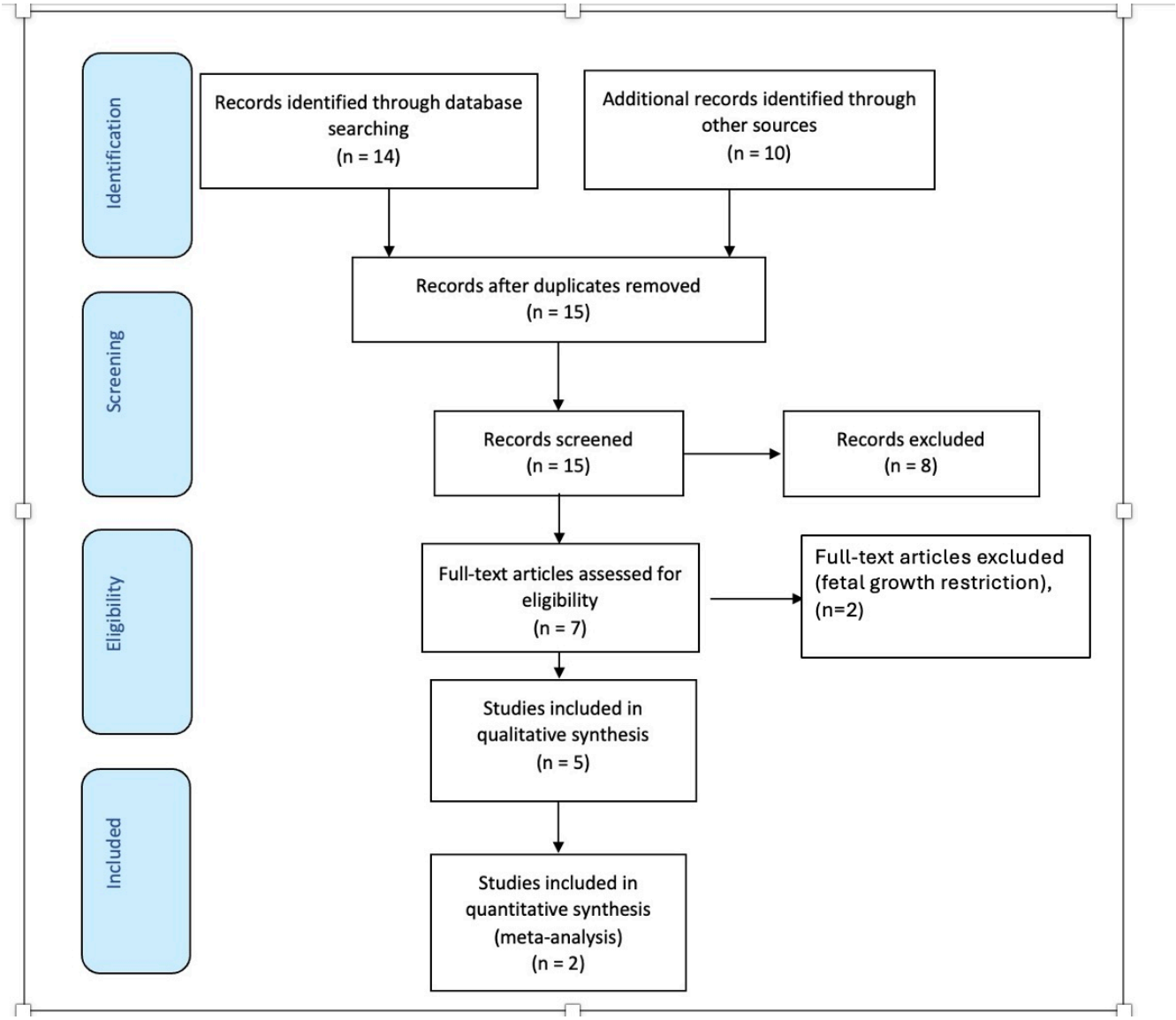

Figure 8 Prisma flow diagram of placental texture.

Study Id	Reviewer	Bias arising in the randomization process or due to confounding	Bias in selecting participants into the study	Bias in classifying interventions for All outcomes	Bias due to departures from intended interventions for All outcomes	Bias due to deviations from intended interventions for All outcomes	Bias from missing data for All outcomes	Bias in measurement of outcomes	Bias in selection of the reported result	Bias in reporting outcomes selectively
		Judgement	Judgement	Judgement	Judgement	Judgement	Judgement	Judgement	Judgement	Judgement
Do 2019	1	low	low	low	low	low	low	low	low	low
Do 2019	2	low	unclear	low	low	low	low	low	low	low
Do 2019	Consensus	low	low	low	low	low	low	low	low	low
Sun 2019	1	low	low	low	low	low	low	low	low	low
Sun 2019	2	low	low	low	low	low	low	high	low	high
Sun 2019	Consensus	low	low	low	low	low	low	high	low	high
Romeo 2019	1	low	low	low	low	low	low	low	low	low
Romeo 2019	2	unclear	low	low	low	low	high	low	low	low
Romeo 2019	Consensus	low	low	low	low	low	low	low	low	low
Chen 2019	1	low	low	low		low	low	low	low	low
Chen 2019	2	low	unclear	low		low	low	low	low	low
Chen 2019	Consensus	low	low	low		low	low	low	low	low
Do 2020	1	low	low	low	low	low	low	low	low	low
Do 2020	2	low	low	low	low	low	low	low	low	low
Do 2020	Consensus	low	low	low	low	low	low	low	low	low

Table 1 Quality assessment of the included studies according to Cochrane quality assessment tool.

General characteristics

All the included studies were of retrospective cohorts, and the total number of populations was 405. The cohorts scanning timeline ranged from (5-10 years) in each single institution. Interestingly, all the published research work was in 2019. The research groups' settings are mainly based in the USA, China, and Italy.

The eligibility criteria in each paper were women at higher risk of developing PAS, history of placenta previa was the major risk factor which is detected during routine ultrasound assessment in the second trimester. The reviewed scanning time was mainly during the late second and third trimesters. The reference standard for PAS diagnosis was histopathology samples, which was provided in all the studies except

in one (Do, Lewis et al. 2019) in which they used intraoperative signs of PAS as their reference.

Quality assessment

The risk of bias was conducted using pre-designed forms for non-randomised studies available in Covidence. It was mainly performed according to three main domains: selection of studies, interventions exposure and outcomes measurements and reporting. Assessment criteria are addressed in the following list:

• Bias arising in the randomization process or due to confounding factors
• Bias in selection of participants into the study
• Bias in classification of interventions for all outcomes
• Bias due to departures from intended interventions for all outcomes
• Bias due to deviations from intended interventions for all outcomes
• Bias due to missing data for all outcomes
• Bias in measurement of outcomes
• Bias in reporting outcomes selectively
• Bias in selection of the reported result

Studies were rated as either low, unclear, or high risk of bias. Inconsistencies were discussed among the reviewers (table 1).

Meta-analysis

We conducted a diagnostic test accuracy review (DTA) to evaluate the methods currently used for textural analysis. To answer the question of whether MRI textural analysis is effective in PAS diagnosis or not. Three papers reported outcome measures for DTA i.e., sensitivity, specificity, accuracy, and AUC (Do, Lewis et al. 2020) (Romeo, Ricciardi et al. 2019) (Sun, Qu et al. 2019). The included studies and the number of patients are described in table 3.

Revman version 5.4 software was used. The data was exported from Covidence to Revman. To create a two-by-two table, the authors were contacted to inquire about missing data. Romeo provided the results, Quyen Do, claimed using receiver operating characteristics to conclude data could manipulate the accuracy of the results if there is not enough knowledge regarding patient management and outcome. We did not use an optimal cut-off to derive the sensitivity and specificity so decided to exclude it from the meta-analysis. Therefore, data entry of texture diagnosis was for two studies only. Other review studies were described narratively to give a summary of the updated measures of placental texture.

MedCal version 19.8 was used to create a meta-analysis of the area under the ROC curve. AUC values and the standard error calculated from the paper were entered to generate ROC summary, forest, and funnel plots (table 4, Fig. 9a and b).

Results

Fifteen research papers were identified, of which eight irrelevant studies were excluded in the title screening phase. In the abstract reading stage, two studies of intrauterine growth abnormalities were excluded. The full-text review was conducted on a total of five studies. Data extraction was performed by the two reviewers using Covidence forms, consensus was reached for inconsistency following meeting and discussion.

Results synthesis

Data were extracted by the two reviewers (table 2).

Authors name	Year	Country	Setting	Institution	Design	Sample size	Maternal age	Inclusion criteria	Exclusion criteria	GA	Group differences	Histology specimens
Quyen N. Do et al.	2019	USA	Single Institution	Department of Radiology, UT Southwestern Medical Center, Dallas, Texas, USA	Retrospective cohort study	62	PAD cases : 33± 5.8 years Control cases : 33± 5 years	MRI for risk of PAD	none	hysterectomy cases: 32± 3.3 weeks non hysterectomy cases: 32 ± 3.1 weeks.	Two subgroups: Hysterectomy group : 40 Non hysterectomy group: 22 (9 accreta, 16 increta, 9 percreta).	histopathology diagnosis was provided. 85% of cases has an evidence confirming the invasion(34 of 40 cases) (6 cases missed due to either poor quality report or non available pathology analysis).
Quyen N. Do and TWICKLER Diane	2019	USA	Single institution	Department of Radiology, UT South western Medical center, Dallas,Texas, United States of America	Retrospective cohort study	44	none	singleton pregnancy, normal or mild ventriculomegaly MR finding, MR acquisitions included T2W, T1W, DWI, and ADC with substantial inclusion of the placenta in the imaging field of view.	Studies with extreme fetal movements resulting in MR artifacts were excluded from the dataset	Gestational age ranged from 23 to 36 weeks	25 cases determined to be normal and 19 cases with mild central nervous system (CNS) ventriculomegaly based on MR findings.	No histopathology confirmation
Eric Chen et al	2019	USA	Single Institution	Department of Radiology, University of Illinois at Chicago	Retrospective cohort study	80	aged 21-45 (mean±S.D., 35.1±5.1)	pregnant females at risk of PAD	none	gestational ages ranged from 14 to 41 weeks (mean 28.8±5.8). The majority of patients had an MRI scan during the early third trimester from 29 to 35 weeks (45 patients) or late second trimester from 21 to 28 weeks (21 patients). Only six patients had an MRI scan from 36 to 41 weeks, and 11 patients were scanned at 14 to 20 weeks gestational age	34 normal cases and 46 with abnormal invaded placentas	Histopathology diagnosis used as the referance standard
Valeria Romeo et al	2019	Italy	Single Institution	Department of Advanced Biomedical Sciences, University of Naples Federico II, Naples, Italy.	Retrospective cohort study	64	mean age of (34.4± 4.9 years)	> 18 year old patients with placenta previa who performed an MRI examination and for whom a histological report was available.	incomplete MRI examinations due to patient claustrophobia and MRI images significantly affected by fetal/mother movements	mean GA (34.6± 2.3 weeks)	64 patients with placenta previa and suspicion of PAS. 20 cases positive for PAS (12 placenta acreta, 7 placenta increta and 1 placenta percreta). 44 negative for PAS.	Histology was used as the reference
Sun and Qu first authors, Zhou last author	2019	China	Single institution	Hospital of Sichuan, Sichuan, China	Retrospective cohort study	155	The mean age for the Placenta invasion group (30.86 ± 3.49 years, range from 21 to 38) was significantly higher than the simple placenta previa group (28.84 ± 3.34 years, range from 19 to 35).	Women with suspected abnormal placentation due to the presence of placenta previa on routine second trimester, ultrasound examinations were initially selected.	Multiple pregnancy , those who underwent MRI scan before 24 gestational weeks , presence of significant fetal/maternal anomalies, severe motion or other type of artifact on either imaging sequence , and deliveries performed outside of the institution (resulting in lack of final diagnosis)	Pregnancies of more than 24 weeks gestation	first group of placental invasion (PI), second group of simple placenta previa	All cases were pathologically confirmed

Table 2 General characteristics of the included studies.

Quality assessment

The risk of bias in the reviewed studies was mostly low. A consensus was made about the inconsistent evaluation. There was a high risk of bias in the measurement and reporting of the outcome in one study (Sun, 2019, table 1). The areas of bias were in measurements of outcomes as only 10 significant features were reported and bias in reporting outcomes selectively. Also, the study did not clearly state the difference between normal and abnormal placentas. In addition, the outcomes GLRLM, GLDM, GLCM and GLSZM were reported in p-values and missing data was found. Overall, the inter-rater reliability was 0.59 (Cohen's Kappa).

Heterogenous methods: Texture analysis process

The major difference in the available published studies lies in the methods. The continuous rising interest in machine learning and the availability of newly developed software programs are part of the reasons behind it. In the reviewed papers, placenta segmentation had been performed manually or using semi-automated machine learning. For example, Quyen N. Do et al. conducted a manual segmentation in their two studies (Romeo, Ricciardi et al. 2019, Sun, Qu et al. 2019). While machine learning analysis was explored by Romeo et al. (Romeo, Ricciardi et al. 2019), textural analysis through software applications such as MATLAB was used by Chen et al. (Chen, Mar et al. 2019), It-Ksnap used by Sun et al. (Sun, Qu et al. 2019).
To examine publication bias in the two studies, a funnel plot was interpreted (Fig. 9b). It showed asymmetrical plot which means that there is bias in those studies. Sun et al. study was more biased (0.96) than Romeo et al. (0.98) as shown in the plot.

Gestational age and texture

It is worth noting the effect of gestational age as a confounding factor to placental texture since placental ageing alters texture as the growing cotyledons mature and assemble into a highly organised structure (Teo, Law et al. 2009, Derman, Nikac et al. 2011, Do, Lewis et al. 2019). Quyen N. Do et al. explored the former effect in their

study using second order Haralick texture features. The texture increases with gestational age (Do, Lewis et al. 2019). Sun et al. also showed an effect of GA on non-uniformity and coarseness for which linear detrending was conveyed prior to image analysis (Siauve 2019). Others grouped images according to gestation to help eliminate the GA effect (Chen, Mar et al. 2019).

Data and analyses

Data tables by test

Study ID	TP	FP	FN	TN
Romeo 2019	77	2	1	78
Sun 2019	64	11	2	78

Table 3 Meta-analysis results: Data table

Meta-analysis: Area under ROC curve

Variable for studies	Refrence
Variable for Area under ROC curve (AUC)	AUC
Variable for Standard Error of AUC	SE

Study	ROC Area	Standard Error	95% CI	z	P	Weight (%)	
						Fixed	Random
Sun et al.	0.960	0.0178	0.925 to 0.995			29.45	29.45
Romeo et al.	0.980	0.0115	0.957 to 1.000			70.55	70.55
Total (fixed effects)	0.974	0.00966	0.955 to 0.993	100.846	<0.001	100.00	100.00
Total (random effects)	0.974	0.00966	0.955 to 0.993	100.846	<0.001	100.00	100.00

Test for heterogeneity

Q	0.8907
DF	1
Significance level	P = 0.3453
I^2 (inconsistency)	0.00%
95% CI for I^2	0.00 to 0.00

Publication bias

Egger's test	
Intercept	-3.1746
95% CI	
Significance level	P < 0.0001
Begg's test	
Kendall's Tau	-1.0000
Significance level	P = 0.3173

Table 4 Area under the curve of placental texture.

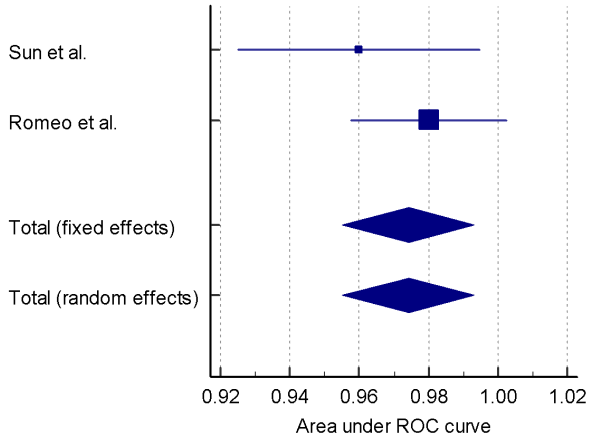

B.

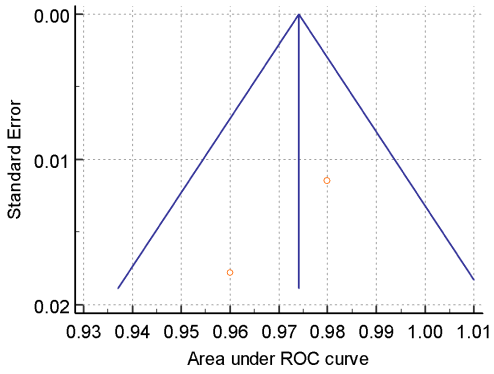

A.

Figure 9 Forest plot (a) and funnel plot (b) of placental texture meta-analysis.

Discussion

Textural analysis is useful to evaluate placental invasion. Meta-analysis showed AUC of 0.97 with P<0.001. Sun et al. and Romeo et al. studies were evaluated in depth. The qualitative and the quantitative assessments revealed bias in one or two areas and judgment has been made for the need for placental texture evaluation. The variation between the two studies can be justified for many reasons. As several MRI models were undertaken, this might be the source of heterogeneity. For example, in Sun et al. study, 14 models were concluded from a tree-based pipeline optimization tool (TPOT). Only 2 models (5 and 6) exhibited the highest diagnostic accuracy (Romeo, Ricciardi et al. 2019). The second reason is the difference in the threshold where different studies used different models, algorithms, and machine learning programs. This has put a difference in what is regarded as abnormal versus normal texture.

Manual (Do, Lewis et al. 2020) and automatic placenta segmentation (Chen, Mar et al. 2019, Do, Lewis et al. 2019, Romeo, Ricciardi et al. 2019, Sun, Qu et al. 2019) were used in the studies. The third reason for heterogeneity is the small population size (n=141), which can reflect a higher chance of variability.

Histogram analysis was assessed by Chen et al., and interestingly, abnormal placentas expressed higher values than normal (Mean of 350 vs 150 respectively),

and a higher SD of pixel intensity in the abnormal group (3.7 versus 2.5 for normal placenta)(Chen, Mar et al. 2019). Inconsistency in methodologies to measure TA, and the wide availability of software programs which aided in machine learning and artificial intelligence made it harder to gather the available data into one meta-analysis. There is a need to apply machine learning for placenta textural assessment.

Overall, there is sufficient evidence to suggest that textural analysis may be able to aid the diagnosis of placental accreta spectrum but insufficient evidence to suggest that it can aid the diagnosis of the difference degrees of placenta accreta spectrum. Further work on larger data sets, accounting for gestational age effects and with detailed pathological correlation is required.

1.3
Assessing the diagnostic accuracy of the two main MRI signs of invasion and comparison with ADC and texture analysis to detect PAS

Abstract

Background

Diagnosis of placenta accreta spectrum (PAS) comprises a challenge in clinical practice. Identification of magnetic resonance (MRI) invasion signs requires specialized/high experience. It is important to determine the degree of invasion since the deeper the invasion is, the higher possibility of a catastrophic outcome (Do, Lewis et al. 2020). Studies have found a significant reduction in mortality rates when there was a planned multidisciplinary approach. The need for an objective approach arises to aid in the evaluation and assessment of placental diseases thus improving maternal and fetal outcomes. Diffusion and textural analysis have shown a correlation with some types of breast and brain tumours (Sarioglu, Sarioglu et al. 2020). Textural analysis (TA) can help measure the degree of heterogeneity of tissue by analysing the degree of grey level and pixel intensity, which in turn, may aid in PAS diagnosis. The aim of this study was to apply ADC and TA on PAS images to assess their potential to help aid diagnosis.

Method

A retrospective review of 127 cases. ADC values were obtained from the area above the bladder and the entire placenta on a midline sagittal image by 2 readers (HA and Supervisor). Heterogeneity of the placenta and placental dark bands were also noted. Pathological diagnosis was obtained from medical records. Three subgroups (normal, accreta/increta and percreta) were identified.

For placental texture, a retrospective review of 44 MR images was performed. Texture was analysed using radiomics program (LIFEx). Placentas were manually segmented to obtain two 3D areas, where the entire placenta area and a small caesarean scar area were analysed. A total of 104 textural features were extracted which were then analysed among PAS groups.

Results

- ADC values were higher in invaded placentas than normal. ADC of total placental area and CS area showed non-significant difference among normal and invaded placentas.

- Heterogeneity and dark bands were significantly different in normal and invaded placentas.
- There was a significant difference of texture values between normal and invaded placentas. Placental texture was proportional to the degree of placenta heterogeneity.
- ROC curve for texture of local placenta area gave a significant difference between normal and invaded groups. linear regression of texture showed a significant difference between the texture of accreta, percreta and normal groups.
- Results of high-order statistics analysis showed that out of 104 variable outcomes, 47 variables for global placental texture and 43 for local CS area showed a significant difference between normal and abnormal placentas.

Conclusion

Combining objective and subjective approaches may help differentiate between the suspicious and actual cases of PAS. Heterogeneity and dark bands did not have a diagnostic accuracy of PAS of 100% but ADC values did not aid in the diagnosis or determining the severity of PAS and whilst textural features showed a trend among placenta subgroups with significant differences between normal and invaded groups the diagnostic accuracy was not good. Further research is needed.

Introduction

The study highlights the potential possible value of the techniques in the diagnosis of PAS. As documented in the previous systematic review and meta-analysis, there is increasing interest in textural analysis to aid the diagnosis and extent of PAS. ADC biomarkers are also potentially useful. During the COVID pandemic lockdown the following study was conducted to look at the value of ADC and textural analysis in the diagnosis of PAS.

The reason for investigation of the data was that previous small studies had suggested that both ADC and texture could potentially aid in the diagnosis of PAS. The systematic review and meta-analysis presented above also showed a potential role for using textural analysis to aid the diagnosis and different degrees of PAS. The ADC value reflects the blood flow and composition of the placenta and it is known that placenta accreta spectrum is associated with abnormal blood vessels and fibrin deposits so the ADC valued is very likely to be different between normal placentas and cases of PAS.

In addition, the heterogeneity used as a sign of PAS on the MRI images and thought to reflect the multiple lacunae seen on the ultrasound images in cases of PAS should therefore be reflected in increased texture on textural analysis and the normal homogeneous placenta will have much less variation on textural analysis.
The systematic review on texture studied both the whole placenta and regions of interest. As on MRI the features are not specific to the basal layer of the placenta but more full thickness it was decided to look at the whole placenta and a region of interest at the previous caesarean section scar site.

The usefulness of heterogeneity, dark bands and ADC value for the diagnosis and extent of PAS on MRI.

Hypothesis

1. The 2 main diagnostic features of PAS on MRI, heterogeneity and dark bands, accurately predict PAS and its severity.
2. The ADC value will also predict the degree of invasion.

Null Hypothesis: The ADC value will not predict the degree of invasion.

Different forms of invasion may coexist in the same placenta, and they may also change with advanced gestation. It is still challenging to set specific diagnostic criteria to assess the depth of invasion on ultrasound. Accurate diagnosis is critical for adequate clinical therapy and patient counselling and is mandatory to avoid the dangerous complications of this condition. As a result, defining MRI diagnostic criteria is essential for the best use of this technique. Lax et al. have examined the utilization of MRI features in the diagnosis of PAS but they failed to examine the subgroups of placental invasion, i.e. subjects who had placenta accreta, placenta increta, and placenta percreta (Lax, Prince et al. 2007). MRI has been reported as a useful technique to assess the depth of placental invasion, especially when the ultrasound diagnosis is not clear or doubtful (Derman, Nikac et al. 2011, Elhawary, Dabees et al. 2013). Ultrasound-reported sensitivity and specificity in the diagnosis of PAS are 77–93% and 71–95%, respectively (Elsayes, Trout et al. 2009). Whereas MRI has a sensitivity of 75–100% and a specificity of 65–100% (Rahaim and Whitby 2015). These techniques should be used together when high risk cases are presented with inconclusive findings (Cuthbert, Teixidor Vinas et al. 2016). The aim of this study is to define the diagnostic accuracy of the 2 main MRI features in cases of PAS (heterogeneity and dark bands), measure the placental ADC and correlate it with the conventional MRI markers and outcome measures.

An already partly completed data base of 127 patients was provided for analysis. The grading of the dark bands and heterogeneity had been completed by 2 experienced senior consultant radiologists (each with over 9 years' experience of MRI of the placenta) initially independently and the final score agreed by consensus if there was any difference. The outcome data had already been collected by one of the radiologists. In addition, I undertook analysis of the individual diffusion weighted images for each case to obtain the ADC values and undertook textural analysis of a subset of cases.

Materials and methods

Participants and images acquisition

This was a retrospective study conducted on 127 pregnancies referred to Sheffield Teaching Hospital. The reason for referral was an abnormal ultrasound scan in

pregnancies with previous caesarean deliveries and a low-lying placenta. The gestational age ranged from (21- 38) weeks. Images were analysed by two experienced radiologists using the proprietary software. The definitive diagnosis of placental invasion was made based on the surgical (if the placenta was removed without any need for myomectomy or hysterectomy) or pathology results (when the placenta had required resection).
The time frame was from (Nov. 2011 to Feb. 2020), the majority of the MRI scans were performed on one of 2 Siemens 1.5T scanners (Aera and Advanto) based in Sheffield. To minimize the effect of gestational age on placental maturation, placentas were divided according to gestational age into the second and third trimesters.

The two experienced consultant radiologists who had graded the images reviewed MRI scans obtained from the hospital's electronic database. The following characteristics were provided in an incomplete dataset completed by the clinical team:
(1) normal or abnormal placenta.
(2) proposed depth of placental invasion (placenta accreta, increta, or percreta) based on MRI features within the placenta.
(3) the presence of MRI signs to diagnose PAS - heterogeneity and dark bands
(4) blood loss at delivery – a clinical marker for the degree of invasion and increased vascularity
(5) number of hospital stay days – a clinical marker for the degree of difficulty of the surgery.
None of the cases had any additional pathology, for example infarction or haematoma.

MRI images analysis

1. MRI signs of placenta invasion

Retrospective data of MRI signs of invasion were reviewed. These were analysed by the 2 experienced radiologists. They included placental heterogeneity and dark bands. Heterogeneity was assessed as the presence or absence of local or widespread irregular dark areas that appeared on T2W images. Dark bands, on the

other hand, were assessed according to irregular thick bands that arise from the placenta's maternal side. Four categories were used: none, single, <5 or >5 dark bands. These are the features used clinically by the team and were investigated for sensitivity, specificity and accuracy before they were used as a comparator for other ADC and texture.

2. DWI-ADC

As part of the imaging protocol, used in clinical practice a DWI sequence was performed. Images were obtained in sagittal and axial planes. The imaging parameters included: slice thickness of 3mm-6mm and b values of 0, 600 and 1000. Using the ADC map produced two regions of interest (ROI) defined with two circles of (1-10 cm) dimension were placed within the placenta. One ROI was global and included as much as the placenta on the slice chosen as possible. The other was a regional ROI at the site of the presumed previous lower segment C-section scar site (above the maternal bladder). Placenta accreta spectrum changes (heterogeneity and dark bands) on MRI are either local or global and include the full thickness of the placenta not just the area of attachment. ADC readings were recorded for both categories: whole placenta ROI and regional ROI (Fig. 10).

Statistical analysis

Data were analysed using IBM SPSS Version 27. The results of ADC in the two ROIs were compared with the presence or absence of placental heterogeneity, dark bands, and histopathology. The number of hospital stay days was also compared with them. This was taken as a degree of severity of the condition as the more severe the condition the more complicated the delivery, the more likely there are to be complications and the larger the impact on the patient. It would be beneficial to the clinicians to know if the imaging features could predict the likely length of stay too.

In order to test the normality of the data, Q-Q plots and histograms were used. Subgroups of accreta, increta and percreta were compared with the two ADC groups (ADC-whole placenta and ADC CS area). As the number of increta group was small we combined increta and accreta into one group. (These are both treated as a potential increta in the clinical setting whilst the percreta cases require significantly more

resources for safe delivery and the MRI imaging features are also similar whilst those of percreta are more extensive). The number of cases per subgroup for normal, accreta and percreta were 77, 28 and 22 respectively.

Heterogeneity and dark bands

Normal and invaded cases were compared to check the correlation between heterogeneity and placenta pathology, Pearson correlation was applied. The same test was also applied to test dark bands and placenta pathology. Placenta accreta spectrum correlation with MRI signs, we performed an ANOVA test.

The area under the curve was then tested for each sign. AUC and sensitivity of heterogeneity and dark bands were calculated for the diagnosis of PAS. Then, heterogeneity and dark bands were combined to predict the validity of diagnosing PAS, and sensitivity and area under the curve were calculated.

ADC and GA

To demonstrate the relationship between ADC values and placenta growth, ADC values were tested across gestational age.

ADC in normal and invaded placentas

Placentas of normal and PAS cases were compared.

In case of whole placenta ADC and placenta groups, Mann Whitney U test was used to compare the means of 2 groups. While for regional ADC and placenta groups, independent t test was applied as the distribution of data was normal.

ADC in placenta subgroups

Placentas of normal group were compared with subgroups of invaded ones (accreta and percreta). Comparisons were made using a univariate ANOVA test.

ADC and MRI signs of PAS

We assessed the 2 main features used for the diagnosis of PAS which are heterogeneity and dark bands and compared these to new features - ADC values to see if they could be used as biomarkers for diagnosis of PAS.

ADC and heterogeneity

Logistic regression was used to test the correlation between whole placenta ADC of 3 subgroups (normal, accreta and percreta) and heterogeneity. Kruskal Wallis test was used to test the correlation of ADC (of normal and invaded groups) and heterogeneity. For regional ADC and heterogeneity, ANOVA test was applied.

ADC and dark bands

In the case of dark bands and whole placenta ADC, the data were not normally distributed, so the Independent-Samples Kruskal-Wallis test was used. While for regional ADC and dark bands, Anova test was used.
To assess the specific features against outcome, the following were used:

Number of hospital stay days

Independent tests were applied to test the correlation of hospital stays with dark bands and heterogeneity. Nonparametric independent Kruskal Wallis test was applied. The degree of placental invasion was correlated with the number of hospital stay days to look at their correlation. Hospital stay was compared with ADC and texture of the placental areas to look for the association.

Blood loss

The amount of blood loss was compared with heterogeneity, dark bands, ADC, and texture to test the association.

Hysterectomy

MRI signs, ADC and texture were also compared with caesarean hysterectomy.

Pathology

Pathological diagnosis was obtained from medical records. Three subgroups (Normal, accreta/increta and percreta) were identified if available. If no pathology was available (as was often the case for normal and accreta cases) then if the placenta was delivered

complete and intact and there was no mention of increased adhesiveness at surgery, it was assumed normal. If the placenta needed manual traction or was delivered incomplete with mention of increased difficulty in separation at delivery it was assumed accreta. Increta and percreta cases were all diagnosed from pathological analysis.

Reliability (intra and Inter class agreement)

To assess reliability of measurements, 2 raters independently collected data from a random selection of 64 cases. The same number were measured twice for ADC whole and regional areas. Both total and regional placental ADC were tested for inter and intra-rater agreement and potential bias. The test used for our continuous data was Bland Altman plot. An independent t-test of the mean difference around zero and linear regression to evaluate the evidence of proportional bias was also used. While intraclass agreement were tested using the reliability test.

Figure 10 Placenta ADC MRI of a sagittal section illustrates regions of interest, the whole placenta and a small region above the bladder.

Results

Not all cases were treated in Sheffield, so a definitive diagnosis was not available in 8 cases and 39 cases were excluded due to poor image quality or missing ADC

sequences leaving a total of 127 patients for analysis. 50 cases were abnormal with a placental invasion of different severities. 77 cases were normal.

Data distribution was undertaken to assess normality of data or not and select the appropriate test for the data set (see appendix).

a) MRI diagnostic features currently used clinically

113 cases were graded for heterogeneity and 112 for dark band features and compared with placenta pathology.

1. Heterogeneity

We conducted two groups of comparisons:

a. Normal and invaded placentas

There was a significant strong correlation between heterogeneity and placental pathology, (Spearman's correlation r=0.682, p=0.000) where the significance level was 0.05. The distribution of cases according to the degree of heterogeneity is shown in (Fig.11).

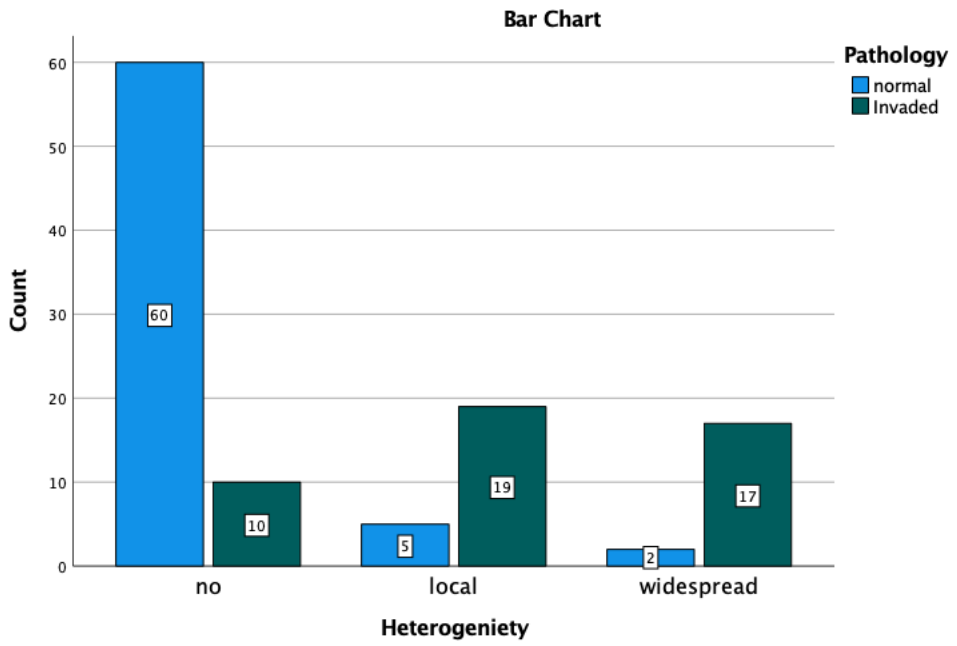

Figure 11 Bar chart shows the level of heterogeneity in normal and invaded placentas. The blue bar represents normal while green represents invaded placentas, the number of cases is labelled on each bar.

b. Normal and PAS (accreta+ increta and percreta)

Normal and 2 groups of PAS were compared with heterogeneity categories (accreta and increta were combined into one group due to small numbers of increta cases which were treated by local resection not hysterectomy, could be treated in the women's hospital and did not require an ITU bed). Normality checks and Levine's test were carried out and the assumptions were met. There was a significant relationship between heterogeneity and PAS, (Pearson's Chi-Squared test $p < 0.001$).

2. Dark bands

a. Normal and invaded placentas

Different dark band categories (none, single, <5 and >5) were compared with placenta groups (normal and invaded). A positive strong correlation was found, which was significant (Spearman correlation, r=0.69, p=0.000). The distribution of dark bands in normal and invaded placentas are described in Fig.12. The level of significance was 0.05.

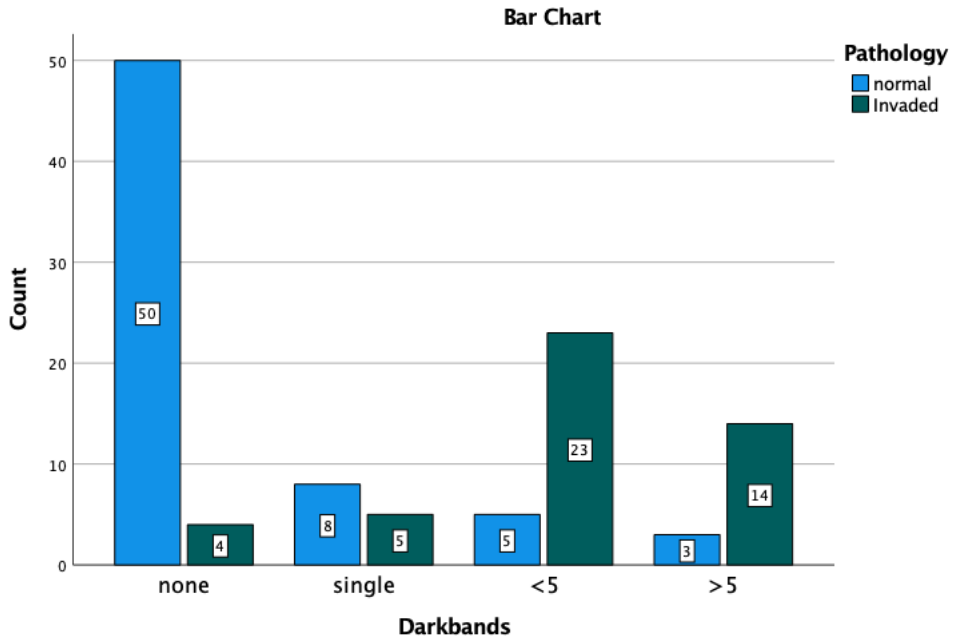

Figure 12 Cluster bar chart describes the presence of dark bands in normal and invaded placentas. The blue bar represents normal while green represents invaded placentas.

b. Normal and PAS (accreta+ increta and percreta) groups

There was significant evidence of an association between the two groups (non-parametric Spearman's correlation, $p < 0.001$).

Diagnostic accuracy of MRI signs currently used clinically for PAS

The ROC curve for both dark bands and heterogeneity was 0.84 which is an excellent test quality. Combining both signs resulted in a higher curve (AUC=0.87) (Fig.13).

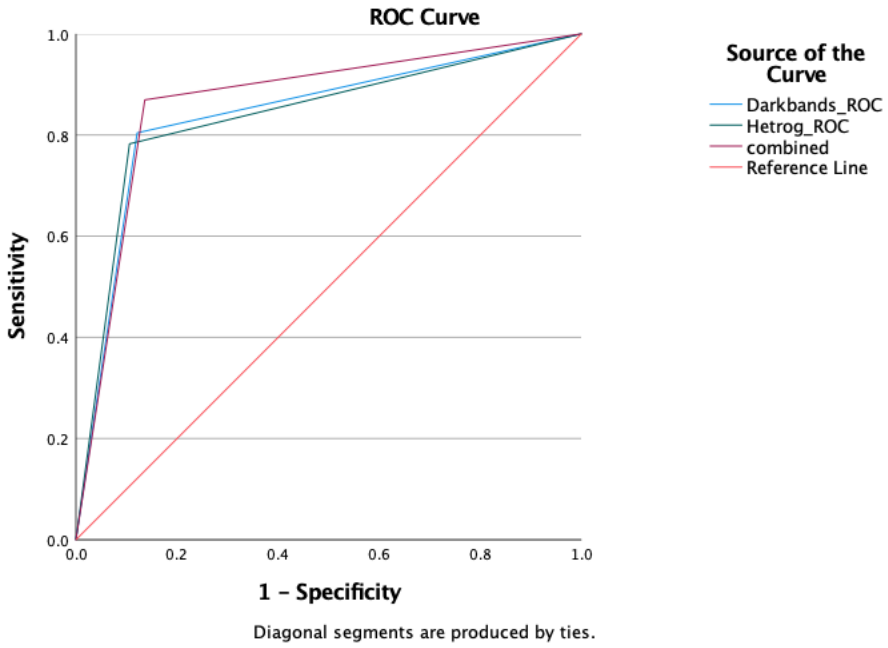

Figure 13 Receiver operator characteristic (ROC) showing the diagnostic accuracy of heterogeneity and dark bands to detect PAS.

Sensitivity, specificity, and accuracy

While the highest specificity was reported with heterogeneity (89.6%). Combining both heterogeneity and dark bands gave the highest sensitivity than of each sign alone (87%) and the highest accuracy (86.7%). Dark bands sensitivity was higher than that of heterogeneity (80.4 % vs78.3% respectively).

The above analysis demonstrates that the 2 signs relied on currently to diagnose PAS on MRI are sensitive, specific and have a high diagnostic accuracy.

Further analysis was undertaken to assess the prognostic ability re outcome measures.

Prediction of patient outcome using MRI features, number of hospital stay days, blood loss and hysterectomy

1. Hospital stay days

The duration of hospital stay was used as a marker of severity of the surgery. The longer the stay the more significant the surgery. It was assumed that the more significant surgery was the more likely to have complications and increase the length of stay too.

The duration spent in the hospital for patients with placenta accreta spectrum was compared with those with normal placentas. The average time spent for normal group was 3 days (SD= 3.158) compared to 10 days in percreta group (Fig.14 and 15).

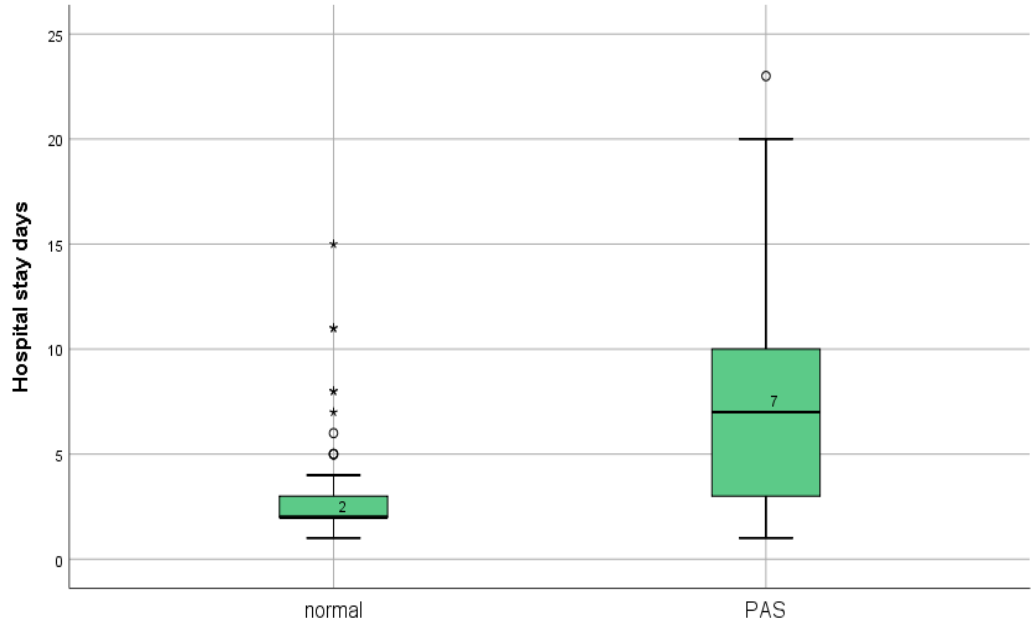

Figure 14 Box and whisker plot of hospital stay for patients with caesarean deliveries with normal and invaded placentas. The median in normal group was 2 and 7 days in PAS.

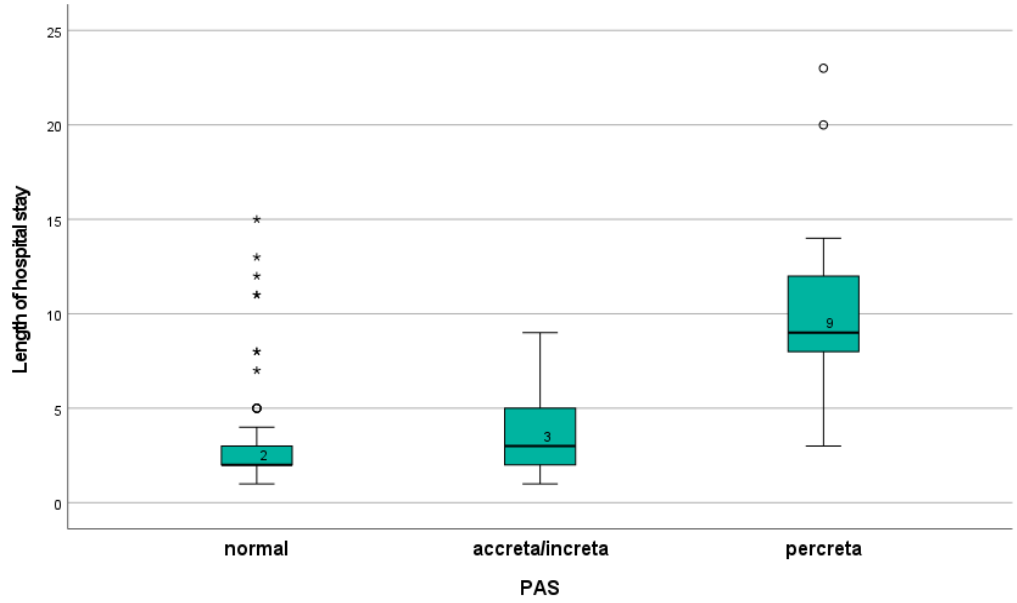

Figure 15 The length of hospital stay in normal and PAS groups. The median stay of the normal group was 2 days. In case of accreta/increta groups, the stay was 3 days compared to 9 days in percreta.

a. Duration of hospital stay and heterogeneity (normal and invaded placentas)

When heterogeneity was assessed to predict the period spent in the hospital, the median was proportional to the degree of placental invasion (Fig.16). There was evidence of a difference between the non-heterogenous and local heterogeneous groups (p=0.044, adjusted using the Bonferroni correction) and stronger evidence (p=0.00) adjusted significant difference between homogenous and those with widespread heterogeneity.

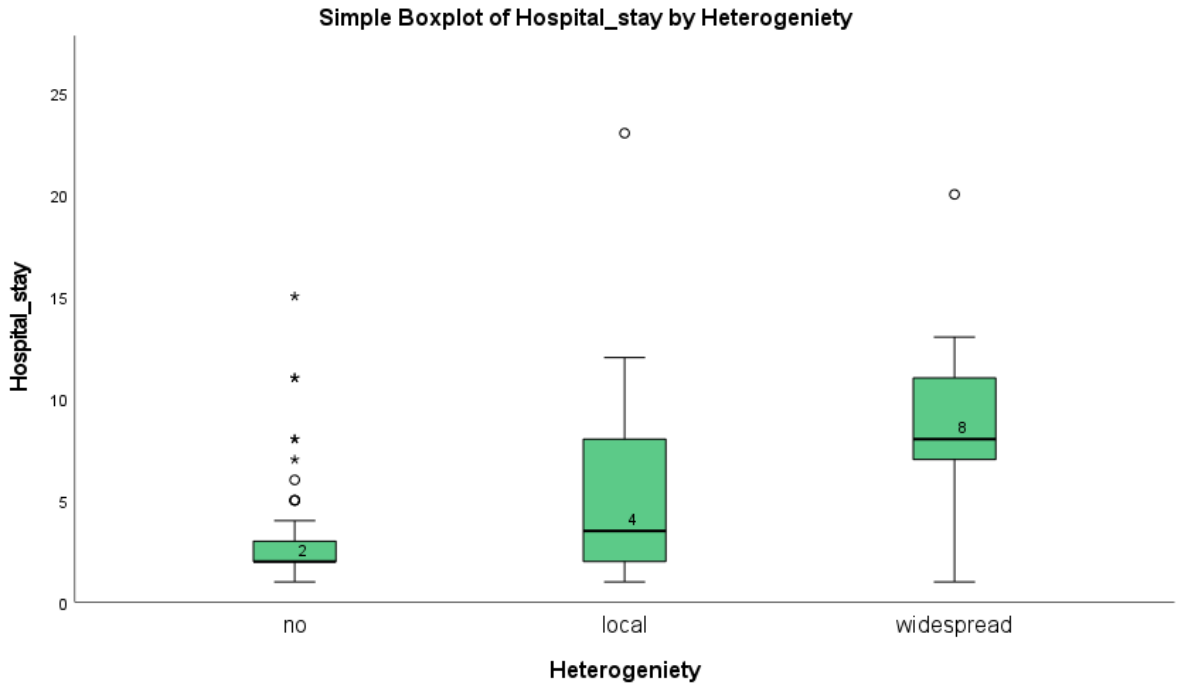

Figure 16 Hospital stay according to the degree of placental heterogeneity. Widespread heterogenous placenta is an indicator to increase the number of hospital stay days.

The median length of stay for the group having no heterogeneity was 2 days compared to 4 days in the group with local heterogeneity and 8 for the group with widespread heterogeneity. There was no significant difference for the groups of local versus widespread heterogeneity in terms of hospital stay days.

b. Duration of hospital stay and dark bands (normal and invaded placentas)

The length of stay was proportional to the presence of dark bands (Fig. 17). There was strong evidence (p=0.016, adjusted using the Bonferroni correction) of a difference between groups of none and single dark bands and stronger evidence (p=0.00) adjusted significant difference between groups with no and >5 dark bands. The median length of stay for the group having no dark bands was 2 days compared to 5 days in the group with a single band and 8 for the group with >5 bands. There was no significant difference among <5 dark bands and >5 dark bands.

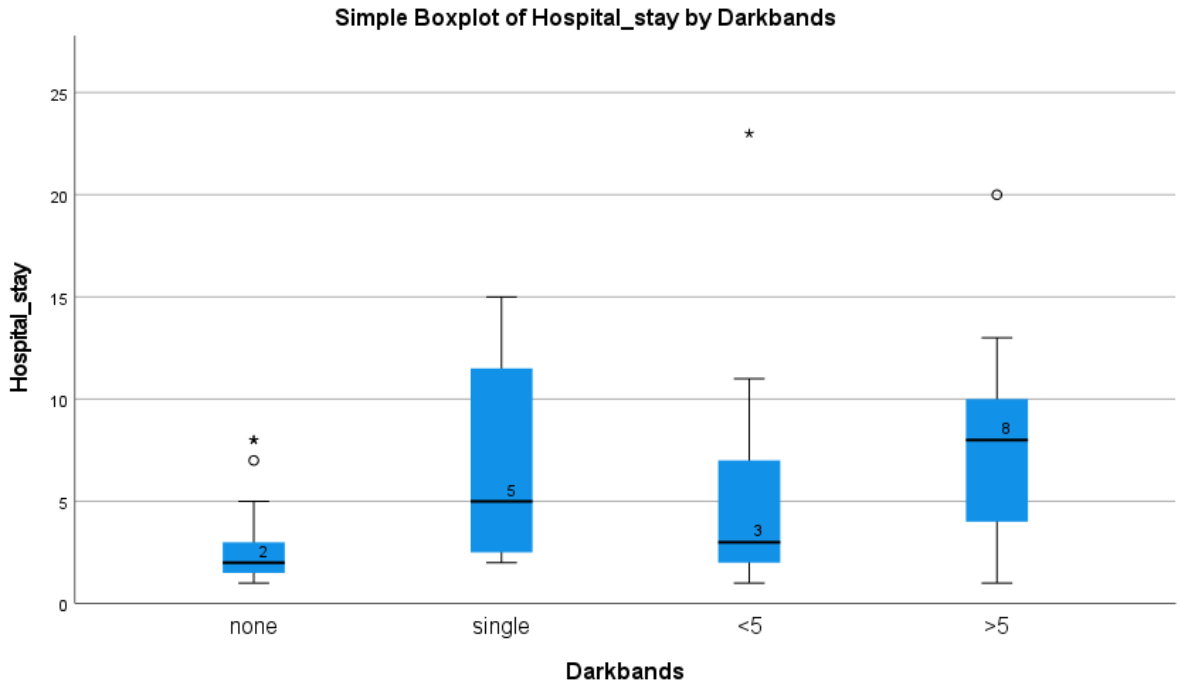

Figure 17 The length of hospital stay according to the presence of placental dark bands. As it is shown, the more the dark bands present the more days of stay.

2. Blood loss

By far the greatest amount of blood loss following management of placenta accreta spectrum was the highest when dark bands were >5 and widespread heterogeneity by reaching almost 6 litters.

a. Blood loss and heterogeneity

Assessing placenta heterogeneity may allow the prediction of blood loss. There was a significant difference between heterogeneity groups: no+ local (p=0.014), no+ widespread (p=0.00) and local+ widespread (p=0.037) (Fig. 18).

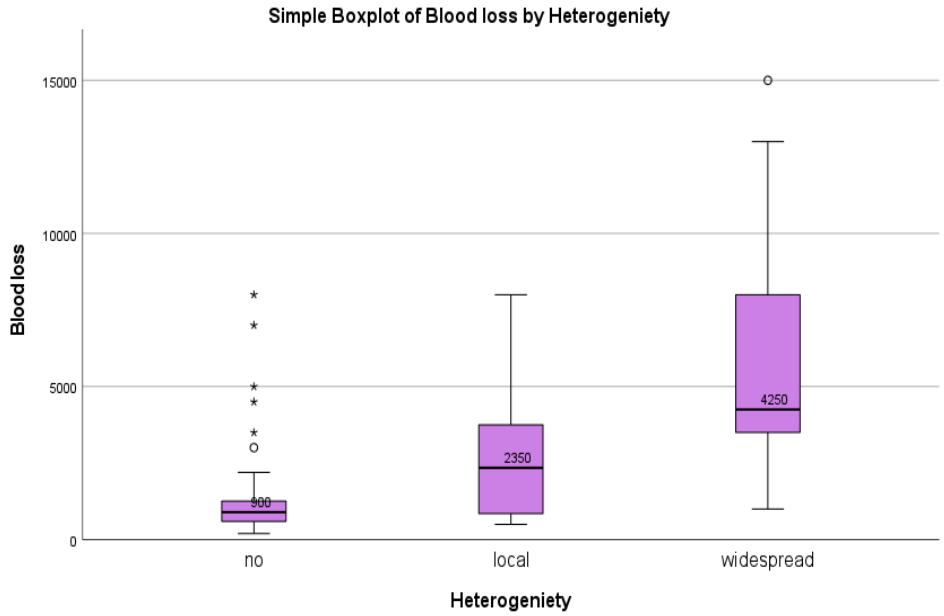

Figure 18 Boxplot of blood loss and heterogeneity. The median blood loss was proportional to the degree of heterogeneity starting from 900 mL in the non-heterogenous placenta to 4250 mL in placentas with widespread heterogeneity.

b. Blood loss and dark bands

Dark bands may also predict blood loss during a CS. 96 data complete data set were analysed. There was strong evidence of a difference between groups of none- <5 and none- >5 dark bands (adjusted using the Bonferroni correction, p=0.014, p=0.000 respectively) as shown in Fig. 19.

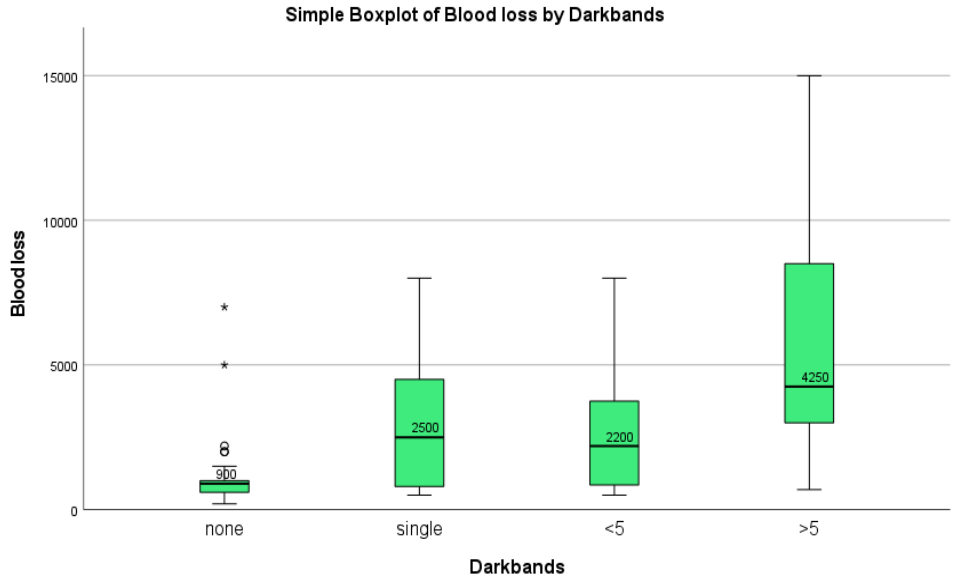

Figure 19 Boxplot of blood loss in different placentas. The amount of blood loss was different in each group of dark bands category. Placentas with >5 dark bands bled more than 4 litres at delivery.

3. Hysterectomy

Outcome results were sorted into binary data of whether there was a hysterectomy or not. This has been compared with MRI signs of heterogeneity and dark bands. There was missing outcome data of 25.9% for dark bands and 25.2% for heterogeneity.

Both heterogeneity and dark bands were independently associated with the requirements for a hysterectomy (Pearson's Chi-squared, $p < 0.001$) for heterogeneity and ($p < 0.001$) for dark bands. When hysterectomy outcomes were compared with heterogeneity. 60 cases of uneventful deliveries were in non-heterogenous placentas, and 24 cases with heterogenous placentas ended up with hysterectomy (Fig. 20). All placentas with no dark bands were delivered without hysterectomy. 3, 10, and 13 cases with single, <5 and >5 dark bands respectively had a hysterectomy (Fig. 21).

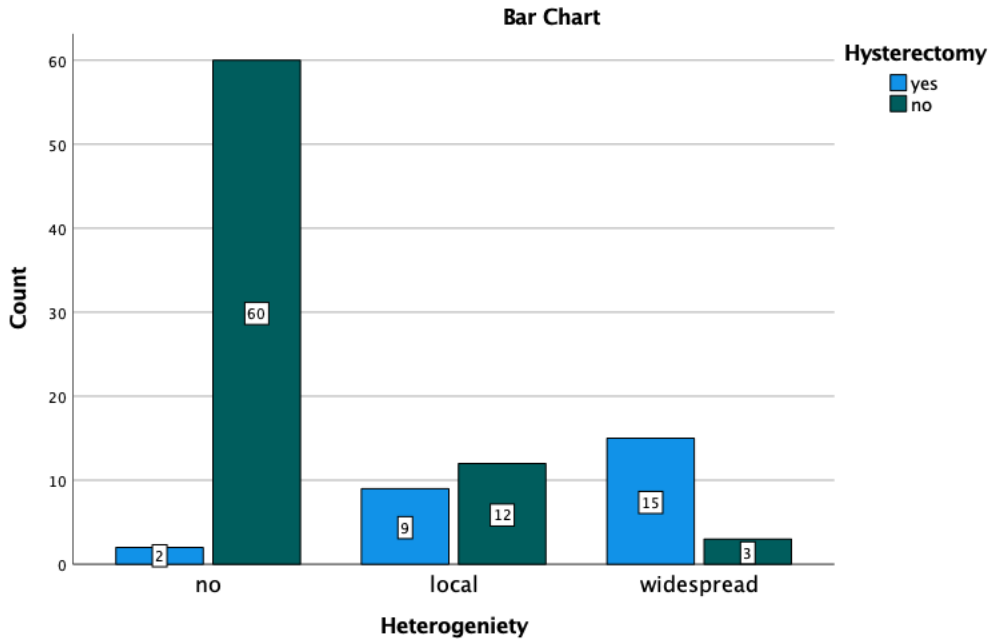

Figure 20 Bar chart of hysterectomy outcome with heterogeneity.

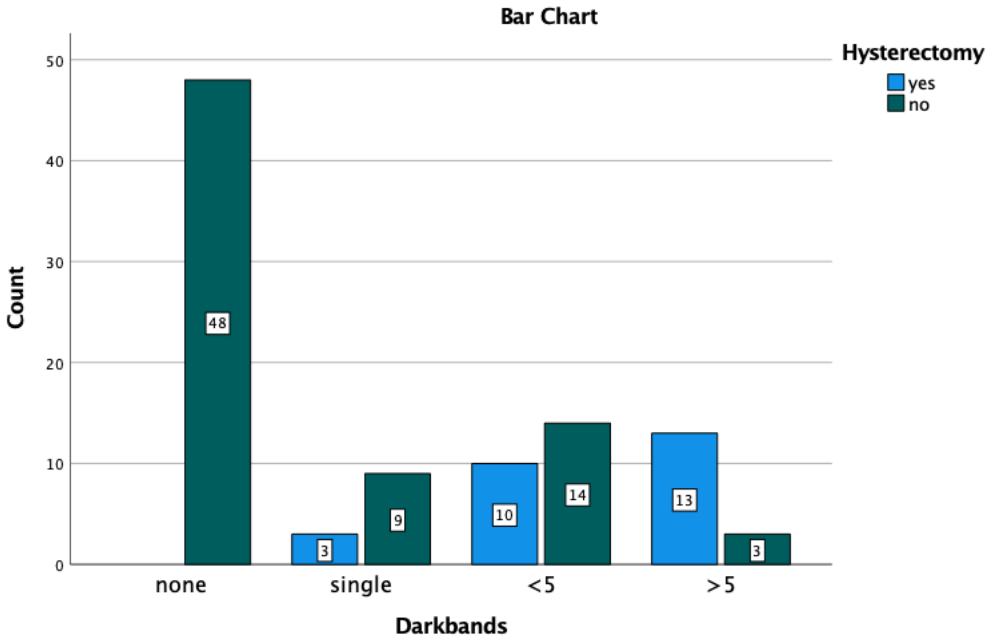

Figure 21 Bar chart of dark bands and delivery complications.

Heterogeneity and dark bands are sensitive specific and have a high diagnostic accuracy for PAS on MR images. They are also predictive of the outcome in terms of surgery most likely to be required (hysterectomy or not), and severity of the procedure measured as hospital stay and blood loss.
Having established the value of the 2 main signs use clinically in current practice the value of the ADC measurement was assessed:

MRI of the placenta and the value of ADC in diagnosis and severity of PAS:

The ADC value was measured by both myself (PhD student) and an experienced radiologist (Supervisor). Repeat measurements were taken and inter and intra observer variation calculated. All data was assessed for normality or skew to allow selection of the correct statistical tests (see appendix). ADC data were normally distributed.

b) ADC

Inter-rater agreement

64 data cases were measured by the same two investigators and checked for their agreement. Both the total and regional placental ADCs were tested for the inter-rater agreement and potential bias. The test used for continuous data was the Bland-Altman plot.
There was poor reliability between the observers for ADC values for both the whole placenta and ROI, detailed below:

Regarding total placental ADC
The first measurement (A) mean was higher than the second measurement (C) and the SD was also higher. Inter class correlation (ICC) was 0.45 and the 95% CI was (0.23-0.62, p=<0.001). In conclusion, there was poor reliability between the two observers.

Regarding regional placental ADC

The mean of the first measurement (A) was higher than the second measurement (C). Inter class correlation (ICC) was 0.46 (p=<0.001). In conclusion there was poor reliability to support the repeatability of this measurement.

Intra-class reliability

ADC whole placenta

The data of 64 cases were measured twice by the same investigator at two different occasions. The mean of the first measurement (B) was higher than the second measurement (C) and the SD was also higher. Intra-class correlation (ICC) was 0.87 and the 95% CI was (0.79-0.91, p=0.00). In conclusion there was good evidence to support the repeatability of this measurement.

ADC regional area

The evidence of reliability for 64 cases of ADC regional placenta was tested. Two measurements (B and C) were compared. The values of C were higher than B. ICC was 0.78 with 95% CI (0.67-0.86) which mean there is evidence of reproducibility.

a. ADC and gestational age (GA)

The association of ADC levels with GA was assessed using simple linear regression. A model was created relating the ADC in the whole placental region (A) and regional placenta (B) with gestational age. There was a downward trend in ADC value with increasing GA in both normal and those with PAS placentas. This was most obvious in the whole placental ADC(r=-0.09); little variation was seen in regional ADC with advancing GA (Fig. 22). The correlation was not significant (ADC whole placenta p=0.2) and regional ADC, p=0.4). The same trend was seen in both, normal and invaded groups combined (accreta, increta and percreta).

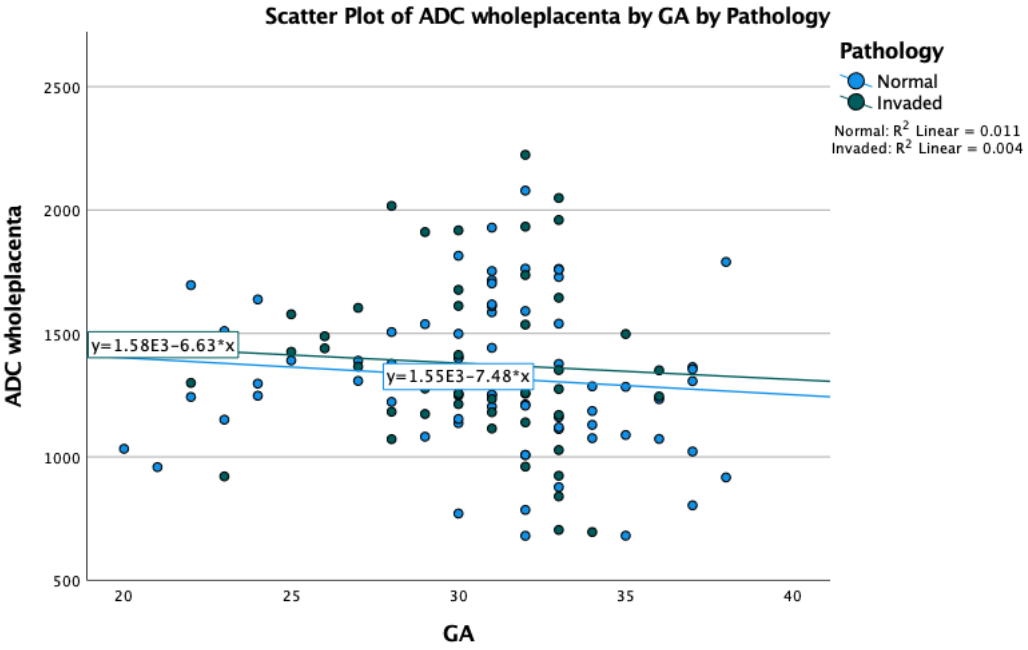

A.

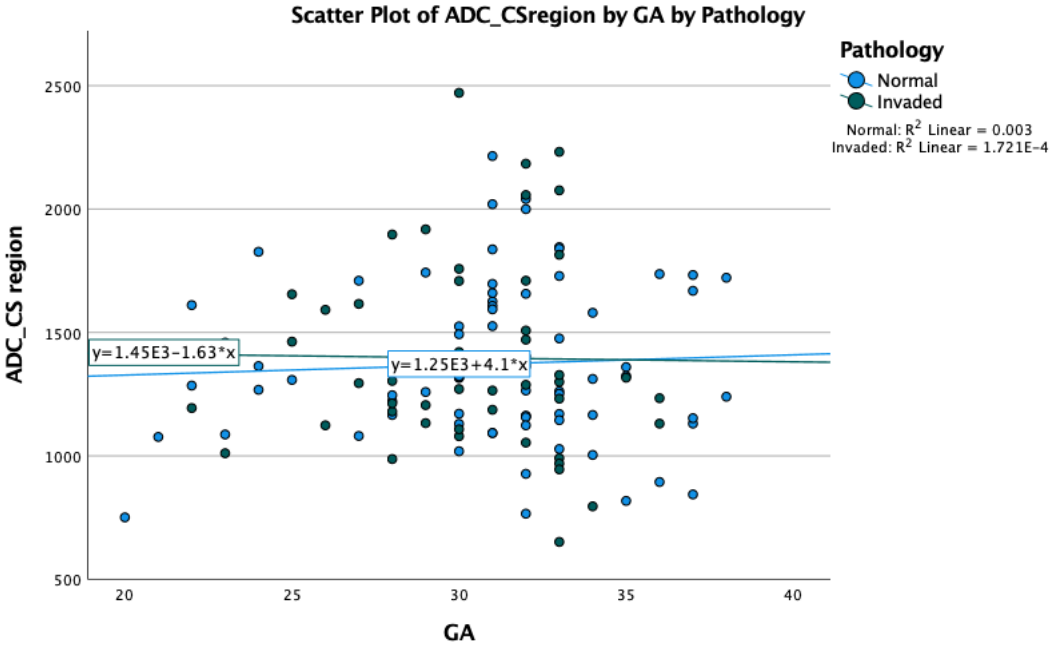

B.

Figure 22 Scatter plots showing the distribution of ADC whole placenta (A) and regional placenta (B) across gestation.

b. Duration of hospital stay and ADC

There was no significant correlation between ADC whole placenta and CS area with hospital stay (Spearman's correlation p=0.92 and p=0.67 respectively).

c. Blood loss and ADC

ADC values did not predict blood loss. The correlation was non-significant with whole placenta and regional ADC (Spearman's correlation, p=0.6 and p=0.4) respectively.

d. Hysterectomy and ADC

There was no association between ADC values either whole placenta or regional with hysterectomy (Mann- Whitney U test, p= 0.9, p=0.8).

As there was no significant correlation with GA with ADC values, we dismissed GA. ADC mean was higher in invaded placentas than in controls for both whole placental area and regional area.

e. ADC and PAS (normal, accreta, and percreta)

Sample characteristics

A sample of 135 cases was analysed. Two ADC measurements (whole placenta and regional) were compared with placenta pathology of invasion and MRI invasion signs (heterogeneity and dark bands). 8 cases were missing for ADC measurements either due to missing ADC sequences or poor quality of images. The remaining was 127 total sample size.

Control cases comprised more than half of the sample (58.8%). While PAS groups were percreta: 17% (n=23), accreta: 18.5 % (n=25), increta cases were the lowest at 2.2% (n=3).

ADC whole placenta was higher in accreta and percreta than normal. The increta group showed the lowest ADC values (median=1235 mm^2/sec). ADC ROI on the other hand showed the lowest values in accreta cases (median=1265 mm^2/sec) than in controls (median=1319 mm^2/sec). Percreta cases showed the highest values (median=1400 mm^2/sec).

ADC whole placenta and pathology

The number of cases in each group was 77 normal, 28 accreta, and 22 percreta. The mean ADC of each subgroup was 1320 mm^2/sec in normal, 1337 mm^2/sec for accreta, and 1428 mm^2/sec in percreta. This was not statistically significant (univariate analysis, p=0.4).

Regional ADC and pathology

The mean ADC of each subgroup was 1372 mm^2/sec in normal, 1350.8 mm^2/sec in accreta, and 1455.6 mm^2/sec in percreta. This was not statistically significant (univariate analysis, p= 0.5).

ADC as a diagnostic test for PAS

ROC curve shows the poor diagnostic accuracy of ADC for PAS, the AUC of 0.5 is the equivalent of random chance. Dark Bands and heterogeneity were far better with AUC of 0.9 and 0.8 respectively (Fig. 23).

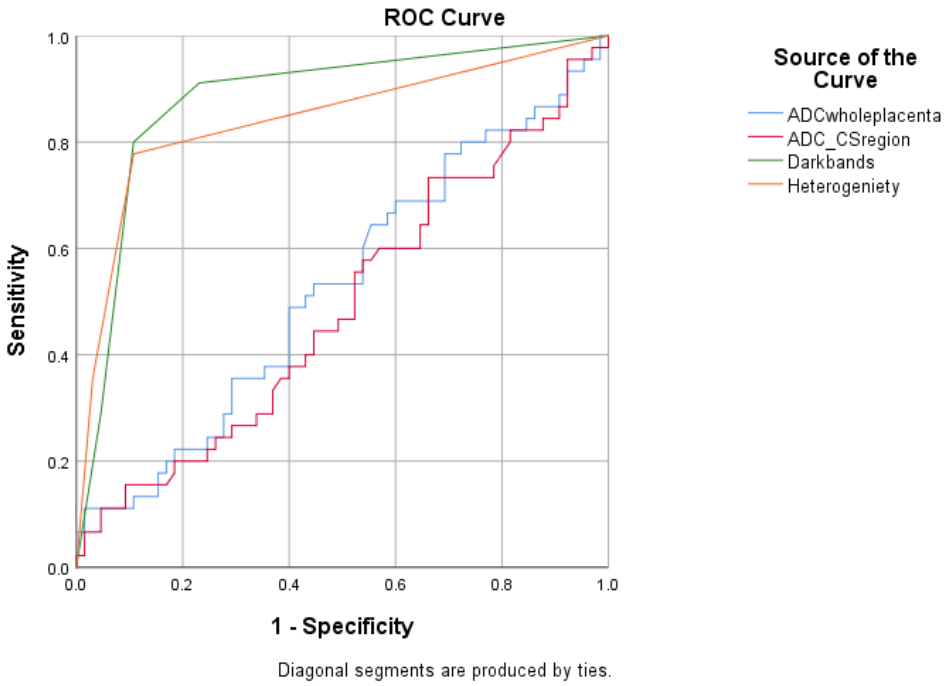

Figure 23 ROC curve of ADC whole and regional placenta ROI compared to dark bands and heterogeneity.

f. ADC and MRI signs of placental invasion

Testing the association of ADC and MRI signs of PAS

The data was normally distributed (Kolmogorov-Smirnova test was applied, p-value was not significant).

Heterogeneity

The level of ADC (whole placenta) showed a trend with the degree of placenta heterogeneity. ADC was higher in percreta group with local heterogeneity, (median=1737 mm^2/sec) than in the normal group (median=1355 mm^2/sec).

Dark bands

The median whole placental ADC in the invaded placentas was higher than in normal ones. Only in placentas with >5 dark bands, the ADC whole placenta was less than normal (1162 mm^2/sec).

1. **ADC whole placenta and MRI signs**

There was no significant difference between ADC whole placenta and MRI signs of invasion. Results of the ANOVA test were non-significant for dark bands (P=0.38), heterogeneity (P=0.68), dark bands and heterogeneity (p=0.14).

2. **Regional ADC and MRI signs**

There was no significant difference between dark bands and regional ADC and heterogeneity and ADC values. Results of the ANOVA test were none significantly different for dark bands, heterogeneity, and both: Dark bands (p=0.3), heterogeneity (p=0.9), dark bands and heterogeneity (p=0.5).

Overall ADC was not a useful value to aid in the detection of and determining the severity of PAS on MR images.

To assess the value of textural analysis of the MR images in cases of PAS:

c) Texture analysis

A retrospective review of a randomly selected subset of cases n=44 MR images was performed. Due to limited availability of anonymised images and (COVID pandemic). The texture was analysed using radiomics program LIFEx (Version 6.73.7, www.lifexsoft.org). A semi-automated program for 3D textural analysis. At the time of analysis, the reader was blind to the outcome of the cases analysed.
Using the T2-haste sagittal and axial section images, the entire placenta and a small area of the caesarean scar area (above the urinary bladder) were manually segmented to generate two 3D areas. The two ROIs were manually drawn in each sequence (Fig. 24, 25).
The texture protocol was used in the Lifex software. The input parameters were chosen according to the Lifex protocol provided:

1. Spatial resampling: spacing between x, y, and z of 2 mm, as it should be the same for all voxels (same voxel size) as textural values depend on voxel size.
2. Intensity discretization: number of grey levels 1.0 (automatically comes up when the size of bin is entered, the size of bins is 128 according to user advice for fixed bin width.
3. Intensity rescaling: relative rescaling in which the ROI lies between the min and max intensity values for the drawn ROI.

Textural features (TFs)

Selected from the systematic review as potentially the most likely to provide useful information and also those that were available in the software available to use 95 textural features were automatically extracted from each ROI (global and CS). First-order, second and high-order statistics were generated. First-order statistics were conventional and histogram features, which include minimum, maximum, SD and mean, skewness, kurtosis, energy-uniformity, entropy, etc. The second-order stat is textural features (table 5).

Textural features included:

1. Conventional: 12 features
2. Discretized: 12 features
3. Histogram: 5 features
4. Shape: 5 features
5. Grey-level co-occurrence matrix (GLCM): 7 features.
6. Grey-level run-length matrix (GLRLM): 11 features.
7. Neighbourhood grey-level different matrix (NGLDM): 3 features
8. Grey-level zone length matrix (GLZLM): 11 features

LIFEx manual describes the features and mathematical basis (Nioche, Orlhac et al. 2018).

Conventional/Discretized	Histogram	Shape	GLCM	GLRLM	NGLDM	GLZLM
CONV/DISCRET(min, mean, sd, max) CONV/DISCRET_peak 0.5 ml CONV/DISCRET-peak 1ml CONV/DISCRET_CAS CONV/DISCRET_TLG CONV/DISCRET_RIM_ (min, mean, sa,max,..) CONV/DISCRET_(Q1, Q2, Q3)	HISTO_Skewness HISTO_Kurtosis HISTO_Entropy_log10 HISTO_Entropy_log2 HISTO_Energy	SHAPE_Volume (mL) SHAPE_Volume (# vx) SHAPE_Sphericity SHAPE_Compacity Shape-Surface area	GLCM_Homogeneity GLCM_Energy GLCM_Contrast GLCM_Correlation GLCM_Entropy GLCM_Entropy log2 GLCM_Dissimilarity	GLRLM-SRE GLRLM-LRE GLRLM-LGRE GLRLM-HGRE GLRLM-SRLGE GLRLM-SRHGE GLRLM-LRLGE GLRLM-LRHGE GLRLM-GLNU GLRLM-RLNU GLRLM-RP	NGLDM-Coarseness NGLDM-Contrast NGLDM-Busyness	GLZLM-SZE GLZLM-LZE GLZLM-LGZE GLZLM-HGZE GLZLM-SZLGE GLZLM-SZHGE GLZLM-LZLGE GLZLM-LZHGE GLZLM-GLNU GLZLM-ZLNU GLZLM-ZP

Table 5 Extracted textural features.

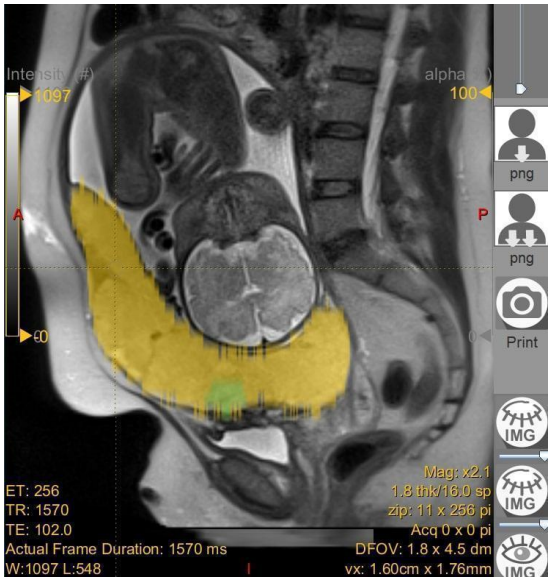

Figure 24: T2 sagittal section of the placenta, textural analysis is performed with 2 ROIs, global placenta (yellow) and local CS (green).

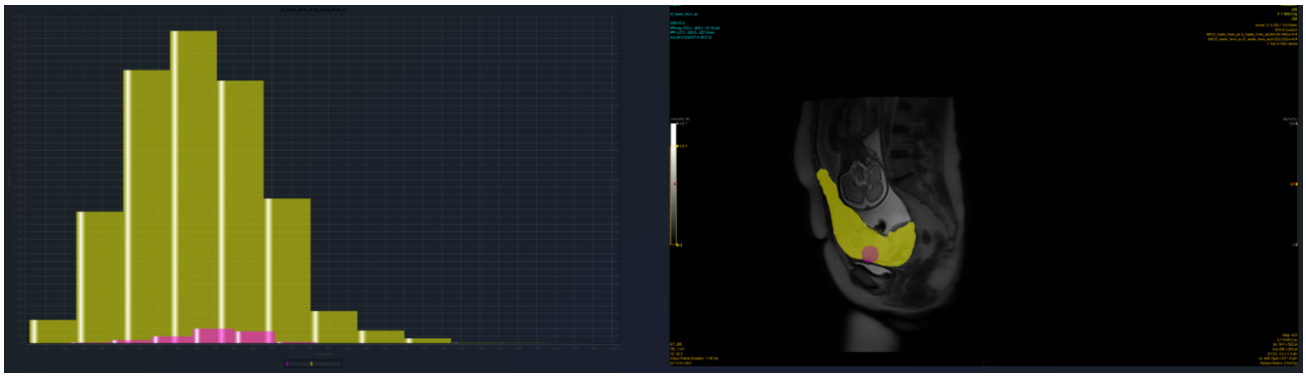

Figure 25: Textural analysis of the placenta, 2 ROIs were drawn, global placenta (yellow) and local CS (pink).

Statistical analysis

Texture conventional mean (first-degree statistics) was used to refer to texture. We tested the normality of the data; the whole placenta texture was not normally distributed, but the texture of the local CS area was normally distributed. Multiple logistic nominal regression was applied to test the correlation of mean texture, and ADC with placental invasion. The area under the curve was also tested to look at the

diagnostic value of texture for placental invasion. The area under the curve was examined to determine the difference between ADC, texture, and MRI signs in the diagnosis of PAS. Wilcoxon test was applied for group comparison of textural features between normal and invaded placentas.

Texture and ADC

Population

A data set of n=130 was available. Since gestational age may affect textural values, we ranked them according to GA into two groups: second trimester of 23 cases and third trimester of 107 cases. The texture of 44 cases was then matched with ADC readings (whole and regional ADCs). Then, the mean of texture measured in two ROIs were compared with placental pathology, MRI signs of invasion, and ADC. Characteristics of ADC and texture readings are given in table 6.

	Mean	95%CI	Median	Std. deviation	Std. error
ADC whole placenta	1395.3	1303 to 1487.5	1358	303.3	45.7
ADC CS	1467.7	1358.7, 1576.8	1412	358.7	54.1
Texture whole placenta	288.1	206.8 to 369.4	237.8	267.4	40.3
Texture CS	221.4	170.9 to 272	205.1	166.2	25.1

Table 6: Descriptive statistics of ADC and texture values of whole placenta and CS area.

Data distribution: was assessed prior to statistical analysis see appendix.

A. Texture and heterogeneity

The texture of the whole placental and CS area was not significantly associated with heterogeneity i.e., none, local, or widespread (Kruskal Wallis test, p=0.9 and p=0.09) respectively.

B. Texture and dark bands

The texture of the whole placental and CS area was not significantly associated with dark bands (none, single, <5 and >5), (Independent-Samples Kruskal-Wallis, p=0.8, 0.06) respectively.

C. Blood loss and texture

Regional placental texture may predict blood loss. Spearman's correlation was weak for regional texture (p=0.03) and non-significant for whole placental texture (p=0.32).

D. Hysterectomy and texture

There was no association between the texture of either whole placenta and regional placenta with hysterectomy (Mann- Whitney U test, p= 0.9 and p=0.06) respectively.

E. Texture and pathology texture, and placental pathology

The texture of both the whole placental and CS region showed a significant association with placental pathology (multinomial linear regression, p=0.000).

F. Duration of hospital stay and texture

No significant correlation was present between the texture whole placenta and hospital stay (Spearman's correlation p=0.45). However, this was significant with the texture of the CS area (Spearman's correlation, p=0.01).

Texture

Textural features describe several radiological characteristics in two different ways:

1. Morphology (shape features) such as roundness and convexity.
2. Statistical features in simple as a histogram (entropy, mean, variance, skewness, kurtosis, percentiles) and complex as higher order grey level statistics such as grey level co-occurrence matrix (GLCM) and grey level run length matrix (GLRLM).

a. Histograms; first-order features

Two histograms were extracted from each image, total placenta and localised ROIs, features were either conventional which means original images were used to extract the TFs, or discretized means using discretized images for that purpose (table 7). Features were minimum, mean, standard deviation, maximum, and quartiles.

Kurtosis measures the shape of the grey level distribution (flat or peaked) While skewness measures the asymmetry of data (Fig. 26).

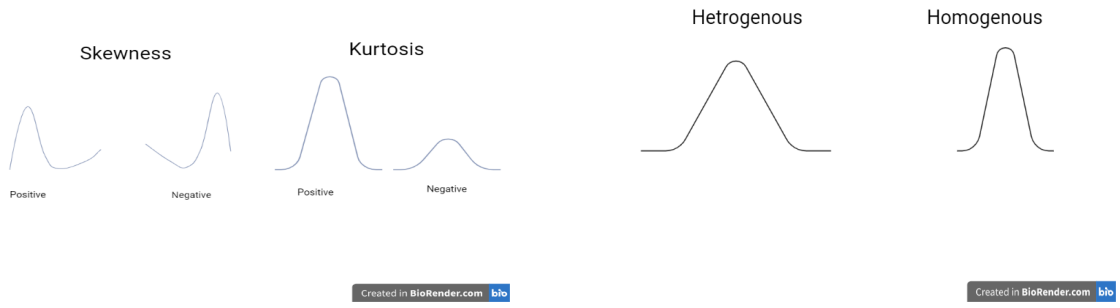

Figure 26: A basic description of skewness and kurtosis.

Assessment of a normal placenta showed a narrow histogram that reflects the characteristics of a homogenous placenta (Fig. 27).

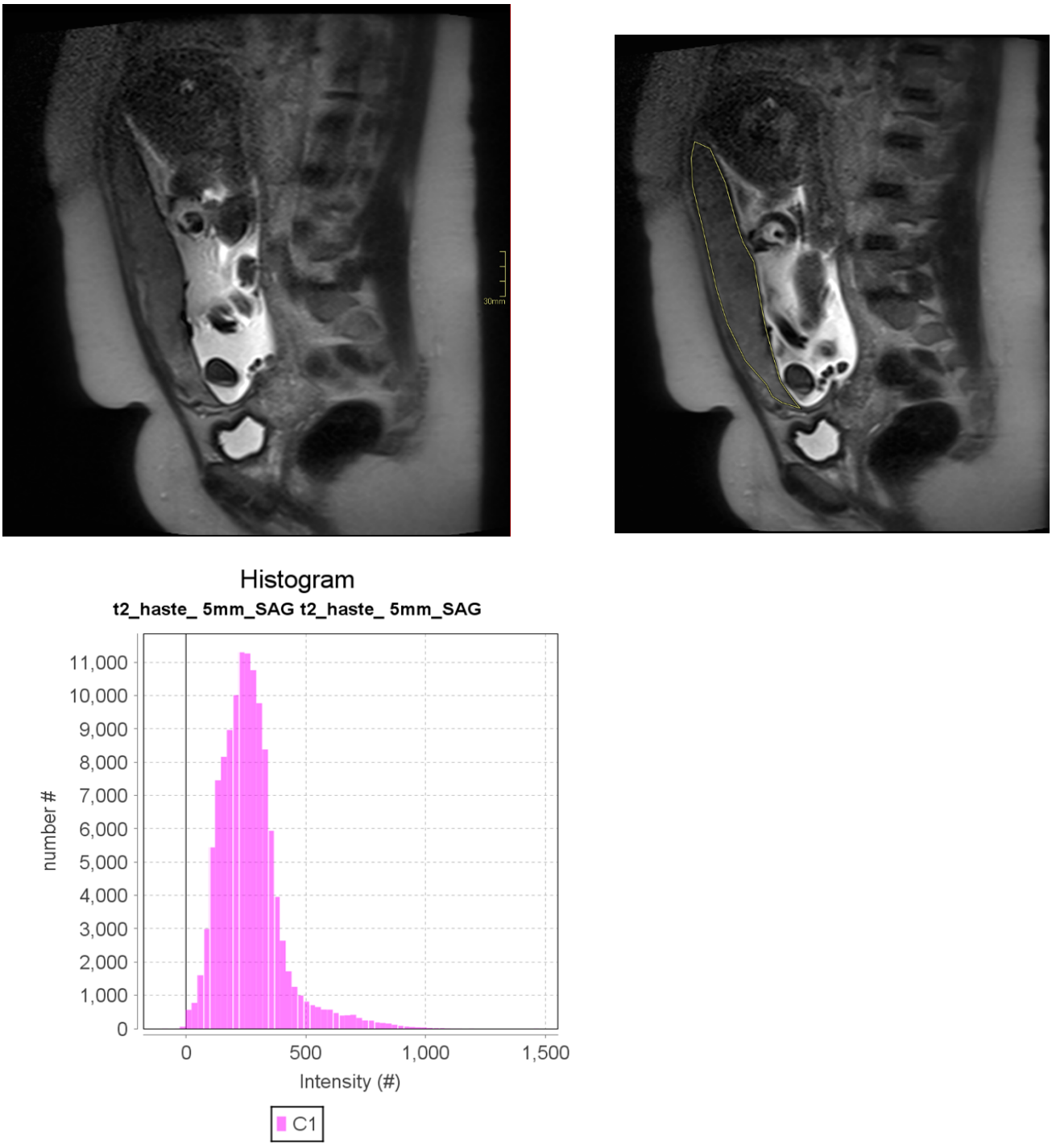

Figure 27: 30 weeks placenta, normal placental histology, narrow histogram, homogenous placenta.

While another patient with placenta percreta was assessed for histogram features. The area above the CS area was highlighted with a pink ROI. Values were widely distributed in this case reflecting a heterogenous placenta (Fig. 28).

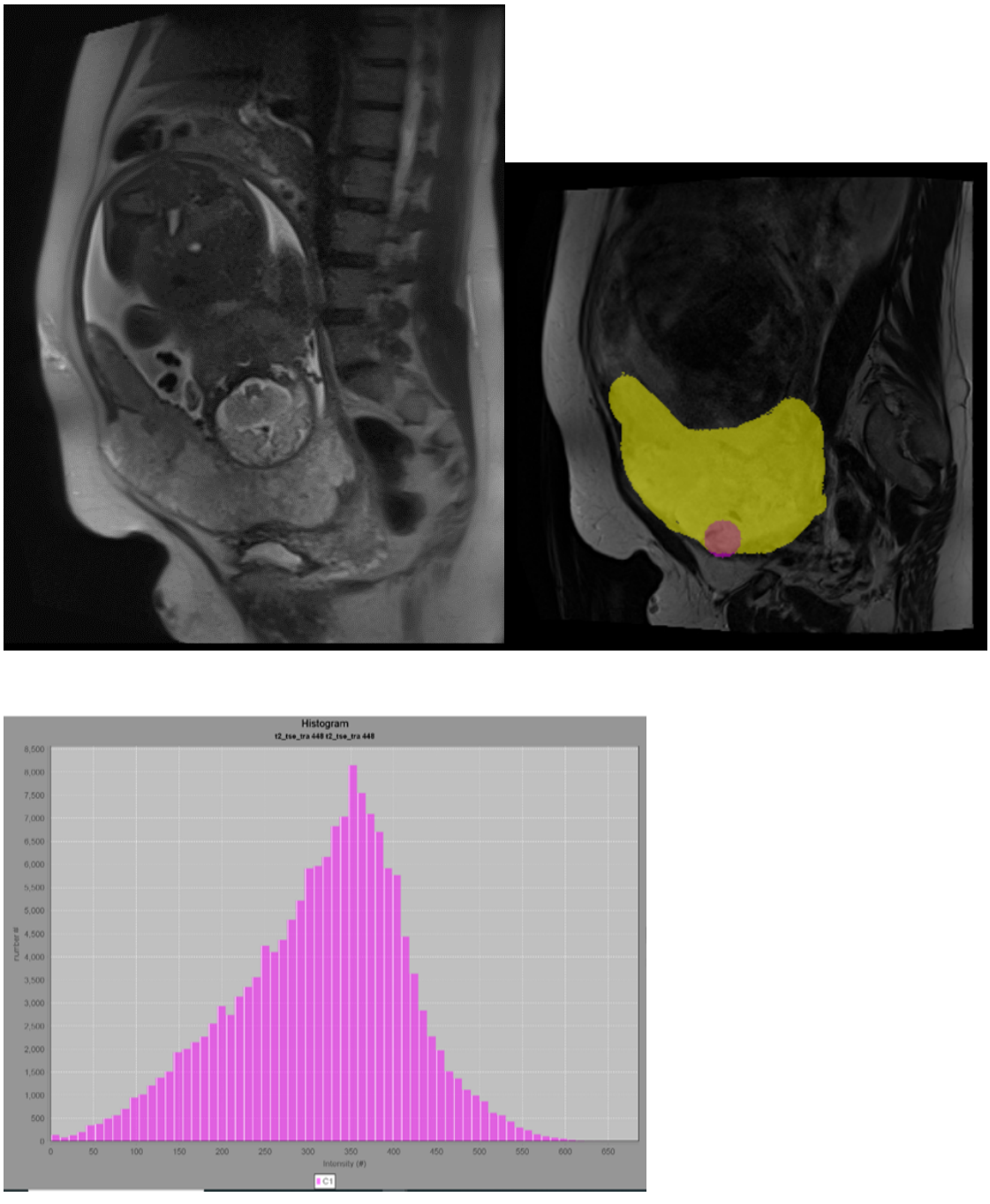

Figure 28: The pink circle is represented by the histogram below. The wide heterogeneity might give a clue to the diagnosis of PAS. 34 weeks placenta, percreta, the outcome was hysterectomy and 1-liter blood loss.

b. Advanced textural analysis (TFs)

These features are listed in appendix XI. Several features were extracted. Grey level co-occurrence matrix (GLCM) describes how voxels are arranged together with respect to homogeneity, energy (uniformity), contrast, correlation, entropy (randomness), and dissimilarity. The second feature was the neighbourhood grey-level difference matrix (NGLDM) which explains the difference in grey levels between one voxel and its 26 neighbourhoods in 2 dimensions (coarseness, contrast, and crowdedness). Also, the grey level run length matrix (GLRLM) describes the size of homogenous runs for each grey level. It includes short and long-run emphasis (SRE, LRE), low grey-level run emphasis (LGRE), high grey-level run emphasis (HGRE), short-run, low and high grey emphasis (SRLGE, SRHGE), and long-run low and high grey emphasis (LRLGE, LRHGE).

The grey level zone length matrix (GLZLM) is the size of homogenous zones for each grey level in 3 dimensions. (e.g., short zone emphasis (SZE) and long zone emphasis (LZE) GLZLM, low grey-level zone emphasis (LGZE) and high grey-level zone emphasis (HGZE) GLZLM, short zone low grey level emphasis (SZLGE) and short zone high grey level emphasis (SZHGE), long zone low grey level emphasis (LZLGE) or long zone high grey level emphasis (LZHGE). Grey level non-uniformity for the zone (GLNUz) and zone percentage ZP.

Morphometric and textural features and associated meaning	
Normalized mean grey level	Measures the average grey level for all pixels in an image, normalized per patient
Normalized variance	Measure of coarseness; describes the variance in grey level values; low values reflect image homogeneity
Kurtosis	Measure of uniformity; using the pixel histogram, measures magnitude of distribution; high values reflect greater uniformity
Skewness	Measure of asymmetry; using the pixel histogram, measures distribution of grey values; low values reflect more low grey level.
Energy	Measure of homogeneity; higher values have higher orderliness, reflecting homogeneity

Entropy	Measure of homogeneity; higher values have higher regularity, reflecting homogeneity
Inverse different movement	Measure of homogeneity; higher values reflect more homogeneity
Inertia	Measure of local homogeneity; low values reflect more homogeneity
Cluster shade	Measure of asymmetry; low values reflect greater symmetry
Cluster prominence	Measure of asymmetry; low values reflect small variation in grey levels or greater symmetry
Short run emphasis	Measure of coarseness; high values reflect greater distribution of short runs in an image or finer texture
Long run emphasis	Measure of coarseness: high values reflect greater distribution of long runs in an image or coarser texture
Grey level non-uniformity	Measures similarity of grey level values; low values reflect greater similarity of grey values
Run length non-uniformity	Measures similarity of run lengths; low values reflect similar run lengths
Low grey level emphasis	Measures runs of low grey levels; high values reflect images with more runs of low grey levels
High grey level emphasis*	Measures runs of high grey levels; high values reflect images with more runs of high grey levels
Short run low grey level emphasis	Measures short runs and low grey levels; high values reflect images with many short runs and low grey levels
Short run high grey level emphasis	Measures short runs and high grey levels; high values reflect images with many short runs and high grey levels
Long run low grey level emphasis	Measures long runs and high grey levels; high values reflect images with many long runs and high grey levels
Long run high grey level emphasis	Measures long runs and high grey levels; high values reflect images with many long runs and high grey levels

Table 7: Textural features meaning definitions.

(Castellano, Bonilha et al. 2004, Davnall, Yip et al. 2012, Andescavage, Dahdouh et al. 2019).

Whole placenta texture analysis

31 cases of invaded placentas with global textural features were compared with 11 cases of normal placentas. 46 TFs were significantly different among the two groups. ROC curves were also calculated. For the significant results, AUC was at a maximum of 0.8 for GLZLM_SZE.

Local placenta texture analysis

30 cases of invaded placentas with local textural features were compared with 11 cases with normal placentas. 43 features were significantly different between the two groups. The AUC was the highest for GLRLM SRE = 0.7.

Analysis

The distribution of data was abnormal. The most significant parameters were calculated using Wilcoxon tests and ROC analysis was performed. Table 8 shows the cut points and ROC metrics for the significantly different TA features (see appendix).

Whole placental texture

19 features of whole placental texture were of acceptable AUC (0.7 and more).

Whole placental texture	**controls Mean**	**Invaded Mean**	**P-value**	**ROC curve**
Symmetry and homogeneity				
DISCRETIZED mean	5.5	**23.4**	0.000	0.8
DISCRETIZED max	14.5	**62.7**	0.000	0.7
DISCRETIZED Q2	5.6	**22.9**	0.000	0.7
DISCRETIZED Kurtosis	6.6	**7.1**	0.231	0.7
DISCRETIZED Excess Kurtosis	3.6	**4.1**	0.231	0.7
DISCRETIZED HISTO_Entropy_log10	**469.2**	108.1	0.000	0.7
DISCRETIZED HISTO_Entropy_log2	**58636**	13401	0.000	0.7
Image coarseness and voxel based spatial arrangement				
GLCM Contrast Variance	4.2	**43.2**	0.000	0.8
GLCM Entropy log10	0.7	**1.7**	0.000	0.7

GLCM Entropy log2 Joint Entropy	**31.6**	14.7	0.003	0.7
GLCM Dissimilarity	0.5	**3.1**	0.000	0.8
GLRLM SRE	**30.9**	1.9	0.000	0.8
GLRLM SRHGE	**5426**	2754	0.000	0.8
GLRLM LRHGE	168.9	**1650.6**	0.000	0.8
NGLDM Contrast	**4590127**	718191	0.002	0.7
GLZLM SZE	**35.1**	2.1	0.000	0.9
GLZLM SZHGE	199.4	**1004.7**	0.000	0.8
GLZLM GLNU	28	**394.2**	0.000	0.8
GLZLM ZP	0.1	**0.25**	0.465	0.8

Table 8: whole placental textural features in controls and invaded placentas (values in bold are higher).

Local placental texture

3 features of local texture were of good diagnostic accuracy between normal and invaded placentas (table 9).

Local placental texture	**Controls Mean**	**Invaded Mean**	**P-value**	**ROC curve**
GLRLM SRE	**26.1**	2.18	0.000	0.7
GLZLM SZE	**29.2**	2.3	0.000	0.7
GLZLM ZP	0.4	0.4	1	0.7

Table 9: local placental textural features in controls and invaded placentas (higher values are in bold).

ROC curves

The area under the curve of the conventional mean texture for both whole and regional placental areas was 0.6 and 0.5 respectively. ADC AUC was 0.5 for both placental areas, and heterogeneity and dark bands diagnostic accuracy was higher (0.8 and 0.9) respectively (Fig.29).

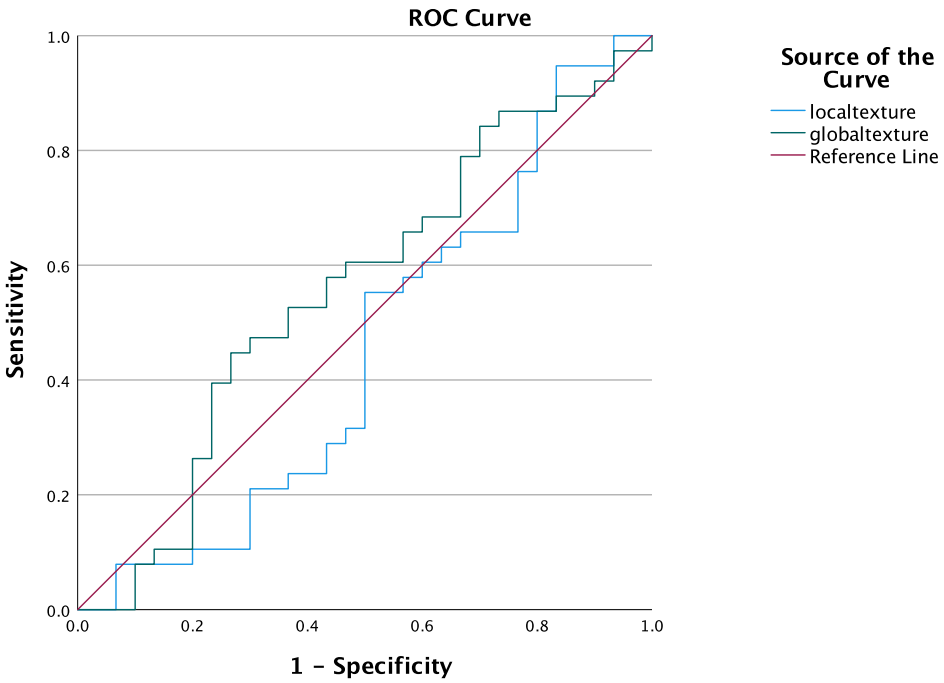

A.

B.

Figure 29: Area under the curve for texture (A) and ADC and MRI signs (B).

Discussion

In this study, we assessed the usefulness of MRI signs in the diagnosis of PAS. The most important clinically relevant findings were:

a) MRI diagnostic features and PAS

MRI visual signs of invasion such as heterogeneity and dark bands offer high diagnostic accuracy. The sensitivity of intra-placental dark bands was higher than heterogeneity (80.4% vs 78.3%) respectively whereas heterogeneity was slightly more specific (89.6%) than dark bands (87.9%). Our study also clarified the differences in MRI signs in normal and invaded placentas and differentiated between PAS groups as there was a significant association between dark bands and PAS ($p < .001$). Also, the diagnostic accuracy and AUC of both heterogeneity and dark bands were similar

(85% and 84%) respectively. Furthermore, combining both signs gave a higher diagnostic accuracy and AUC (86.7 and 87%) respectively.

Our data were comparable to previous studies. The efficacy of MRI diagnosis was reported in the literature, dark bands had a sensitivity of 60.5 and a specificity of 95.8 (Bourgioti, Zafeiropoulou et al. 2018). A systematic review by Rahaim and Whitby published in 2015 summarised the diagnostic index of both intra-placental dark bands and heterogeneity. Dark bands scored a sensitivity of 86.4% (Alamo, Anaye et al. 2013) and 100% in other studies (Teo, Law et al. 2009, Derman, Nikac et al. 2011, Lim, Greenberg et al. 2011). In general, the specificity of MRI ranged from 65 to 100% (Rahaim and Whitby 2015). However, each sign separately has a specificity range from 25-100% for heterogeneity (Derman, Nikac et al. 2011, Lim, Greenberg et al. 2011) and 50-100% for dark bands (Teo, Law et al. 2009, Lim, Greenberg et al. 2011, Shweel 2012).

This wide variability was most likely due to poor MRI sequences as noted in old studies and improved diagnostic experience in recently published research. A mild-to-moderate degree of heterogeneity was considered a non-useful indicator of invasion (Rahaim and Whitby 2015). These results suggest that dark bands might better help to identify placentas with suspicious findings, but heterogeneity helps to exclude the false positive results. If step by step approach is followed, it could help to maximise the accuracy of the diagnosis. For that reason, it is important to combine both signs to offer a more robust diagnosis.

Hysterectomy and MRI features of invasion

Predicting hysterectomy hazards in high-risk pregnancies is fundamental. It can help the surgical team to plan for a comprehensive approach. In this study, MRI features of PAS were strongly correlated with the risk of hysterectomy with heterogeneity ($p < .001$) and with dark bands ($p < .001$). The degree of heterogeneity and the presence of multiple dark bands can indicate a complicated delivery. Placentas that ended up with hysterectomy presented with multiple dark bands and were heterogeneous. This could be due to the higher placental surface area and depth of invasion which has been previously explained in other research studies (Clark, Ng et al. 2020). As the mortality in peripartum hysterectomy is more than 25 times higher than in hysterectomy cases performed for reasons other than pregnancy (Wright, Devine et

al. 2010). Early prediction of complicated caesarean hysterectomy may help reduce comorbidities and thus improve maternal outcomes (Silver, Landon et al. 2006).

Blood loss and MRI features of invasion

The next section of the project linked the amount of blood loss in different cohorts. Assessing placental dark bands and heterogeneity can efficiently help to predict the amount of blood loss. Placentas with multiple dark bands and heterogeneity are at risk of severe bleeding at delivery. An average of 6 litres of blood loss were linked to placentas with widespread heterogeneity and dark bands. There was a significant difference between the normal and PAS groups. Widespread heterogeneity (median of 4250 mL) and multiple dark bands (>5) (median of 4250 mL) were associated with massive obstetrics haemorrhage. This point has not been reported in previous research. Obstetrics haemorrhage has been related to the length of placental dark bands; dark bands' maximum length of more than 35.65 mm was associated with massive obstetrics haemorrhage (Wu, Zhou et al. 2022).

In this research, the average blood loss was 1.4 litres which is much less than the findings in previous research (Mitric, Desilets et al. 2019). Invasive placentas bleed more as more branching blood vessels are present, leading to more blood loss (Palacios-Jaraquemada, Bruno et al. 2013). Another reason is the volume of blood vessels in the invasive placentas is bigger than the normal size as it was described in research by Azour et al. (Azour, Besa et al. 2016). The AUC for predicting significant intraoperative bleeding in pregnant women with PAS by intra-placental fetal vessel (IFV) was 0.80, according to Bourgioti et al. (Bourgioti, Konstantinidou et al. 2021).

This research used retrospective clinical data which is always a limitation however the surgery in these cases is done by specialist centres that are used to dealing with high-risk cases. The surgical and anaesthetic notes were used for blood loss data and although these are often an estimate, they do include cell salvage data, weight of swabs and sheets plus measured blood loss in clearing suction techniques and is as accurate as possible. The findings of this study have several important implications for future practice as predicting blood loss prior to surgery allows selection of techniques for the surgical approach and also requesting the correct amount of blood products thus rationalising valuable resources.

Hospital-stay days and MRI features of invasion

Another interesting finding is the strong association of the length of hospital stay with placental pathology. The median ranged from 2 days for normal placentas to 9 days for perecreta cases. This is consistent with the findings in other studies. Peripartum hysterectomy caused by placenta accreta was reported to have a duration of hospital stay of 9.8 ± 13.5 days in large data in the United States (Wright, Devine et al. 2010). While in another study reported from Canada, the length of stay was 5.2 days instead of the previously mentioned 6 to 9.8 days (Mitric, Desilets et al. 2019). The period of stay can be affected by multiple factors, including the type of hysterectomy and complications. Subtotal hysterectomy has been linked with a reduced hospital stay (Lethaby, Ivanova et al. 2006). There was strong evidence of difference among different grades of placental heterogeneity (p= 0.000). Hospitalization ranged from 2 days in homogenous placentas to 4 days in placentas with local heterogeneity and 8 days in those with widespread heterogeneity. Another important finding was the strong evidence of a difference in groups with different numbers of dark bands (p=0.000). Two days hospitality stay when the placenta showed no dark bands but 5 days stay in placentas with a single band and 8 days stay for more than 5 dark bands. In the cases when the bands were less than 5, hospitalization was from 2-7 days. These results indicate that placental MRI is not only important in planning for surgery and placenta topography but also to predict postoperative complications and hospitality period which should be considered while dealing with PAS cases.

b) ADC and PAS

In this research, we addressed the properties of placenta invasion in terms of describing the perfusion and diffusion features. No previous papers have described this aspect before. ADC importance has been widely covered in several studies in the assessment of embryonic kidney illness and brain development (Schneider, Berman et al. 2009). In women with PAS diseases, placental invasion depth and topography are the primary determinants of surgical outcome (Palacios-Jaraquemada, Bruno et al. 2013, Marcellin, Delorme et al. 2018). Our hypothesis was that ADC in two ROIs is different according to the degree of placental invasions. ADC whole placenta was higher in percreta and accreta than in normal cases. Regional ADC was only higher in

percreta cases. Accreta cases showed closer values to normal (median =1288 vs 1319 mm^2/sec in controls).

This feature allows for the interrogation of placental function that is invisible to the human eye. By the movement of water from the extracellular to the intracellular space, the increase in intracellular space and the decrease in extracellular space may decrease the ADC values and high signal intensity of DWI in the invaded placentas (Sotak 2004).

Although there was a trend in the ADC values in both ROIs, the difference was not significant. This is consistent with Lu et al. research (Lu, Wang et al. 2022). Lu et al. assessed the microstructural function of the placenta in cases of uterine invasion (Lu, Wang et al. 2022). This study included placenta previa cases of 11 controls and 62 PAS. They used DKI (diffusion kurtosis imaging) which is another enhanced DWI model and has been extensively utilised to evaluate cancers and neurological illnesses. DKI provides more accurate water molecule mobility and distribution in biological tissues. In this study, it was combined with IVIM which is a conventional DWI to assess placental function. One of their diffusion parameters was MD which is parallel to ADC. Their reported ADC mean values were closer to ours but were non significantly different between normal and invaded placentas ($1.5x10^{-3}$ mm^2/sec for normal and $1.55x10^{-3}$ mm^2/sec for invaded ones) with p=0.15.

As ADC reflects tissue density, the more the placenta is invaded, the more highly vascularised and less dense tissue is there. According to Capuani's study, a normal placenta has a high cell density and a lot of cytoplasm, which prevents water from diffusing through it (Capuani, Guerreri et al. 2017). This confirms our results as ADC values were lower in normal placentas than those with higher abnormal vascular perfusion. Accreta cases demonstrated closer ADC value to controls, as there is usually a minimal change in placental structure while the change was higher in perecreta and increta cases which showed higher ADC values. These results are in keeping with those reported by Lu et al. (Lu, Wang et al. 2022), using a different technique but measuring a similar effect.

ADC of the whole placenta was not significantly correlated with gestation. ADC value decreases with placental maturation, which was also the case in a study by Sefidbakht et al. which suggested a good correlation between ADC and Grannum classification. The study included 38 normal placentas and measured ADC values obtained from

different b values. ADC values with b values of 0 and 1000 showed a significant correlation with gestational age and Grannum grades respectively. B values of (50, 400 and 800) were not correlated with GA. Because of their small sample size, this study could not establish a set of normal values for different ages of gestation (Sefidbakht, Zeinali-Rafsanjani et al. 2019).

Regional placental ADC was not correlated with GA. We hypothesized that they may possess extra pathological characteristics as the fibrosed scarred CS area could result in changes in tissue characteristics. Normal placentas need to be investigated in a holistic way to look at their inherited changes.

Previous research describing healthy pregnancies is consistent with the declining trend in ADC values over GA (Bonel, Stolz et al. 2010, Hutter, Slator et al. 2019). However, they did not link ADC values with gestational age or Grannum classification. For that reason, reference values for normal ADC values in the placenta were needed (Bonel, Stolz et al. 2010).

This was the first study that combined conventional MRI diagnostic signs of invasion with perfusion function. ADC values were none significantly different when the degree of placental heterogeneity and dark bands increase. When compared to normal cases, ADC was higher in placentas with local heterogeneity of the invaded placentas (1737 and 1355 mm^2/sec). Placentas with more dark bands also expressed higher ADC values except with dark bands >5. The difference was non-significant between these groups. One of the reasons why ADC was not directly correlated with the degree of heterogeneity and dark bands could be due to the subjective analysis of these signs as MRI is not usually a routine assessment tool (Barzilay, Brandt et al. 2020) and the possibility of the presence of pathologies other than invasion.

This might confirm the need for combined techniques to reach the final diagnosis as MRI signs of invasion may present in normal placentas. Combining objective and subjective approaches may help differentiate between the suspicious and the actual cases. Heterogeneity and dark bands diagnostic accuracy of PAS is not 100%. The use of combined MRI signs (4 and more) to diagnose PAS gave an AUC of 0.87 which was higher than using a smaller number of signs (Barzilay, Brandt et al. 2020). Different outcomes may be seen in situations with the same degree of placental invasion depending on the site of the invasion (Cali, Forlani et al. 2019). Most previously published studies assessing the accuracy of ultrasound and MRI in

diagnosing PAS disorders have concentrated on the detection of the presence of PAS and not the extent of invasion (D'Antonio, Iacovella et al. 2014).
In conclusion, ADC measurements did not show the expected diagnostic accuracy, sensitivity or specificity and is unlikely to help in the overall interpretation of MR images for the diagnosis and extent of PAS. Our sample size was relatively small which our limitation was. Further work is required to reach this stage and a large multi-centre prospective study is needed.

c) Texture and PAS

Applications of radiomics to analyse tissues' texture have shown a correlation with some types of breast, brain and lung tumours (Orlhac, Soussan et al. 2015, Goya-Outi, Orlhac et al. 2018, Lafcı, Celepli et al. 2023). Few study groups conducted on the placenta were parallel to our findings (Chen, Mar et al. 2019, Do, Lewis et al. 2019, Romeo, Ricciardi et al. 2019, Sun, Qu et al. 2019, Do, Lewis et al. 2020). We designed a model to fit the diagnostic biomarkers that could potentially differentiate between PAS subgroups and normal placentas. The results of the model were significantly different as the mean texture of the 2 ROIs was significantly different in accreta and percreta cases, ADC was not different across these subgroups.

Prediction of PAS groups using texture analysis is a novel finding as we have provided a method to distinguish different stages of placental invasion using textural analysis. A study published by Ren et al. did not assess the differences across PAS subgroups (Ren, Mori et al. 2021). Their study conducted a comparison between visual analysis of invasion signs and textural analysis in different MRI sections. Results have shown TA in coronal and sagittal sections have ROC curve of 0.98 which was higher than that of the visual analysis (AUC=0.75). Our diagnostic accuracy was comparable to Romeo et al. and Ren et al. and less than that of Do et al. (Romeo, Ricciardi et al. 2019, Do, Lewis et al. 2020, Ren, Mori et al. 2021). We performed advanced TA which showed 46 significant TFs for the whole placenta and 43 for regional texture. Their diagnostic accuracy was higher in the whole placental ROI (AUC=0.9 for GLZLM SZE) while the maximum AUC results for regional texture was 0.7 for GLRLM SRE, GLZLM SZE and GLZLM ZP. Our AUC was lower than previously published research, Do et

al. reported AUC = 0.75 and Romeo et al. reported an accuracy equal to 0.98 (Romeo, Ricciardi et al. 2019, Do, Lewis et al. 2020).

Placental textural features are compatible with MRI signs of invasion. Conventional whole placental TFs presented higher diagnostic prediction than that of the local placental region (0.6 and 0.5 respectively). TFs were consistent with the diagnostic accuracy of placental heterogeneity (AUC=0.84) and dark bands (AUC=0.88). However, texture of the local placenta was less accurate (AUC = 0.5). This could be justified by the inherited features of the specified ROI. There might be other features in the placenta that were not able to be assessed enough using the specified ROI. Increased heterogeneity of that area leads to different textural features than the usual placental tissue (Lafcı, Celepli et al. 2023).
It is disappointing that the TFs did not add to the diagnostic accuracy over and above that visualisation of dark bands and heterogeneity.
Histograms describe the standard distribution of first-order statistics and give an idea about the overall voxel intensity of the lineated ROI. In the context of placental texture, a wider distribution histogram reflects a heterogenous invaded placentas. Narrow histograms were shown in normal placentas while wider histograms were demonstrated in invaded ones. This finding was also reported by Chen et al. (Chen, Mar et al. 2019). Thus, may help in clinical diagnosis when visual assessment is not clear.
Entropy is a measure of a source's level of randomness. Entropy results greater than the threshold value point to tissue heterogeneity (Maes, Collignon et al. 1997, Lafcı, Celepli et al. 2023). Even though interpretation is difficult, a higher value of entropy may imply a stronger variety of intensity values. Higher-order statistics were good predictors of placental heterogeneity (AUC> 0.6). These indices include NGLDM, GLRLM, GLCM, and GLZLM. They are used to characterise how voxels or pixels are statistically related to one another. Although this was a complicated analysis as it is challenging to describe each TFs and their relation to PAS, they allow microscopical interpretation of the placental tissue.

As in the Grannum classification, the placental texture is largely affected by placental maturation. The use of radiomics clarifies the effect of GA on placental heterogeneity (Sun, Qu et al. 2019). As only specific features are affected by placenta growth such

as cotyledon and septum formation (Blaicher, Brugger et al. 2006). These are dependent and run length matrix features (i.e., GLRLM and NGLDM) which change along with placental maturation (Sun, Qu et al. 2019). GLRLM is a method of characterising voxels with the same grey-level value that occurs in a line across a specific direction (Tang 1998). It calculates how evenly distributed voxel lines are. This statistic increases when a few outliers in line length dominate the histogram and decreases when lines are evenly distributed in length (Sun, Qu et al. 2019). The distance of voxels from the central voxel is measured by the dependent matrix, NGLDM is a dependent matrix that dominates mostly with grey levels in the histogram. Conversely, the features that reflect placental abnormalities are GLCM and GLSZM which may reflect placental coarseness that has shown significant differences among PAS placentas. The co-occurrence matrix defines how voxels with the same discretized grey level are arranged pairwise at a specific offset (Haralick, Shanmugam et al. 1973). This has many subtypes, and an increment reflects fibrosis or abnormal microvascular structures. The number of voxel zones counted in with the same discretized grey level comprises GLSZM giving the zone percentage. The greater values suggest that the targeted region is made up of tiny zones. This together with entropy reflects placental heterogeneity and it is not affected by gestational age (Sun, Qu et al. 2019).

The involvement of radiomics in the radiological assessment allows quantitative analysis of the placental tissues. This could replace other invasive yet late diagnostic techniques such as histopathology. However, this cannot replace the role of radiological features but could help to make a robust diagnosis. Apart from the retrospective nature of the study and the small sample size, there have been a few limitations. Although the segmentation process was largely aided using semi-automated software, there was some subjective element in terms of drawing the size of the ROI, as it could affect the results of the analysis. There is a continuous update in the software which we haven't tested in another study. The analysis of textural elements was relatively complex and needs time and skills to run through all features. For that reason, we have not repeated the analysis. Hence no test of repeatability was conducted. We recommend running further studies to count the reproducibility and feasibility of the study. Unlike the case of ADC, special software is needed to run this analysis as it is not available on the ordinary proprietary system. Despite this

encouraging result, it is challenging to understand the distinct mathematical changes that result in the small changes of heterogeneity. It would be useful to carry out more research on the biological factors underlying various heterogeneity metrics.
In conclusion, texture results were a novel finding as there is sparse availability of similar data.

Overall features of heterogeneity and coarse texture were higher in the invaded placentas. Invaded placentas were more symmetrical and had higher uniformity (higher kurtosis and excess kurtosis), whereas entropy features were higher in controls reflecting more randomness in their histograms and grey levels voxel pairs. Long-run features with high grey emphasis (GLRLM-LRHGE) were more in the invaded placentas than short-run features (GLRLM-SRE, GLZLM-SZE) reflecting the coarse and heterogenous structure of the invaded placentas. Also, GLZLM-GLNU (grey level zone length matrix-grey level non-uniformity) was higher in invaded placentas reflecting less similarity of grey values (more heterogeneous). Textural features of the local placental area were mostly short-run metrics that were higher in the controls (GLRLM SRE, GLZLM SZE) reflecting homogenous and smooth placental texture.

The run-length metrics, which are measures of textural coarseness, showed that textural smoothness increases with gestation in healthy pregnancies. Furthermore, high grey level emphasis reflects tissue heterogeneity which has been reported to increase with GA as tissue heterogeneity increases (Andescavage, Dahdouh et al. 2019). Placentas with FGR were presented with homogenous and symmetrical signal intensity than controls. Also, they have larger numbers of short-run features and smaller numbers of long-run features than that of controls reflecting smoother and less coarse features of the FGR placentas (Andescavage, Dahdouh et al. 2019).

Limitations and conclusion

This study's limitations include its retrospective design, and the small sample size is given that adherent placenta is a rare condition. Particularly, increta cases for that reason, we combined them with the accreta group to optimize study statistics. Some cases missed the pathology reports and outcome data as those delivered outside

Sheffield hospitals were rather challenging to follow up which could be a major limitation. Another issue is that some mild forms of placental invasion pass into delivery unrecognised and present during the time of operation as an adhesive placenta, prolonging active stage of labour and PPH. These cases are mostly accreta which does not undergo further clinical assessment.

As mentioned above the blood loss data is based on hospital notes and will always be an estimated blood loss. The strength of the blood loss data in this study is that the surgery and anaesthetic staff are a set team of super specialists, the same hospital, the same equipment, and the same process to calculate blood loss so their variability of the data will be reduced. The fact that the MRI features enable us to predict the estimated blood loss allows the team to select the correct use of appropriate resources.

Further limitation is that we did not have a histologic reference standard for all pregnancies.

While texture values calculation is a more accurate representation of the microperfusion component, daily radiology work does not directly allow for measurement of these values, necessitating complex post-processing and advanced calculations, as opposed to the straightforward measurement of ADC values on a PACS workstation.

Conclusion

Further investigation of textural analysis may aid the visual interpretation of the MRI for diagnosis of PAS but currently the 2 main signs, heterogeneity and dark bands remain the most accurate for diagnosis and prognosis. ADC values do not appear to be predictive or helpful for the diagnosis of PAS.

Section 2

Fetal growth restriction (FGR)

Overview about FGR

The placenta is often a neglected organ yet is essential for fetal development and wellbeing. The basic morphology, e.g., volume, surface attachment, thickness, and other imaging characteristics, e.g., areas of abnormal signal, collection of blood, and venous lakes, all have the potential as “biomarkers” for the fetal outcome. It is confirmed that the placenta is often the problem in fetuses that have abnormal growth, e.g., small for gestational age (SGA) and fetal growth restriction (FGR) (Andescavage, Dahdouh et al. 2019). In cases of maternal diabetes, the fetus is often large (macrocosmic) (Kc, Shakya et al. 2015). Fetal MRI is now established in clinical practice; however, there has been little interest in using MRI technology to investigate the placenta. Previous studies have concentrated on blood flow, diffusion, and perfusion characteristics, neglecting simple morphology. We aimed to look at SGA/FGR/diabetes mellitus (DM) cases and controls and their placentas. In this section, I will summarise current knowledge of the role of the placenta in these conditions.

Fetal growth restriction (FGR) is a multifactorial disorder, but currently, little clinical interest has been given to the placenta. The placenta has many roles in the development of the fetus; for that reason, significant maternal and fetal health issues may arise due to abnormal placental development. A recent study has shown that placental conditions are the leading cause of growth restriction in stillborn fetuses (Burton and Jauniaux 2018). The latest research showed that approximately one in every 300 pregnancies would end up having a stillbirth, and FGR affects about 10% of the population (Flenady, Wojcieszek et al. 2016, Andescavage, Dahdouh et al. 2019). Fetuses affected by abnormalities of growth are still unfortunately common and poorly understood, and additional features that help predict the outcome early in gestation can then be the focus of research on an intervention to alter the outcome in the long term.

The consequences of GDM on fetal growth can be either large for gestational age babies in pregnancies with bad glycaemic control or SGA when there is a relatively normal blood glucose level (Macara, Kingdom et al. 1996). Doppler US is not an effective tool for screening SGA in diabetic pregnancies as it has limited value in the detection of placental insufficiency. Moreover, Doppler parameters, including the

middle cerebral artery (MCA), umbilical artery associated nephropathic and vasculopathic complications are not recognised by Doppler. Further studies are needed to investigate for SGA in diabetic pregnancies.

Learning to identify placental morphological changes on MRI may help to introduce timely interventions that can benefit the outcome of the pregnancy. Fetal growth restriction cases have been missed during clinical practice; however, some cases were regarded as abnormally small for gestation but considered normal according to their inherited parental and ethnic demographics. The high detection rate of FGR results in unwanted maternal anxiety of inaccurate diagnosis. This may be reduced by identifying the constitutionally small for date fetuses from the real FGR, consequently, preventing unnecessary maternal anxiety. The result may have a significant impact on the mother and the developing fetus.

2.1 Background of FGR

Fetal growth restriction (FGR) can result from maternal, fetal and uteroplacental vascular insufficiency or a combination of more than one factor. However, placental abnormalities account for 25–30% of FGR cases (Nardozza, Caetano et al. 2017). It affects approximately 5- 10% of the population (Lausman, Kingdom et al. 2013, Leon, Li et al. 2018). It is difficult to define the term due to the absence of standard criteria regarding the cut-off points. In recent years, there have been various terminologies, diagnostic techniques, and monitoring tools. Yet a large proportion of constitutionally small babies are still difficult to diagnose until after delivery. However, FGR may be defined as the failure of the fetus to exhibit the standard growth potentials of a specific population (Gordijn, Beune et al. 2018). Small for gestational age (SGA) refers to fetuses with a birth weight of two standard deviations smaller or less than the 10th percentile of the average weight for a specific population (Sharma, Shastri et al. 2016). The critical point to highlight is that not all SGA fetuses are FGR. According to the RCOG green-top guidelines, 50-70% of the diagnosed SGA are constitutionally small (RCOG 2013). Fetal growth restriction accounts for 42.9% of the perinatal mortality rate (Gardosi, Kady et al. 2005). The significance of recognizing FGR is proved by the decrease in the rate of stillbirth rates (Gardosi, Giddings et al. 2014). In the UK, stillbirth rates have dropped from 5.25/1000 stillbirths in the last ten years to 4.01/1000 stillbirths in 2019 as a result of implementing the growth assessment protocol (GAP) (Gardosi, Giddings et al. 2014). The reason for that is partly because unexplained causes of stillbirth are due to fetal growth abnormalities, and early recognition and management help in stillbirth management. Disturbances in fetal growth might happen along with fetal life.

FGR is pathological growth that could either be early or late than 32 weeks of gestation. The majority of babies with early-onset FGR are SGA, yet 40% of babies with a birth weight below the 10th percentile have healthy constitution (Khalil, Morales-Rosello et al. 2015). On the other hand, in late-onset FGR with placental insufficiency, fetal growth may be limited in relation to their growth potential, but the birth weight will still fall within the normal range (i.e., AGA) (Gordijn, Beune et al. 2016, Damhuis, Ganzevoort et al. 2021). In fact, fetuses classified as AGA account for up to 70% of prenatal mortality (Pacora, Romero et al. 2021).

Early FGR develops before 32 weeks of gestation. In this category, preeclampsia comprises the major cause and the challenges rely on the management rather than the diagnosis (Figueras, Caradeux et al. 2018). Placental insufficiency is the main reason for late FGR, which is still underdiagnosed. The diagnostic challenge occurs because later in gestation, the placenta can compensate for damage by shifting blood into fetal vital organs. Often, there is a minimal change or normal cerebral Doppler and umbilical Doppler indices and no evident cardiovascular abnormalities.

Consequently, screening parameters may be inconsistent. Ultrasound can detect abnormal abdominal circumference, but other parameters tend to be healthy (head circumference, biparietal diameter, and femur length) (Sharma, Shastri et al. 2016). Undetected fetal growth restriction can lead to a significant rise in perinatal mortality (Gardosi, Madurasinghe et al. 2013). The risk of stillbirth rises approximately four folds in cases with FGR, and failure to identify it antenatally raises the risk further by eight fold in comparison with healthy pregnancies (Gardosi, Madurasinghe et al. 2013).

Clinically, identifying high-risk fetuses of developing SGA can be performed by using customized fetal growth charts for age, gender, and ethnicity. These are better than the population-based charts in detecting high-risk fetuses for serial US measurements. The high-risk population is defined as either having abnormal uterine artery Doppler at 20-24 weeks or symphysial fundal height (SFH) plotted below the 10^{th} centile using customized growth charts. These should be referred to as serial ultrasound measurements of fetal size (RCOG 2013). SFH, a quick and simple measure of uterine size that is thought to reflect fetal size, is of limited quality if the woman is obese or has a fibroid or abnormal fetal lie (RCOG 2013). A study of a large population investigated the effectiveness of SFH in SGA resulted in only 27% sensitivity and 88% specificity (Persson, Stangenberg et al. 1986). Whilst the use of customized fetal growth charts resulted in higher sensitivity (48%) (Gardosi and Francis 1999). Current diagnostic approaches according to SGA green top guidelines, assume using US measurements of estimated fetal weight (EFW) and abdominal circumference (AC) (RCOG 2013).

Fetuses with a birth weight lower than the 10th percentile may not have growth abnormalities. Similarly, their birth weight may range from the 10th-90th percentile, i.e., appropriate for gestational age (AGA) or even more than the 90th percentile, i.e., large for gestational age (LGA) but they might also present with FGR features. Some manifestations of growth restriction can be recognized in utero, and this is regarded

as FGR (Sharma, Shastri et al. 2016). Only 60% of the diagnosed SGA are growth restricted, and approximately 21% are physiological (Gordijn, Beune et al. 2018). While ultrasound is a convenient screening and diagnostic tool, its usage has many limitations in reaching the definitive diagnosis of growth-restricted fetuses. An added dilemma is the wide variability of fetal parameters for growth charts and the absence of an international agreement regarding the average growth for a specific population (Papageorghiou, Ohuma et al. 2014).

FGR and placental changes

FGR placentas express a wide range of findings, in cases with lesions present, two types of lesions were identified:

- Macroscopic changes include patchy placental infarction in 25% of term FGR cases (Wigglesworth 1964).
- Microscopic changes have been classified into general and those linked to UA Doppler changes according to Mifsud et al. They are either:

- General changes

These are identified in most FGR placentas, but they can be encountered in non FGR placentas as well (Sandstedt 1979, Rayburn, Sander et al. 1989). Placental abruption/retroplacental haemorrhage, villous morphological abnormalities (e.g., syncytiotrophoblast "knots"), excess cytotrophoblast cells, thickened trophoblastic basement membrane, villous fibrosis, hypovascular terminal villi, reduced villous volume, reduced intervillous space, and non-specific inflammatory lesions (villitis of unknown aetiology (VUE)) are examples of villous infarcts or hypovascular terminal villi. Furthermore, histological characteristics such as insufficient "physiological change," fibrinoid necrosis, and acute atherosis (a dense perivascular lymphocytic infiltration with intimal arterial foamy macrophages) may be seen, which indicate faulty remodelling of spiral arteries into uteroplacental veins (Mifsud and Sebire 2014).

- Changes when UA Doppler abnormalities are present.

These cases were studied as thought that abnormalities in the UA doppler would increase the positive predictive values of the changes in the placental tissues. Abnormalities in the uteroplacental flow were among most charges noticed (Mifsud and Sebire 2014).

Feto-placental flow or fetal stem arteries were examined in other studies, which found their relation with FGR placentas (Las Heras, Baskerville et al. 1985, Fok, Pavlova et al. 1990, Salafia, Pezzullo et al. 1997), where they investigated feto-placental circulation in placentas with abnormal Doppler results. This included stem vessel wall thickening in 90% of cases, which was observed in cases with absent end-diastolic flow (EDF).

The broad patterns of placental changes that might be reflected in the MRI imaging used in this study include:

- **Maternal vascular malperfusion:** these are common placental findings. They include:

a) **Gross features:** intervillous thrombus, retroplacental haemorrhage and infarcts.
b) **Microscopic features:** villous agglutination, increased syncytial knots, distal villous hypoplasia, peri villous fibrin deposition, decidual vessels with acute atherosis/fibrinoid necrosis of the vessel wall, muscularized basal plate vessels and increased cell islands**.**

- **Fetal vascular malperfusion:**

a) **Gross:** thrombi in umbilical/ chorionic vessels
b) **Microscopic:** groups of avascular hyalinized villi, vascular ectasia in chorionic plate/stem villi, villous stromal karyorrhexis, nucleated RBCs, fibrin/re-canalizing thrombi.

- **Umbilical cord abnormalities:**

  Gross: coiling of cord (hyper and hypo coiling), insertion of the cord (marginal, velamentous, para central/ eccentric) (Sundari Amirthakatesan, Devi Chandramohan et al. 2023).

Risk factors of FGR

Recent research on fetal growth has shown several risk factors that can exert an effect on fetal growth. Some of them can be summarised as:

1. Maternal age

Maternal age may expose a significant impact on fetal growth. In a recent observational study, fetuses were delivered one week earlier in mothers who were five years older (Khong, Mooney et al. 2016). This suggests that in older age mothers, there is less adequate placental perfusion and hence, earlier delivery with a higher likelihood of FGR.

2. Maternal height

Short maternal stature has been associated with an increased risk of FGR. A shorter stature may be linked to a smaller pelvic size, potentially affecting fetal growth (Kozuki, Katz et al. 2015).

3. Maternal weight and BMI

Underweight: Maternal underweight is often associated with an increased risk of FGR. Inadequate maternal nutrition and low weight can contribute to insufficient fetal growth (Lewandowska 2021).

Overweight and obesity: Maternal overweight and obesity are also associated with an increased risk of FGR. Obesity can lead to various complications, such as gestational diabetes and hypertension, which may contribute to fetal growth issues (Lewandowska 2021).

Maternal nutritional status is a critical factor influencing fetal growth. Poor maternal nutrition, regardless of weight, can negatively impact fetal development (Marshall,

Abrams et al. 2022). Certain medical conditions associated with extreme weights, or BMIs, such as anorexia nervosa or morbid obesity, may increase the risk of FGR (Eagles, Lee et al. 2012, Tanner, Brock et al. 2022).

4. Racial origin

The relationship between racial or ethnic origin and fetal growth restriction is a complex and multifactorial issue. While there may be observed differences in the rates of FGR among different racial or ethnic groups, it's essential to understand that these variations are influenced by a combination of genetic, environmental, and socioeconomic factors (Nasiri, Moodie et al. 2020).

Genetic factors can play a role in determining fetal growth. Different populations may have genetic variations that influence factors such as maternal metabolism, placental function, and fetal development (Wang, Fernandez-Boyano et al. 2022). However, it's important to note that genetics alone do not explain all the observed differences. Socioeconomic factors, including access to healthcare, nutrition, education, and socio-economic status, can significantly impact fetal growth. Racial and ethnic groups may experience disparities in health conditions that can affect pregnancy outcomes. Conditions such as diabetes, hypertension, and obesity, which are more prevalent in some populations, can contribute to an increased risk of FGR. Cultural practices, including dietary habits and lifestyle choices, can impact maternal and fetal health. Variations in cultural practices may contribute to differences in FGR rates among different racial or ethnic groups. Geographic and regional factors can also play a role. For example, populations living in certain geographical areas may face different environmental exposures, which can influence pregnancy outcomes (Frisbie, Biegler et al. 1997).

5. Parity

Some studies suggest that multiparity (more than 5 births) may be associated with an increased risk of fetal growth restriction (Mohammad, Sohaila et al. 2018). This could be due to factors such as changes in the uterine environment, maternal age, or increased likelihood of underlying health conditions with multiple pregnancies. On the

other hand, being a first-time mother (primiparity) may also be associated with an increased risk of FGR. Primiparous women may have a higher likelihood of certain risk factors, such as advanced maternal age or underlying medical conditions (Mohammad, Sohaila et al. 2018).

6. Pregnancy interval

The time between pregnancies, known as the interpregnancy interval, is another factor to consider. Short interpregnancy intervals may be associated with an increased risk of adverse pregnancy outcomes, including FGR. This could be related to insufficient time for maternal nutritional replenishment between pregnancies (Agrawal, Chaudhary et al. 2022).

7. Gestation weight gain

Both insufficient and excessive gestational weight gain can be associated with an increased risk of adverse pregnancy outcomes, including fetal growth restriction. The relationship between gestational weight gain and FGR is complex and can be influenced by various factors. Here's how inadequate and excessive gestational weight gain may impact fetal growth:

1- Inadequate gestational weight gain:

Risk of FGR: Inadequate weight gain during pregnancy can be associated with an increased risk of fetal growth restriction. Insufficient maternal nutrition may limit the supply of nutrients to the developing fetus, affecting its growth and development (Mohammad, Sohaila et al. 2018).

Low Birth Weight: Babies born to mothers with inadequate weight gain are more likely to have a low birth weight, which is a common characteristic of fetal growth restriction (Hulsey, Neal et al. 2005).

2-Excessive gestational weight gain:

Risk of FGR: Excessive weight gain during pregnancy, particularly beyond recommended levels, may also be associated with an increased risk of fetal growth restriction (Leddy, Power et al. 2008).

Gestational diabetes and hypertension: Excessive weight gain can contribute to the development of gestational diabetes and hypertension, both of which are risk factors for FGR.

Macrosomia: While excessive weight gain is more commonly associated with large babies (macrosomia), it can still have implications for fetal health, including potential complications during delivery (Weschenfelder, Lehmann et al. 2019).

8. Current or previous history of essential HTN and pre-eclampsia

High blood pressure during pregnancy can pose risks to both the mother and the developing fetus, including an increased risk of fetal growth restriction (Muhammad, Khattak et al. 2010, Mohammad, Sohaila et al. 2018). Here's how high blood pressure can impact fetal growth:

- Uteroplacental insufficiency:

Hypertension can lead to reduced blood flow to the placenta, a condition known as uteroplacental insufficiency. The placenta plays a crucial role in delivering nutrients and oxygen to the fetus. When blood flow is compromised, it can result in inadequate nourishment for the developing baby, affecting its growth (Krielessi, Papantoniou et al. 2012).

- Preterm birth:

High blood pressure, particularly when it progresses to conditions like preeclampsia, is a known risk factor for preterm birth. Babies born prematurely are at an increased risk of experiencing growth restriction (Bertagnolli, Luu et al. 2016).

- Intrauterine growth restriction:

Hypertensive disorders of pregnancy, such as preeclampsia, are associated with an increased risk of intrauterine growth restriction (Burke, Unterscheider et al. 2014).

- Oxygen and nutrient supply:

Hypertension can lead to vasoconstriction (narrowing of blood vessels), reducing the supply of oxygen and nutrients to the developing fetus. This can negatively impact fetal growth and development (Gathiram and Moodley 2016).

- Risk of low birth weight:

Babies born to mothers with hypertension, especially if associated with preeclampsia, may be at an increased risk of having a low birth weight. Low birth weight is a common characteristic of fetal growth restriction (Nakimuli, Starling et al. 2020).

9. Diabetes

Diabetes mellitus is a serious health problem for pregnant women as there are several complications for the mother and fetus. Although many researchers have studied the effect of diabetes in pregnancy on the growing fetus, there is little evidence regarding the role of the morphology of the placenta. Many studies have examined the pathological changes in the placental tissue post-delivery. It is necessary, however, to find significant placental characteristics which can be detected using imaging techniques during pregnancy.

Several studies have determined the effect of diabetes on the fetus, targeting the pathology of the placenta. Pedersen's hypothesis states that poor glycaemic control during gestation leads to maternal and fetal hypoglycaemia. This results in fetal hyperinsulinemia. As a result, macrocosmic babies developed due to a higher rate of lipogenesis (Pedersen 1955). Pregestational and gestational diabetic placentas can exhibit significant pathological manifestations. Macroscopically, the most frequent pathological changes were an increase in size, volume, and weight of the diabetic's placenta. Microscopically, however, there were observed pathological changes, such as villous immaturity, villous edema, fibrinoid necrosis, syncytial nodes, and fibrin thrombus (Edu, Teodorescu et al. 2016). The macroscopic changes can be detected during gestation, and the reported variable alterations in placental growth should be easily characterized by placental MRI. For example, in cases with pregestational diabetes, 20% of placentas are relatively small for gestational age, and 25%-30% is relatively large for gestational age (Starikov, Inman et al. 2014, Rais, Starikov et al. 2019). The proposed mechanism behind this is that the diabetic's placenta has raised insulin resistance, which promotes placental growth and decreases the exchange efficacy. This is due to immature villous development, which is a common histological finding (Tanaka, Yamada et al. 2018). Type 1 DM placenta exhibits the most notable findings in terms of abnormal villous growth. The longest period of hyperglycaemic

exposure occurs in pregestational diabetes, while gestational diabetes, which develops in the second half of pregnancy, has less of an effect (Dubova, Pavlov et al. 2011).

Starikov et al. in 2014 concluded that women with type 2 diabetes have a higher incidence of placental insufficiency and maternal decidual vasculopathy compared to type 1 diabetes. However, placentas of type 1 diabetes display higher rates of vasculitis associated with fetal vasculitis, preterm premature rupture of membranes (PPROM), and admissions into the newborn intensive care unit (NICU). These findings confirm that the degree and type of placental tissue pathology suggest different mechanisms involved in the disease (Starikov, Inman et al. 2014). Pregestational diabetes may have longer-acting effects than gestational diabetes on the development of the placenta. In the beginning, the placenta adapts to the excessive glucose level by buffering the higher glucose concentration and raising vascular resistance; this could decrease the effect on fetal growth (Desoye and Hauguel-de Mouzon 2007). Normally, when the glucose level is increased, the placenta should eliminate it. When a defect in this process occurs, that results in fetal macrosomia (Desoye and Hauguel-de Mouzon 2007). Placental adaptation mechanisms include an increased weight due to the raised level of fibroblast growth factor. The latter is responsible for angiogenesis and hyper-capillarization, especially in diabetes type 1 (Hill, Tevaarwerk et al. 1995, Arany and Hill 1998). As a result, the placental exchange surface area may be larger than usual (Desoye and Hauguel-de Mouzon 2007). This can protect infants from the effect of chronic hypoxemia (Daskalakis, Marinopoulos et al. 2008). Placentas of gestational diabetes mellitus (GDM) express independent pathological changes whatever glycaemic control is. In other words, glycaemic control does not change the already established early placental growth defects, as this is due to the placental adaptation that has occurred before the diagnosis of the GDM. Optimal glycaemic control, however, may preserve the fetal weight within the standard limit. As a result, the fetal/placental weight ratio tends to be lower than average (Daskalakis, Marinopoulos et al. 2008).

Current imaging knowledge of diabetic's placentas is limited. 3-D US imaging findings of the placenta in gestational diabetes compared with healthy controls revealed a significantly larger placentas (Pala, Artunc-Ulkumen et al. 2015). Most recent research identified a potential ultrasound predictor for a diabetic's placenta which is an immature appearance of the placenta (Patil, Srinivas et al. 2019).

In conclusion, there seem to be factors other than glycaemic control or body mass index (BMI) affecting placental morphology in diabetic pregnancies (Rais, Starikov et al. 2019). Diabetic placenta tends to be less efficient, and this may cause severe growth abnormalities. However, there is still a lack of reporting on the effect of a diabetic placenta on fetal growth and how matching with placental morphology could be related.

10. Autoimmune diseases

The impact of autoimmune diseases on fetal growth can vary depending on the specific condition, its severity, and how well it is managed during pregnancy (Anaya, Shoenfeld et al. 2013). The impact could be due to many factors, including:

- Inflammation and immune response:

  Chronic inflammation associated with autoimmune diseases can potentially impact the developing fetus. Inflammatory processes may interfere with the normal processes required for fetal growth (Adams Waldorf and Nelson 2008).

- Maternal health:

  The overall health of the mother, including the management of her autoimmune disease, can influence fetal growth. Uncontrolled or severe autoimmune diseases may contribute to complications that affect pregnancy outcomes (Merz, Fischer-Betz et al. 2022).

- Medications:

  Some medications used to manage autoimmune diseases may have potential effects on fetal growth (Scott 1977).

- Specific autoimmune conditions:

  The impact on fetal growth can vary among different autoimmune diseases. For example, conditions such as lupus (systemic lupus erythematosus) and antiphospholipid syndrome are associated with an increased risk of adverse pregnancy outcomes, including FGR (Limaye, Buyon et al. 2020).

- Vascular complications:

  Certain autoimmune diseases may increase the risk of vascular complications, such as vasculitis or blood clotting disorders. These complications can affect

blood flow to the placenta, potentially leading to FGR(Bleau, Patenaude et al. 2016).

- Antiphospholipid syndrome:

Antiphospholipid syndrome, an autoimmune disorder characterized by abnormal blood clotting, has been associated with an increased risk of recurrent miscarriages and fetal loss. This syndrome may also contribute to FGR due to impaired placental blood flow (Xu, Chen et al. 2022).

11. Pre-existing vascular diseases

Pre-existing vascular diseases can pose risks to fetal growth that may lead to fetal growth restriction. Vascular diseases can affect the blood vessels and circulation, impacting the delivery of oxygen and nutrients to the developing fetus. The impact on fetal growth is due to impaired blood flow, placental dysfunction, hypertension and preeclampsia, diabetes and its associated vascular complications, vasculitis, thrombophilic disorders and aneurysms and vascular abnormalities (Adam 2017).

12. Pre-existing renal diseases

Pre-existing renal diseases can increase the risk of FGR and other complications during pregnancy. When a woman has pre-existing renal diseases, renal functions may be compromised, potentially impacting fetal development. According to one research (Holley, Bernardini et al. 1996), women with CKD had a five-fold increased risk of IUGR and a three-fold increased risk of SGA (Kimmerle, Zass et al. 1995). The risks of pre-existing renal disease on fetal growth include impaired renal function, hypertension and preeclampsia, proteinuria, electrolyte imbalances, impact of medications, vascular changes, and preterm birth risk.

13. Prior stillbirth

Experiencing a prior stillbirth can be a challenging and emotionally distressing event, and it may have implications for subsequent pregnancies. While there is an association between prior stillbirth and certain pregnancy complications, including fetal

growth restriction, it's important to note that each pregnancy is unique, and not every woman who has had a stillbirth will experience complications in subsequent pregnancies (Malacova, Regan et al. 2018). The risk of FGR could be due to many factors such as: placental insufficiency, underlying conditions such as HTN and diabetes, uterine abnormalities, thrombophilic disorders, chronic health conditions, maternal age and lifestyle factors and psychological factors.

14. Mode of conception

The mode of conception, referring to whether a pregnancy resulted from natural conception or assisted reproductive technologies (ART), can have implications for fetal growth. Various factors associated with ART and fertility treatments may contribute to differences in pregnancy outcomes, including the risk of fetal growth restriction (Ghazi, Spielberger et al. 1991). These factors are multiple pregnancies, preterm birth, advanced maternal age, underlying causes of infertility, ovulation stimulation and hormonal medications, lifestyle, and behavioural factors.

15. Alcohol

Alcohol consumption during pregnancy poses serious risks to fetal development, and one of the potential consequences is fetal growth restriction (Pielage, El Marroun et al. 2023). The key risks associated with alcohol consumption during pregnancy, particularly concerning FGR include: fetal alcohol spectrum disorders (FASDs), impaired placental function, increased risk of preterm birth, neurodevelopmental impairments, low birth weight and organ development issues.

16. Recreational drugs

The use of recreational drugs during pregnancy can pose serious risks to fetal growth and development, including an increased risk of fetal growth restriction. The impact of recreational drugs on pregnancy outcomes varies depending on the specific substance, the timing and frequency of use, and individual factors. Here are some general considerations regarding the risks of recreational drug use on fetal growth:

1. Illicit Drugs and FGR

The use of illicit drugs, such as cocaine, heroin, methamphetamine, and ecstasy, has been associated with an elevated risk of fetal growth restriction. These substances can negatively affect placental function, blood flow, and nutrient delivery to the developing fetus (Currie and Tough 2021).

2. Marijuana and FGR

The use of marijuana during pregnancy is associated with various risks, including an increased likelihood of FGR. Tetrahydrocannabinol (THC), the psychoactive component of marijuana, crosses the placenta and can impact fetal development (Natale, Gustin et al. 2020, Lo, Hedges et al. 2022).

3. Prescription drug abuse

Misuse or abuse of prescription drugs, such as opioids, benzodiazepines, or stimulants, can have adverse effects on fetal growth (Jones and Fielder 2015).

17. GA at birth

The risk of gestational age at birth on FGR is an important consideration, and it's crucial to understand the relationship between these factors.

Preterm birth and low birth weight

Preterm birth is associated with an increased risk of low birth weight, which can be a result of FGR. Preterm infants may not have had sufficient time to achieve their full growth potential in the womb (Hediger, Scholl et al. 1995).

Late-term and post-term pregnancies

Pregnancies that go beyond the due date (post-term) may also have a higher likelihood of complications, including FGR. The placenta's function may decline in post-term pregnancies, potentially affecting fetal growth (Clausson, Cnattingius et al. 1999).

Growth velocity

Beyond gestational age alone, growth velocity or the rate of fetal growth over time is an important factor. Fetal growth should follow a typical trajectory based on gestational age, and deviations from this pattern may indicate FGR.

Intrauterine environment

The intrauterine environment, influenced by factors such as maternal nutrition, health, and placental function, plays a significant role in fetal growth. These factors interact with gestational age to impact fetal development.

Gestational age and placental function

The placenta is a key organ in nutrient and oxygen exchange between the mother and the fetus. As pregnancies progress, changes in placental function may influence fetal growth. Placental insufficiency can lead to FGR.

18. Heavy first trimester vaginal bleeding

Heavy vaginal bleeding in the first trimester of pregnancy can be a concerning symptom and may indicate various underlying issues. While heavy bleeding itself may not directly cause fetal growth restriction (FGR), the potential complications associated with bleeding could indirectly impact the developing fetus.

Threatened miscarriage

Heavy first-trimester bleeding is often associated with threatened miscarriage. While some pregnancies progress successfully. Unfavourable pregnancy outcomes include neonates with low birth weight were reported among pregnancies with threatened miscarriage (Ahmed, El-Sammani Mel et al. 2012).

Subchorionic hematoma

A number of unfavourable obstetric outcomes, including term premature rupture of the membranes and FGR, were linked to the presence, size, and duration of an asymptomatic subchorionic hematoma found between 5 and 10 weeks of gestation (Pan, Lan et al. 2023).

Placental abruption

In rare cases, heavy bleeding in the first trimester may be associated with placental abruption. Placental abruption occurs when the placenta separates from the uterine wall before delivery. This condition can potentially affect fetal oxygen and nutrient supply, impacting growth (Ananth and Williams 2013).

19. Increase nuchal translucency

If there are concerns about fetal growth restriction or other complications, additional assessments and monitoring, such as serial ultrasounds and Doppler studies, may be recommended to evaluate fetal growth and well-being. While an increased NT itself is not a direct risk factor for fetal growth restriction, it serves as an indicator of potential underlying issues that could impact fetal health (Kalem, Ellibeş Kaya et al. 2019).

20. Prior FGR or SGA

Prior fetal growth restriction (FGR) or being born small for gestational age (SGA) in a previous pregnancy can be associated with an increased risk of FGR in subsequent pregnancies. There is a 20% to 30% chance of recurrence for women whose last pregnancy was impacted by FGR (Blue, Page et al. 2021).

Underlying causes

Understanding the underlying causes of FGR or SGA in the prior pregnancy is crucial. Various factors can contribute to restricted fetal growth, including placental insufficiency, maternal health conditions (such as hypertension or diabetes), and genetic factors. Identifying and addressing these factors is important for managing the risk in subsequent pregnancies.

Placental health

FGR is often linked to issues with the placenta, such as insufficient blood flow or impaired nutrient exchange. Placental health is a critical factor in fetal development, and problems in a previous pregnancy may indicate a potential risk in subsequent pregnancies.

Maternal health

Maternal health plays a significant role in fetal growth. Conditions such as chronic hypertension, diabetes, or certain autoimmune disorders can contribute to FGR.

Managing and optimizing maternal health is essential for reducing the risk in subsequent pregnancies.

21. Paternal or maternal SGA

SGA can result from a variety of factors, including genetic and environmental influences. If either the father or the mother was born SGA, it may influence the risk of fetal growth restriction (FGR) in subsequent pregnancies.

Maternal SGA

Growth-restricted mothers are twice as likely to give birth to FGR babies (Chew LC 2023). This could be associated with factors affecting placental function or nutrient exchange, potentially influencing fetal growth in subsequent pregnancies. Maternal SGA may be linked to underlying health conditions that affect reproductive health. Conditions such as chronic hypertension, diabetes, or certain autoimmune disorders can impact both maternal health and fetal development (Sharma, Shastri et al. 2016). There may be genetic factors contributing to both the mother's SGA status and the risk of FGR in subsequent pregnancies. Genetic factors can influence how the placenta functions and how nutrients are transported to the developing fetus (Sharma, Shastri et al. 2016).

Paternal SGA

Negative birth outcomes were substantially correlated with the risk factors of paternity, which included age, race/ethnicity, and educational attainment. Compared to the matching maternal risk factors, these paternal risk factors were more accurate in predicting low birth weight (Meng and Groth 2018).

22. Malformations

Fetal growth restriction and congenital malformations are distinct but can sometimes be associated with each other. Although weak, there appears to be a correlation between birth weight and congenital abnormalities (Puccio, Giuffré et al. 2013).

Fetuses whose (EDD) varies between the measurement made by the last menstrual cycle and the measurement made by second-trimester ultrasonography appear to be more susceptible to congenital abnormalities, such as chromosomal abnormalities (Nikkilä, Källén et al. 2007).

23. Placental insufficiency

FGR can result from placental insufficiency, where the placenta is unable to provide sufficient oxygen and nutrients to support normal fetal growth. Severe placental insufficiency can potentially contribute to both FGR and malformations.

Common underlying causes

Some underlying causes or risk factors may be shared between FGR and congenital malformations. For example, genetic factors, environmental exposures, or maternal health conditions can impact both fetal growth and organ development.

Chromosomal abnormalities

Certain chromosomal abnormalities can be associated with both FGR and congenital malformations. For instance, trisomies (such as Down syndrome) can affect both fetal growth and lead to structural abnormalities.

Teratogenic exposures

Exposure to teratogens (substances that can cause birth defects) during critical periods of fetal development can contribute to malformations. Depending on the timing of exposure, teratogens may also impact fetal growth.

Genetic syndromes

Some genetic syndromes involve both growth-related issues and congenital malformations. These syndromes often have a genetic basis and can affect various aspects of fetal development.

Maternal health

Maternal health conditions, such as poorly controlled diabetes or certain infections during pregnancy, can increase the risk of both FGR and congenital malformations.

Uteroplacental blood flow

Inadequate blood flow to the uterus and placenta can contribute to FGR and may also affect organ development, potentially leading to malformations.

24. Folic acid

It is well-known that folic acid supplementation during the first trimester of pregnancy decreases the likelihood of fetal growth abnormalities (Damodaram, Story et al. 2010). However, recently, it has been found that continuous folic acid supplementation beyond the first trimester can be associated with decreased SGA rate (Wallace, Bhattacharya et al. 2013).

25. Smoking

Smoking renders a severe effect on the growth of the placenta and the fetus. It has been found that the SGA and perinatal mortality rate doubled in smoker mothers (Hayward, Lean et al. 2016) (Marcos, Semelka et al. 1997). The primary mechanism behind it is still under debate; however, placental infarction was noticed in SGA smokers' placentas (Bonel, Stolz et al. 2010). Interestingly smokers' placentas expressed two significant abnormalities. The first placental weight to fetal birth weight ratio was larger in the smoker's placentas than in the controls. This concludes the fact that the placenta compensates for fetal hypoxia by increasing its tissue mass. Secondly, smokers often deliver earlier than non-smokers, which results in fetal prematurity with its accompanied complications (Marcos, Semelka et al. 1997).

26. Heavy metals exposure

Fetal growth abnormalities have been linked to metal exposure (Baker, Johnson et al. 1994). Cadmium raises the risk of FGR while selenium and zinc render a protective effect (Derwig, Lythgoe et al. 2013).

27. Socioeconomic and geographical distribution

Poor areas with low socioeconomic status have a higher rate of abnormal fetal growth development (Mifsud and Sebire 2014). Hence within the same community, fetal growth is primarily influenced by factors other than ethnicity and infectious diseases. The explanation can partly be attributed to the fact that maternal access to essential life sources is difficult in these areas as well as the biological, and environmental differences (Mifsud and Sebire 2014).

Diagnosis of FGR

Ultrasound of the placenta in FGR

Pregnant women may have multiple risk factors that increase their susceptibility to having an underdeveloped baby. These can be classified into pre-pregnancy modifiable and non-modifiable risk factors as well as obstetric risk factors. The advantages of identifying risks might increase the effectiveness of screening for FGR (Monier, Blondel et al. 2016). Reported US detection rate range from 40% to 60% for cases with moderate to severe fetal growth abnormalities respectively, a large portion of those detected are confirmed postnatally as physiologic or constitutionally small fetuses and not true FGR (Monier, Blondel et al. 2016). By assessing signs of placental malfunction, it may be possible to differentiate constitutionally small-for-date fetuses from real restricted ones (Nardozza, Caetano et al. 2017).

As most cases of placental insufficiency present late in gestation, the first and most effective diagnostic indicator is the abdominal circumference (AC) (Sovio, White et al. 2015). This is mainly due to the reduction in liver size as part of the adaptation mechanism. When the third trimester expected fetal weight (EFW) is less than the 10th percentile, FGR should be suspected (Sovio, White et al. 2015). FGR caused by placental insufficiency can be diagnosed using Doppler US velocity parameters, for instance, measuring arterial resistance pulsatility index (PI) in particular central and peripheral vessels (Sharma, Shastri et al. 2016). It is thought that changes in these arteries are sequential. Earlier changes in velocity parameters occur in the peripheral arteries (uterine artery, umbilical artery and middle cerebral artery), while central arteries (ductus venous and aortic isthmus) express abnormalities later in gestation (Ferrazzi, Bozzo et al. 2002). However, uterine artery perfusion is found to be influenced by maternal demographic factors such as age, BMI, smoking, parity, as well as gestational age which may affect the accuracy (Hafner, Metzenbauer et al. 2001). Uterine artery Doppler gives an inadequate prediction for screening FGR Pregnancies (Andescavage, duPlessis et al. 2017). While more than half of FGR pregnancies delivered less than 34 weeks have positive uterine artery Doppler (UtAD) findings, this percentage decreased to just 24% for deliveries of FGR at or more than 34 weeks (Nardozza, Caetano et al. 2017). Unlike the uterine artery pulsatility index (PI), maternal variables may have no effect on the placental volume (Hafner, Metzenbauer et al. 2001). Placental volume has been widely used as a screening indicator for

placental insufficiency. It constitutes an indirect predictor of how well the placenta invades the uterus. A first-trimester US examination of pregnant women using both vascular indices and placental volume increased the efficacy of detecting FGR. However, these models have low sensitivity in clinical practice (Gonzalez-Gonzalez, Gonzalez-Davila et al. 2017). Second trimester 3D US is usually performed at 22-24 weeks as a routine antenatal assessment to detect FGR and preeclampsia. Increased PI as a result of high arterial resistance is a useful measure (Hafner, Metzenbauer et al. 2006). Since FGR is a serious problem, many wish to identify an earlier effective diagnostic tool. 3D Doppler US was not effective in diagnosing FGR in the first trimester. Several studies have concluded that placental volume and uterine artery PI in the first trimester are not useful. The sensitivity was 27% vs 28% for both measures respectively (Soongsatitanon and Phupong 2018).

Placental quotient (PQ) is a recently designed measure using 3D US. It can diagnose FGR as early as in the first trimester 11-13 weeks of gestation (Hafner, Metzenbauer et al. 2006). It provides an important evaluation, which is equivalent to placental perfusion but at a much earlier date. Usually, uterine artery PI can detect abnormalities in the 22nd week of gestation. PQ is calculated by dividing the value of placental volume on a given fetal size, i.e., crown-rump length (CRL) (Metzenbauer, Hafner et al. 2001). In addition to earlier detection, PQ has been reported to have a higher sensitivity compared to uterine artery PI measured in the second trimester (Hafner, Metzenbauer et al. 2006). However, another study has reported that this measurement is mainly ineffective (Soongsatitanon and Phupong 2018). A combined study of both placental volume and functional placental study has been proposed to raise the sensitivity of the FGR screening rate (Hafner, Metzenbauer et al. 2006).

US is not accurate enough for the diagnosis of FGR. In the UK, the routinely applied imaging protocol does not include ultrasound screening during the third trimester. Further assessment commences when the pregnant woman presents with risk factors or pregnancy complications (Monier, Blondel et al. 2015). Excessive US screening has been shown to raise the FGR detection rate. In a study that compared women who had the US in their third trimester with those who did not, approximately 2% of growth-restricted fetuses have been found in the non-SGA proportions. However, several studies have shown that a third trimester US increases the rate of iatrogenic complications, including maternal anxiety, higher rates of caesarean sections as well as higher admission rate into neonatal care units (Monier, Blondel et al. 2015).

Current diagnostic tools are insufficient to diagnose placental defects. Fetal Doppler has confounding limitations in assessing fetal growth. This has been mainly encountered in late gestational diabetes cases where umbilical artery Doppler is often normal in diabetic women diagnosed in their third trimester. The reason behind this is the physiological compensation of ductus venousus that tend to shunt blood to spare vital fetal organs as each fetus expresses its growth potentials, which is governed by parental and fetal factors. It is still challenging to reach a consensus on specified fetal growth velocity for each gestational age (Macara, Kingdom et al. 1996). The findings on fetal Doppler US can be categorized according to gestational age: first trimester Doppler can detect early fetal anomalies when CRL is abnormal. While second trimester Doppler has a false predictive ratio affected by ethnicity as the abdominal circumference is falsely influenced by the effect of genetic factors on free fat mass. For example, fetuses of south Asian origin usually have a smaller body size, estimated weight, and abdominal circumference but they have higher free fat mass in comparison with fetuses of European descent (Macara, Kingdom et al. 1996). On the other hand, European fetuses grow in a faster trend and show a smaller size in contrast with non GDM pregnancies. As a result, the abdominal circumference is not a useful predictor in assessing fetal growth in Asian and European diabetic mothers. In summary, US needs an adjuvant tool that aids in giving the final decision regarding diagnosis of FGR, especially in high-risk pregnancies.

MRI of the placenta in FGR

Fetal MRI is established in clinical practice. However, there has been little interest in using MRI technology to investigate the placenta. Utilizing MRI along with US has several advantages in clinical practice. 3D US provides a cheap, rapid, and widely available instrument that assesses fetal and placental wellbeing. However, certain drawbacks are associated with the use of the US. The images have low contrast resolution, which is necessary to differentiate between the placental basal plate and the uterus. As a result, US has limitations in some cases where the measurement of placental volume is needed. It also has a narrow field of view mainly in the second trimester and beyond (Leon, Li et al. 2018). Furthermore, US has poor imaging quality in cases of maternal obesity, abnormal amniotic fluid volume and posterior placenta

(Andescavage, du Plessis et al. 2015). MRI, on the other hand, can diagnose fetal and placental abnormalities accurately and may help detect the onset and mechanism of placental insufficiency (Andescavage, duPlessis et al. 2017). Doppler US can identify abnormalities in placental perfusion indirectly by measuring vascular resistance to flow which is called the pulsatility index (Andescavage, Yarish et al. 2015). MRI, however, assesses placental tissue without the need for a contrast medium. Several MRI advanced techniques have been developed providing better resolution to reduce artefacts caused by maternal and fetal motion. These limitations have previously hampered MRI studies (Do, Lewis et al. 2019).

Usually, the placenta at (19-23) weeks appears as a homogenous structure with higher signal intensity on T2 than on T1. While at (24-31) weeks, the placenta becomes more lobulated which results in higher heterogeneity on MRI due to the development of septa (Allen and Leyendecker 2013).

Accurate MRI detection of placental abnormality can provide further insight into the mechanism and onset of FGR and hence may prevent further fetal growth damage (Leon, Li et al. 2018). Leon et al. suggested that MRI detection of placental morphological features such as volume may provide a hint into fetal growth abnormalities. This study observed healthy pregnancies of 112 retrospective cases. It used two MRI scans for placental sequencing which were either Half-Fourier acquisition single-shot fast spin-echo (SSFE) or balanced steady-state free precession (SSFP) gradient echo sequence. The results revealed a positive correlation of placental volume with gestational age and confirmed what Damodaram et al. suggested in previous work. However, Damodaram et al. study was more extensive, as it addressed for the first time different placental morphological features. It concluded that an insufficient placenta has different morphology that differentiates healthy from growth-restricted fetuses, and this correlates directly with the degree of severity (Damodaram, Story et al. 2010).

Moreover, the volume of the placenta runs parallel to fetal weight and gestational age and can only be accurately measured by MRI (Leon, Li et al. 2018). Damodaram et al. evaluated 20 cases with FGR suspicion included in a prospective study, along with 28 controls. MRI scanning was performed only once at different gestational age. In this study, there was a long gap between antenatal and postnatal pathology assessment. Additionally, some cases did not undergo a histological examination to confirm the diagnosis. Studies have found that many factors may influence birth weight and

placental weight. Multiparty, fetal gender, maternal diabetes, and congenital heart diseases have been associated with placentas that have a larger volume than average (Andescavage, Yarish et al. 2015) (Wallace, Bhattacharya et al. 2013, Hayward, Lean et al. 2016).

Leon et al., on their cross-sectional study, suggested that maternal age, BMI, hypertension, and diabetes do not appear to affect placental volume; however, they only had 8 cases with DM and 12 cases with hypertension. Furthermore, their study was retrospective; in approximately 18% of cases medical records were not available to access, and significant data was missing regarding their disease treatment control and fetal growth outcome (Leon, Li et al. 2018).

MRI is needed over other imaging modalities as it is a safe, efficient modality that investigates the placenta in vivo. Other modalities including Doppler USS are unable to assess the changes in placental structure and function due to multiple limitations. Doppler imaging can measure placental and fetal Doppler blood flow that changes secondary to fetal hypoxia. Also, USS-measured estimated fetal weight and small growth trajectories such as abdominal circumference, don't always differentiate between pathological FGR and constitutional SGA (Figueras, Caradeux et al. 2018). There are growth charts that are not customised for specific populations to reflect their normal growth potentials. These are indirect techniques that assess fetal growth and placental function (Aughwane, Mufti et al. 2021). There have been 2/3 of cases of stillbirth in the UK that are undiagnosed (Maternal and Health 2009). Cases of FGR especially those are resulted from placental insufficiency can occur even in cases with AGA. This is because in late FGR, hypoxia or reduced nutrition due to placental insufficiency could pass on to stillbirth without having obvious abnormality using the currently available diagnostic techniques. Using MRI scan have the potential to detect smaller placentas in FGR cases which could offer earlier and accurate diagnosis (Damodaram, Story et al. 2012).

MRI has the advantage of detecting many changes in fetal organs parallel to placental abnormality. For instance, an MRI study of fetal brain volume and placental volume beyond the first trimester revealed a marked decrease in cases with SGA (Andescavage, duPlessis et al. 2017). It has been reported that placental volume is 120 cm^3 lower than the average for the same GA and uterine artery PI is 1.87 ml higher in cases with SGA. This is an impression of diminished placental perfusion as a cause or may indicate how and when FGR has developed in utero (Andescavage, duPlessis

et al. 2017). In their prospective cohort study, 114 women were collected including 35 FGR cases and 79 healthy controls. Cohorts had two longitudinal MRI scans in the second and third trimesters; Andescavage et al. were able to identify only moderate placental morphological changes in comparison with healthy controls. However, 50% of the cases diagnosed with SGA antenatally were born AGA. This confirms the need for an ongoing follow-up which may detect any fetal neurological defect to confirm FGR diagnosis. Also, the placental histological assessment was not performed which is necessary to identify any pathological tissue.

There are no large studies examining MRI and placenta, the available data are either on PAS or placental perfusion. However, the correlation and complementary findings are listed below.

Correlation:

1. Structural assessment

MRI allows for detailed structural assessment of the placenta, including evaluation of size, shape, and vasculature. Correlations have been reported between MRI findings and histopathological examinations of the placenta.

2. Blood flow and perfusion:

Functional MRI techniques, such as dynamic contrast-enhanced MRI, can provide information about blood flow and perfusion in the placenta. These parameters may correlate with measures of placental function and fetal well-being.

3. Placental abnormalities

MRI has been used to identify and characterize placental abnormalities, such as infarctions, haemorrhages, and lesions. Correlations between MRI-detected abnormalities and clinical outcomes have been explored.

Complementary information:

1. Functional insights

MRI can provide functional information about the placenta, such as perfusion, oxygenation, and diffusion. This complements the structural information obtained from

other imaging modalities and may offer insights into the dynamic aspects of placental function.

2. Non-invasive evaluation:

MRI is a non-invasive imaging technique, and its use in assessing the placenta allows for detailed evaluations without the need for invasive procedures. This can be particularly valuable in monitoring high-risk pregnancies.

3. Whole-placenta assessment:

MRI enables the visualization of the entire placenta in three dimensions. This comprehensive view can be beneficial in identifying abnormalities throughout the entire organ.

4. Monitoring changes over time:

Serial MRI scans during pregnancy can track changes in placental structure and function over time, providing a dynamic assessment of placental health.

5. Quantitative measures:

Quantitative MRI parameters, such as relaxation times and diffusion coefficients, can be analysed to derive numerical metrics related to placental function. These measures can be valuable for research and clinical purposes.

While MRI and placental findings can concur, the use of MRI is often considered in conjunction with other diagnostic methods, such as ultrasound and clinical assessments. The integration of multiple modalities allows for a more comprehensive understanding of placental health and fetal well-being.

A normally growing placenta is similar to a flat disc in shape with two tapered ends. It is larger in surface area and size than underdeveloped placenta (Damodaram, Story et al. 2010, Andescavage, Dahdouh et al. 2019). FGR placentas resemble a globular structure with an increase in thickness in comparison to volume. Which can be referred to as placental thickness-to-volume ratio; the ratio has proved to be significantly increased in cases of placental insufficiency (Damodaram, Story et al. 2010). The shape of the placenta tends to be normal in later onset FGR cases, while the volume is defective in all growth-restricted cases (Andescavage, Dahdouh et al. 2019). This may provide an essential significance in the timing of FGR incidence. Andescavage et al. findings were novel in describing the relation of placental textural and morphological changes with FGR. The study included 66 pregnant women for MRI imaging, but only

10 cases had longitudinal MRI imaging. In addition to that, no histological examination was conducted. Several risks for FGR mean that further research is warranted. We suggest including larger homogenous samples (200 cases), specifying risk factors for placental insufficiency (Diabetes, SGA, and FGR) and conducting the postnatal histological study. This can help to detect microstructural changes and more considerable specific results that may support Andescavage et al. findings.

The developing placenta reveals an increase in heterogeneity with advanced gestation. Heterogeneity has been observed on T2 MRI of abnormal growing placentas compared to controls in a retrospective study of 112 cases (Sharma, Shastri et al. 2016, Leon, Li et al. 2018, Do, Lewis et al. 2019). However, another study showed that FGR placentas have homogenous signals (Andescavage, Dahdouh et al. 2019). An assessment of placental morphology, i.e., shape, and texture (how smooth or coarse it is), has also received little attention in the current literature, especially in association with FGR. No existing studies are focusing on the obstetric risk factors such as diabetes and its effect on the placental texture and morphology.

Contrast media is contraindicated in pregnancy, and this has led to the development of new MRI sequences. In 1997, Marcos et al. studied the standard appearance of the placenta using gadolinium contrast media. The aim was to obtain a basic understanding of how to diagnose earlier placental insufficiency (Marcos, Semelka et al. 1997). The clinical application of this was limited as gadolinium use is contraindicated in pregnancy. Consequently, new modalities have been developed such as diffusion-weighted MR imaging (DW MRI) and T2*. Using MRI, along with the US, has raised the sensitivity of placental insufficiency detection from 73% to 100% and specificity from 90% to 99% reported in one study (Bonel, Stolz et al. 2010). The functional characteristics of the placenta have been observed using MRI. This study has assessed ADC (apparent diffusion coefficient) and placental morphology in terms of hypertrophy, infarction, or haemorrhage. It has also compared MRI results with US data. Results showed that the US diagnosis of fetal growth abnormalities is considered normal in some instances that reveal growth abnormalities using MRI. However, placental morphological assessment was not detailed enough to diagnose growth abnormalities (Bonel, Stolz et al. 2010).

The placenta can appear in many forms, for example, very flat with tapered ends (pancake), (Fig 30a), medium thickness with two tapered ends (crumpet), (Fig 30b), or globular (cupcake); (Fig.30c). This highlights an important issue concerning placental volume measurement when various placental forms can give the same volumetric value as the volume represents the result of total three-dimensional measurements. Similar volume numbers are not always the same, and hence other morphology characteristics have to be studied together. The majority of work relates to placental volume or placenta weight at delivery and neglects the shape of the placenta.

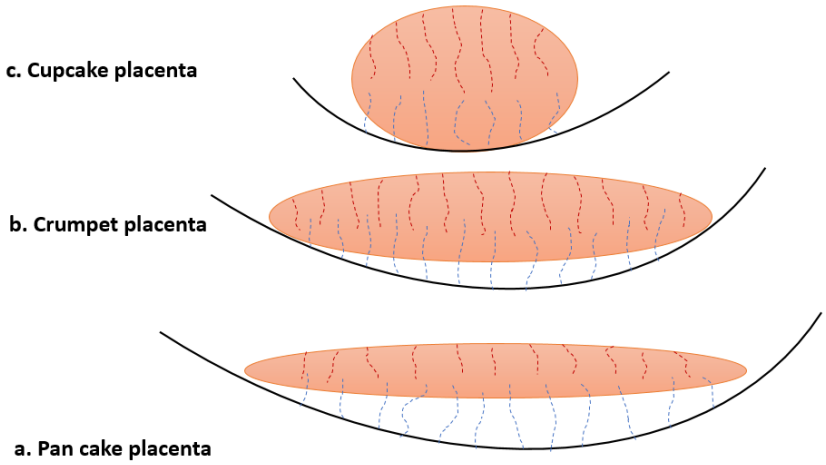

Figure 30 Shows three basic placental shapes; note that the average volume in all three plots is similar.

The hypothesis of this research relies on the believe that the placental surface area of attachment is an essential determinant of function, which means that a specific area of attachment has to be measured alongside with placental volume and midpoint thickness. The mean placental area measured by MRI has been referred to in a single published paper, which was 2.67*104 mm^2 (Sd=9.6 $\times 10^3$) in normal placentas and 1.62 × 104 (7.1 × 10^3) in insufficient placentas with GA <30 weeks in 11 fetuses and >30 weeks in 14 fetuses (Ohgiya, Nobusawa et al. 2016). Placentas with smaller surface areas as in the globular placenta might be pathological due to the lower

surface area for feto-maternal exchange. Similarly, pancake placentas might have a larger surface attachment area, but their thickness will be compromised. We also hypothesize that in FGR placentas, the blood supply is disrupted and T2* values could be reduced. Therefore, we sort to try and predict placental changes on T2* values.

2.2 A systematic review of placental morphology on MRI in normal cases and cases of fetal growth restriction (FGR)

Introduction

Placental insufficiency affects 5-7% of pregnancies (Leon, Li et al. 2018). Fetal growth restriction (FGR) is a serious complication, which has many drawbacks to the fetus. Several studies have used MRI to detect specific placental features present in restricted fetuses including abnormal volume, thickness and surface attachment. Literature suggests that low volume may indicate a poor outcome (Stables D 2010) or low birth weight (Gude, Roberts et al. 2004) however, there is no current consensus. We conducted a literature review to assess if there were any trends or more conclusive data in recent literature. The systematic review aims to identify papers where the morphology of the placenta was studied and the consensus of opinion across the published data.

Materials and Methods

A systematic search was performed by myself and checked by a further student using two database systems. PubMed, May 2009-May 2019. Web of science database in August 2019 (May 2009-Aug 2019) to identify any additional relevant papers. Search terms 'MRI of the placenta' and 'fetal growth restriction.' The inclusion criteria were all the English studies published during the last ten years (MRI is a new technology that has rapidly developed over the last 20 years and has only recently been employed for imaging in pregnancy, in fact its use is still very limited to specialist centres. Any data over 10 years old is unlikely to be of sufficient quality to be useful).

Reviews, case reports, and animal studies were excluded. Following that, a comprehensive review was conducted by reading abstracts to exclude irrelevant articles. The final group of included articles was under the title of placental morphology (table 10).

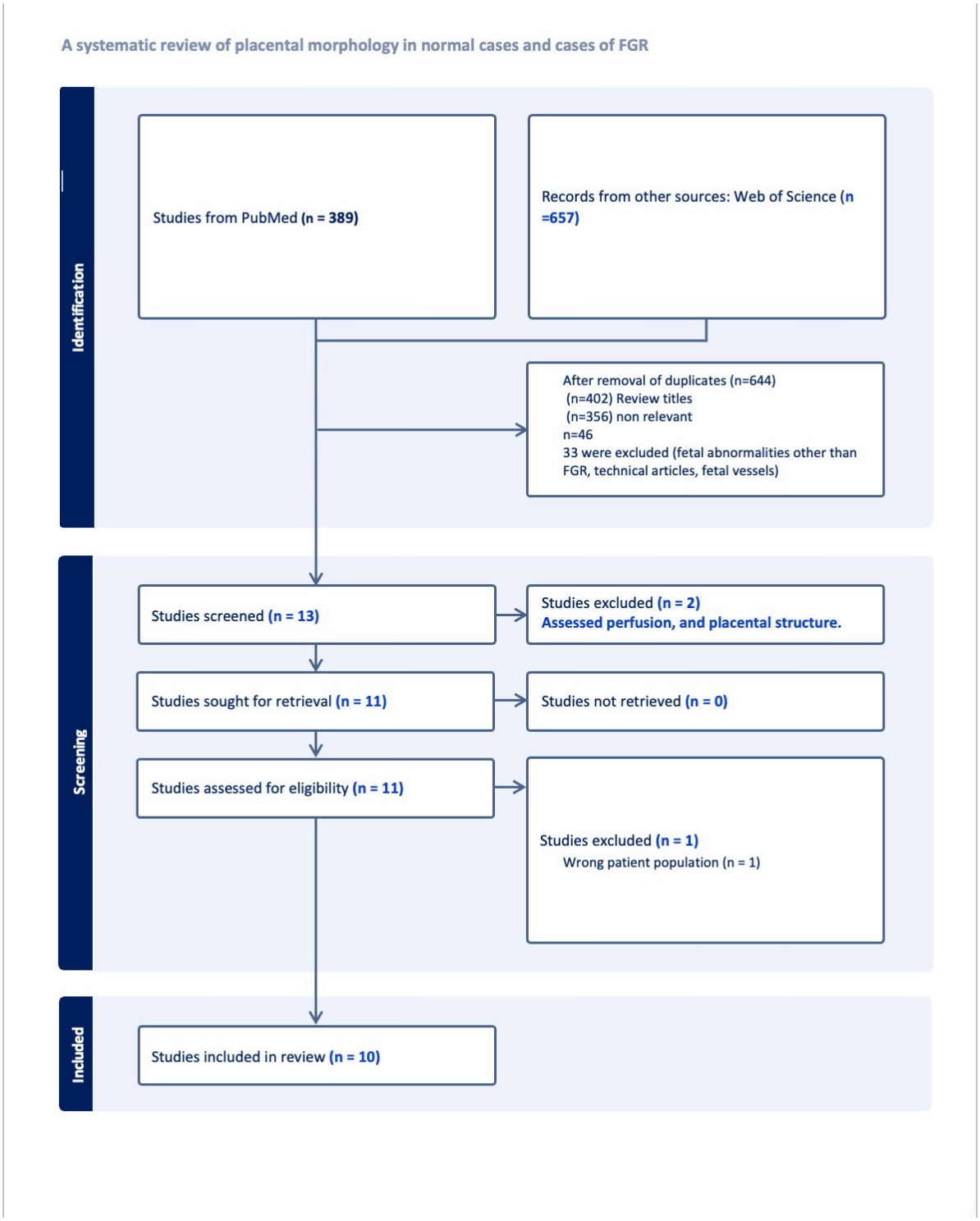

Table 10 Prisma flow diagram of MRI based placental morphometry.

Results

Pub Med search total number of papers obtained was 389 papers on placental MRI. While the Web of Science search was 657 studies. Following the exclusion of duplicates and non-relevant reviews, 33 out of 46 articles were excluded as they were

on either placental adhesive disorders or placental function. Only 13 studies were included for further in-depth reading and investigation. 3 papers were excluded as they looked at placental perfusion and structure rather than morphology. The final number of papers about placental morphology in controls and FGR was 10.
Quality assessment was conducted by two reviewers (PhD student and an experienced radiologist) for the current knowledge on placental morphology (table 11) where the risk was either low, high, or unclear.
A meta-analysis was deemed inappropriate due to the heterogeneity of the papers and therefore was not performed.

The risk of bias was assessed using Covidence template and included the following domains:

1. Bias arising in the randomization process or due to confounding factors
2. Bias in the selection of participants into the study
3. Bias in classification of interventions for all outcomes
4. Bias due to departures from intended interventions for all outcomes
5. Bias due to deviations from intended interventions for all outcomes
6. Bias due to missing data for all outcomes
7. Bias in the measurement of outcomes
8. Bias in reporting outcomes selectively
9. Bias in the selection of the reported result

- Papers were highly biased for the randomization process as their controls and FGR groups were not blinded in the reviewed studies.
- Andescavage et al. 2015 was scored high by both reviewers for bias in the selection of participant into the study because the groups were known to the person measuring the placenta.
- Damodaram et al. 2010 was also scored high for the selection of participant as there was a small GA range of FGR cases.
- Shapira-Zaltsberg et al. 2018 and Andescavage et al. 2015 were both highly biased for the selection of participants as they compared controls and fetusus with CNS abnormalities and CHD respectively.

Study Id	Reviewer	Bias arising in the randomization process or due to confounding factors		Bias due to departures from intended interventions for all outcomes	Bias due to deviations from intended interventions for all outcomes	Bias due to missing data for all outcomes	Bias in classification of interventions for all outcomes		Bias in measurement of outcomes	Bias in reporting outcomes selectively	Bias in selection of participants into the study		Bias in selection of the reported result
		Judgement	Comments	Judgement	Judgement	Judgement	Judgement	Comments	Judgement	Judgement	Judgement	Comments	Judgement
Derwig 2011	1	low		low	low	low	low		low	low	low		low
Derwig 2011	2	high		low	low	low	low		low	low	low		low
Derwig 2011	Consensus	high		low	low	low	low		low	low	low		low
Andescavage 2017	1	high		low	low	low	low		low	low	high		low
Andescavage 2017	2	high		low	low	low	low		low	low	low		low
Andescavage 2017	Consensus	high		low	low	low	low		low	low			low
Andescavage 2015	1	high		low	low	low	low	no intervention as such , all cases were measured the same	low	low	high	Pre-selected so the group was known to the person measuring the placenta	low
Andescavage 2015	2	high		low	low	low	low		low	low	high		low
Andescavage 2015	Consensus	high		low	low	low	low		low	low	high		low
Ohgiya 2016	1	high		low	low	low	low		low	low	high		low
Ohgiya 2016	2	high		low	low	low	low		low	low	low		low
Ohgiya 2016	Consensus	high		low	low	low	low		low	low			low
Leon 2018	1	low		low	low	low	low		low	low	low		low
Leon 2018	2	high		low	low	low	low		low	low	low		low
Leon 2018	Consensus	low		low	low	low	low		low	low	low		low
Langhoff 2017	1	low		low	low	low	low		low	low	low		low
Langhoff 2017	2	high		low	low	low	low		low	low	low		low
Langhoff 2017	Consensus	low		low	low	low	low		low	low	low		low
Victoria 2011	1	low		low	low	low	low		low	low	low		low
Victoria 2011	2	high		low	low	low	low		low	low	low		low
Victoria 2011	Consensus	low		low	low	low	low		low	low	low		low
Damodaram 2010	1	high	also small GA range of IUGR cases	low	low	low	low		low	low	high	small GA range	low
Damodaram 2010	2	high		low	low	low	low		low	low	low		low
Damodaram 2010	Consensus	high		low	low	low	low		low	low	high		low
Andescavage 2019	1	high		low	low	low	low		low	low	high		low
Andescavage 2019	2	high		low	low	low	low		low	low	low		low
Andescavage 2019	Consensus	high		low	low	low	low		low	low			low
Shapira-Zaltsberg 2018	1	high		low	low	low	low		low	low	high		low
Shapira-Zaltsberg 2018	2	high		low	low	low	low		low	low	high		low
Shapira-Zaltsberg 2018	Consensus	high		low	low	low	low		low	low	high		low

Table 11 Quality assessment of placental morphometry reviewed in the literature

The diagram (Fig. 31) shows the results of the systematic search according to the assessment of different placental morphological features. Note some papers included more than one morphological feature e.g. both volume and surface area.

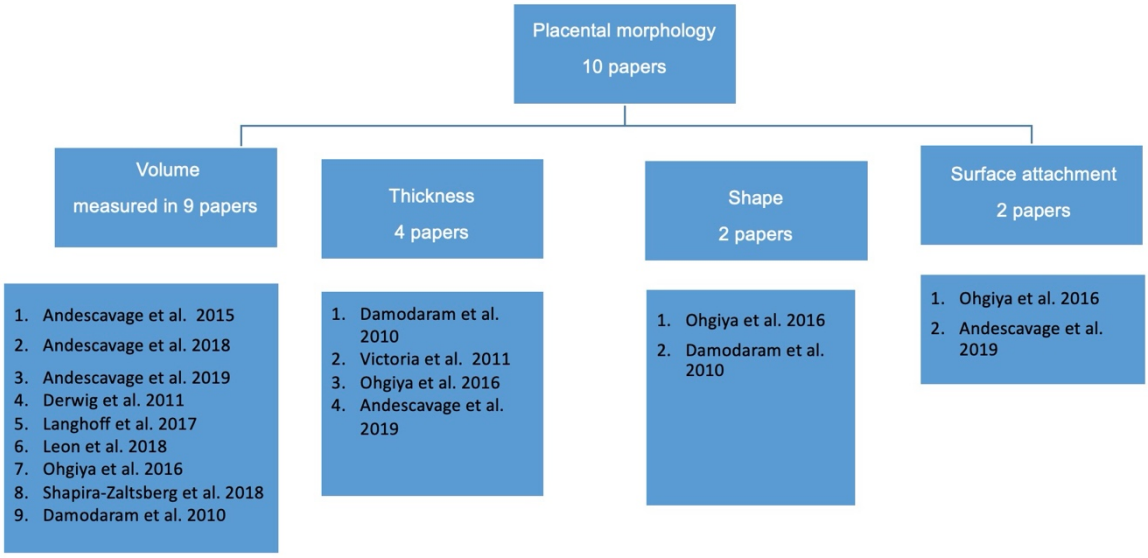

Figure 31 Diagram of placental morphology features (volume, thickness, shape and surface attachment) mentioned in the reviewed papers. Note that some papers reported more than one feature.

The outcome of this search has been summarised according to our targeted placental measures that were covered in previous literature:

1. Volume

Placental volume was measured in several research studies. Nine papers reviewed had placental volumetric outcomes. As clarified in table 12, placental volume increases exponentially with fetal growth (Derwig, Akolekar et al. 2011, Andescavage, Yarish et al. 2015, Langhoff, Gronbeck et al. 2017, Leon, Li et al. 2018). Normal placental volume reference values were scattered among different papers. The available normal reference values collected from different references can be seen in table 13. Most studies did not scan cases longitudinally, only Langhoff et al. reported longitudinal changes in normal volume values. In their study, 20 participants underwent seven MRI scans during the second and third trimesters (Langhoff, Gronbeck et al. 2017).

Published data has failed to address abnormal cases to assess any pathological relationship. Leon et al. examined normal retrospective placental volume; however, they did not consider other morphological features (Leon, Li et al. 2018).

It is worth mentioning that the methods used were heterogeneous among studies. Ohgiya et al. proposed a specially designed equation to calculate placental volume based on 50 retrospective cases (Ohgiya, Nobusawa et al. 2016). Andescavage et al. used IT-KSNAP to manually segment the placenta and calculated the volume. Derwig et al. used EasyMeasure software to measure the placental volume in a stereological approach. Leon et al. used another software (Philips Intellispace Tumor Tracking Tool) to draw the placental ROI and measure volume based on slice thickness. Langhoff et al. used software developed for cardiovascular assessment which was not very effective in segmenting the placenta and then manually measured and calculated placental volume. Damodaram et al. used ImageJ to manually sketch the region of interest on each slice with placental tissue present to determine placental volume. Shapira-Zaltsberg et al. used "Functool" software by which the placenta and fetus were manually delineated on sequential pictures in the sagittal plane, and volumes were estimated. The variety of methods and approaches in these studies highlights the ongoing exploration and development of techniques for placental volume measurement, each with its strengths and limitations and potential applications in medical research and practice. Limitations included a delay in placental histological assessment.

Fetal pathology may or may not affect the placenta but it has been shown that there was no difference in fetal and placental volumes between groups with and without fetal CNS disorders but placentas from fetuses with CNS disorders have a slower rise in fetal to placental volume ratio with GA (Shapira-Zaltsberg, Grynspan et al. 2018).

Andescavage et al. performed three pieces of research measuring placental volume. The first one showed a significant correlation of volume with an increment in gestational age in fetuses with congenital heart diseases (CHD) (Andescavage, Yarish et al. 2015). The cohort did not include cases with placental insufficiency or high-risk pregnancies to form a comparable data set. In addition, volume results showed no significant results in cases with and without CHD ($p=0.134$). In the second paper, Andescavage et al. compared the placental volume of both FGR placentas and controls (Andescavage, duPlessis et al. 2017). However, the analysis did not consider the other morphological features, which can be abnormal. Placental volume in both

groups increased with gestational age. FGR group had a considerably reduced median placental volume (414.3 vs 581.2 cm^3) than the controls when adjusted for GA.

In their third study, Andescavage et al. employed a comprehensive approach, combining both morphometric and textural analysis techniques to examine structural changes in the placenta throughout pregnancy. The inclusion of both healthy pregnancies and those complicated by FGR allowed for comparative analysis, aiming to identify features that may serve as indicators of placental insufficiency. The finding showed that placentas undergo significant increases in size during the study period and that signal intensity remains relatively constant suggests that the study is tracking dynamic changes in placental structure (Andescavage, Dahdouh et al. 2019).

Damodaram et al. showed a significant association between volume and growth restriction in a small sample size, which included 20 cases of FGR that had a single MRI scan (Damodaram, Story et al. 2010).

Overall, it appears that the placenta increases in volume with increasing GA but little is known on the differences of normal and FGR placenta volume.

2. Thickness

This can be abnormal as in the case of the globular placenta (Damodaram, Story et al. 2010). The incremental increase in thickness has been linked with fetal pathologies such as chromosomal anomalies, and maternal diabetes. However, no single paper addressed the question of why diabetes placentas may result in large for dates babies or abnormally grown infants. Research measuring placental thickness had little coverage. Four studies in this review have included placental thickness. The normal measured values reported within the second trimester are (2.4 ± 0.8) cm, and (3.3 ±0.6) cm in the third-trimester (Victoria, Johnson et al. 2011).

Research on placental thickness was retrospective (Victoria, Johnson et al. 2011, Ohgiya, Nobusawa et al. 2016) and prospective (Damodaram, Story et al. 2010, Andescavage, Dahdouh et al. 2019). Ohigiya et al. concluded different values for median placental thickness in normal and insufficient placentas, 36.9mm and 49 mm respectively. The study was for 50 comparable groups of normal controls and FGR. Interestingly the accuracy of placental insufficiency diagnosis was higher when

combining thickness with the decrease in flow voids (FVs) than assessing thickness alone (Ohgiya, Nobusawa et al. 2016). Victoria et al. (Victoria, Johnson et al. 2011) reported normal cases only, missing any pathological correlation with placental thickness. Whilst Damodaram et al. (Damodaram, Story et al. 2010) found a significant increase in placental thickness to volume ratio in growth-restricted placentas, but they failed to assess thickness and placental surface attachment**.**

Overall placental thickness appears to have some sort of relationship to pathology including FGR.

3. Shape

The placental shape also had little coverage in literature, with only two papers mentioned the relation with fetal growth abnormalities. It is important to note that placental volume alone may correlate with fetal growth assessment but can be affected by other co-existing pathologies for example large placentas can result from diabetes pregnancies that also have fetal growth abnormalities.

Two pieces of research mentioned globular placentas in cases of fetal growth abnormalities (Damodaram, Story et al. 2010, Ohgiya, Nobusawa et al. 2016). The shape can be disturbed as a result of changes in thickness or surface attachment. Ideally all aspects of morphology need to be combined in any study to assess the correlation of placenta morphology and pathological fetal growth.

4. Surface attachment

Only two papers in the review included the surface area of attachment (Ohgiya, Nobusawa et al. 2016, Andescavage, Dahdouh et al. 2019). Surface attachment (SA) is reported to be decreased in placental insufficiency. Ohigiya et al. described the area of the maximum transverse diameter of the placenta at the midpoint of thickness, which was then used to calculate the total placental area (Ohgiya, Nobusawa et al. 2016) but did not measure this directly. The normal average diameter of surface attachment has been measured and reported using ultrasound as (16 to 20) cm (Barker, Thornburg et al. 2010). However, MRI has no normative reference value for SA.

Andescavage et al. measured placental elongation in a prospective study comparing controls and FGR cases. This has been reduced significantly in early onset FGR cases while it was masked in late onset FGR (Andescavage, Dahdouh et al. 2019). The reason behind it is the longer time the placental units were damaged in cases with early FGR in comparison with the late onset.

Author	Population	Study type	Intervention	Comparison	outcome
Derwig et al. 2011	83 cases, GA (24-29) weeks	Prospective	Doppler US measured UTaPI and MRI measured the Volume	Three groups of cohorts (according to EFW and Doppler artery PI)	Median placental volume increased with GA in normal neonates while placental volume was smaller in SGA cases
Langhoff et al. 2016	20 normal cases, GA (14-38) weeks	prospective	7 Longitudinal MRI scans with four weeks interval	Only normal cases were assessed	Mean volume showed linear increment through GA with a median of 856ml at delivery, and this was positively correlated with weight
Andescavage et al. 2015	135 cases, GA (18-39) weeks	prospective	2 Longitudinal MRI scans	94 controls, 41 complicated with congenital heart disease (CHD)	Placental volume increased with GA and birth weight, but the degree of increment was higher in cases with CHD than controls
Andescavage et al., 2018	114 cases, GA (18-39) weeks	Prospective	2 Longitudinal MRI scans	79 controls and 35 FGR cases	Placental volume was significantly correlated and increased with GA. Placental and fetal brain volumes were

					significantly smaller in FGR cases than controls
Andescavage et al. 2019	66 cases, GA (20-40) weeks	Prospective	2 Longitudinal MRI scans	32 controls and 34 FGR cases were compared. Placental texture and morphometric features (volume, thickness, and elongation) were assessed.	FGR placentas were smaller in size and more homogenous than controls.
León et al., 2018	112 cases, GA (6-39) weeks	Retrospective	MRI images were assessed	Only normal cases were assessed	Placental volume increased with GA and in coordination with estimated fetal weight and birth weight
Shapira-Zaltsberg et al. 2018	97 cases	Retrospective	MRI scans were assessed	32 controls versus 65 cases with CNS abnormalities.	Placental apparent diffusion coefficient (ADC) was reduced in cases with CNS abnormalities. No difference was found in fetal and placental volumes between groups
Ohgiya et al., 2016	50 cases, mean GA is 29.3 weeks	Retrospective	MRI scans were assessed	25 normal placentas and 25 insufficient placentas	Volume was lower in cases with FGR, insufficient placenta tends to have a globular shape

Damodaram et al. 2010	20 FGR cases and 28 normal controls at varying GA.	Prospective	1 MRI scan and placental histopathology	Normal versus women with FGR	Placental volume was significantly lower in cases with FGR, and this was significantly correlated with FGR severity and estimated fetal weight
Victoria et al. 2011	60 cases (second and third trimester)	Retrospective	MRI images were reviewed	Only normal cases were assessed	Placental thickness measured to provide normative values

Table 12 Characteristics of studies included in the systematic review.

	Surface attachment	Volume	Thickness
US	19.42 ± 3.27 cm^2 at 22 weeks(Kingdom, Audette et al. 2018).	51-55 cm^3 at 12 weeks. 113 cm^3 at 20 weeks (Hafner, Philipp et al. 1998).	2.68 ± 0.66 cm at 22 weeks (Kingdom, Audette et al. 2018).
MRI	17.1-18.5 cm at 31 weeks (Andescavage, Dahdouh et al. 2019).	363 cm^3 at 24 weeks (Derwig, Akolekar et al. 2011). 515 cm^3 at 29 weeks (Derwig, Akolekar et al. 2011). 628.98-657.22cm^3 at 31 weeks (Andescavage, Dahdouh et al. 2019).	5.6 -5.8 cm at 31 weeks (Andescavage, Dahdouh et al. 2019).

Table 13 normal reference values of placental surface attachment, volume, and thickness as described in papers measured by ultrasound and MRI.

Conclusion

Changes in placental morphology have been linked to fetal pathological growth. This has been inconsistently analysed and reported in a small number of heterogeneous studies.

Volume increases with increasing GA.

Thickness potentially increases in cases with FGR and diabetic mothers.

Surface area of attachment may be reduced in cases with FGR.

Further MRI Studies of morphology along with histology postnatally is warranted before placenta MRI is used in clinical practice. Most available research focuses on assessing placental adhesion disorders and perfusion. Scientists mentioned that a diabetic's placenta has abnormalities, but no single paper addresses the MRI diagnostic features. There is missing information regarding the normative placental dimension values and how that could affect fetal growth pathology. Research on this

area is heterogeneous, a systematic approach is needed in both controls and growth-restricted fetuses.

2.3 Retrospective study of FGR

Whilst waiting for ethical approval for the prospective study I undertook a similarly design retrospective study with data obtained in clinical practice. This lacked any patient demographics but allowed me to develop the skills to identify and measure the placenta and assess if our data showed the trends seen in the published data studied in the systematic review presented above.

Introduction

The study aims to determine placental morphological features on MRI that may help predict the outcome of the pregnancy and the health of the coming baby. Earlier and more accurate diagnosis of severe SGA fetuses might decrease the rate of perinatal death and neonatal admissions. Early medical intervention to improve survival and to plan the timing of delivery would enhance the outcome. Fetal MRI has detected how the placental features change during gestation and that there is a wide variety of appearances in apparently normal placentas. Given that some of these cases are FGR and others are stillborn raises the possibility that the appearance of the placenta might hold clues to the outcome of the pregnancy. If this study shows that the basic morphology or any specific pathological features do influence the outcome of the pregnancy, it might be possible to detect these by MRI early in pregnancy, and this will allow changes in management, e.g., early delivery or treatment changes. The findings will also open research opportunities to develop management or treatment strategies further.

Aim:

i) To obtain normal placental measures and determine the relationship between gestational age and placental growth.

ii) To assess the morphology of placentas in both controls (normal pregnancies) and patients with a small for gestational age fetus.

Hypothesis

i) The placenta grows along a defined trajectory as the pregnancy advances.

ii) The placentas of small for gestational age fetuses are thicker and have a smaller surface area of attachment, but the same volume as normal pregnancy placentas.

Null Hypothesis:

i) Placental growth is not related to gestational age.
ii) The placentas of SGA fetuses and normal pregnancies show no morphological difference.

Materials and methods

The study was conducted on 30 normal singleton pregnancies and 5 pregnancies with FGR. A research passport was issued to approve access to data. The data were available on NHS software. The specialist radiologist reported the patient list previously. As the data was part of routine clinical care, consent was not required. The project was registered under the Sheffield Teaching Hospital (STH) registration number 18743, the service evaluation number 5520, and the University ethics number 007380. All the cases were anonymized. The manual segmentation of the placenta was then performed for each case.

MRI measurements

Images were obtained on a Seimens 1.5T Avanto MRI scanner (Erlanghen, Germany) using amongst other sequences required for clinical needs, either a T2 weighted HASTE (Half-Fourier Acquisition Single-shot Turbo Spin Echo Magnetic Resonance Imaging) or SS-FSE (Single-shot fast spin-echo). These provided clear anatomical definition of the placenta. Manual segmentation of two sections; axial and sagittal sections was performed. Each section had 11 slices as a minimum and 42 as a maximum. The placenta was drawn with a line to quantify the perimeter area and midpoint thickness (Fig. 32). The volume was calculated by multiplying the total number of areas in each section with slice thickness. The surface attachment was measured by counting the perimeter, which was a read from the software. Subtracting the perimeter from the line on the fetal surface to give the maternal surface attachment. The total number of surface attachment of all slices were added and multiplied by the slice thickness. Lastly, placental midpoint thickness, was calculated by measuring the

vertical line in the middle area. As there were many slices for each section. The maximum, minimum, range, median, mean and SD were calculated.

Figure 32: Placental segmentation using property software was conducted on a sagittal section-imaging scan of 21-week gestation pregnant.

Statistical analysis

Analysis was performed using SPSS version 27 for windows group analysis. The correlation between gestational age and placental measures was tested using a correlation coefficient. Pearson test was applied to show the degree of that correlation. Cohen's scale was applied to show the strength of the correlation. Linear regression was tested. A p-value < 0.05 was considered significant. Assumptions were applied to histograms to look at the distribution of data.

Results

Study population

A total of 30 pregnant women's scans were interpreted. Gestational age ranged from (18-37) weeks. The indication for MRI referrals were to diagnose the placental accreta spectrum, all outcomes were normal. Each participant underwent one scan, except for

three participants who had a second follow-up scan. Their analysis was then utilised to assess placenta growth patterns over pregnancy.

Distribution of data

Distribution of data was assessed for normality or not prior to statistical analysis to ensure choice of correct test.

Statistical tests showed that the placenta increased in size with increasing GA.
(Spearman's correlation test showed an R-value of 0.3 for (surface area, volume and mid-point thickness).

Placental Volume

At 18 weeks gestation, the mean placental volume was (153.6- 193.9) cm^3 and following that there was a positive correlation between GA and volume reaching (832.02-883.70) cm^3 at 37 weeks. Regression test showed a significant correlation (p-value= 0.03).
B-value was 19.1, which means on each week of gestation, the volume increases by 19 cm^3.

Placental surface attachment

The surface attachment of the placenta showed a direct correlation with gestational age. This association was significant (p=0.03). The measured surface area of the placenta started from (21.70-78.06) cm^2 at 18 weeks gestation and reached (312.55-383.54) cm^2 at 37 weeks. The correlation coefficient test showed a B value of 8, which means for each extra week of gestation, the surface attachment goes up by 8 cm.

Placental midpoint thickness

There was a non-significant correlation with gestational age (p =0.05).
The negative correlation (B value of -0.1) implied an inverse corelation between gestation and placental thickness, and hence for each extra week increment, there is about a 0.1 mm decrease in midpoint placental thickness.

Results of control and FGR cases

Volume

Independent t-test and Mann-Whitney U test showed no significant difference between the 2 groups and their correlation to increasing volume with increasing GA (p= 0.2). The volume of the placenta in both groups increased with increasing GA and there was no significant difference between the rate of growth (Fig. 33a).

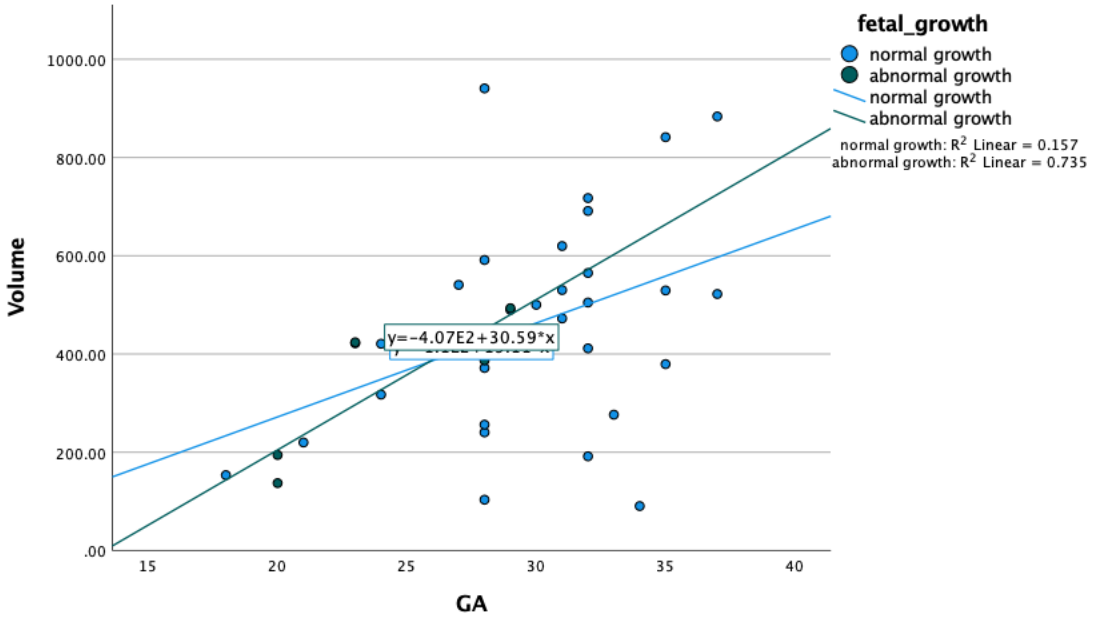

a.

Thickness

The midpoint thickness showed a significant difference between the 2 groups (p= 0.01).

This time the rate of growth was very different with the normal cases demonstrating decreased thickness with increasing GA whilst the FGR cases showed an increasing thickness with increasing GA (Fig. 33b).

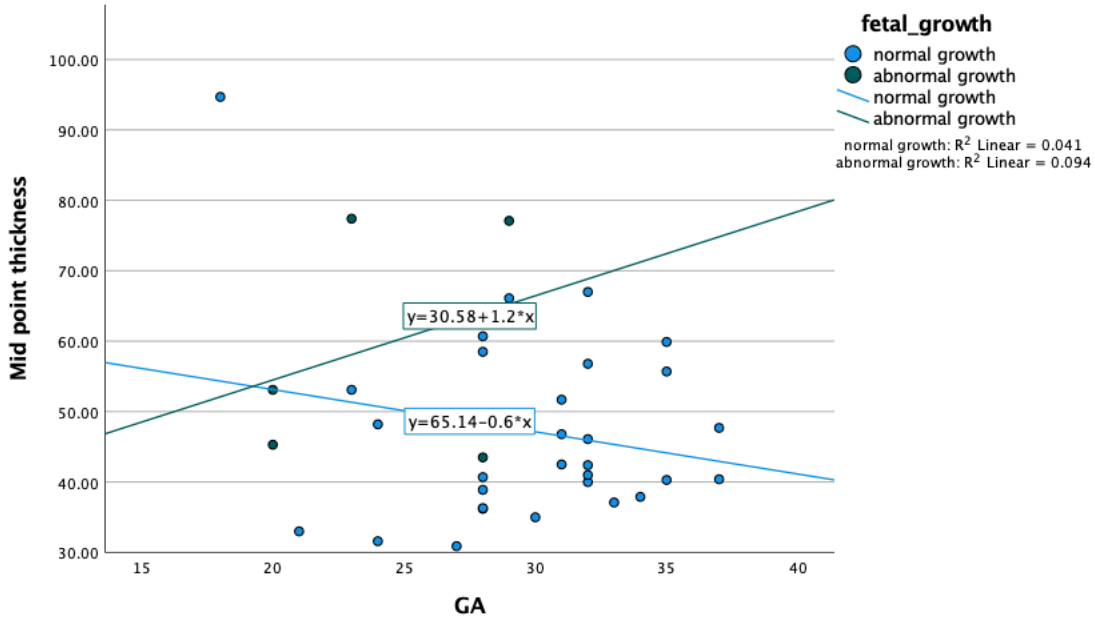

b.

Surface area of attachment

The surface area of attachment of the placenta increased in both groups with increasing GA. There was a non-significant difference in the surface attachment between the 2 groups, (p= 0.08) (Fig. 33c).

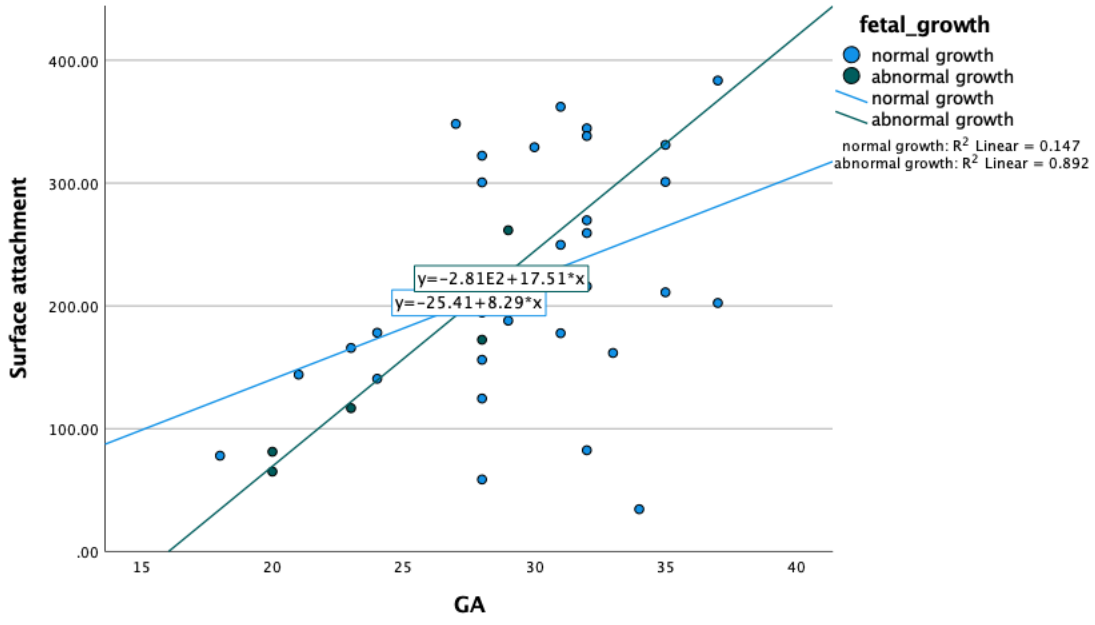

c.

Figure 33: Scatter plots showing the relation of placental volume (cm3) (a) surface attachment (cm2) (b), and midpoint thickness (mm) (c) with GA (weeks).

Follow-up scans analysis

Three subjects included in our study had two longitudinal MRI scans. Scans were in the second and third trimesters. Analysis revealed a direct correlation between volume, surface attachment, and GA but an inverse correlation of placental thickness with GA.

Summary of results

- N= 30 normal and 5 abnormal cases.
- Placental volume increased with increasing gestational age (R= 0.3 and p= 0.03) (Fig. 33a).
- Placental surface attachment increased at a rate of 8 cm^2 per week (Fig.33b).
- Statistical analysis showed no significant difference between the FGR and the normal group for both volume; (p=0.2), and surface attachment (p value=0.08) but a significant difference of midpoint thickness with fetal growth (p=0.01) (Fig. 33c).
- The largest mean midpoint thickness was 3.7cm.
- Abnormal fetuses demonstrated a globular shape placenta with a smaller volume and surface area of attachment but a larger thickness.

Discussion

In the retrospective study, we investigated a practical method for the evaluation of the normal placenta. We reported, for the first time a systematic approach of placental morphology across gestation. As expected, fetal growth influenced placental elongation and increment in size. However, there were no clear points regarding placental thickness. Placental insufficiency is the result of placental dysmorphic changes, which might happen earlier than abnormalities in Doppler ultrasound. As the results showed, the placental thickness was higher earlier in gestation; this emphasized the placenta tends to be flat in shape later in development. Previous research has not undertaken a comprehensive approach to the placenta as the majority were concentrating on measuring single measurements (Victoria, Johnson et al. 2011, Linduska, Messerschmidt et al. 2012, Leon, Li et al. 2018). Victoria et al. and Linduska et al. measured placental thickness while Leon et al. focused on placental volume measurement and linked it with GA and fetal weight.

Our study provided a database for the normative values, which can be regarded as a standardized reference. One of our limitations is the small sample size, which is why the correlation was not very strong. However, both the published ultrasound and MRI data available, although limited, agreed with our retrospective data.

We have demonstrated the placental phenotype in normal pregnancies in the second and third trimesters. In terms of findings, Damodaram et al. supported an increment in placental volume with fetal age (Damodaram, Story et al. 2010). The link between placental shape and volume has been neglected in the published literature, yet there might be an association with fetal outcomes. Adverse fetal outcome has been found to have an association with globular placenta (Fisteag-Kiprono, Neiger et al. 2006), again supporting our findings.

It should be noted that although the limited published data in general support our findings our MRI-measured placental surface attachment was higher than the reported US numbers and not comparable with other MRI studies. In our study, placental surface attachment, measurements ranged from 78 cm^2 at 18 weeks to 383 cm^2 at 37 weeks of gestation with a rate of 8 cm^2 increment per week. This result has not been reported previously using MRI. Ultrasound measurements of the average placental

area were found in previous studies, which were 19.42 ± 3.27 cm^2 at 22 weeks (Kingdom, Audette et al. 2018).

Placental length measured by MRI has been previously reported (Andescavage, Dahdouh et al. 2019) at 31 weeks of gestation to range from 184.69 to 171.22 mm. Whilst others (Ohgiya, Nobusawa et al. 2016) reported the MRI-measured surface area in placentas with and without insufficiency as 2.67×10^4 mm^2 in normal placentas and 1.62×10^4 mm^2 in insufficient placentas. Their calculation uses a formula based on placenta thickness rather than a direct measurement, so comparison is not possible with ours.

Increased placental thickness has been associated with fetal growth abnormalities (Elchalal, Ezra et al. 2000). It was reported that normal thickness on MRI is less than 4cm (Victoria, Johnson et al. 2011). The largest mean midpoint thickness in our research was 3.7cm, which means that there are consistent results among MRI placental measurements, as Grannum et al. stated, the placenta becomes thinner as it matures (Grannum, Berkowitz et al. 1979).

Published data is very limited but both the published ultrasound and MRI data available agreed with our data.

In summary, we have established a useful technique to evaluate placental morphology using MRI during the second and third trimesters. This will be the foundation to identify MRI placental abnormalities in future studies. In addition, we have also shown, in a small sample, that FGR cases potentially have different placenta thickness, volume and surface area that supports out hypothesis and warrants further investigation in a prospective study.

2.4 Prospective study of FGR

Abstract

Background

Diagnosis of fetal growth abnormalities presents a challenge in clinical practice as Doppler ultrasound does not reliably indicate placental insufficiency (Figueras and Gratacos 2017). There is growing evidence that placental function can be assessed by magnetic resonance imaging (MRI) (Bonel, Stolz et al. 2010). We hypothesized that placenta shape and perfusion function can be assessed using MRI.

Methods

An observational, prospective pilot study of 59 participants in four groups: (controls, diabetics (DM), small for gestational age (SGA), and SGA with DM). 13 participants contracted COVID-19 during pregnancy. MRI scans were performed in the second and third trimesters. The total number of scans was 88.

Manual segmentation of the placenta was performed to measure volume, thickness, and surface attachment. Apparent diffusion coefficient (ADC) was obtained using propriety software. T2* was measured using multi-echo T2 star images obtained from all participants, using the MRI protocol gre_Multiecho_T2star_Ax. ADC, T2* and placenta morphological measurements were tested in the different groups and COVID was tested as a covariate.

Results

- GA significantly affected the placental growth pattern.
- Diabetes, COVID-19 infection, birth weight and birth centile, GA at birth, and autoimmune diseases had no effect on placenta growth.
- Placental thickness was not significantly different between the groups (control, diabetics (DM), small for gestational age (SGA). It had an upward trend with GA in all groups.
- In diabetics placenta, surface attachment (SA) was significantly different in diabetics and diabetics with SGA (p=0.029).
- Placental volume was the highest in diabetics while SGA with diabetes placentas was the smallest.

- Surface attachment was highest in diabetics and smallest in the SGA+DM group.
- SGA placentas had the highest thickness 47mm while this was lowest in diabetics 34mm.
- SA took an upward trend over gestation and was significantly different between SGA and controls.
- ADC was lower in SGA cases and higher in diabetics than controls (p=0.04).
- T2* was not significantly different in placentas among the three groups. The pattern was increasing slightly in both controls and SGA placentas and decreasing in diabetics' placentas.

Conclusion

In conclusion, the study sheds light on the complex interplay of factors influencing placental growth patterns. While gestational age emerges as a prominent determinant, other factors such as diabetes and small for gestational age (SGA) status exhibit nuanced effects on specific placental characteristics.

Interestingly, diabetes appears to influence surface attachment and volume of the placenta, with diabetic placentas exhibiting distinct patterns compared to those with SGA and controls. Moreover, SGA placentas demonstrate unique features such as higher thickness and altered apparent diffusion coefficient (ADC), underscoring the intricate relationship between fetal growth restriction and placental structure.

However, amidst these variations, certain parameters like placental thickness and T2* show consistency across groups, suggesting fundamental aspects of placental development unaffected by these factors. Whilst the numbers in this study are small and further studies are needed this is the first study to look at multiple biomarkers, account for covariables and consider more than a single pathological group. All other studies have been restricted to a single pathology and little if any follow up. The study supports our hypothesis that the placentas of SGA babies may be a similar volume to normal babies but are thicker and have a smaller surface area of attachment. These features are likely to explain the changes seen in ADC and T2* that reflect blood flow. COVID did not appear to influence the MRI biomarkers and was found not to be a confounding variable in this study.

This research shows trends suggesting that placental thickness, volume, SA, ADC and T2* are a potential biomarker to investigate for placental growth and function that need further research.

Further research is warranted to elucidate the underlying mechanisms driving these observed differences, with potential implications for maternal-fetal health and clinical management.

Introduction

Explained in page 152.

Methods

Study design and population

The study design is a cohort observational study. Subjects were approached in the maternal-fetal unit (FMU), antenatal and specialist antenatal diabetic clinics at Sheffield teaching hospital. The Obstetricians were also referring a few cases who were at higher risk of developing fetal growth abnormalities. Our cohort included: normal pregnancy control cases, cases where the fetuses was suspected to be small for gestational age (SGA), cases with intrauterine growth restriction (IUGR), maternal diabetes, or cases who had contracted COVID-19 during the pregnancy. Specific cases were required for the study and due to the delays during COVID-19 pandemic a targeted recruitment was necessary. These groups were identified in the fetal medicine clinic using clinically used definitions for each group based on ultrasound criteria.

Control group

Normal pregnancy cases.

Diabetes group

All types of diabetes were included (type 1, type 2, and gestational diabetes).

SGA group

Participants with fetal growth below the 10th centile.

COVID positive group

Any pregnant woman who had the infection during pregnancy at anytime point was included. Usually, COVID-19-positive women received a daily phone call (for 10 days) from a registered midwife after testing positive. This midwife asked the woman if they are interested in this study. At this stage it was an expression of interest, and the patient was giving verbal consent for her name and hospital number to be given to the research team who then forwarded additional information. All scans were conducted in the post-isolation or during the recovery period. If their condition deteriorated, they had access to the care system as normal and were only scanned when recovered. If an appointment was made and then they deteriorated the scan was rescheduled.

Exclusion criteria

Preeclampsia, multiple pregnancies, fetuses with known chromosomal abnormalities, and any exclusion on the MRI safety questionnaire (mainly pacemakers and unsafe body implants) or severely claustrophobic patients at the time of recruitment. Only second and third-trimester cases were scanned, if the patient volunteers before this time, scan dates were given at 20 weeks of gestation onwards.

Sample size

This was a pilot study. The sample size planned in the protocol was 250; It was proposed ideally to have fifty patients of each of the five groups to be collected as the target was to have a minimum of 30 completed data sets in each.

Recruitment

Recruitment included adverts in Jessops Feto-Maternal Unit (FMU) and antenatal clinics combined with a direct approach (advert attached in the appendix p.335). Fully informed written consent was obtained from all participants. Participants were recruited from clinics and identified by the clinician responsible for their care. They were also given an information sheet, and the study was explained. An appointment was then made for the MRI scan. At the time of the appointment, the chief investigator (CI) and the principal investigator (PI) were there to explain the study again and answer any questions the volunteer might have. The consent form was filled in at this point in case it was not signed at the time of recruitment and to give the participants time to withdraw from the study if required. The MRI scan was then performed (approximately 20 mins); the participant was made comfortable on the scanner with cushions and pillows. After the scan, the participants were able to see their images, which included the baby in most cases, and have these ‘talked’ through with them by an expert radiologist. They were also offered a selection of their images by e-mail. A further appointment was made between 4 and 8 weeks later for a second scan. The scans were processed using proprietary software to obtain measurements and were reported by the specialist radiologist (CI) for any pathology. The responsible clinician was told about any pathology. A ‘flag’ was put on the patient’s maternity records to request that the placenta is sent to the pathology department at Sheffield children’s hospital (SCH) after delivery. The data required on the baby were obtained from the delivery notes. From the patient’s perspective, the second scan was their last active involvement in the study; all other data were obtained from hospital records. All

principal investigator documents and the site file are in Dr Whitby's office. All data were anonymized at the time of analysis (Fig.34).

COVID-19 impact

COVID pandemic has impacted the research timeline. Following the ethical approval by the health research authority (HRA) and health and care research Wales (HCRW) which was approved in November 2019, the project was halted by the beginning of the COVID-19 pandemic. The recruitment process did not commence as ethical approval was withdrawn locally and only re-instated 18 months later. Following that, amendments to the project were requested on how or when participants were seen to avoid exposing them to COVID-19 to reduce the burden on clinical services. Recruitment finally started in August 2021.

Ethical approval

The project was approved by the health research authority (HRA) and health and care research Wales (HCRW). Application process was introduced through the integrated research application system (IRAS). Agreement letter (STH20937, IRAS 260951, REC 19/LO/1656) was obtained on 24th August, 2021. The study commenced in August 2021. Further amendments were undergone to include COVID cases with the cohort obtained on 29th November 2021. COIVD was added as this was starting to be linked to placental changes including fibrin deposition. This was therefore likely to a covariable that would impact on our results. By the addition of COVID group we could account for its potential impact. The recruitment stages followed are as in the diagram below.

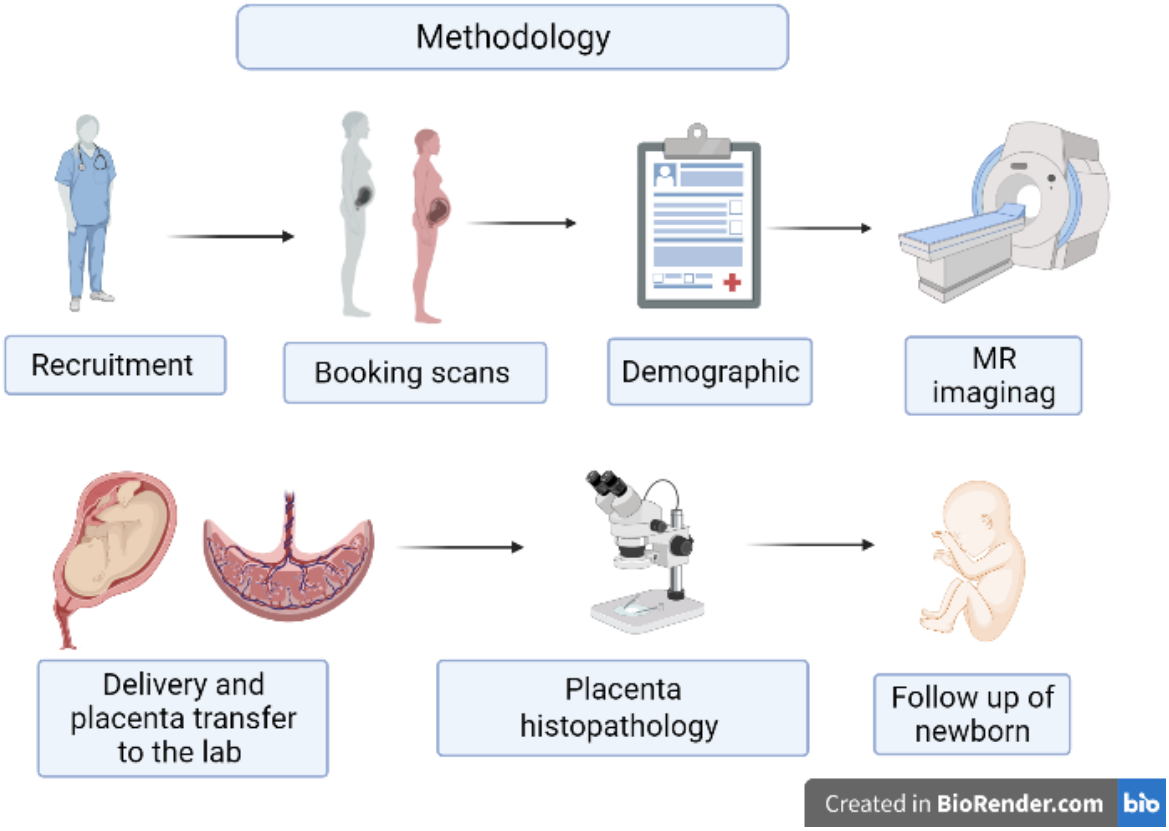

Figure 34 Illustration of the research methodology

Participant information

Demographics, obstetric, and medical history were provided by each participant. A form (see appendix) was filled out by participants on the day of their scan. Follow-up of the participants' clinical data was obtained through hospital notes i.e., obstetrics complication, ultrasound scan, and date of delivery.

MR imaging

Participants were scanned in Sheffield teaching hospital NHS radiology department. After that, the scans were processed using proprietary software to obtain measurements and reported by the specialist radiologist (CI) for any pathology. The responsible obstetrician was told about any pathology. MRI 1.5 T scanner (Advanto, Siemens healthcare) was used, and different imaging protocols were applied to all participants to obtain T2, T2 star, and DWI image sequences (table 14).

Delivery and placenta transfer to the lab

A 'flag' was placed on the patient's maternity records to request the placenta be sent to the pathology department at SCH after delivery. Data required on the baby were obtained from the delivery notes.

Post-delivery notes, the placenta was sent to the children's hospital for full comprehensive assessment (pathology form attached in appendix). The estimated date of delivery (EDD) was recorded from the hospital notes. Access to delivery notes enabled us to follow up on the actual date of delivery. The histopathology lab is based in Sheffield children's hospital and to transfer the placenta from Jessop wing maternity hospital into Sheffield children's hospital, a note was given to each participant on the scan day to hand it to the medical team on their delivery day. Another flag notice along with a copy of the participant's consent and pathology request forms were enclosed with delivery notes. Pathology request forms were sent to Sheffield children's hospital. On the delivery day placentas were stored in a bucket in the ward fridge to be sent to the histology lab in the following day.

Placenta histopathology

Placentas were sent to the lab to assess their macro and microstructural features. Fetal sex, ethnicity, COVID infection during pregnancy, weight of the delivered babies and group of scanned placentas were noted in the request forms. The pathologist reported the placenta to assess the features of the normal vs abnormal placentas i.e., diabetic, intrauterine growth restricted and COVID infection. Analysis was performed on fresh, unfixed tissue. The data obtained was used to compare the features that are known to reduce maternal or fetal perfusion with the ADC and T2* of the MRI to see if there was any correlation that would allow MRI imaging features to predict perfusion and/or potential pathology.

COVID was added due to the evolving links of COVID and placenta pathology.

Follow-up of newborns

Baby delivery notes were accessed through hospital electronic system. Date of delivery (DOD), mode of delivery, gender, weight, birth centile as well as admission into the neonatal unit (NNU) and Apgar score were noted.

Subject withdrawal

Participants were free to withdraw at any point during the study.

Outcome measures

Variability in the placenta morphology and appearances and any indication that this links to either fetal growth abnormalities or stillbirth. As correlated with gross morphology and histology of the placenta.

Costing schedule

This was a funded study. No additional NHS costs, all scans and histopathology costs were covered.

Funding arrangements

Iraqi ministry of higher education.

Images analysis

We enrolled 59 singleton pregnancies recruited from August 2021 to June 2022. The data were available on NHS software. The specialist radiologist reported the patient list previously. All the patients' names and data were anonymized. A sample was divided into subgroups of normal control, diabetics, SGA and COVID-positive. The Diabetic and SGA group where both conditions were present in the same patient was too small for statistical analysis so this was not performed although trends are shown.

1. Placenta morphometry

Manual segmentation of the placenta was performed for each patient scan. Measurements of the placenta have been calculated for volume, midpoint thickness, and surface attachment. We have adopted the same methodology that has been used in retrospective analysis. The surface attachment was measured in a slightly different way (Fig. 35, 36, 37).

Surface attachment

Multiple lines were drawn along the placenta edge facing the uterine wall. The measurement in mm were recorded for each slice in the section. The summation of those measurements multiplied by the slice thickness resulted in the surface attachment.

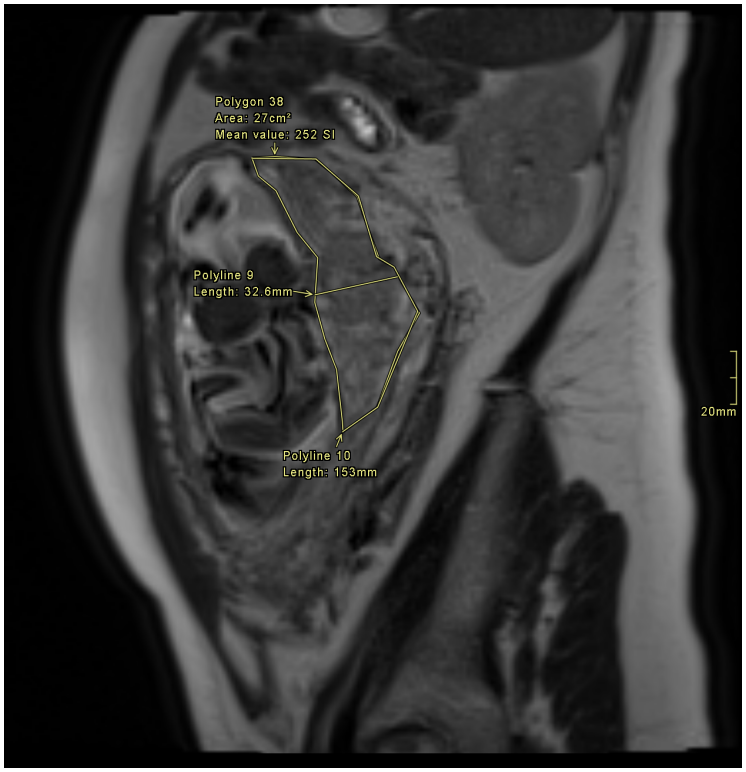

Figure 35: 28 weeks scan of COVID-19 positive placenta.

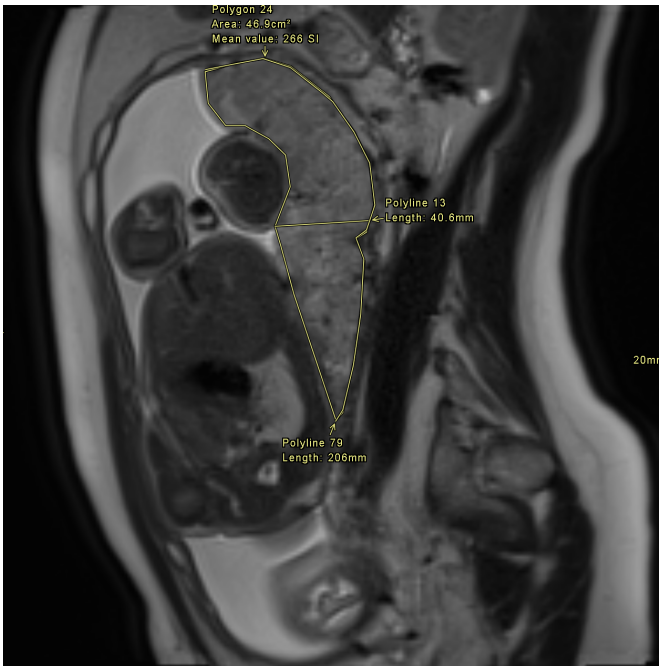

Figure 36: 32 weeks +5 of COVID-positive placenta.

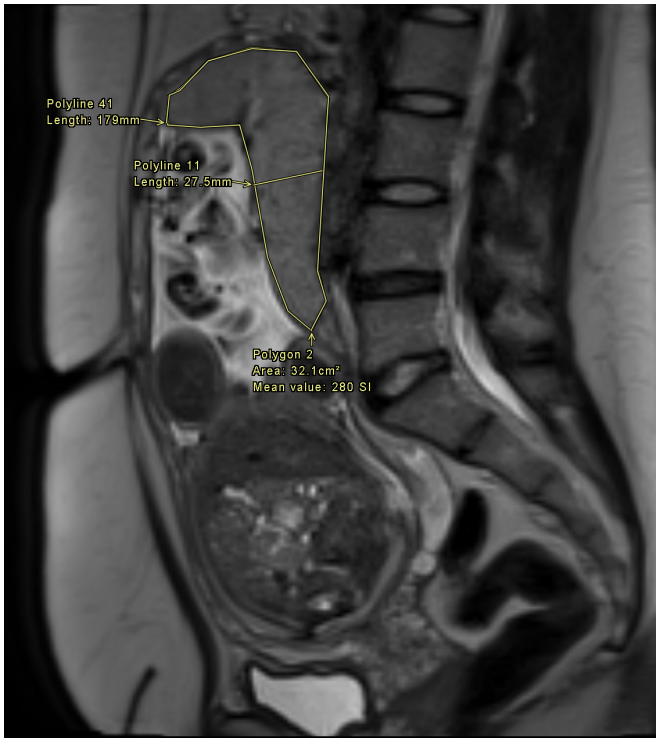

Figure 37: T2 sagittal MRI section, 31 weeks with SGA and small placenta.

2. ADC

MRI images were obtained using a 1.5 T scanner (Avanto, Siemen's healthcare, Erlnaghen, Germany), Using the proprietary software, apparent diffusion coefficients (ADCs) maps were generated when performing DW image sequences on the MR scanner. MRI parameters used are listed in table 12. Images were archived into the NHS-PACS system and retrieved for analysis. Analysis was performed by a single reader (myself - PhD student). Using the DWI protocol, b values from 0-1000 mm^2/sec can be combined into one series where zero is a control image as T2 sequence and 1000 is the highest bipolar gradient and highest diffusion. Manual segmentation includes an ROI of the placenta as a whole on a midline sagittal DWI sequence (Fig.38). On DWI image series, the markup was then displayed on the same geometrical location of all series which then appeared in ADC images sequence. As the ADC map was automatically plotted into other sequences of other b values. It was not required to note down the b value. Mean and standard deviation were recorded.

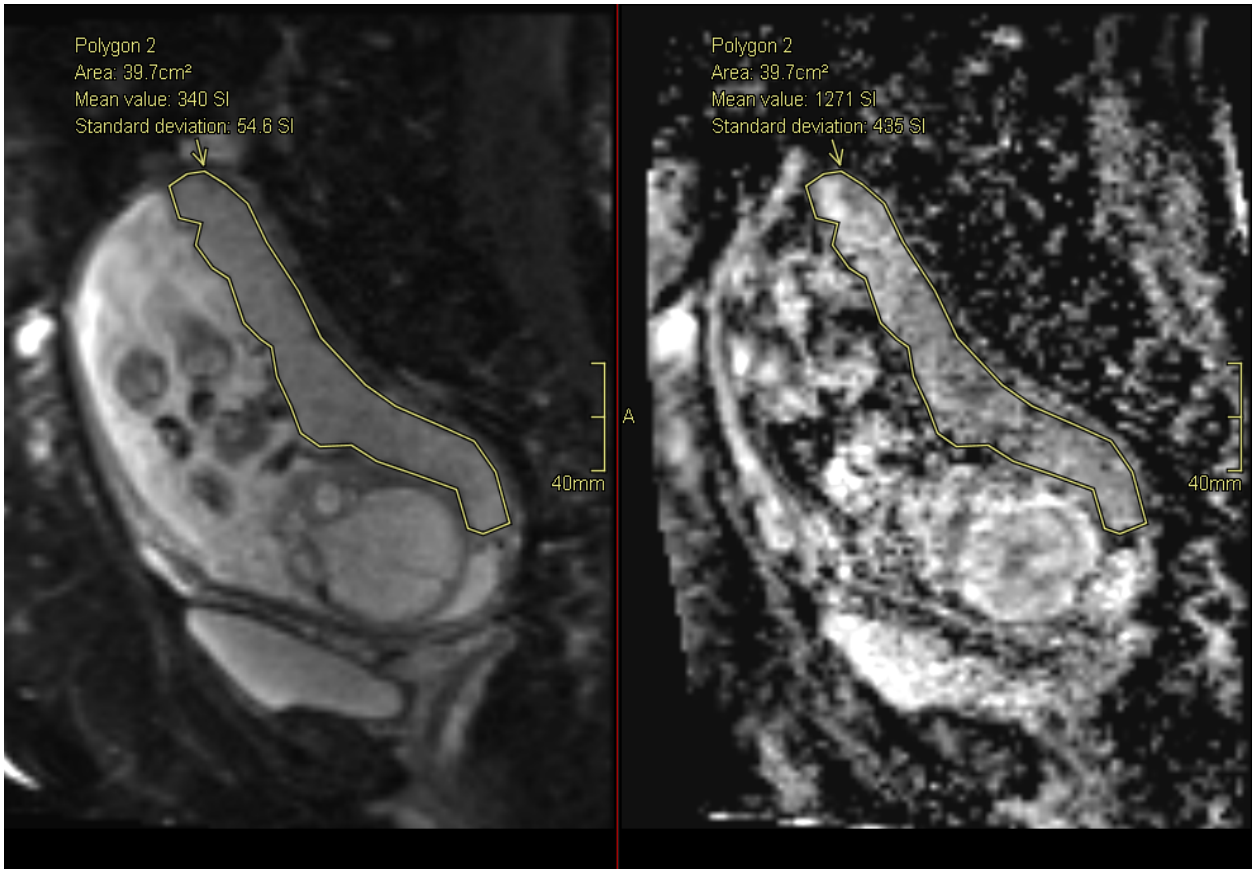

Figure 38: 1.5 T sagittal section, DWI and ADC sequences of normal placenta at 25 weeks gestation. ROI of the whole placenta was drawn first in the DWI sequence (left), it automatically appeared on ADC figure (Right).

3. T2*

Images acquisition

Multi-echo T2 star images were obtained from all participants, using the MRI protocol gre_Multiecho_T2star_Ax. The gradient placed in the middle of an axial section of the placenta to include the largest part. The parameters followed were as shown in table 22. Multi-echo T2* Images were then anonymized.

Images analysis

The program used was Image J adapted by the department MRI physicist and integrated into Image J plugins. This allowed a T2 * map to be created by (by myself-PhD student) by following the addition of the images to the program, the T2* map is selected. The whole placenta was contoured, and the T2 images were synchronized to improve recognition. Images used were either axial, sagittal, or coronal sections. The map size was then adjusted to only include the placenta and only one

ROI was drawn and localized inside the placenta according to map shape. Contouring around the organ of interest was then performed. The number of pixels was selected as 256 (which is automatically added to the program during the programming process). Outputs measures then appear, the values measured were mean and SD.

Acquisition	Imaging frequency	Repetition time (msec)/echo time (msc)	Matrix	Slice thickness (mm)	Flip Angle	Echo numbers	Number of phase encoding steps
T2-weighted 2D 1.5 T (magnetic field strength)	63.67 Echo train length 117	1000/89	Matrix size 192 x 192 y Acquisition matrix 0\192\192\0	4mm Slice gap 4	143	1 Field of view = 288x288	233
T2* MR acquisition type: 2D 1.5 T Protocol name: gre_multiecho_T2star Scanning sequence=GR Acquisition type= 2D	63.67 Echo train length 12	272/3	Matrix size 384x 512 y Acquisition matrix 256\0\0\144	10mm spacing between slices 12	20	1 FOV = 337x450	144

ADC protocol name ep2d_diff_b0_600_1000_sag_p2 Sequence name: ep-b0-1000 Scanning seq=EP	63.6 Echo train length=62	5900/79	Matrix size 112px138 Acquisition matrix 0\138\112\0	Slice thickness 4.3 Spacing between slices=4.3	90	1 FOV 248X305	125

Table 14: MRI parameters of T2-weighted, DWI ADC and T2 sequences.*

Statistical analysis

IBM SPSS version 26 was used. A test of normality was performed. Histogram and q-q plots were drawn to show the distribution of data.

Placenta morphometry

Analysis of covariance ANCOVA was applied, dependent variables were placenta volume, thickness, and surface attachment, COVID infection was a covariate. The following were examined:

1. Characteristics of participants' demographics
2. The correlation of GA with placenta development (V, MPT and SA) of different groups (normal, SGA, diabetics, SGA+ diabetics) was examined.
3. Correlation of placental morphometry with abnormal fetal growth. i.e., SGA and diabetics.

ADC

A univariate ANCOVA test was applied, ADC and placenta morphometry were tested in the different groups (control, SGA, DM, SGA, and diabetics), and COVID was tested as a covariate.

1. The difference of ADC in placentas of normal and SGA groups, diabetics, SGA+ diabetics.
2. Correlation of ADC of normal pregnancies with GA.

T2*

1. T2* mean with birthweight centiles and GA as covariates.
2. T2* with GA.
3. Birth weight (centile) with GA.

Results

All analysis were completed using the antenatal grouping of SGA, diabetes, and controls.

Morphology (shape, size, surface attachment, and volume)

A total number of 59 participants had MRI scans in the second and third trimesters. Four groups (controls, diabetics (DM), small for gestational age (SGA), and SGA +DM). The total number of scans was 88, 27 participants had only a single scan and 29 had 2 scans at two-time points. One participant had 3 scans. 13 cases had COVID at some point during pregnancy. The number of scans per group was: 60 controls, 18 diabetics, 7 SGA, and 3 SGA+DM (table 15, Fig. 39 and 40). 2 participants from SGA groups did not consent to scan but agreed to offer their placentas post-delivery for examinations. Their data was not used in the current study. The DM+SGA group was too small for meaningful statistical analysis and trends, although the trends are shown here for completeness. COVID was distributed in all groups and was therefore treated as a confounding variable rather than a separate group.

Technique	Participants	Number of scans
First scan	27	27
Second scan	29	58
Third scan	1	3
Only pathology	2	0
Total	59	88

Table 15 Details of prospective cohort MRI scans and pathology.

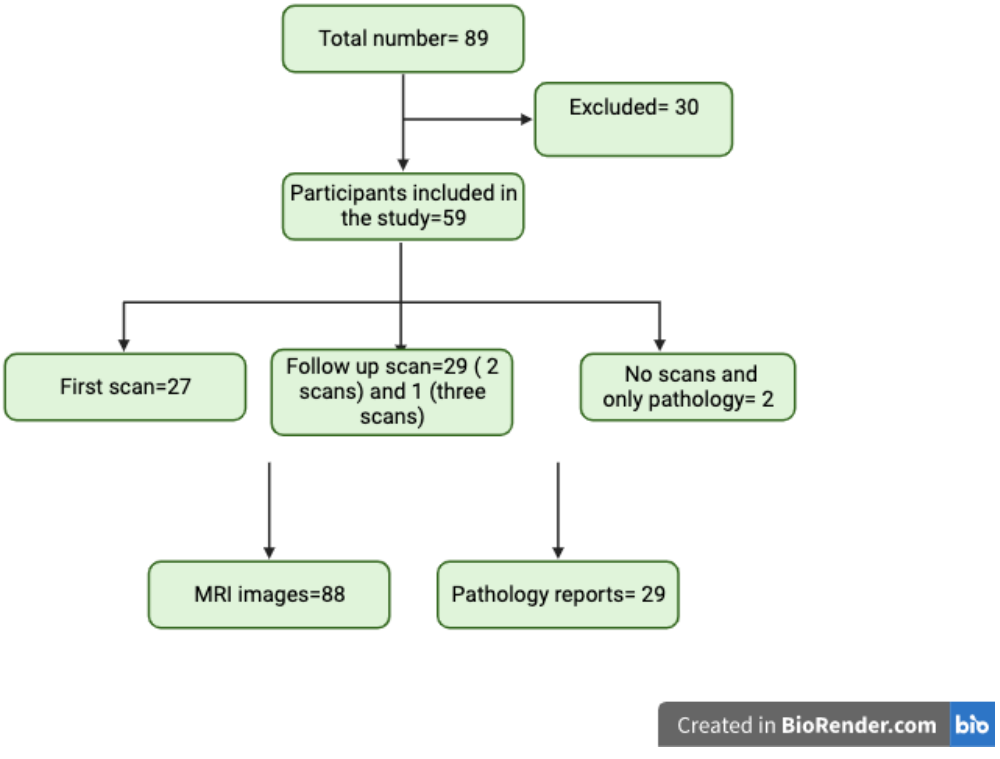

Figure 39 Recruitment process.

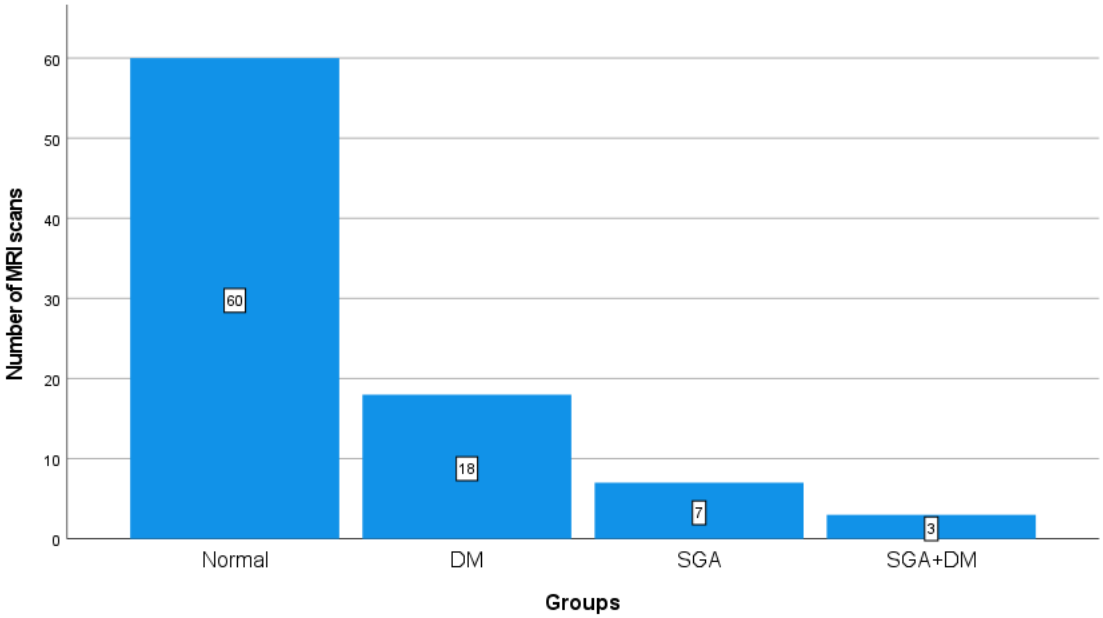

Figure 40: Bar chart showing the groups of the total sample analysed.

Recruitment Timeline

An electronic research management system-EDGE was used to document all participants. The recruitment timeline was from 26/08/2021 to 10/10/2022 where a total of 96 participants were involved. 37 of them were withdrawn (Fig. 41).

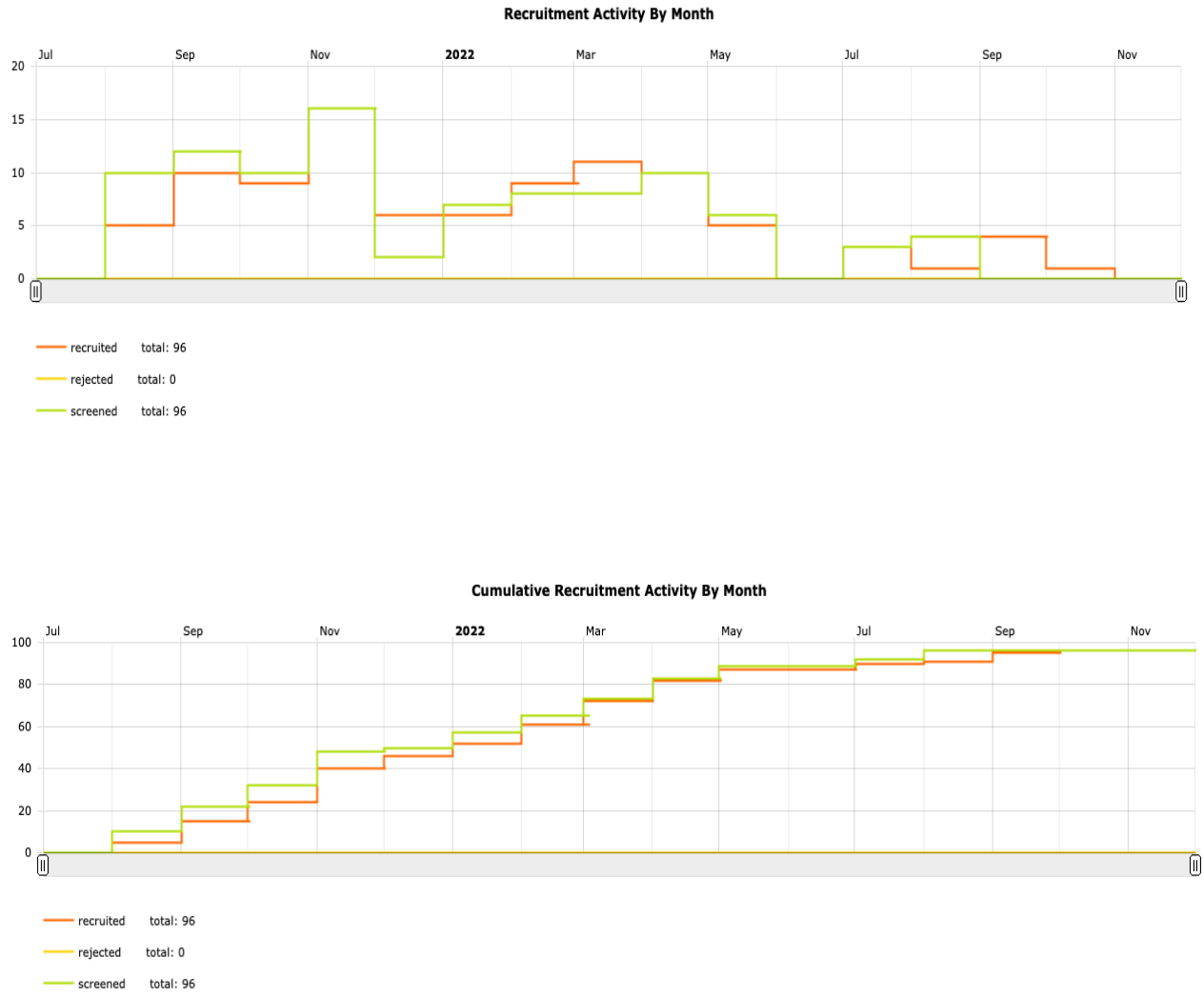

Figure 41: Recruitment timeline by months.

Participants leaving the project

There was a significant number of participants who declined their scan appointments for various reasons. 37 participants left the project at different points of recruitment. The reasons were either clinical in 8.11% (n=3) or patient decision in 91.89% (n=34) as shown in the pie chart (Fig. 42). Each reason is divided into different categories. Clinical causes include:

- COVID 19 infection at the time of appointment in 2.7% (n=1).
- Disease progression (patient was overweight (BMI=48.9), and there was a query about whether she could fit the MRI scanner. The participant also has been reported to have high blood pressure and pregnancy complications, was sick and was admitted into the hospital).

Patients' causes include:

- Family, carer, and social reasons (childcare, partner non-agreement, ethnic minority) in 16.22% (n=6).
- 54% of withdrawn participants did not give any reason.
- 18.92% had none of the above, participants had other reasons for withdrawal, e.g., recruitment late in gestation and not being able to book an unurgent scan, neglecting the scan date for anxiety over fetal health, accessibility, and weather issues.

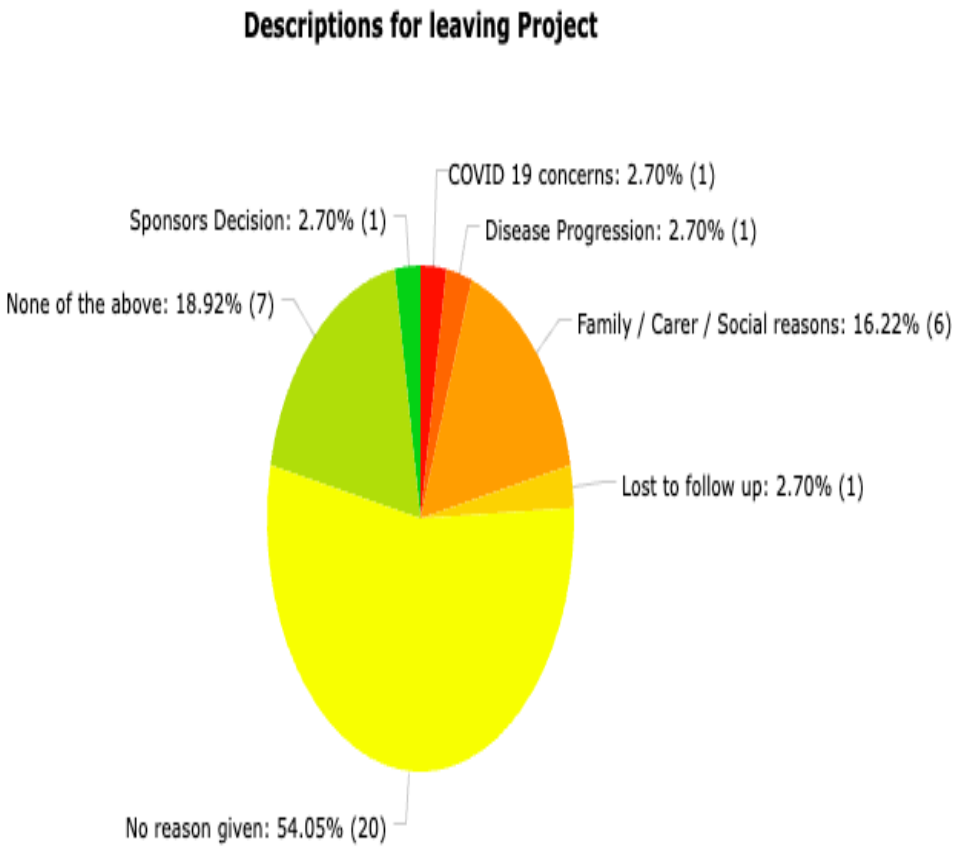

Figure 42: Pie chart providing the reasons of participants' withdrawal.

Participants demographics

Population

The mean age of mothers scanned was 33.6 years (SD=5.5). Ethnicities were white (n=46), Asian=5, mixed=2, black= 1 and other=2. The mean gestational age of the first scan was 26.8 weeks with a range from (19-37) weeks. While the second scan was of a mean of 30.9, with a range from (23-38) weeks, only one participant had a third scan at 33 weeks. Maternal weight measured at the time of scan in Kgs was compared across groups. The mean weight was 81.2kg, the minimum was 54 kg, and the maximum was 151 kg. It was noted that DM group had a higher mean weight than the controls and SGA groups (88.9 vs 81.2 and 75.2) respectively. The mean height was 165.8 centimetres. Regarding BMI, the total mean was 29.3. It was noted that BMI was the highest in groups with diabetes and diabetes with SGA. The mean in women with SGA and diabetes was 42.5 in comparison to 27.4 in the control group. The parity mean was 1 (SD=1) and the gravity mean of pregnancies was 2.7 (SD=1.5). The mean period between pregnancies was 1.9 years (SD=3.1). As it was stated in the inclusion criteria, all pregnancies were with a single fetus. There was one participant involved in the study with twin-to-twin transfusion syndrome (TTTS) and loss of one fetus. Two participants experienced heavy first-trimester bleeding, and this had no effect on the outcome.

COVID infection

13 participants contracted COVID-19 during pregnancy. The timing and severity of infection were different for each patient ranging from being asymptomatic to having flu-like symptoms non requiring hospital admission. 6 participants were infected during the first trimester, 5 in the second trimester and 2 in the third trimester (table 16). COVID infection was distributed throughout the groups so was treated as a confounding variable rather than a separate group.

COVID-19 infection trimester			Groups		
First	Second	Third	Normal	SGA	DM
6	5	2	6	4	3

Table 16: Frequency of covid-19 infection at each trimester with their groups.

Hypertension (HTN)

Four women were diagnosed with gestational hypertension. They were controlled with antihypertensive medications. Only one was controlled with diet. Additionally, five pregnancies were diagnosed with essential hypertension, four of them were in the diabetics group. None of the SGA group were diagnosed with HTN. No cases had preeclampsia.

Autoimmune diseases

Few pregnancies were diagnosed with autoimmune diseases. These include antiphospholipid syndrome (APS), hypothyroidism, celiac disease, Graves' disease, anti-nuclear antibodies (ANA), colitis developed following COVID-19 infection and prothrombin gene mutation. Five of them were in the control group and 4 were in the diabetic's group.

Renal diseases

One participant had poly cystic kidney disease and was in the control group.

Vascular diseases

No vascular diseases present.

ART (assisted reproductive techniques)

These are listed in table 20.

Smoking

7 participants currently smoked. There were 4 ex-smokers, three paternal smokers. 5 of them were in the control group, one maternal ex-smoker was in the SGA group and one in the DM group.

Alcohol drinking prior to dx of pregnancy

The number of alcohol units' consumption per week were recorded, the mean was 1.1(0-14) units per week. Most of the participants were not drinking during pregnancy and the units were mostly in the weeks' prior diagnosis of pregnancy.

Recreational drugs

Two pregnancies had a history of drugs misuse. One with marijuana use occasionally (pre-pregnancy) in the diabetic group and one with non-specified drugs misuse in the control.

Medications

Blood thinners (aspirin and dalteparin)

Aspirin was prescribed to 14 participants. The indications were different, most of the cases were in the DM and SGA groups (n=6 and 5 respectively). Dalteparin was prescribed for 5 cases. The indications were:

1. SGA baby and COVID infection (n=1)
2. SGA and smoking (n=1)
3. COVID infection and positive antinuclear antibody (n=1)
4. Positive anti phospholipid syndrome (APS) and previous SGA (n=1)
5. GDM and COVID infection with high BMI (n=1)

Insulin

Insulin was prescribed in 7 cases of diabetics (table 17). Diabetic control (HbA1c) was not available for all patients although most patients were under follow-up.

DM type	number	Insulin prescribed
type 1	3	3
type 2	2	2
GDM	9	2
HBA1c	Not available for all participants	

Table 17: Diabetics participants.

Metformin

8 participants were prescribed metformin tablets, 7 of them were diabetics and 1 was in the normal group (BMI=34.6) with positive antinuclear antibody (ANA).

USS results

Ultrasound was the primary diagnostic tool for SGA fetuses included in the study. Any estimated fetal weight below the 10th centile was included. Excluding the causes of preeclampsia. Only one case diagnosed with SGA was included in the cohort, after which the estimated weight normalized and the baby was delivered with normal weight.

Prior FGR or small baby

5 out of 9 cases who had SGA baby previously had normal pregnancies.

Maternal or paternal SGA

In 6 cases, constitutional SGAs was diagnosed in two cases in the normal group. Others were maternal preterm and premature birth in 3 cases and one paternal SGA.

Fetal malformations

There were several unexpected malformations among scanned pregnancies that had not been detected on the antenatal US. In total, 4 fetal malformations were reported. Half of them were in the SGA group. 1 in the control and the other one in the diabetic's group. These were a dilated left kidney in the control group, ectopic renal pelvis, and hypospadias with minor chordee in SGA group and spina bifida in the diabetics group. All cases were referred to the fetal medicine unit for further management and the parents informed by the consultant radiologists at the time of their research placenta scan.

Perinatal outcomes

The data set that was analysed for placental morphometry, ADC and T2* and pathology included 57 participants. 2 patients only agreed to placental pathology and follow up of their perinatal outcomes, so we did not scan them giving another data set of 59 sample. Only 50 were reported for outcomes and 9 were missing. The missing data included 6 pregnancies were not delivered at the time of analysis and 3 women's data were not reported on the system (doesn't deliver in Sheffield hospital). These are described in table 21. Fetal outcomes were analysed for 59 participants in total excluding 9 who's their data were missing or not delivered (Fig. 43).

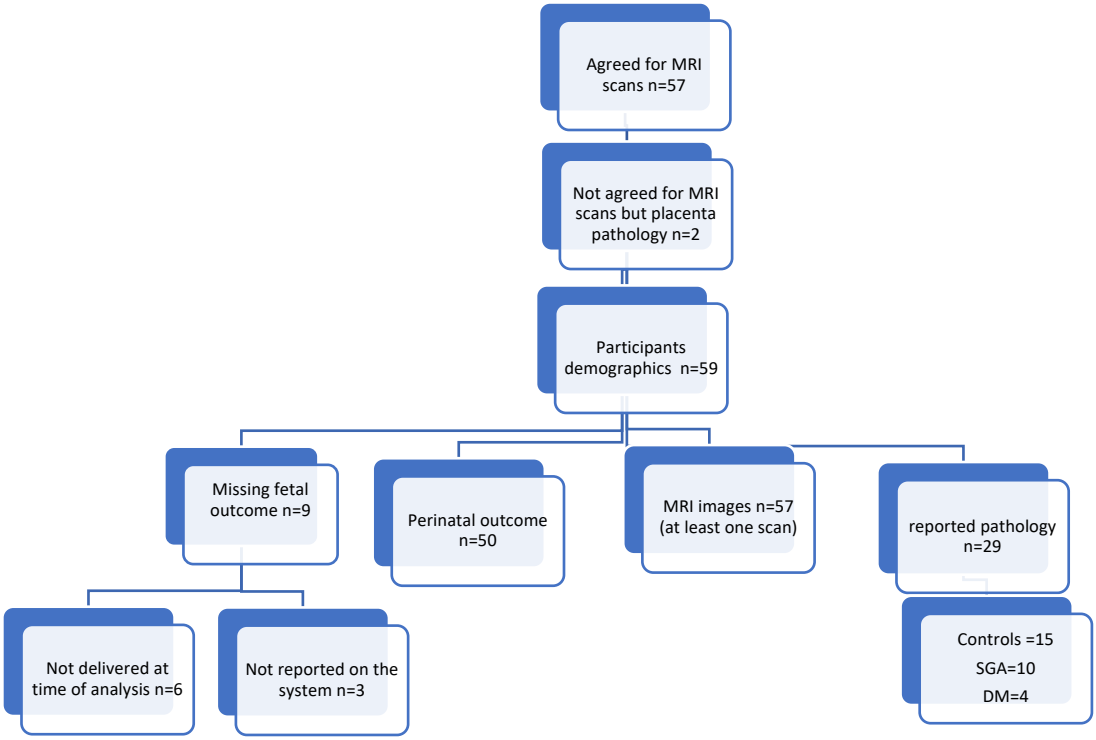

Figure 43: Participants included in the study.

Outcome (normal or SGA)

The fetal outcome was not always as expected from the prenatal diagnosis. One stillborn case was unfortunately diagnosed at 38+4 weeks. Although the patient had two MRI scans, the fetus developed sudden fetal death. Placental pathology revealed a knot in the cord.

7 participants with a normal prenatal diagnosis delivered SGA babies.

3 participants were diagnosed with SGA pregnancy but delivered with a normal weight baby.

SGA

Small for gestational age pregnancies recruited from FMU were scanned. US scans were abnormal in 11 cases, (SGA group and diabetics with SGA). As in table 26, birth weight was normal in 36 cases (61%), prenatal SGA was 9 (15.3%), prenatal diabetics 12 (20.3%). Diabetics with SGA diagnosis 2 (3.4%). Overall number of SGA cases (diabetics and non-diabetics) were 11(18.7%).

Post-natal SGA

At birth, the number of SGA babies delivered less than 10th centile was 15. Post-natally (30%) including 2 undiagnosed cases and 2 cases from the diabetics' group (table 18). Undiagnosed SGAs were 7/15 (46.6%) including 5 cases in normal and 2 cases in the diabetics' group. One SGA case had a small centile during pregnancy that normalised over pregnancy and born with normal weight. Out of all diabetics, 28.6 % (4/14) were born as SGA, although prenatally only 2 were followed up in FMU as SGAs.

Groups	Prenatal	Postnatal	Change	No change
Control (normal)	36	35	5 SGA	31
DM	12		2 DM+SGA	10
SGA	9	15	3 Controls	6
SGA+DM	2			2
Pregnancies did not deliver during the timeline of research	4			
Missing data	5			
Total	59	50	10	49

Table 18: Prenatal and postnatal classification of groups. Diagnosis was made according to hospital protocols using fetal biophysical profile, birth charts and centiles.

Fetal sex

Fetal sex and birth weight

Birth weight was normally distributed. The mean birth weight for male babies was 3101 gm (SD=815.261) and for female babies was 2996.20 gm (SD=804.171). There was no relation between the birth weight and sex (p=0.65).

Fetal sex and placenta morphometry

Surface attachment and thickness data were normally distributed. Volume, ADC and T2* data were not. Non-parametric tests were applied and showed no difference in T2* whole placenta (p=0.8). Placental morphology was not related to sex of fetus (independent t-test), all data are listed in table 19.

Feature	Mean (SD)		P-value
	Male	Female	
Thickness	4.35(1.4)	3.9(1.3)	0.26
SA	200.8(73.5)	213.3 (73.5)	0.96
Volume	448.6(227.7)	428.3(182.7)	0.4
ADC	1272.65(255.5)	1306.81(209.7)	0.5
T2 star whole placenta	50.02(25.9)	46.4(27.7)	0.6
T2 star of ROI	43.3(29.3)	46.6(30.6)	0.8
Birth weight	3020.9(888.5)	2956.4(813.7)	0.9
Birth weight centiles	35.2(26.4)	35.1(35.2)	0.9

Thickness (cm), SA=surface attachement (cm^2), Volume (cm^3), ADC (mm^2/sec), T2 star (ms).

Table 19: Placental morphometric features, ADC and T2 star difference according to fetal sex.

Table 20: Maternal characteristics

Factors	Total Mean (Min-Max)	Control Mean (Min-Max)	SGA Mean (Min-Max)	DM Mean (Min-Max)	SGA+DM Mean (Min-Max)
Maternal age	33.6(21-44)	32.5(22-42)	30.6(21-42)	35.7(27-42)	33(28-38)
GA at first scan	26.8 (19-37) wks.	25.3 (19-37)	32.71(30-36)	mean=26.8 (19-36)	28(27-29)
GA at 2nd scan	30.9(23-38)	31.6(23-38)	none	28.3(23-35)	only one (GA=31)
Maternal weight	81.2(54-151)	76.2(57-127)	75.2(63-91)	88.9(65-151)	86.48(83-90)
Maternal height	165.8(146-188.9)	165.3(153-188.9)	165.4(155.5-176.7)	165.9(153-179.8)	166.3(165-167.6)
BMI	29.3(20-52)	27.4(21-47)	27.1(23-32)	33.8(22-51)	42.5(33-52)
*Obesity	normal=21, overweight=5, obese=13	normal=17, overweight= 6, obese=7	normal=1, overweight=2, obese=4	normal=3, overweight=0, obese=8	normal=0, overweight=0, obese=1
Ethnicity	White=46, Black= 1, Asian=5, Mixed=2, Other=2	White=29, Black=0, Asian=1, Mixed=2, Other=1.	White=8, Black=0, Asian=1, Mixed=0, Other=0.	White=8, Black=1, Asian=2, Mixed=0, Other=1.	White=1, Black=0, Asian=1, Mixed=0, Other=0.

Parity	1(0-5)	1.3(0-5)	0.3(0-2)	1.3(0-3)	1.5(0-3)
Gravity	2.7(1-6)	2.7(1-6)	1.7(1-3)	3.6(2-6)	3.5(1-6)
Inter-pregnancy interval	1.9(0-18)	1.7(0-9)	0.7(0-4)	3.9(0.2-18)	0.2(0-0.3)
Hypertension during pregnancy	normal=52, abnormal=4	normal=34, abnormal=1	normal=7, abnormal=0	normal=9, abnormal=3	normal=2, abnormal=0
Previous preeclampsia	n=1	n-1			
Essential HTN	n=5	n=1	n=0	n=4	n=0
Autoimmune diseases	APS, hypothyroidism, celiac, Graves' disease, ANA, colitis, prothrombin gene mutation	n=5	n=0	n=4	n=0
Renal diseases	Poly cystic kidney disease	n=1	n=0	n=0	n=0
Vascular diseases	0	0	0	0	0
ART (assisted reproductive techniques)	ICSI=1, sperm donor=2, IVF=1, IUI=1.	n=3	n=1	n=2	n=0

Smoking (paternal and maternal)	ex-smoker 3, maternal 1, paternal 3	n=5	n=1	n=1	n=0
Alcohol units drinking prior to pregnancy dx	1.1(0-14)	1.2(0-14)	1.1(0-7)	3.5(0-10)	0
Recreational drugs	marijuana occasionally (pre-pregnancy), drugs misuse	n=1(not specified)	n=0	n=1(marijuana prepregnancy)	n=0
Aspirin	n=13	n=2	n=5	n=6	n=1
Dalteparin	n=5	n=2	n=2	n=1	n=0
Metformin	n=8	n=1	n=0	n=7	n=0
Heavy first trimester bleeding	2	n=1	n=0	n=1	n=0
Multiple pregnancy	one with TTTS caused stillbirth for one baby	n=1			
Prior stillbirth	pregnancy TTTS (1)				
prior FGR	n=9	n=5	n=0	n=3	n=1

paternal or maternal SGA	n=6	n=2	n=2	n=1	n=1

*Groups were ranked into normal (BMI of 18.5-24.9), overweight (BMI of 25-29.9) and obese (BMI of >24.9).

Perinatal outcome	Total mean (min-max)	Control mean (min-max)	SGA mean (min-max)	DM mean (min-max)	SGA+DM mean (min-max)
GA at birth	37.9(27-43)	39.5(37-42)	36(31-42)	37.4(33-40)	34.5(31-38)
fetal gender	male=24, female=26	male=14, female=15	male=3, female=6	male=5, female=5	male=2, female=0
CS	56% (28/50)	n=13	n=7	n=7	n=1
Birth weight (grams)	2987.4(955-4340)	3569.3(2585-4340)	1951.7(1180-3530)	3103.8(2160-3950)	2059(1318-2800)
Birth weight centile	35.2(0.20-99.60)	43.8(2.1-99.6)	9.7(0.2-34.5)	39(0.8-97.8)	4.6(1-8.3)
NNU admission	n=10	n=5	n=1	n=2	n=1
Malformations	n=4	n=1	n=2	n=1	n=0

Table 21: Perinatal outcome of our cohort.

Placenta morphometry, ADC and T2*

Interclass and intraclass correlation

10 cases were repeated by the same examiner (PhD student) (A and D) to measure intra class correlation and two other examiners (B Supervisor and C MSc student) to measure inter class correlation (ICC). All tested cases were normal. Inter and intra relator reliability was excellent apart from for the ADC measurements where it was poor.

Placental volume

Raters A and B

Overall, it appears that investigator B measures slightly higher and more variably than investigator A. Our estimated reliability between investigators A&B was 0.92, with 95% CI (0.712, 0.979), which is quite 'wide'.

Raters A and C

Investigator C measured slightly higher and more variably than investigator A. The estimated reliability between investigators A&C was 0.884, with 95% CI (0.602, 0.97).

Intra class correlation

The same investigator repeated the measurement of placental volume twice in 10 normal cases. The ICC was 0.890 with 95%CI (0.62,0.97).

Midpoint thickness

Raters A and B

It appears that investigator B measured slightly higher and more variably than investigator A. The ICC calculations of the estimated reliability between investigators A&B was 0.908, with 95% CI (0.67, 0.97).

Raters A and C

The MPT of examiners A and C were also compared. Measurements were slightly higher than C. The ICC was 0.879 and 95%CI was 0.587 and 0.968.

Intra class correlation

Raters A and D

The ICC of the two readings measured by the same examiner was 0.959 and 95%CI of 0.84 to 0.99.

Surface attachment

Raters A and B

The SA measured by investigators A&B were compared. The ICC was 0.74 and 95% CI was between 0.254 and 0.929 which is wide.

Raters A and C

ICC of the two readings was 0.658 and 95% CI was between 0.093 and 0.903.

Intra class correlation

ICC was 0.867 and 95% CI was (0.55, 0.96).

Summary

The ICC between the three examiners was

SA: 0.74 and 0.65

Volume: 0.92 and 0.88

MPT: 0.9 and 0.87

The ICC for the same examiner on different occasions was:

SA: 0.86

Volume: 0.89

MPT: 0.95

ADC

A and B (second examiner)

Unfortunately, due to time constraints the rater of this section had not completed this assessment at the time of writing.

Intra class correlation

ADC values were repeated in 10 cases by the same examiner to measure the reliability. The mean of the second measurement was slightly higher (1320.5 vs 1271) mm/sec^2. The ICC was poor (0.489).

T2 star test of reliability

Unfortunately, due to time constraints the rater had not completed this assessment at the time of writing.

Data distribution

Thickness and surface attachment data were normally distributed. Volume, ADC and T2 * whole placenta were not. For mid-point thickness and surface attachment analysis of covariance, ANCOVA was applied. GA was a covariate and COVID-19 infection was a confounder. Kruskal-Wallis test was applied for volume, ADC and T2* with groups as they were not normally distributed (appendix XII).

A. Placenta morphometry and GA

Thickness

Simple linear regression showed a significant relationship between gestation and placental midpoint thickness ($p<0.001$). Pearson's correlation coefficient showed a strong positive correlation ($r=0.6$). In the diabetic's group, $R^2=0.64$ so 64% of placental thickness can be explained by GA, while in the control R^2 was equal to 28% (Fig.44a). The slope coefficient was 0.13 in controls, 0.16 in the DM group, 0.1 in SGA and 0.16 in SGA+DM. So, placental MPT increases differently each week according to group. Placental MPT increases in all groups with increase in GA although the trend line is slightly different in each group.

Volume

Placental volume was significantly correlated with GA ($p<0.001$) and Pearson's correlation coefficient showed a strong positive correlation ($r=0.7$). In the diabetic's group, the R^2 was equal to 0.73 means 73% of placental volume in diabetics is explained by GA. While in the control group, 54% of the volume could be predicted by GA ($R^2=0.54$) 21% in SGA+DM and 1% in SGA (Fig.44b). The slope was 29.68 in the control group, and 37.65 in DM, 3.86 in SGA and 13.74 in SGA+DM. So, placental volume increases by different numbers per week gestation according to group. Placental volume increases with increase in GA in all groups. The trend lines are very similar for controls, diabetics and SGA and diabetics. The trend line for the SGA group appears very different although shows an incremental increase with GA.

Surface attachment

As with thickness and volume, SA was also correlated with GA. Pearson's correlation coefficient showed a strong positive correlation ($r=0.6$). Over gestation, there was a steep rise in SA in diabetics', control, and SGA+DM groups. In SGA on the other hand, SA remained steady over gestation (Fig.44c). R^2 was 44% in control, 47% in diabetics, and 11% in SGA+DM. The slope was 9.06 in control, 10.3 in DM, 0.3 in SGA and 4.98 in SGA+DM. In SGA R^2 was equal to 0.002, which means there is barely a change in SA with GA in SGAs.

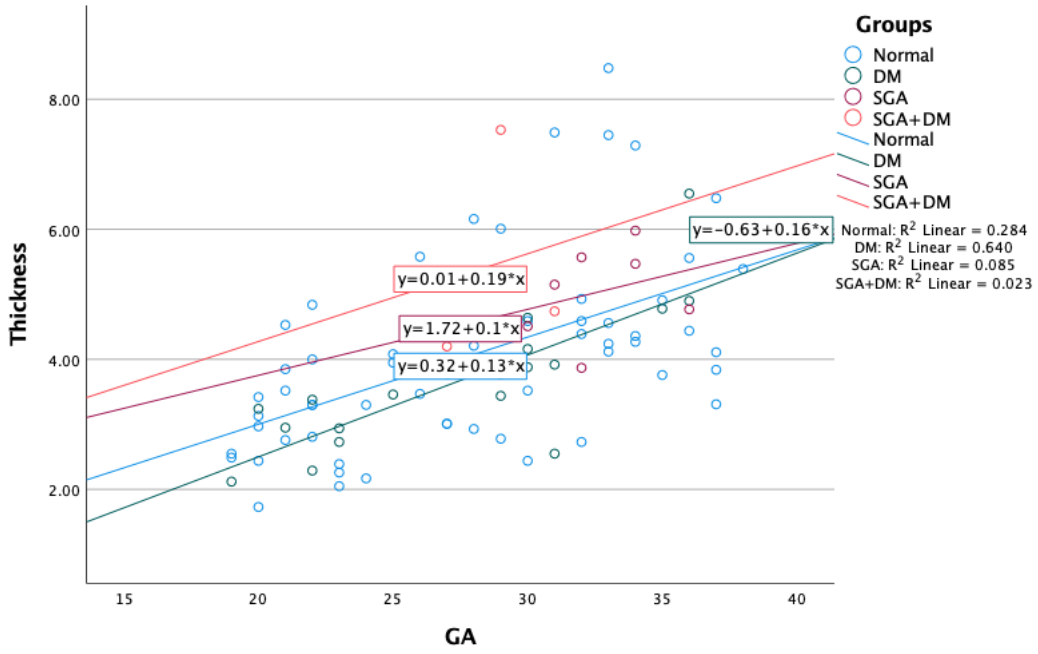

a.

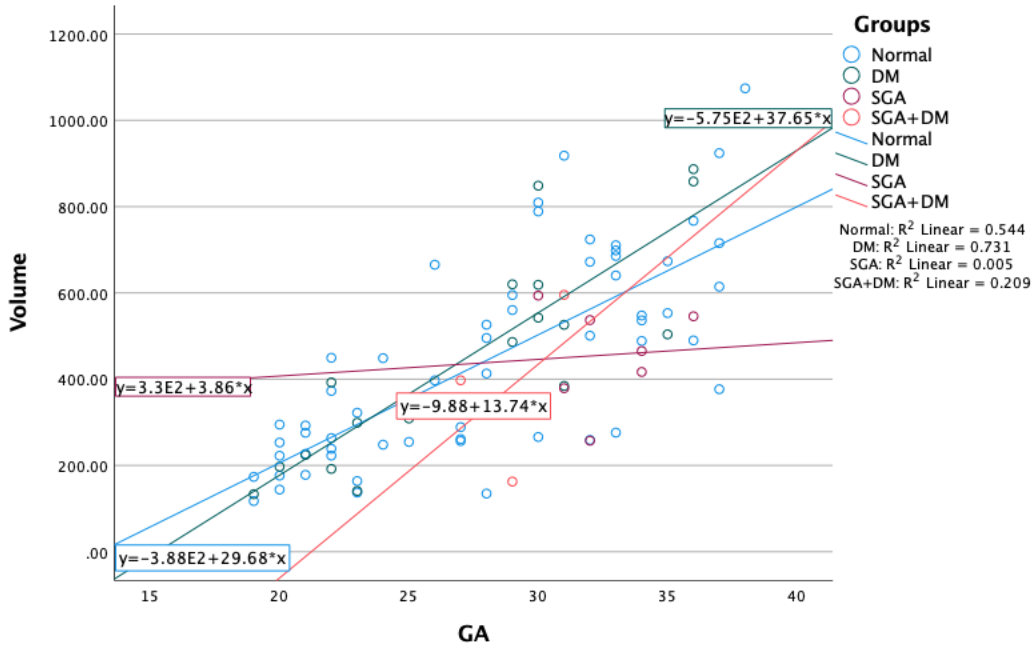

b.

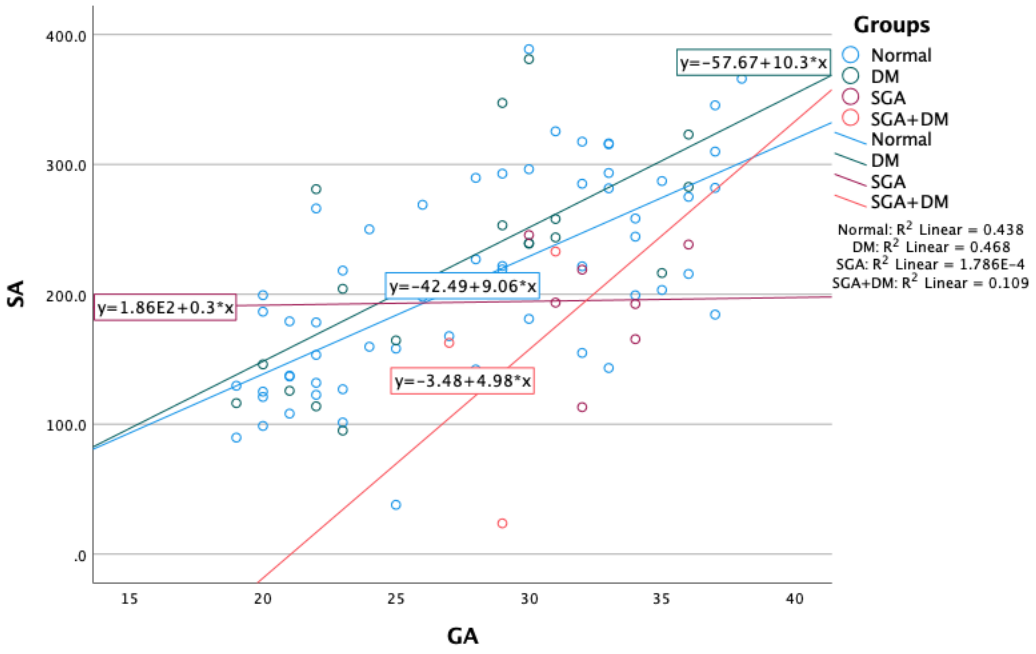

c.

Figure 44: Scatter plot showing the relationship between GA (weeks) at the time of scan (weeks) and placental morphometric values: thickness(cm) (a), volume(cm3) (b) and surface attachment (cm2) (c). When COVID-19 was a factor in the analysis of the effect on gestation.

In summary of placental morphology

- Controls: larger SA than SGA
- SGA: smaller SA, thicker and smaller volume
- DM: similar thickness to controls (largest SA and volume).
- SGA+DM: was too small for any trends to be noted.

B. ADC and GA

Pearson's correlation was carried out to look for relationships between ADC and GA. There was significant evidence (r= -0.2, p=0.024). GA was weakly corelated with ADC and this correlation was negative. ADC remained steady over gestation in the diabetics group and showed a steep rise in SGA+DM group (Fig.45). R2 was 8% in controls, 0.007 in SGA and 91% in SGA+DM. The slope coefficient for gestation was -8.746, So the ADC reduces by 8.746 for each week of gestation. In controls, this was -9.37. -0.54 in diabetics', -6.04 in SGA and 35.3 in SGA+DM.

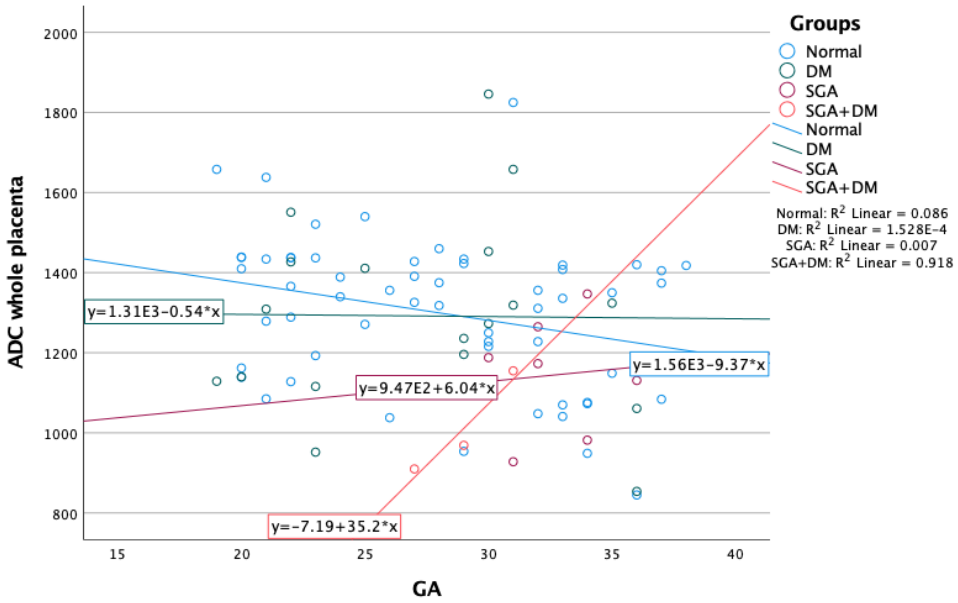

Figure 45: Scatter plot of ADC whole placenta (mm2/sec) in different groups.

C. T2*

The process of T2* segmentation and measurements of ROIs are clarified for normal and SGA examples (Fig. 46 & 47).

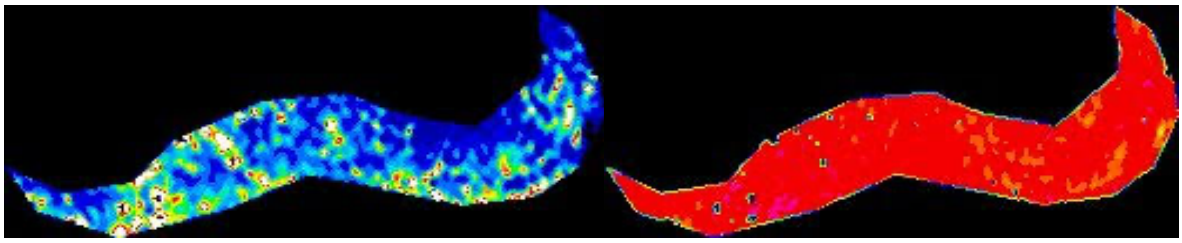

Figure 46: Gradient multi-echo MRI sequence of 35 weeks+3 days gestation of normal placenta. The mean T2 of the whole organ was 65.212 millisecond (ms) and SD was 70.98 ms.*

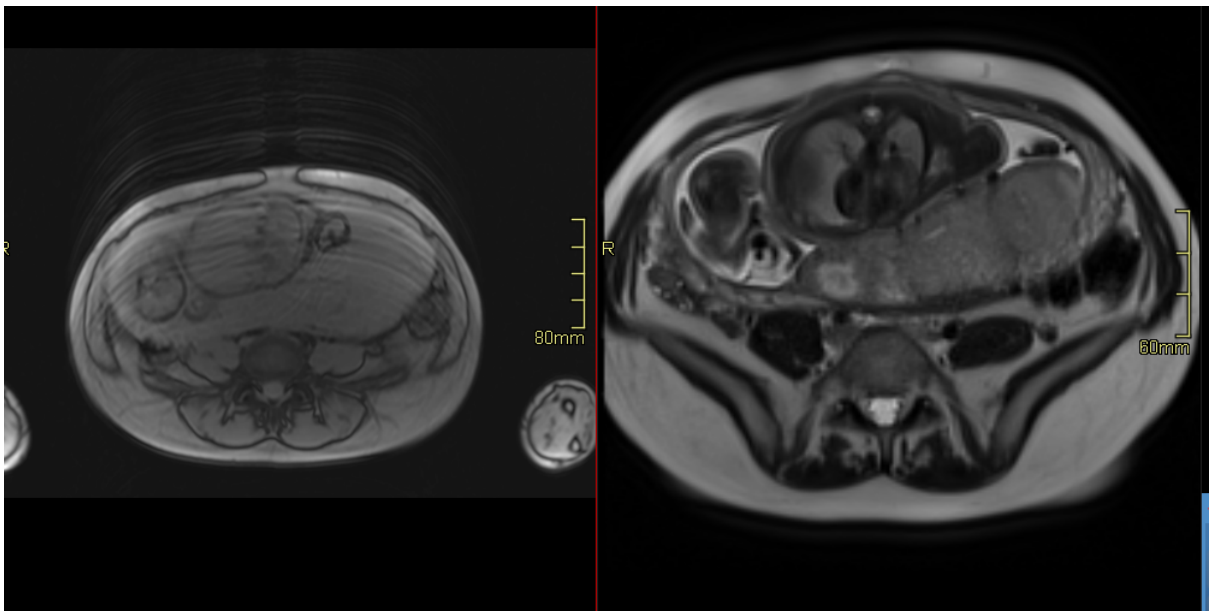

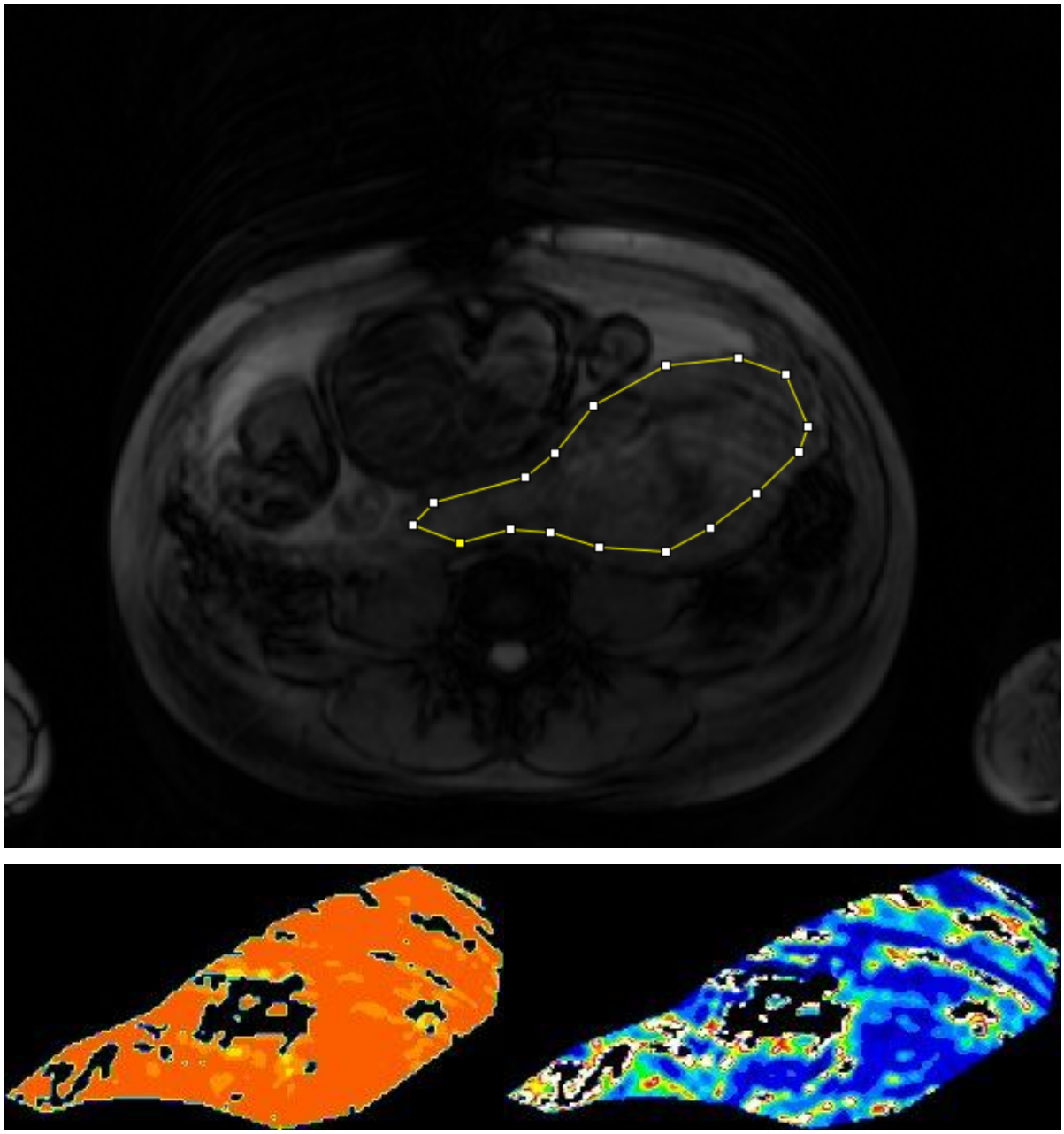

Figure 47: Gradient multi-echo MRI sequence of SGA placenta at 35 weeks gestation. The steps of manual segmentation are shown. T2 mean of the whole placenta was 71.67 ms and ROI was 34.87ms.*

Nonparametric Tests

The distribution of T2* of whole placenta sample was abnormal, so nonparametric tests were applied (appendix). 76 placentas were tested for whole placental T2*.

The results of the independent-sample Kruskal-Wallis test showed a non-significant difference in T2* whole placenta across groups (p=0.616).

GA and T2*

GA has weakly correlated with T2* whole placenta and the correlation was not significant (r=0.17, p=0.131) (Fig. 48 & 49).

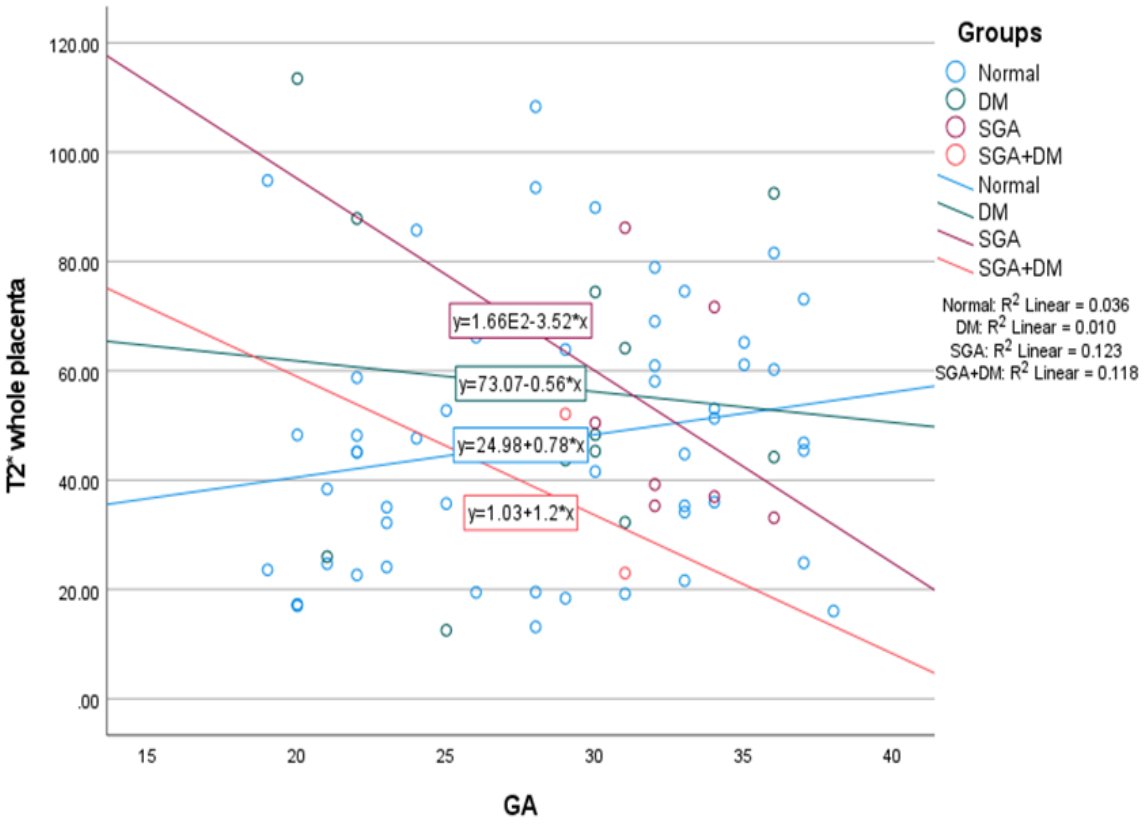

Figure 48: Placental T2 whole placenta (ms) and GA (weeks) in 4 groups of participants. The graph shows that there has been a slight rise in placental T2* of controls (blue line) over gestation. SGAs T2* (red line) has shown a steep fall over gestation.*

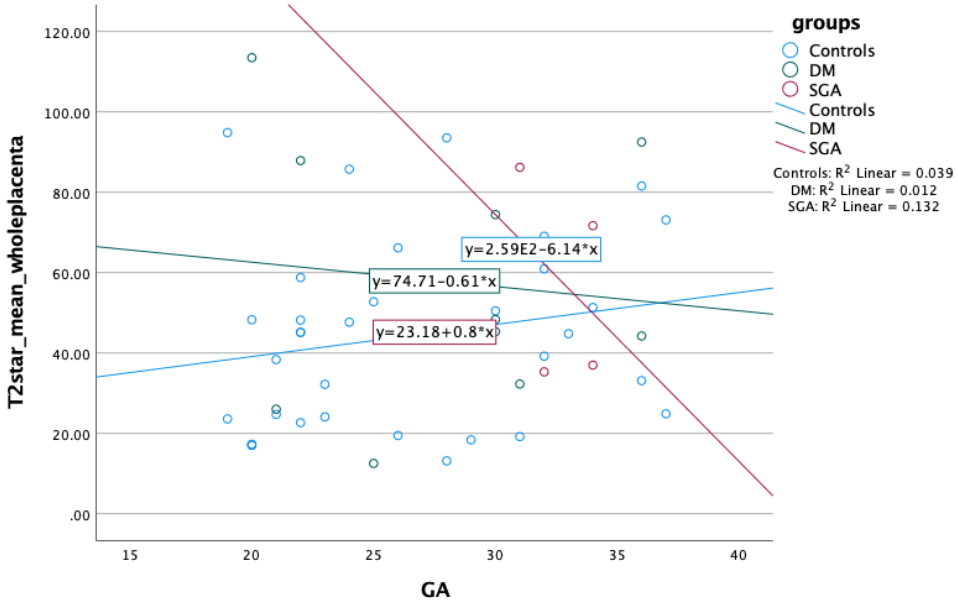

Figure 49: Placental T2 whole placenta (ms) and GA (weeks) in 3 groups of participants.*

Excluding GA as a covariate

When analysing data, we have assessed 2 samples. Due to the small numbers, we assumed that participants who have 2 or 3 scans during the recruitment process will belong to sample 1 (n=88). While for the assessment of perinatal outcomes and maternal characteristics, the original sample was used (n= 57).

Interestingly, there was a difference in results regarding placental measurements and ADC when numbers were changed, this is possibly because the groups were not matched. The predominant group was controls. While SGA and diabetics groups were fluctuating. This was a pilot study and gave an indication to explore more to make a change in clinical practice.

As we excluded SGA+DM group and combined it with SGA group, considering diabetes as a covariate, the samples stats changed especially for SGA group (table 22).

Feature	Control(n=60) and (n=54 in T2* whole placenta and 53 in T2* ROI)		DM(n=18) and (n=12) in T2*		SGA(n=10)	
	Mean	**95% CI**	**Mean**	**95% CI**	**Mean**	**95% CI**
Thickness	4.1[a]	3.7,4.4	3.7[a]	3.1,4.2	5.2[a]	4.4, 5.9
Surface attachment	210.3[b]	189.9,230.7	223.9[b]	182.3,265.6	178.7[b]	129.9, 227.5
Volume	441.2[c]	381.2,501.1	453.7[c]	331.9,575.5	435.2[c]	332.6,537.8
ADC	1300.5[e]	1252.9,1348.2	1291.9[e]	1169.9,1413.9	1104.8[e]	997.7,1211.9
T2* whole placenta	47[d]	40.5, 53.5	57.1[d]	38.1, 76.1	46.1[d]	32.2, 60.1

a= cm, b=cm^2, c=cm^3, e=mm^2/sec, d=ms.

Table 22: Placental features among different groups.

Sample 1

We applied two modules using univariate analysis of variants (ANCOVA). Covariate in Module 1 (M1) was gestational age (GA) only while in M2, GA was a covariate and diabetes with SGA and COVID-19 infection were confounders. Groups were compared with controls to look at the difference in their variance and if confounders have a significant effect on them.

Thickness

Only GA was a significant covariate; coefficient values are noted (table in appendix). Data from group comparisons are summarised. SGA and controls coefficient of correlation was 0.6 and this was not significant. COVID-19 infection and diabetes with SGA confounders had also a non-significant effect on placental thickness.

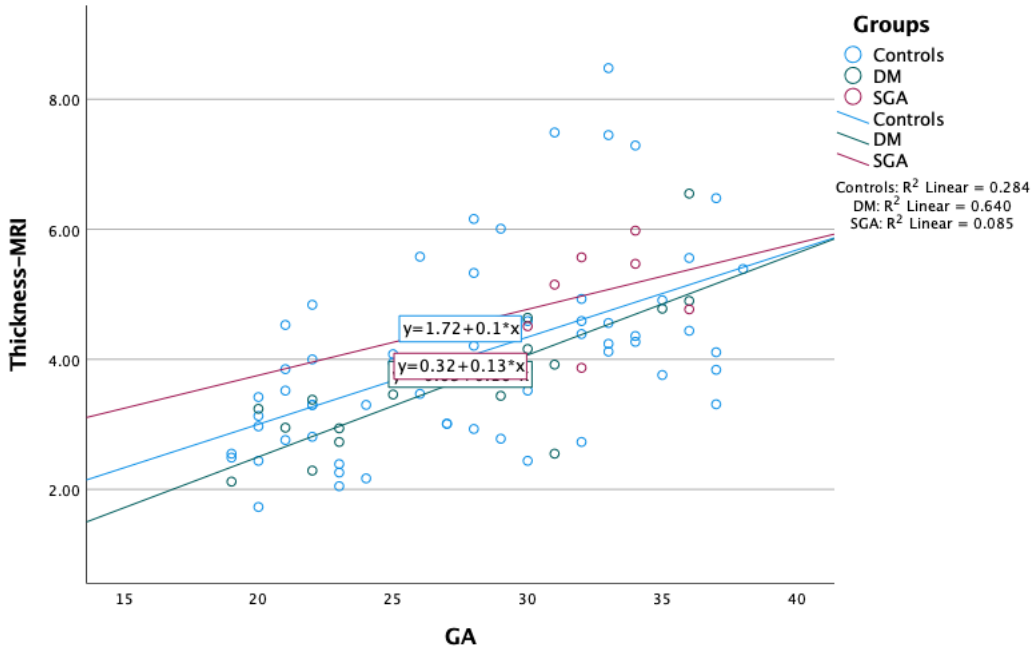

Figure 50: Scatter plot of GA (weeks) and placental thickness (cm) in 3 groups.

To compare the data results from the scatter plot (Fig. 50) and the ANCOVA, it is noted that there are differences in the results of R^2 between the two comparisons. This is largely caused by gestational age (R^2=0.37), in the first instance while in the second form of analysis (M2) R^2 hasn't changed that much (0.38), because diabetes, SGA and COVID-19 infection haven't caused a substantial change in the analysis.

Volume

Gestational age also played a significant role as a covariate in placental volume across different participant groups. Placental volume was significantly different in SGA from controls (table in appendix). In the DM group, the volume was not significantly different from the controls. The trend of placental volume across gestation in different groups is shown in Figure 51.

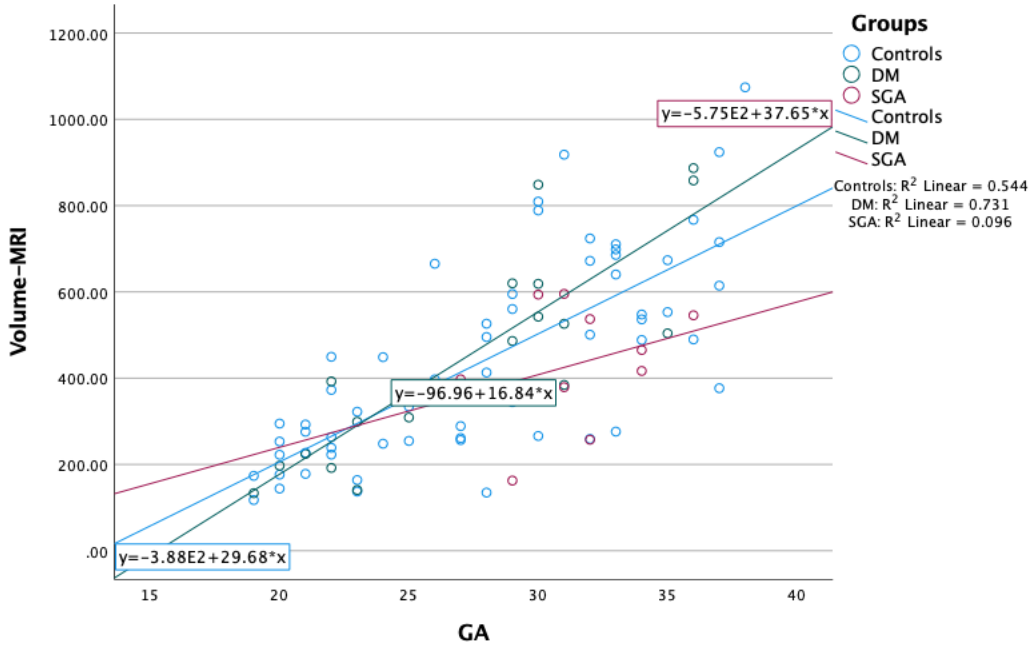

Figure 51: Scatter plot of placental volume (cm3) with GA (weeks).

Surface attachment

Placental surface attachment was significantly different between SGA and controls under the effect of GA, COVID-19, and diabetes covariates (table in appendix) and (Fig.52).

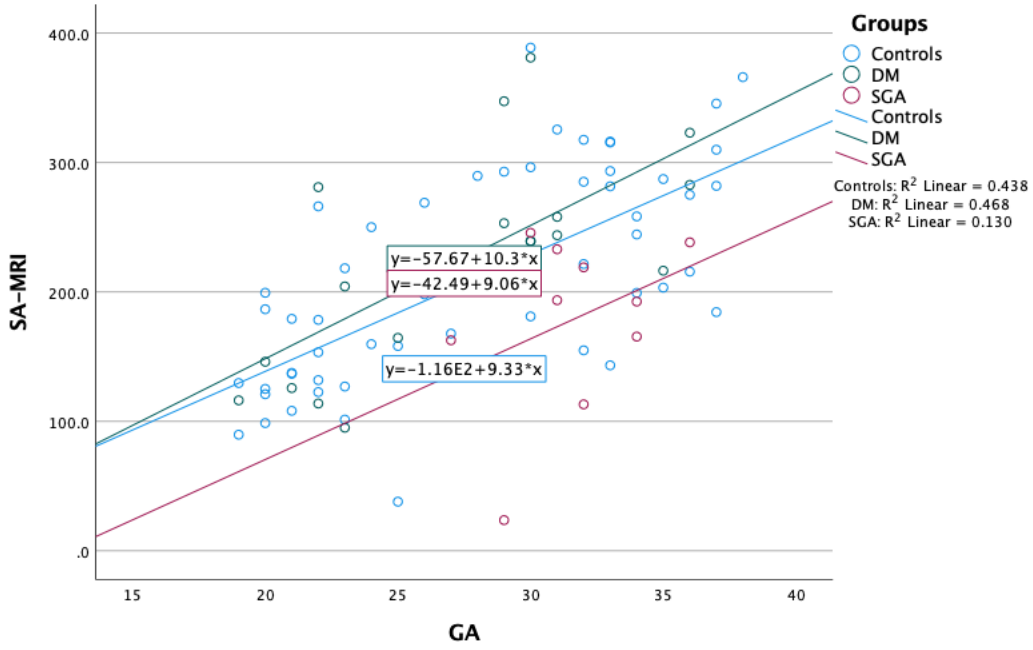

Figure 52: Scatter plot of placental SA (cm2) and GA (weeks) compared in 3 groups.

ADC

The ADC was significantly different between SGA and controls ($p<0.05$). There was a reduction in the ADC for every week of gestation (table in appendix).

In the diabetic group, ADC was not significantly different than in controls (Fig. 53).

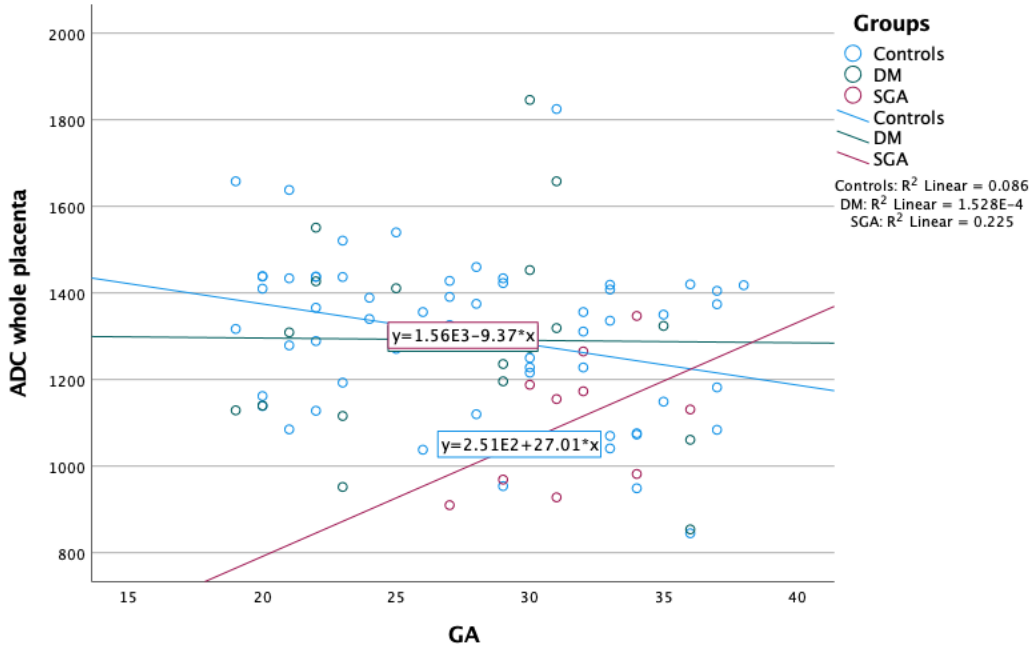

Figure 53: Scatter plot of ADC (mm2/sec) of the whole placenta and GA (weeks).

T2* whole placenta

None of the covariates had a significant effect on the results. There was no significant difference in T2* values between the groups. T2* took an upward trend in controls and was relatively static in SGA groups (table in appendix) (Fig.54).

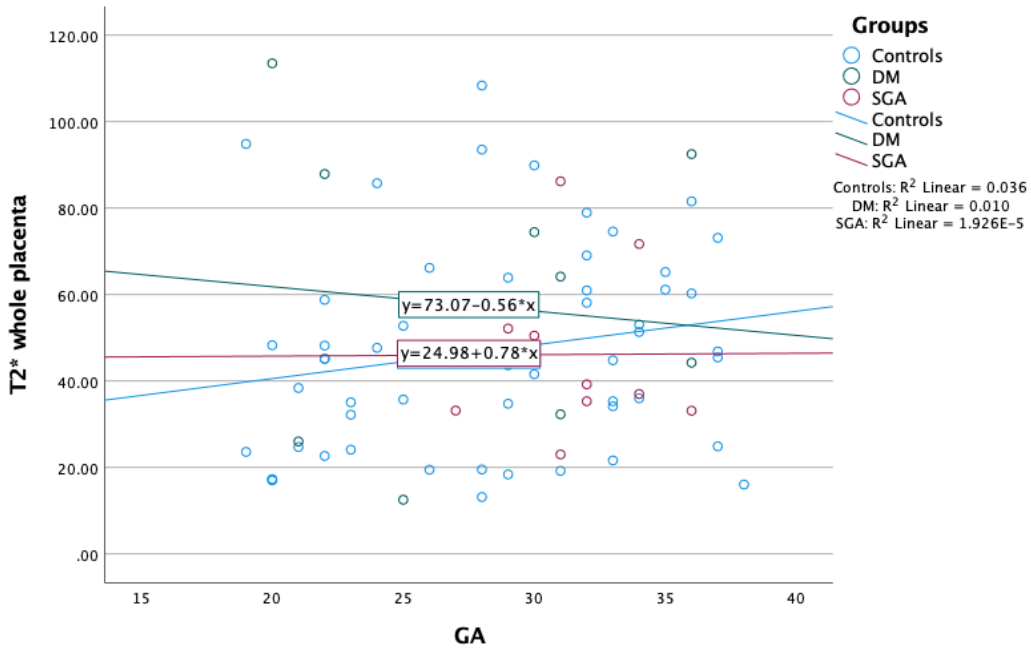

Figure 54: Scatter plot of T2 (ms) of the whole placenta and GA(weeks).*

Sample 2

This sample (n= 57) was used to test the perinatal characteristics and any other potential confounders.

Data distribution

Histogram analysis and Kolmogorov-tests were used to check the distribution of data (appendix). Except for T2* whole placenta, all other data was normally distributed. Univariate analysis of covariance (ANCOVA) was applied. GA was a covariate; confounders were applied to test the effect on the main covariate.

Modules adjustment to test the confounding factors

In module one, gestational age was a covariate. In module 2, we added diabetes with SGA as a confounder. In module 3, we added COVID-19 infection as another confounder. As both COVID-19 infection and diabetes with SGA were both nonsignificant effects. We removed them from the following modules to test the other confounders and kept gestational age as the principal covariate. We then tested all the potential factors, but only significant factors (birth weight and centiles, GA at birth, autoimmune diseases) were reported (tables in appendix).

Thickness

Gestational age was a significant covariate in all seven modules. Diabetes with SGA, COVID-19 infection, birth weight and birth centiles were not significant confounders.

SGAs were compared with controls to look at the effect on placental thickness caused by different confounders. There was a variation in MPT, but the change wasn't substantial ranging from (0.2-0.6) cm. Diabetics and controls were tested as well. There was a non-significant difference in MPT between the groups. The fitness of data to the regression line was between 36% to 45%. The reason for the variation is due to the application of different confounders.

Volume

Gestational age was a significant covariate in all modules. Birth weight, birth centiles and the presence of autoimmune diseases also had a significant effect on placental volume.

Regarding group comparison, there was a significant difference in volume of SGA and controls but not in all modules. In diabetics, placental volume was increasing at each week of gestation. This was significantly different from controls when birth weight was a confounder with a coefficient of 93.8. Diabetics' placental volumes were also significantly different from control when autoimmune diseases were a confounder (B=111.3). The fitness of data to the regression line was good, ranging from 59% to 69%.

Surface attachment

Gestational age acted significantly as a covariate. Regarding confounders, birth weight, centiles, gestational age at birth and autoimmune diseases have significantly affected the placental surface attachment.

SGAs placental surface attachment was significantly different from controls. Diabetics' placentas on the other hand were significantly different from controls when autoimmune diseases were a confounder.

ADC whole placenta

Over gestation, ADC values demonstrated a downward trend in SGAs placentas. There was a significant difference between SGA and controls when birth centiles were

a confounder. The difference in ADC values between SGA and control placentas was significantly influenced by gestational age at birth as well. According to the influence of confounding factors, ADC values in diabetic cases increased over the course of gestation with varying values.

T2* whole placenta

T2* values of the whole placenta were reported with the influence of confounders and GA. None of the factors influenced T2* values. Also, there was no significant difference between the groups (SGA, DM and controls).

The level of T2* pattern in SGAs took two patterns. Increments with a minimal level of less than one for coefficient over gestational age and a second pattern of a reduction in values over gestation under the influence of GA at birth, birth centiles and autoimmune diseases.

Summary of findings:

Factors that could affect the placenta dimensions (volume, MPT, SA, ADC and T2*):

- GA is significantly affecting the placenta growth pattern.
- Diabetes, COVID-19 infection, birth weight and birth centile, GA at birth, and autoimmune diseases had no effect.
- Placental thickness was non significantly different between the three groups. It had an upward trend with GA in all groups.
- The placental volume took an upward trend in all three groups and was significantly different between SGA/controls.
- In sample 2 (smaller size), both volume and SA showed a significant difference between DM and controls.
- SA took an upward trend over gestation and was significantly different between SGA and controls.
- ADC was different between SGA and controls. This was significant with the effect of GA however, COVID-19 and diabetes affected the results.

- Over gestation, ADC values took opposite trends in SGA and controls as it was increasing in SGA and decreasing in controls.
- ADC gave a different result when a smaller sample was tested (sample 2). ADC was insignificantly different between SGA and controls.
- T2* was not significantly different in placentas among the three groups.
- The pattern was increasing slightly in both controls and SGA placentas and decreasing in diabetics' placentas.

Other factors:

When examined with a linear regression model, these showed no significant impact, these were:

- Maternal factors: maternal age, race, maternal height, weight, BMI, obesity, parity, gravity, inter-pregnancy interval, alcohol, smoking and drugs misuse, abnormal BP and essential HTN, first trimester bleeding, use of ART, medications (aspirin, insulin, metformin and dalteparin) and mode of delivery (CS).
- Perinatal outcomes such as fetal sex, NNU admission, previous FGR, maternal or paternal SGA, and malformations.

Placental features and birth weight, centiles

The median birth centile in SGA was 2.10 and 4.65 in the SGA+DM group (Fig.55).

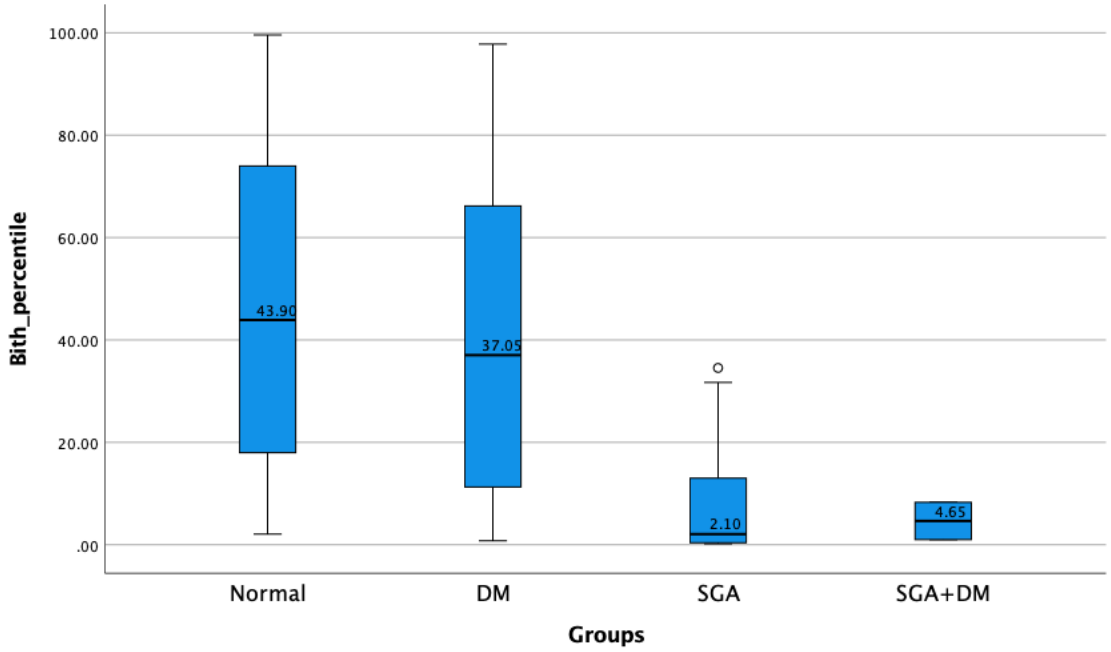

Figure 55: Birth centiles in different groups of participants.

Placental midpoint-thickness

Placental MPT was negatively correlated with birth weight and the correlation was weak and non-significant (r=-0.230, p=0.117). Simple linear regression of birth weight (grams) and MPT (cm) was conducted (R^2=0.053 and a slope of -138.296 (B value) (Fig. 56).

Birth centiles and MPT showed no correlation (r=-0.079, p=0.592).

Linear regression analysis showed (R=0.23, R^2=0.053, B=-138.296, non-significant correlation (p=0.117).

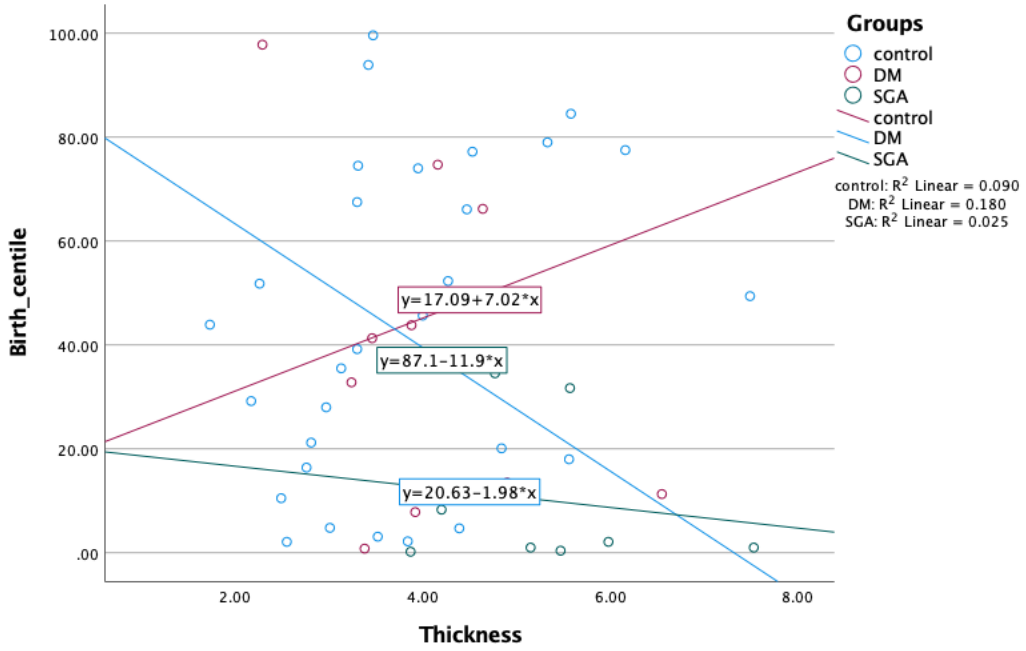

Figure 56: Birth centiles and placental thickness (cm) in different groups of participants.

Placental surface attachment

Birth weight showed a positive moderate Pearson correlation with placental surface attachment (r=0.386). This correlation was significant at the 0.01 level (2-tailed) as p-value was 0.007.

Linear regression results showed:

R=0.386, R^2=0.149, F=8.041, df=1, B=4.274, Beta=0.386, T=2.836.

There was a significant correlation between birth weight and placental SA (P=0.007).

Birth centiles and surface attachment

Placental SA was significantly correlated with birth centiles confirmed with Person's =0.33 (moderate correlation) and p=0.02 at the 0.05 level (2-tailed) (Fig. 57).

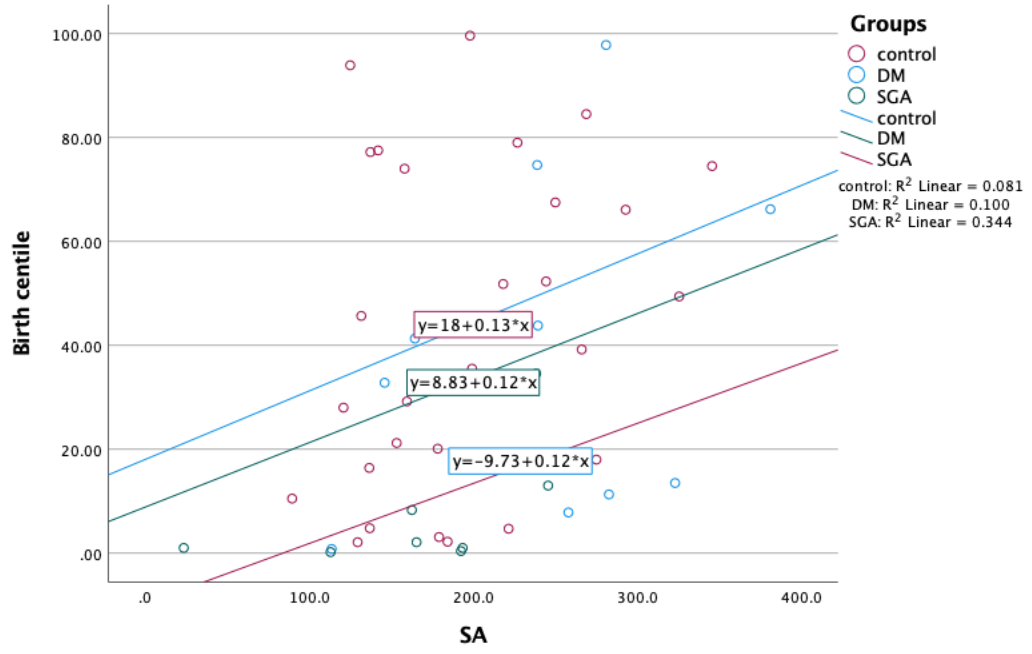

Figure 57: Scatter plot of placental surface attachment (cm2) and birth centiles.

Birth weight and placental volume

Nonparametric correlation of birth weight and placental volume was weak (r=0.173) and not significant (p=0.24).

Birth centiles and volume

Nonparametric correlation showed weak positive correlation (r=0.27, p=0.061) (Fig. 58).

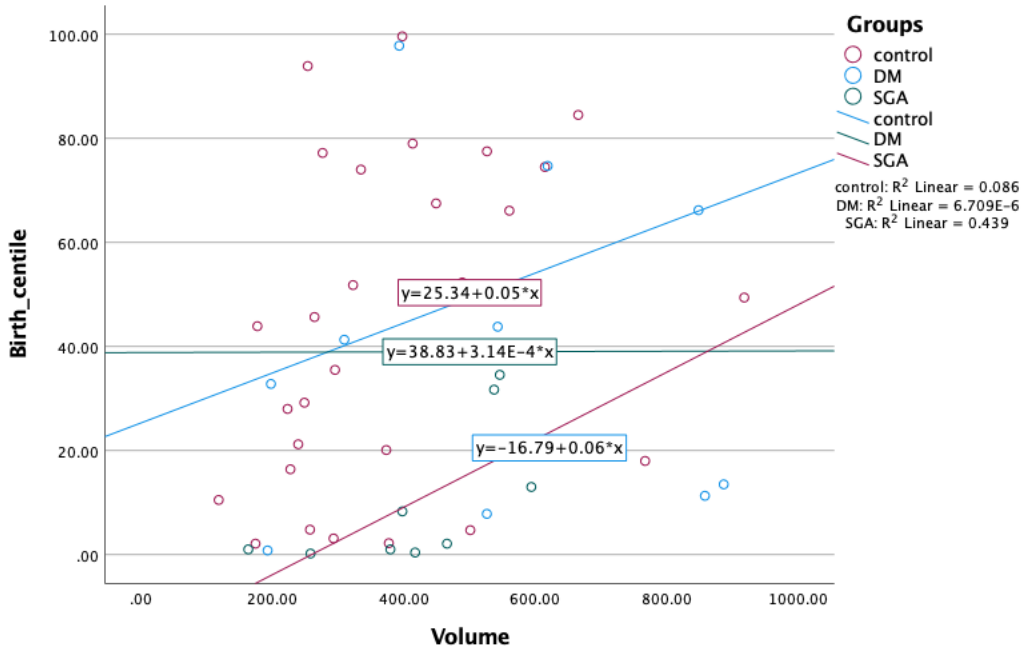

Figure 58: Scatter plot of placental volume (cm3) and birth centiles.

Birth weight and ADC

Nonparametric correlation showed no correlation between ADC of whole placenta and birth weight (r=0.083, p=0.57).

Birth centiles and ADC

ADC was weakly correlated with birth centiles (r=0.105) and the correlation was non-significant (p=0.479) (Fig.59).

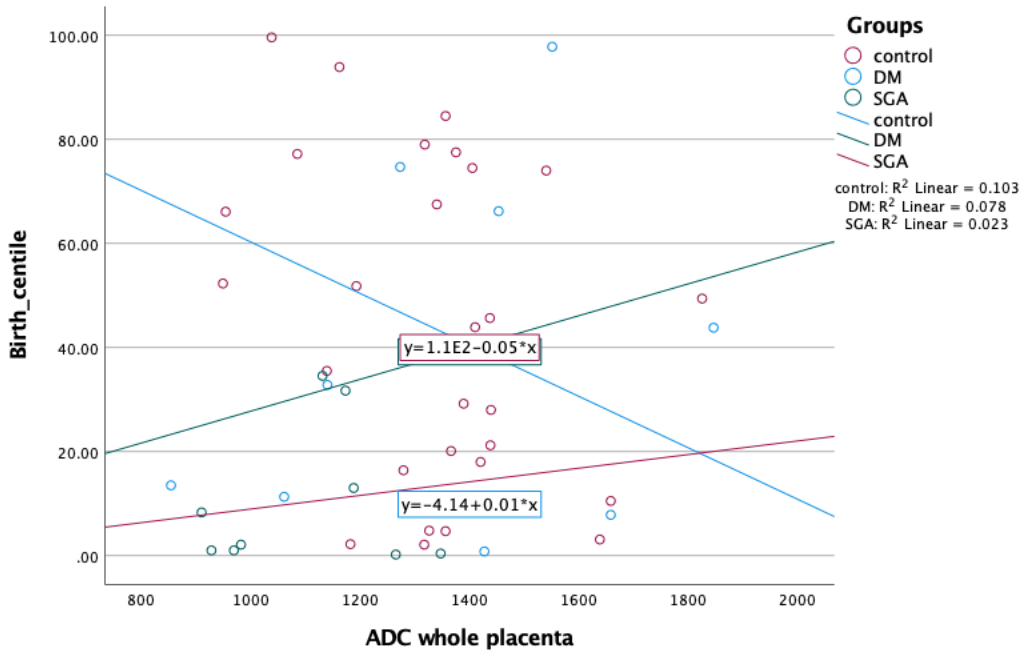

Figure 59: Scatter plot of placental ADC whole placenta (mm2/sec) and birth centile.

Birth weight and T2* whole placenta

Spearman's correlation of birth weight and whole placental T2* showed no correlation (r=-0.07, p=0.65).

Birth centiles and T2* whole placenta

Nonparametric correlations of T2* whole placenta with birth centiles showed no correlation (r=-0.025, p=0.87) (Fig.60).

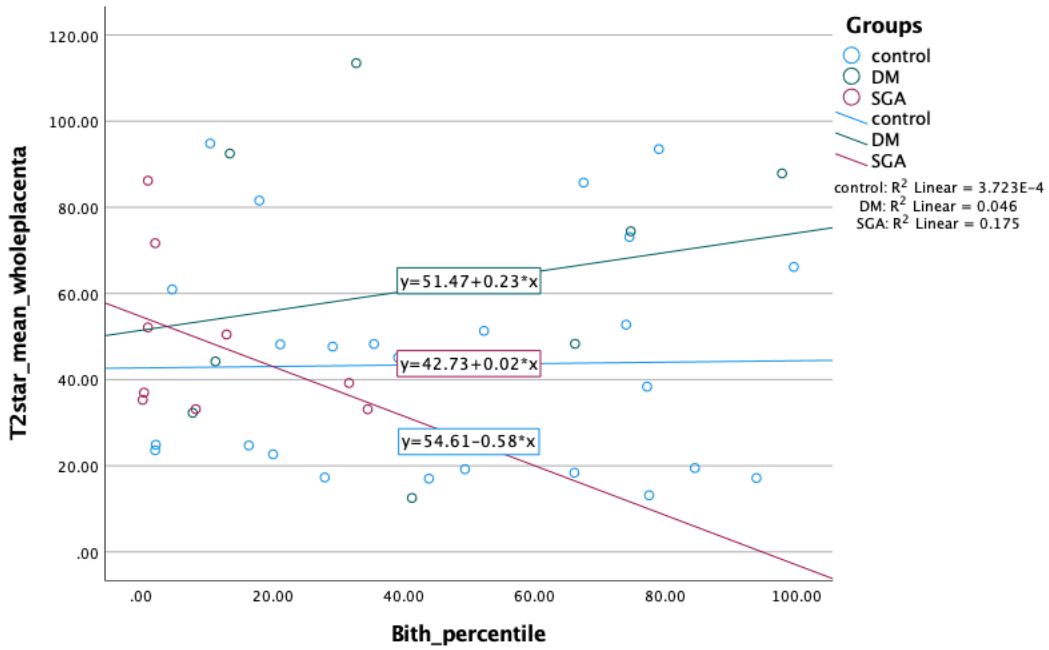

Figure 60: Scatter plot of placental T2 whole placenta (ms) and birth centiles.*

In summary, birth weight and centiles were only correlated with placenta SA measured by MRI.

Discussion

This was a prospective pilot study that used various approaches to look at signs of FGR during the second and third trimesters. It has described longitudinal placental growth in three different groups. SGA placentas were found to be thicker and have smaller volumes and SA whereas diabetics' placentas were bigger than both SGA and controls. These findings were supported statistically and confirmed our hypothesis. Theoretically, a smaller placenta means fewer nutrients and oxygen exchange and higher thickness makes the placenta less efficient.

a) GA and placenta growth

The effect of GA on placenta growth was assessed. MPT, volume and SA significantly correlated with GA ($p<0.001$). Langhoff et al., Andescavage et al. and Leon et al. found a positive correlation between placenta growth and GA (Andescavage, Yarish et al. 2015, Langhoff, Gronbeck et al. 2017, Leon, Li et al. 2018).

In our cohort, term placental volume was 800 cm^3, SA was 320 cm^2 and MPT was 5 cm. We reported measurements of placental volume closer to that reported by Langhoff et al. (Langhoff, Gronbeck et al. 2017) but lower than of Leon at al. and Andescavage et al. (Andescavage, Yarish et al. 2015, Leon, Li et al. 2018). In our cohort placental volume was 800 cm^3 at term, and Langhoff et al. was 787 cm^3 for the same GA range whereas Leon at el. term placental volume was 1,039 cm^3 and Andescavage et al. (Andescavage, Yarish et al. 2015) was 1,000 cm^3. These differences could be due to the variations in the investigated populations, segmentation techniques, equipment used for imaging and practical expertise. Leon et al. cohort (Leon, Li et al. 2018) was large and included multiparous pregnancies, which has been linked in prior research to be related with bigger volume of the placenta (Wallace, Bhattacharya et al. 2013). Although there are not enough studies to compare placental SA, the measured SA in this cohort is closer to the one we conducted in the retrospective study which was 383 cm^2 at 37 weeks. Furthermore, MPT in our controls was higher. Victoria et al. measured thickness of maximum 4 cm in healthy cohort (Victoria, Johnson et al. 2011). A population of 60 included 53 cases in the second trimester of gestation (range 17–26weeks, mean 22±2 weeks) and 7 cases in the third trimester (range 27–34 weeks, mean 31±3 weeks). Their US

measured placental thickness was 1.3-3.7 cm (2.4±0.5 cm) in the second and third trimester was 2.1–3.4 cm (2.9±0.4 cm) (Victoria, Johnson et al. 2011). Their overall MRI placental thickness was 1.7–5.9 (2.9±0.8 cm).

b) Diabetes

In this work, we have described the growth pattern in placentas with diabetes and the effect of various risk factors on them. Placentas were larger in size with higher SA than controls. The mean placental volume measured in our cohort was 453.7 cm^3 with 95%CI (331.9,575.5) cm^3 at GA range (19-38) weeks. A recent study that used quantitative MRI volume and perfusion found a significant increase in volume and a consistent trend of reduced perfusion (Lee, Janzen et al. 2023). Placental volume was measured in 21 participants with GDM and 165 controls on two occasions. The time window of GA was (14-16) weeks and (19-24) weeks. Placental volume with GDM showed a statistical difference from controls. The reference values in GDM placentas were 301.0 cm^3± 84.9 at (19-24) weeks gestation and 255.7 ± 72.2 cm^3 in controls for the same GA window. However, this study was limited only to gestational diabetes, we have shown all types in our cohort. Their numbers are close to our measurements especially the lowest range. There are no other studies to compare MRI findings with and the research focus is on the pathological features rather than finding in vivo changes. We cannot compare other placental measurements in diabetics as only volumetric measurements were reported in literature.

c) SGA

There were significant differences recognized between SGA and controls. Volume and SA are important determinants of placental function. As both showed significant differences between SGA and controls. Also, SGA placentas tend to be higher in thickness, but the difference is not substantial.

The mean placental thickness was 5.2 cm in comparison to controls (4.1 cm). SA was smaller (178.7 cm^2) in SGA while in controls was 210.3 cm^2 and volume was smaller in SGA (435.2 cm^3) while in controls was 441.2 cm^3. Overall, placental MRI measurements may help to predict FGR cases. If the placenta looks like a small cupcake, there is high risk of being insufficient and developing a growth restricted fetus.

Although placental thickness was not significantly different between groups, both volume and surface area were different when GA was accounted for in the analysis. We have also followed up on placenta growth and conducted two different samples analysis, one of them included the longitudinal follow-up scans. Furthermore, morphology at pathology in terms of volume and surface area were correlated with antenatal in vivo placental assessment but not thickness.

Previous studies were not consistent with reporting placental morphological characteristics (measured only volume (Derwig, Akolekar et al. 2011, Andescavage, Yarish et al. 2015, Langhoff, Gronbeck et al. 2017, Leon, Li et al. 2018), only included controls (Langhoff, Gronbeck et al. 2017, Leon, Li et al. 2018). Volume was reported to be smaller in SGA pregnancies (Damodaram, Story et al. 2010, Ohgiya, Nobusawa et al. 2016). Placental thickness was higher in FGR placentas (Ohgiya, Nobusawa et al. 2016, Andescavage, Dahdouh et al. 2019). Victoria et al. measured placental thickness but only controls were assessed (Victoria, Johnson et al. 2011). As in our study, the difference was not substantial. One possible reason for this could be due to the fact that the development of late FGR has more impact on placental volume than shape (Andescavage, Dahdouh et al. 2019) and the importance of the use of combined diagnostic markers. Andecsavage et al. have shown a significant difference in placental volume, no difference in thickness or elongation between normals and FGR (Andescavage, Dahdouh et al. 2019).
The association of globular placenta with poor fetal outcome has been assessed using USS (Fisteag-Kiprono, Neiger et al. 2006) and MRI (Damodaram, Story et al. 2010) but there is limited data in the literature regarding surface attachment. As they are either reported as placental elongation (Andescavage, Dahdouh et al. 2019, Andescavage, Kapse et al. 2021) or measured as the entire surface area which is different from what we did (Ohgiya, Nobusawa et al. 2016) or measured USS (Barker, Thornburg et al. 2010).

In our study, the inclusion criteria of SGA cases were when the EFW is <10th centiles with and without doppler changes. This was different to Andescavage et al. who divided their groups according to Doppler changes but they found the same trends, the reason for that was to increase the diagnostic threshold as there is a significant

number of stillbirths in cases without doppler changes (Andescavage, Dahdouh et al. 2019).

In our cohort, 7 SGA cases (46.6%) were born with normal weight. Monier et al. found that 50% of suspected FGR cases were born with normal birth weight (Monier, Blondel et al. 2015). Besides, not all cases with SGA develop FGR, 21.7% of EFW<10th and 30% of EFW<3rd of SGA diagnosed antenatally have the risk of developing FGR. This raises the suspicion to have more effective biomarkers to detect SGA antenatally. Recent guidelines in the UK focused on the follow-up of fetal growth and observing the pattern of growth over time (Gardosi 2012). The importance lie in the early identification of SGA and regular antenatal visits that could reduce the risk of stillbirth by two folds (Stacey, Thompson et al. 2012).

A comparison of placental indices across genders revealed no difference. Andescavage et al. also identified no differences in the placental morphology (Andescavage, Dahdouh et al. 2019). Interestingly another study by the same group, has reported the impact of gender on placenta growth found a significant difference in the elongation of the placenta in females more than in males' placentas (Andescavage, Kapse et al. 2021).

This study has linked maternal risk factors with placenta growth (i.e., COVID-19 infection, diabetes, hypertension, smoking, autoimmune diseases, etc..). Multivariate analysis has shown that COVID-19 infection did not affect placenta growth, as it was a non-significant covariate. COVID-19 infection has been linked to fetal growth restriction in small and abnormal placenta with infarction and peri villous fibrin deposition (Moltner, de Vrijer et al. 2021, Alessa, Peres et al. 2023). However, histopathology examination has shown no evidence of placentitis in the cohort reported.

Multiple confounding factors have shown no effect on placenta growth. i.e., hypertension had no influence on placental growth. Although research has shown an effect on placenta growth and a smaller surface area was noticed in pregnancies with hypertension (Barker, Thornburg et al. 2010). The reason in our case might be due to

the small number of cases who had HTN during pregnancy (n=4) and none of them were in the SGA group.

Smoking also had no effect on placenta growth as the number of smokers was very small (n=7) and only one case was in the SGA group. Heavy smokers are at high risk of developing FGR (Czekaj, Pałasz et al. 2002). Fetal size and placental volume were smaller when a study of 13 smokers was conducted (Anblagan, Jones et al. 2013). Smoking decreases the density of terminal villi which reduces blood exchange and also causes vasoconstriction (van der Velde, Copius Peereboom-Stegeman et al. 1983) (Castro, Allen et al. 1993).

Birth weight and centiles were correlated with surface attachment, volume, and thickness. While the level of significance was different for these indices, only surface attachment was significant. Reporting of these measures in the literature was inconsistent. Placental volume was correlated with birth weight (Damodaram, Story et al. 2010, Andescavage, Yarish et al. 2015, Langhoff, Gronbeck et al. 2017, Leon, Li et al. 2018). No study has addressed all features in both normal and abnormal cohorts.

Reliability measurements were excellent for placental morphology assessment, it was reported that the intra and inter-rater reliability of normative data for morphometric measures were 0.99 and 0.98 respectively and for ADC were 0.99 and 0.93 respectively (Andescavage, Kapse et al. 2021). This suggests that these techniques are highly reproducible and can be used in clinical practice, however, our results are very different suggesting this is not a reliable method.

In summary, MRI-measured placenta SA and volume (but not thickness) are important predictors of birth weight. These features may provide an in vivo description of placental insufficiency and timely involvement of specialist care for early management and prevention of FGR. Few animal studies have introduced new trials which included the use of melatonin and growth hormones to improve growth-impaired animal models which showed signs of improvement following treatment (de Boo, Eremia et al. 2008, Richter, Hansell et al. 2009). The benefits of MRI in the future could lie in the early detection and monitoring of response to treatment.

d) ADC and FGR

ADC was significantly reduced in SGAs placentas. This finding was supported by previous research. Bonel et al. compared placental morphology and DWI in individuals

with and without FGR, their sample consisted of high-risk pregnancies, but they did not monitor pregnancies over time (Bonel, Stolz et al. 2010). Similarly, Gorkem et al. also concluded that IUGR placentas have lower ADC when compared with controls, their sample consisted of 63 patients and they also did not follow up on their cases (Gorkem, Coskun et al. 2019).

FGR is associated with a reduced placental surface area of exchange at the peripheral villous level, resulting in a smaller exchange area and less diffusion (Carter 2009). Other factors that contribute to reduced diffusion are hematoma and infarctions, these are particularly significant because they cause the placenta to become immature, which reduces its diffusive conductance and restricts blood flow due to tissue ageing and scarring. Diffusion may be impacted by placenta dysmaturity and focal breakdown of the placental barrier (Bonel, Stolz et al. 2010).

ADC was influenced by GA in an inverse correlation in the control group. The effect of GA on placental diffusion had been described in a few papers with various findings, Seidbakht et al. found that GA significantly affects ADC (Sefidbakht, Zeinali-Rafsanjani et al. 2019). Other studies contradicted this concept as there was a non-significant reduction of ADC with advanced gestation (Shapira-Zaltsberg, Grynspan et al. 2018, Andescavage, Kapse et al. 2021). Gorkem et al. also found GA has no effect on the placental diffusion (Gorkem, Coskun et al. 2019).

Our strength was that we conducted two-sample analyses of ADC and placental morphometric measurements and compared them with maternal risk factors. We have also followed up on these measurements and looked at any change in placental perfusion over gestation which other similar published research have not (Bonel, Stolz et al. 2010, Gorkem, Coskun et al. 2019). The GA range was (21–41) weeks in the first study (Bonel, Stolz et al. 2010), and (28-34) weeks in the second study (Gorkem, Coskun et al. 2019). Our cohort has similar GA window if not wider (19-38) weeks.

ADC values may have a prospective role in diagnosing and treating FGR because microstructural and functional changes occur before gross morphological findings (Avni, Neeman et al. 2015). To sustain a healthy rate of nutrients and oxygen exchange within the placenta, proper interactions between maternal and fetal

circulation are required. FGR may develop from impaired fetal trophoblast penetration into the mother's decidua; this condition is clinically assessed by hypoxemia and lactic acidosis' downstream effects on the fetal circulation and upstream effects on the uterine colour Doppler ultrasound. These modifications improve a wide usage of ultrasonography in the diagnosis, follow-up, and management of fetuses with FGR or who are at high risk for FGR (Sefidbakht, Zeinali-Rafsanjani et al. 2019).

e) Diabetics placentas and ADC

The mean of ADC was less than that of controls, however, the difference was not significant. Similar findings of functional MRI (ADC) were in a study that showed reduced perfusion in placentas with gestational diabetes. Although different perfusion parameters were used, the mechanism and trends were similar (Lee, Janzen et al. 2023).

f) T2* and GA

In this part, we reported the T2* reference values of normal placentas for a relatively big sample (n=77). GA had no effect on T2* (p=0.1) and took a positive trend in controls. The possible reason for that is when the fetus grows, oxygen consumption increases, and this produces more deoxygenated haemoglobin and so the T2* also increases. Huen et al. found no correlation with GA (Huen, Morris et al. 2013). Sun et al. found a similar finding when they measured the T2* of the whole placenta. There were fluctuations of T2* in relation to GA taking an upward trend up to 35 weeks and then a downward trend after 35 weeks (Sun, Wu et al. 2023). They also measured T2* in different locations in the placenta and found different T2* values according to their topographic locations (Sun, Wu et al. 2023). As suggested by Sinding et al., we have measured the whole placenta T2* as it is more reproducible than drawing a small ROI (Sinding, Peters et al. 2016). Another study found a downward trend in T2* with GA using a 1.5T MRI system (Wright, Morris et al. 2011). The scientific explanation of reduced T2* over gestation is explained by the reduction of placental oxygenation with maturation and reduced perfusion (Soothill, Nicolaides et al. 1986, Sohlberg, Mulic-Lutvica et al. 2014).

Our T2* values have a positive correlation with GA from 19 to 38 weeks, with upward trend with GA. The relationship between baseline T2* and GA in normal pregnancies

have been discussed in six studies. Four of them have discovered a substantial reciprocal relationship between baseline T2* and gestational age (Sinding, Peters et al. 2016, Sinding, Peters et al. 2017, Sinding, Peters et al. 2018, Hutter, Slator et al. 2019). Only one research found a non-significant negative correlation (Ingram, Morris et al. 2017) whereas Huen et al. found no link between T2* and GA (Huen, Morris et al. 2013). In our study, the baseline T2* was 25 ms in controls at 38 weeks gestation. While the baseline T2* was calculated to be 47-58 ms at 1.5T in normal-term pregnancies (Huen, Morris et al. 2013, Sinding, Peters et al. 2016, Ingram, Morris et al. 2017). Ingram et al. reported a baseline of 17 s-1 controls R2* and not correlated with GA but FGR 26 s-1 R2* where R2* is equal to (1/T2*). In conclusion, our study does not agree with the reciprocal nor the nonsignificant negative correlation trends of the published data.

g) T2* and FGR

T2* took a different trend in diabetics and SGAs, it was the highest in diabetics' placentas and the lowest in SGAs. This could be due to reduced oxygenation in SGAs. In SGAs, T2* was reciprocal with placental weight, birth weight and centiles. This could be due to the reason that T2* measures the perfusion function, areas with lower perfusion have less iron and higher T2* (Wood, Enriquez et al. 2005). Furthermore, smaller placental surface area and higher thickness were reflected with less perfusion and lower T2* mean in SGAs than controls with similar birth centiles.

Published research showed T2* was reduced in cases with FGR (Derwig, Barker et al. 2013, Sinding, Peters et al. 2016, Ingram, Morris et al. 2017, Sinding, Peters et al. 2017, Sinding, Peters et al. 2018). A low placental T2* value was a robust predictor of low birth weight in a prospective cohort study which performed better than uterine artery Doppler flow measures (Sinding, Peters et al. 2017). When FGR patients were compared to normal controls, the baseline placental T2* value was considerably lower. Sinding et al. compared T2* values between normal and FGR cases, their sample size consisted of 24 controls and only 4 cases with FGR with an EFW of <1st centiles. They reported reduced T2* values in FGR cases. The link was only in FGR cases with abnormal Doppler and histology changes. Also, T2* was measured by taking the average of 2 slices while in this project, the T2* map was quantified using the time of decay of signal between the 3 slices (Sinding, Peters et al. 2016).

Sun et al. offered a new approach that uses T2* and diffusion-weighted MRI to automatically classify placental compartments, measure their oxygenation characteristics, and identify placental lesions in vivo. They recruited 27 patients in a prospective study of dual MRI scans. There were 5 cases of complicated pregnancy in which T2* was reduced dramatically in the layer nearest to the chorion throughout the gestation (Sun, Wu et al. 2023). Their major limitations were their small sample size and the wide variety of the group with a complicated pregnancy.
Derwig et al. used EPI to measure T2* in 40 pregnancies of which 25 were diagnosed with SGA (birth weight <10th centile). They found that T2* was reduced in cases with high uterine artery Doppler and low birth weight (Derwig, Barker et al. 2013).

Our data showed a significantly lower T2* baseline than the available published data. The baseline of T2* in SGAs was 38 ms at 32 weeks gestation and 75 ms at 35 weeks gestation. There has been some variation in T2* reference values in SGAs among published papers, according to GA at 1.5T. Anderson et al. reported T2* values were 184 ms at 20 weeks of gestation and 89 ms at 40 weeks (Anderson, Andersen et al. 2021). Few studies were similar to Anderson's in terms of reduced T2* values with GA; their reported values were 100 ms at 35 weeks (Kameyama, Kido et al. 2018) and 149 ms at 27 weeks of gestation (Derwig, Barker et al. 2013). Wright et al. reported higher T2* values of 195 ms at 29 weeks of gestation (Wright, Morris et al. 2011). This variation was justified due to the different cut-off points in the definition of SGAs. Anderson's research defined SGA as birth weight <1st centile while Wright et al. reported low birth weight as <5th centiles. Reduced T2* value can signal placental insufficiency which could be due to fibrosis, vascular constriction, or reduced oxygen saturation. As there is a high rate of false positive diagnoses of placental insufficiency, other causes of SGA should be considered.

Limitations and conclusion

There have been several limitations. First, delay in the project approval and start of the recruitment process was the main limitation. Short timeline of recruitment due to the COVID-19 pandemic made our sample smaller, especially for SGAs.

Secondly, manual segmentation of the placenta is a time-consuming activity.
Not all cases had a histopathological assessment and there was a delay between the histological and antenatal MRI examinations. Some cases were lost to follow-up either due to transfer into another area or they were referred from other hospitals.
The numbers are small especially in the diabetic and SGA group. This may mean that even the trends may not be seen with higher numbers and more detailed analysis was not performed. However, there are more controls and SGA cases and the trends here may be statistically significant in a larger cohort.
A larger cohort would allow additional assessment of co factors.
The histological analysis was not completed due to both the initial delay in recruitment and then the time constraints of the histopathologist both due to the COVID-19 pandemic.
The inter and intra class correlation was good or excellent for all biomarkers except ADC where the inter relator correlation was poor. The reason for this is unclear but it does mean that ADC might not be a reliable or useful biomarker.
The SGA cases were defined by the clinical categorisation, and this is highly variable. It was not split in to early or late and no consistent definition was used in the clinic.
The analysis was performed on the antenatal categories, a repeat analysis on the postnatal category may give slightly different results.

Conclusion

The placenta has been noted to have a wide variety of appearances on MRI, but no formal analysis has been undertaken assessing all the appearances in a single study. Fetal growth restriction (FGR) is a serious complication, which has many drawbacks to the fetus. Several studies have used MRI to detect specific placental features present in restricted fetuses, including abnormal volume, thickness, and general appearances. Literature suggests that low volume may indicate a poor outcome (Dahdouh, Andescavage et al. 2018) or low birth weight (Damodaram, Story et al. 2010); however, there is no current consensus and few studies obtained outcome data, merely reporting the MRI findings between a single pathology, for example SGA and a control group.
This is the first study we are aware of that looks at multiple biomarkers in the same patient and the outcome postdelivery, both the placenta and the baby. In addition, we

have assessed the potential clinical confounding variables that have been neglected in previous studies including Covid.

This research shows trends suggesting that placental thickness, volume, SA, and T2* are all potential biomarkers, independent of other confounding variable to investigate for placental growth and function that need further research. We have also produced normative data for these biomarkers and shown how these changes with gestational age. This relates the surface area, thickness and volume in the same patient which has not been shown previously.

Section 3

Pathology of the placenta in FGR

Histopathology of the placenta in FGR

An examination of placental pathology can identify the underlying causative agent and mechanism. Currently, there is no single pathognomonic sign to diagnose FGR-associated placental insufficiency. This is mainly due to the presence of a wide range of causes and mechanisms (Mifsud and Sebire 2014). The problematic aspect of the diagnosis is that 25% of placentas with FGR do not show any pathological changes (Mifsud and Sebire 2014). Fox H et al. and Mifsud and Sebire et al. mentioned in their papers that one-quarter of FGR placentas don't show any pathological findings (Fox 2007, Mifsud and Sebire 2014). However, another paper mentioned only 2% of placentas didn't show any pathological changes (Sundari Amirthakatesan, Devi Chandramohan et al. 2023). The reason behind that might be due to the difference in the research inclusion criteria, setting, epidemiology and socioeconomic factors. Amirthakatesan et al. studied placentas of neonates with birth weight less than the 10th percentile in India (Sundari Amirthakatesan, Devi Chandramohan et al. 2023). While Fox H et al. conducted a retrospective study of 200 placental tissues. Dilation and evacuation (D&E) technique was used to get the placentas following abortion regardless of the placental pathology. In their review, Mifsud and Sebire et al. mentioned the placental pathological findings in the former research (Fox 2007, Mifsud and Sebire 2014).

Placental insufficiency has been categorized into two essential areas, maternal and fetal vascular malperfusion (Khong, Mooney et al. 2016, Sehgal, Dahlstrom et al. 2019). The former includes placental infarction, distal villous hypoplasia, accelerated villous maturation and decidual arteriopathy. The latter shows thrombosis, segmental avascular villi and villous stromal vascular karyorrhexis (haemorrhagic endo-vasculitis) (Mifsud and Sebire 2014, Sehgal, Dahlstrom et al. 2019).

Most placentas seen in FGR cases tend to exhibit abnormal pathological changes in contrast to those complicated by maternal hypertension which are more likely to have a wide range of gross and microscopic aberrations (So Young Park 2019). For example, placentas have delayed growth, they are therefore smaller and lighter in weight in comparison with those identified in appropriate for gestational age at the same gestational age (So Young Park 2019). The umbilical cord may also show abnormal anatomy and or placental insertion. Insufficient invasion of trophoblast and

disturbed remodelling of smooth muscle vasculature results in vascular atherosis and fibrinoid necrosis. This can lead to an abnormal placental flow (Sehgal, Dahlstrom et al. 2019). Microscopical findings, on the other hand, comprise two major components: 1) those caused by vascular insufficiency (placental infarction, syncytial knotting, presence of nucleated RBCs, distal villous hypoplasia and accelerated villous maturation) and 2) those caused by inflammation (villitis, chorioamnionitis and funisitis)(Macara, Kingdom et al. 1996, Veerbeek, Nikkels et al. 2014, Sehgal, Dahlstrom et al. 2019, So Young Park 2019).

In contrast to AGA, significant pathological differences have been found in FGR placentas. However, no relevant differences seem to be present in non-hypertensive FGR placentas versus those with maternal hypertension. Several studies have concluded that decidual vasculopathy is higher in cases of hypertension-induced FGR (So Young Park 2019). Others have hypothesized that hypertensive placentas have a higher rate of chronic inflammation and syncytial knotting in comparison with normotensive placentas (40% vs. 20%) (Veerbeek, Nikkels et al. 2014).

Pathological assessment is an essential step in the diagnosis of FGR, as it is a way to correlate MRI findings detected during pregnancy with those in real tissues. MRI possesses better detection for specific pathological features than histopathology such as retro-placental haemorrhage, hematoma, subchorionic hematoma, and ischemia. It is nevertheless less reliable in the finding of chorioamnionitis and fibrin deposition (Linduska, Dekan et al. 2009). In conclusion, histopathology can point to defects that may be detectable on antenatal MRI. It is thus necessary to obtain a reliable MRI measure to improve the diagnosis of fetal growth abnormalities.

The key characteristics of severe early-onset FGR, are those of compromised maternal uteroplacental perfusion as a result of faulty extravillous trophoblast invasion and its aftermath. Late-onset FGR is likely more diverse with fewer distinctive histological abnormalities (Mifsud and Sebire 2014).

Fetal thrombotic events may be suggested by a higher incidence of various villous abnormalities, such as fibrosis, hypovascularity, and avascularity, in placentas from FGR at term (Kovo, Schreiber et al. 2010).

While "new" FGR cases (those that followed an AGA pregnancy) were characterised by a higher rate of FVM lesions and lower birthweight, which most likely represent a placental "accident," recurrent FGR was linked to maternal background morbidities during pregnancy, which indicates a chronic repeated insult. These results could imply that the two FGR subgroups have distinct mechanisms of placental malfunction (Levy, Alberti et al. 2020).

In research done by Levy et. al. to investigate the placental differences in new versus recurrent FGR, the main findings were:

1. One third of FGR cases in non-nulliparous women were recurring cases, while the remaining two-thirds occurred following an AGA pregnancy.
2. Compared to the FGR after AGA group, they found that the recurrent FGR group had a higher prevalence of hypertension disorder and diabetes mellitus of any kind during pregnancy. This finding highlights the role of maternal disease and creating a hostile environment as risk factors for recurrent FGR (Vayssiere, Sentilhes et al. 2015).
3. Compared to the recurrent FGR group, the birthweight was substantially lower in the FGR after the AGA group, and placentas from the FGR after AGA group had significantly more FVM (fetal vascular malperfusion) lesions. Both parameters point to insufficient placentation as an unexpected event that may be called an "accident."

Methods

The patients enrolled in the prospective study reported in the previous section agreed to standard pathological assessment of their placenta post-delivery.
The aim was to assess the placentas for any patterns of change within the SGA group not seen in the control group and to then assess the MRI images to determine if these changes could be precited on the imaging. Unfortunately, this did not happen due to time constraints on the pathology department.

Results

Analysis was completed using the antenatal groupings of SGA, diabetics, and controls. The DM and SGA groups contained 3 patients and whilst these were

analysed, and graphs obtained. The group was deemed too small for statistical analysis and any formal conclusions.

Morphology and demographics

Perinatal outcome	Total mean (min-max)	Controls mean (min-max)	SGA mean (min-max)	DM mean (min-max)
GA at birth *	37.9(27-43)	39.5(37-42)	36(31-42)	37.4(33-40)
Fetal gender	male=24, female=26	male=14, female=15	male=3, female=6	male=5, female=5
CS	56% (28/50)	n=13	n=7	n=7
Birth weight (grams)	2987.4 (955-4340)	3569.3 (2585-4340)	1951.7 (1180-3530)	3103.8 (2160-3950)
Birth weight centile	35.2 (0.20-99.60)	43.8 (2.1-99.6)	9.7 (0.2-34.5)	39 (0.8-97.8)
NNU admission	n=10	n=5	n=1	n=2
Malformations	n=4	n=1	n=2	n=1

Table 23: Perinatal outcome

*GA at birth was non significantly different between groups (controls, SGA, DM), (one-way ANOVA test, p= 0.07).

Using the ReCode system (used clinically in all cases in the local pathology department), we systematically classified the pathological features that have been shown to been related to fetal growth restriction into:

Fetus

Infection

feto-maternal haemorrhage

twin-twin transfusion

Fetal growth restriction

Cord

Constricting loop or knot: cord hyper-coiling was common, presented in controls (n=4/16), SGA (n=7/11), DM (n=1/3).

Velamentous insertion

Umbilical cord-other

Placenta

Placental insufficiency

Preterm, small placental centiles

Amniotic fluid

Chorioamnionitis

Oligohydramnios

Polyhydramnios

We had 29 placentas in total assessed for histopathology (15 controls, 10 SGA and 4 diabetics). Features were divided into:

- Gross pathological features
- Placental weight

Descriptive statistics of placental weight in the three groups are shown in (table 24 and Fig. 61).

Groups	Mean weight (gm)	95%CI	Min (gm)	Max (gm)	Range (gm)	SD	Median (gm)
Controls	642	412-511.9	280	602	322	90.2	459
SGA	311.3	237.2-385.5	157	468	311	103.7	308
DM	420	367.6-472.4	387	454	67	32	420

Table 24 Characteristics of placental weight in different groups of participants.

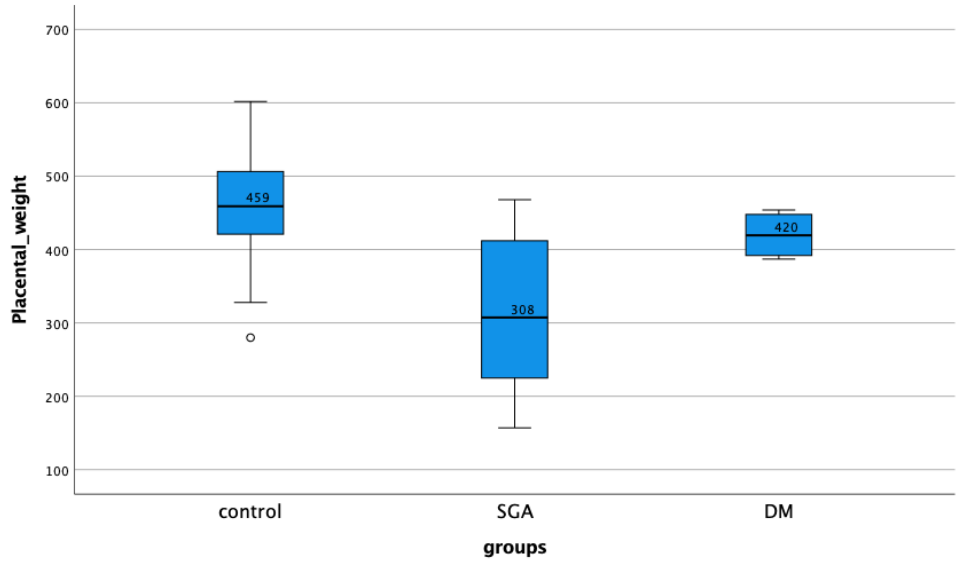

Figure 61: Box and whisker plot of placental weight (gm) showing the three groups' readings.

Placental centiles

To calculate stats, we divided the centiles range into minimum (min) and maximum (max) (table 25, 26).

Groups	Mean min centiles	95%CI	Range	SD	Median
Controls	36	22.4- 49.6	65	24.6	25
SGA	14.6	1.03- 28.2	50	18.9	7.5
DM	36.3	-14.6 - 87.1	65	32	30

Table 25: Characteristics of placental centiles in different groups of participants.

Groups	Mean max centiles	95%CI	Range	SD	Median
Controls	55.7	41.4- 70	75	25.8	50
SGA	25.8	6.2- 45.4	72	27.3	17.5
DM	53.8	0.03-107.5	65	33.8	50

Table 26: Descriptive statistics of placental centiles min and max in the three groups.

Surface area

The surface area was calculated using the formula of an ellipse (x*y*π). These are shown in (table 27 and Fig.62).

Groups	Mean SA (cm2)	95%CI	Min (cm2)	Max (cm2)	Range (cm2)	SD	Median (cm2)
Controls	884	778 - 990	588	1244	656	191.4	895
SGA	648.6	535.1-762	253.7	792	538.3	158.6	691.4
DM	2018	949-3086.8	1015	2442.9	1428	671.7	2307

Table 27: Descriptive statistics of placental SA in the three groups.

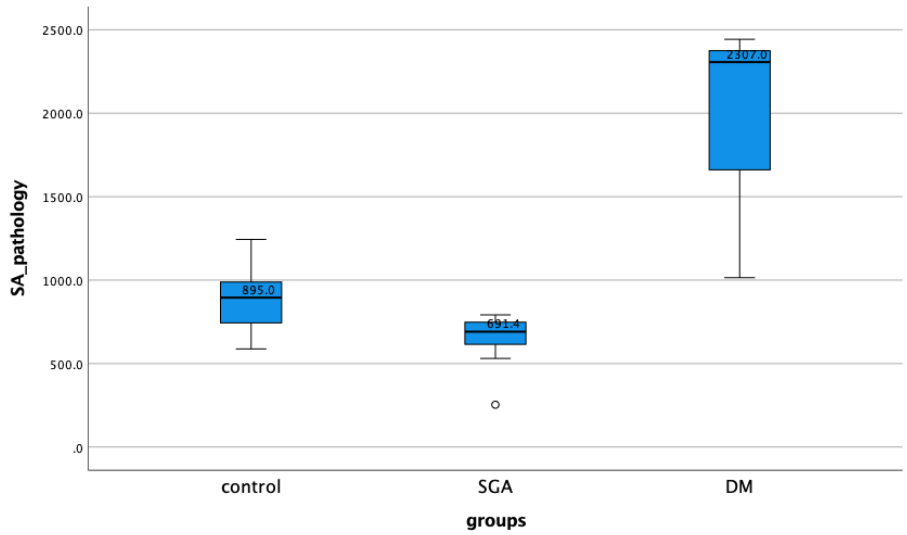

Figure 62: Box and whisker plot of placental surface area (cm2) measured after delivery in three groups.

Volume

Volume was calculated by multiplying the surface area by thickness (table 28 and Fig.63).

Groups	Mean volume (cm3)	95%CI	Min (cm3)	Max (cm3)	Range (cm3)	SD	Median (cm3)
Controls	2566.9	2006- 3127.9	1018	4477	3459	1012	2543
SGA	1572.3	1255.8- 1888.8	634	2243	1609	442.5	1673
DM	5333.8	2269.5- 8398	2538	6922	4384	1925.7	5927

Table 28: Descriptive statistics of placental volume in the three groups.

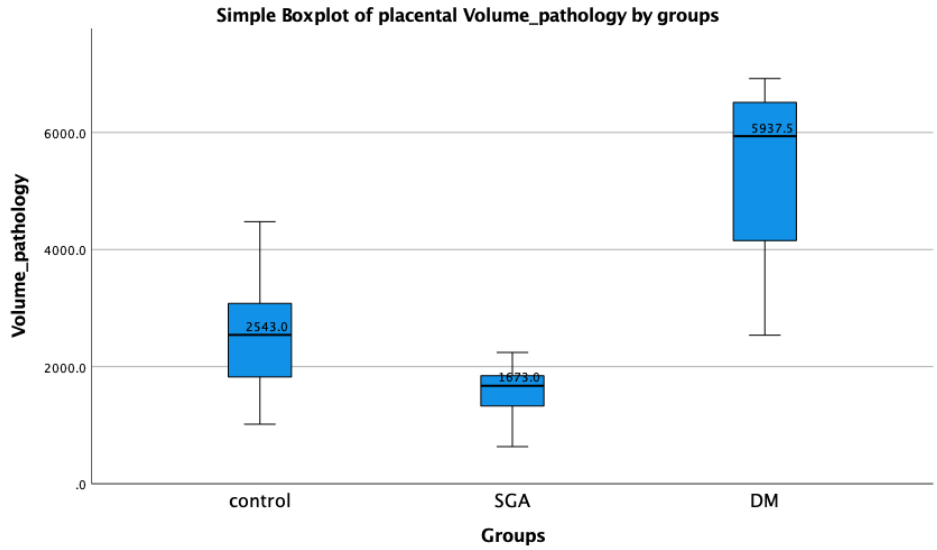

Figure 63: Box and whisker plot of placental volume (cm3) measured after delivery in three groups.

Thickness

Placental thickness statistics are described (table 29 and Fig.64).

Groups	Mean MPT (cm)	95%CI	Min (cm)	Max (cm)	Range (cm)	SD	Median (cm)
Controls	2.9	2.4-3.3	1.5	5	3.5	0.9	3
SGA	2.5	2.1- 2.8	1.5	3	1.5	0.4	2.5
DM	2.6	2.2 - 3	2.5 and 3	3	0.5	0.3	2.5

Table 29: Descriptive statistics of placental thickness in the three groups.

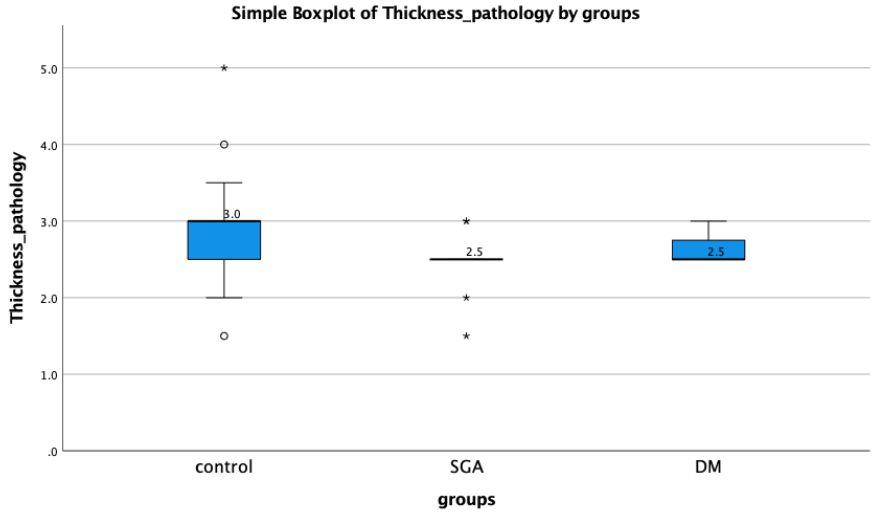

Figure 64: Box and whisker plot of placental thickness (cm) measured after delivery in three groups.

Feto-placental ratio

F/P ratio are described in table 30 and Fig.65, 66.

Groups	Mean F/P ratio	95%CI	Min	Max	Range	SD	median
Controls	6.6	6-7.3	3.9	8.8	4.9	1.2	6.5
SGA	6.8	5.9 -7.7	3.9	8.6	4.6	1.3	7.01
DM	6.6	4.1-9.1	4.9	8.7	3.8	1.6	6.4

Table 30: Descriptive statistics of F/P ratio in the three groups.

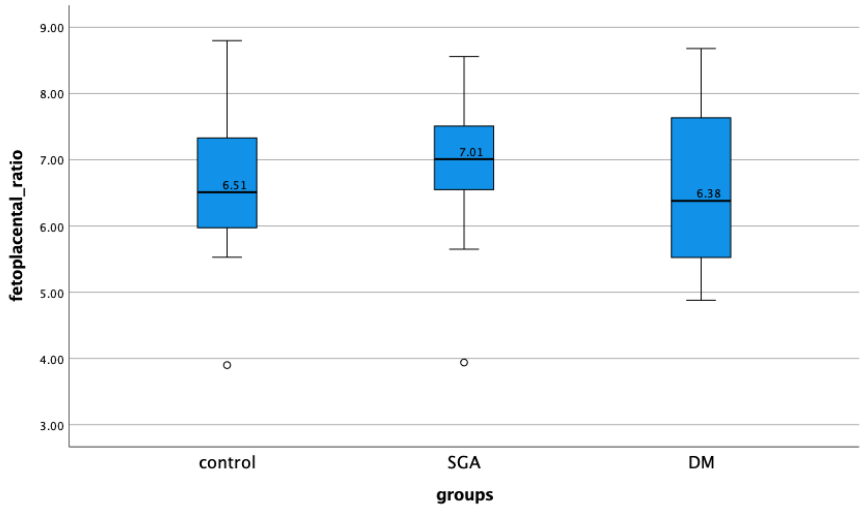

Figure 65: Box and whisker plot of placental feto-placental ratio measured after delivery in three groups.

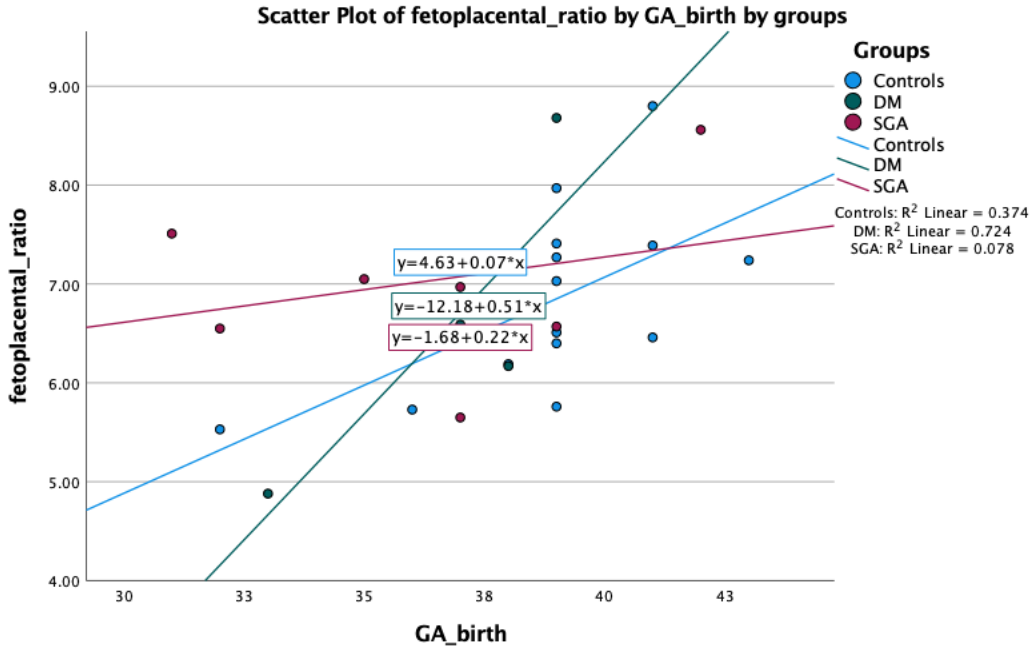

Figure 66: Scatter plot of feto placental ratio over time of delivery of placenta. The ratio is highest for SGA and lowest in diabetics. All ratios were increasing in relation to time of placental birth.

Fetoplacental centiles

Like placental centiles, we divided the F/P ratio centiles into minimum (min) and maximum (max). For controls, the mean fetoplacental centiles min was 42.3 and max mean was 61.9. 95% CI for min and max centiles was (27.9 to 56.8) and (46.8 to 76.9) respectively, with a range of 90 to 92 for both, SD for min 26.1 and 27.2 for max and

median of 50 for min and 75 for max. For SGA, the mean fetoplacental centiles min was 48.3 and max mean was 65.7. 95% CI for min and max centiles were (27.4 to 69.2) and (44.3 to 87.2) respectively, with a range of 92 for both, SD for min 29.2 and 30 for max and median of 50 for min and 75 for max. While in diabetics, the mean feto-placental centiles min was 37.5 and max mean was 55. 95% CI for min and max centiles were (-19.3 to 94.3) and (8.6 to 101.4) respectively, with a range of 80 and 70 for both, SD for min was 35.7 and 29.2 for max and median of 25 for min and 50 for max.

Comparing MRI prediction and pathology for placental measurements

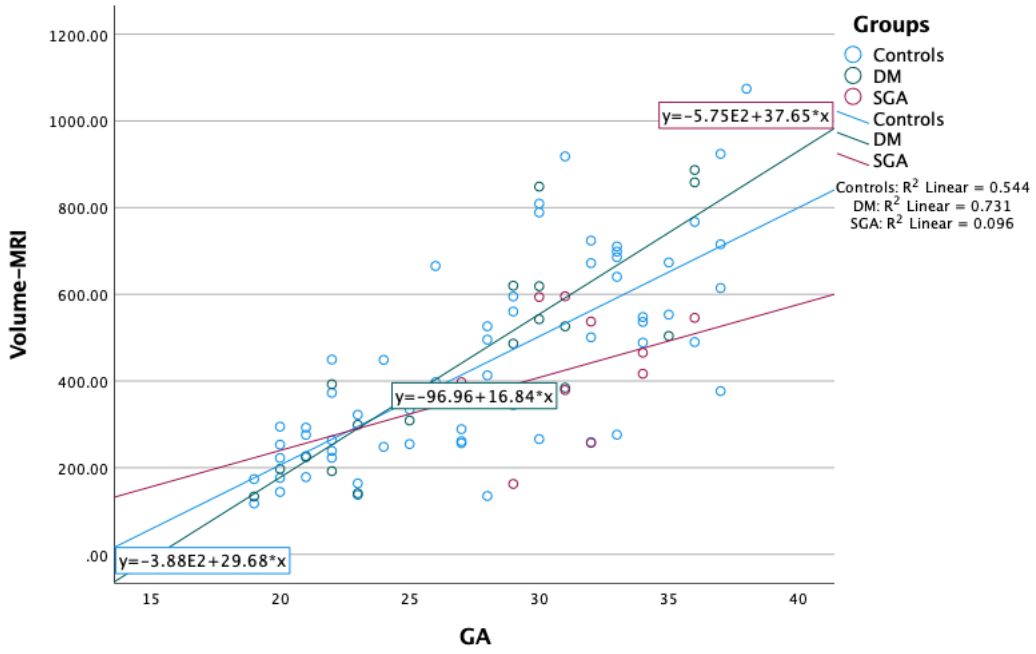

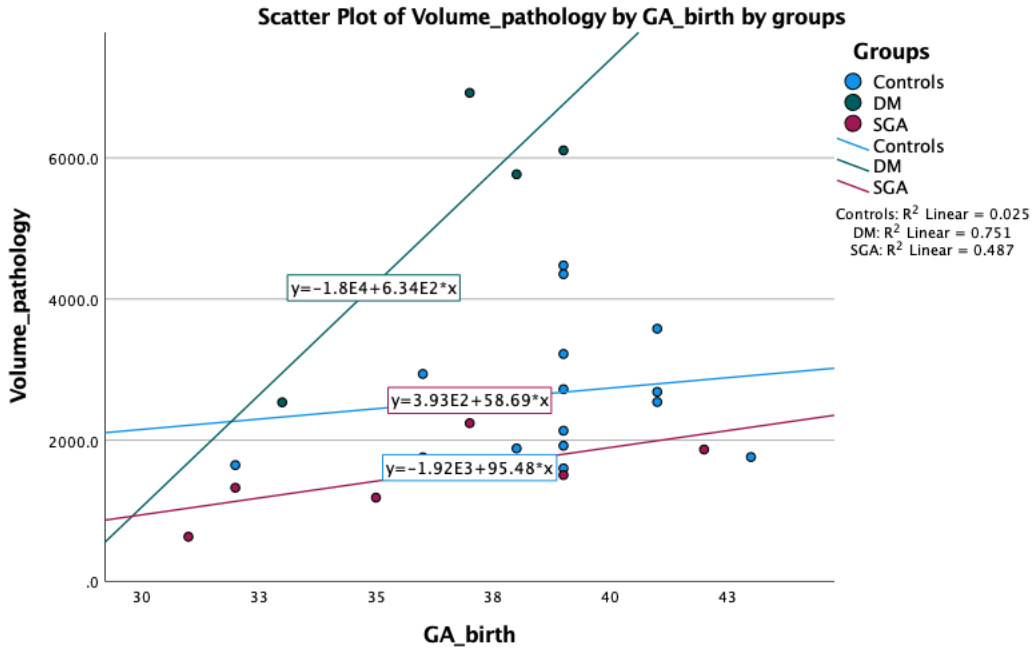

Figure 67: Scatter plot of placental volume (cm3) according to the time of delivery in three groups (diabetics, control, and SGA). Regarding placentas from the control group, it is noticeable that the volume increases slightly with gestational age while in diabetics, volume increment is in a steep line, although there are only four reported placentas. So, the trend is increasing over the gestational age. Comparing the two plots from both MRI and pathology results, both are showing the same trends and patterns in placental volume across gestation in the three groups.

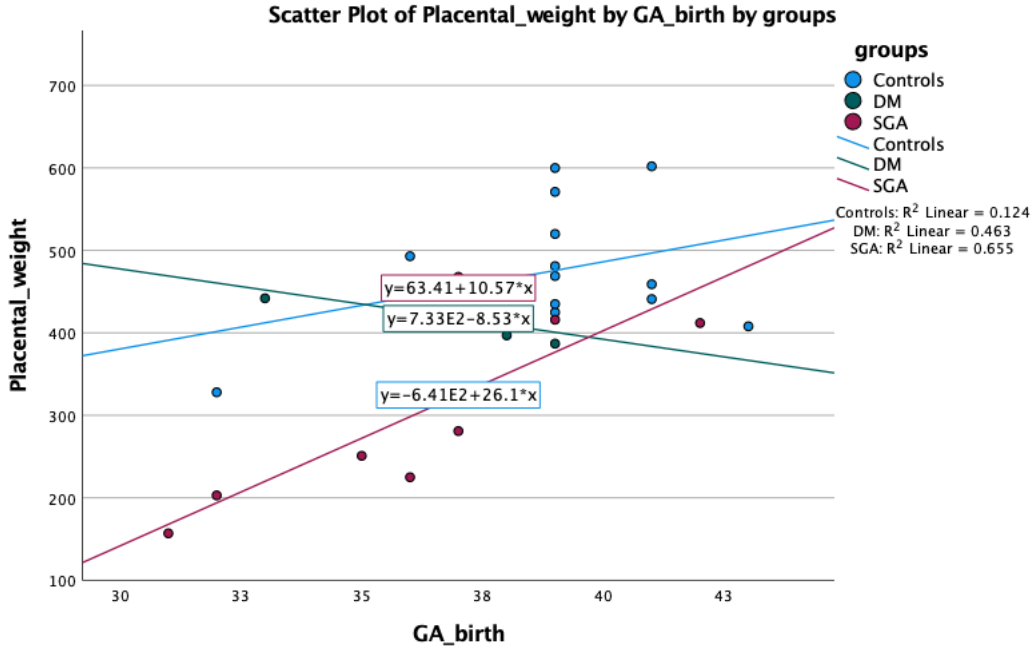

Figure 68: Scatter plot of placental weight (gm) and placental delivery time (weeks). As the gestational age increases the placental weight increases in controls and SGA

however the starting point of the placental weight in SGAs is about 120 gm and lower than in control and diabetics groups. The fitness to regression line is shown in the figure.

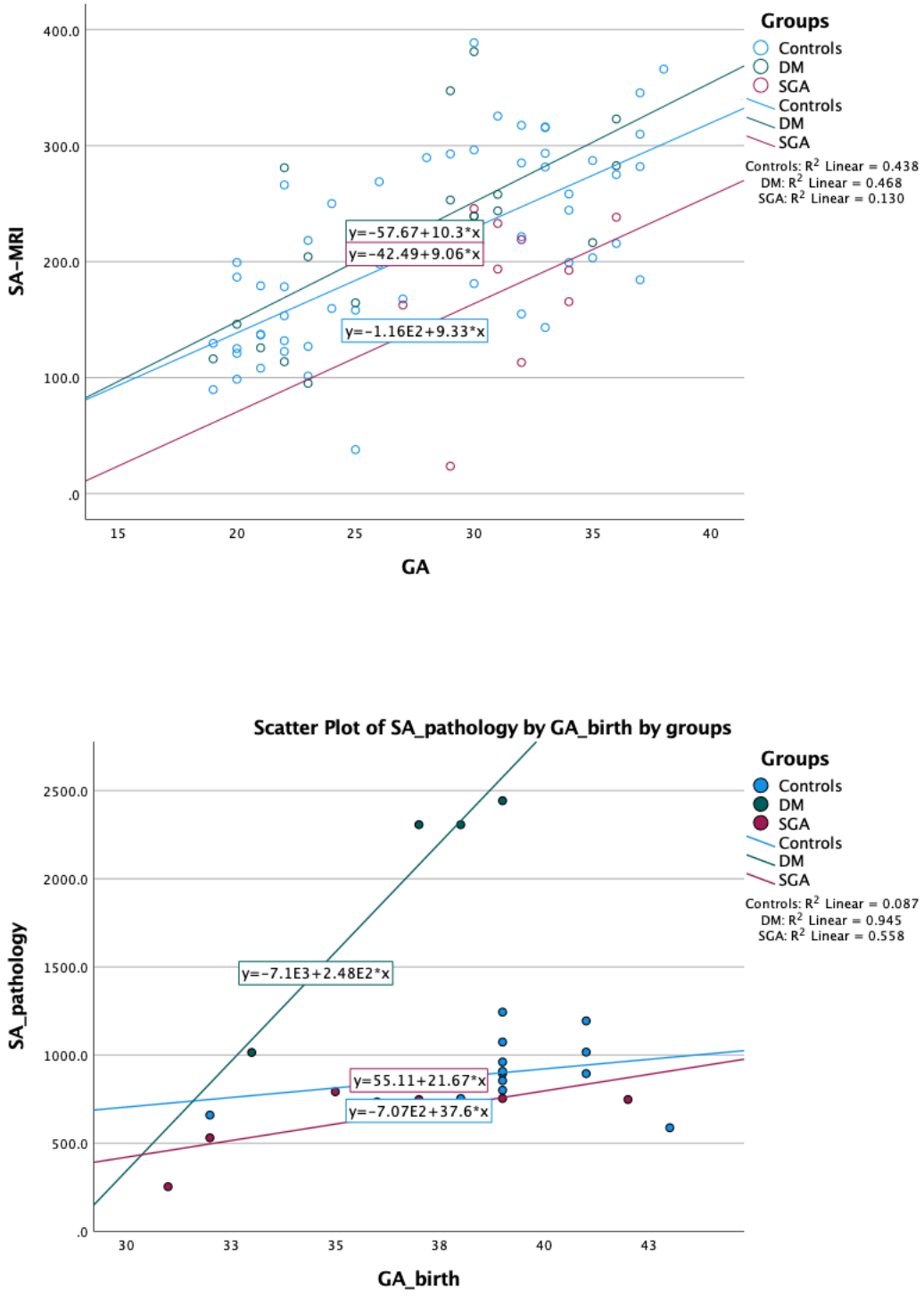

Figure 69: The scatter plots of the two above graphs compare the measured surface area from MRI (cm2) and the surface area (cm2) from placentas after delivery with their gestational age (weeks). Interestingly, the change in surface area is taking the

same trends in the three groups, SGA, diabetics, and control. Although there is a difference in the numbers between the two plots, they are taking the same pattern.

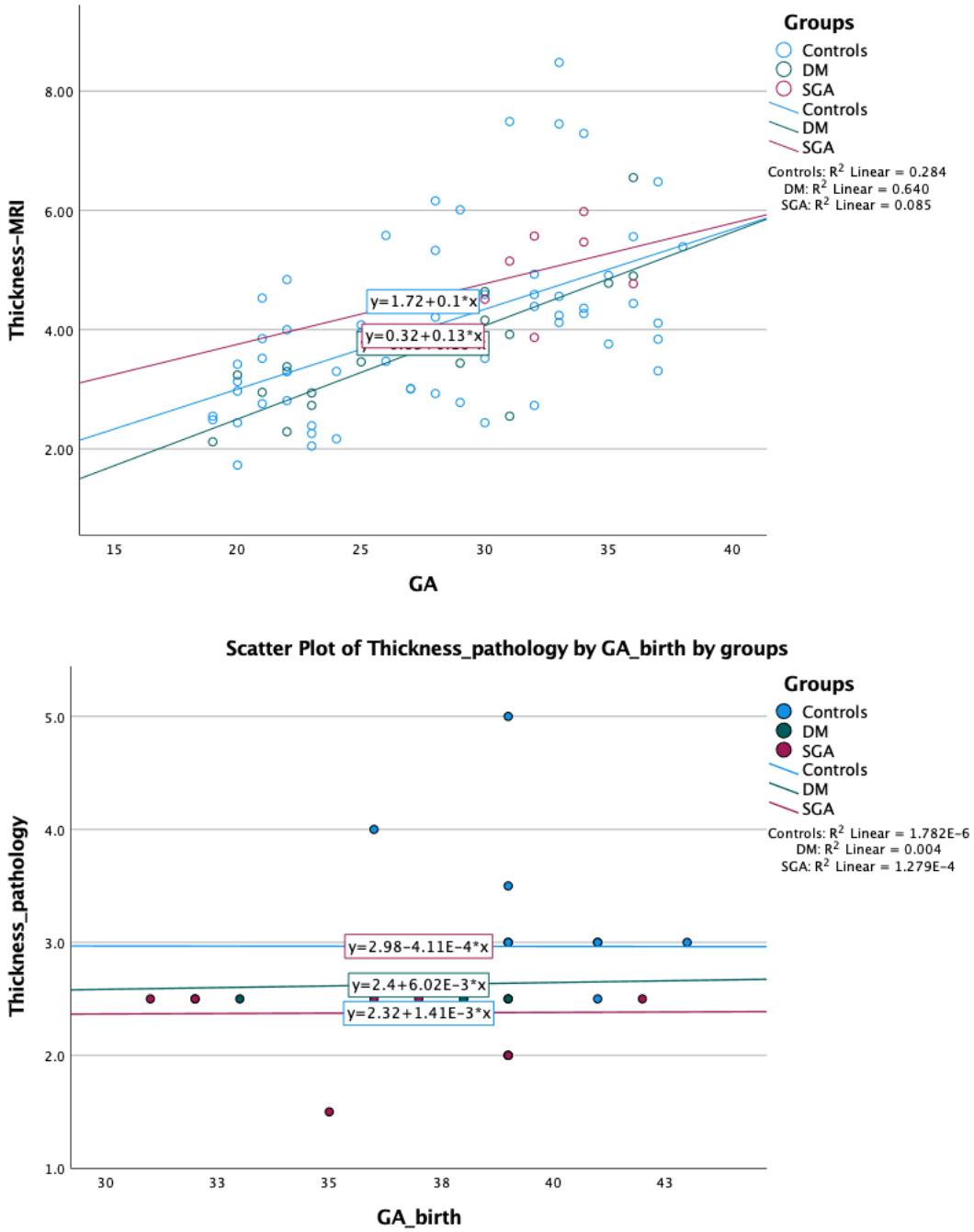

Figure 70: Scatter plots of the placental thickness measured in MRI (cm) (above) and from histopathology (cm) (below chart). The thickness measurements from MR images took an opposite pattern than that from the placenta pathology. The thickness in SGAs

was the highest using MR images, however it was the lowest in histopathology measurements.

Correlation of SGA pathology findings with MRI diagnostic signs and fetal outcome

Linear regression was applied to compare SGA pathological changes with the following factors:

- Placental weight
- Placental centiles
- SA-pathology
- Volume-pathology
- Thickness-pathology
- Thickness-MRI
- SA-MRI
- Volume-MRI
- Birth weight
- Birth centiles

There was a significant correlation between SGA pathology changes and placental weight, MRI thickness and birth weight (logistic regression, p=0.05, 0.024, 0.016) respectively.

Research no.	GA at MRI (week)	GA at US (week)	EFW (estimated fetal weight) (gm)	Umbilical artery PI	MCA (middle cerebral artery) PI	Head circumference (HC)	Femoral length (FL)	Placental T2* (ms) Whole placenta	Birth weight (gm)	Outcome	Histology
11	30	29	1121	1.18 (75-90th centile)		260.5 (<1st centile)		50.49	2700	Normal	Focal delayed villous maturation.
30	31	Not in STH(DRI)	<3rd centile					86.20	1330	SGA	The peripheral membranes show laminar necrosis.
32	34+5	34+5	>10th centile)	1.38 (>90th centile)	2.30 (90-95th centile)	296 (<3rd centile)		39.22	3530	Normal	Focal delayed villous maturation
34	20	21	372	0.93 (5th centile)		181.8	31.7 (<10th centile)	113.49	2160	SGA+DM	Not available
51	34	34+4	1911	1.10 (75-90th centile)	1.10 (<5th centile)	305.5	61.6	37	1770	SGA	Maternal vascular malperfusion/

											insufficiency. Accelerated villous maturation with increased syncytial knot formation.
56	36	35		0.85 (25-50th centile)		304.9	64.4	33.13	2645	Normal	No changes
57	34	35	2072	0.91 (50-75th centile)		303.5	63	71.69	2310	SGA	Not available
60	No scans	34+1	1713	0.90 (25-50th centile)	1.72 (25-50th centile)	295	59.4	-	1960	SGA	No changes
61	29	Not in STH (DRI)	<3rd centile					52.14	1318	SGA	The peripheral membranes show reactive amniotic epithelium. The umbilical cord shows isolated cord phlebitis. The chorionic villous maturation shows distal villous maldevelopmen t. The chorionic villi show

											abnormal villi. The chorionic/stem villous vessels show acute vasculitis and multiple mural thrombosis. The chorionic plate shows acute chorioamnionitis and meconium induced changes. The intervillous space shows acute subchorionitis.
63	27	26+3	789	0.90 (10th centile)	2 (75-90th centile)	236.3	48.7	33.16	2800	SGA	Hypercoiling of the umbilical cord. Diffuse delayed villous maturation with monotonous villi showing centrally placed capillaries. The intervillous space shows multifocal recent intervillous haematoma.

64	No scans	30+2	1144	2.61 (>90th centile)	2.22 (75-90th centile)	270.9	49.7	Patient had no MRI scans	1180	SGA	The maturation is accelerated, with small hypermature villi. There is also frequent villous agglutination. The intervillous space shows prominent chronic histiocytic intervillositis with some excess of perivillous fibrin deposition. The basal plate shows hemosiderin laden macrophages and chronic deciduitis.
84	32	32	1199	1.16 (75-90th centile)	1.13 (<5th centile)	268.9	54.9	35.32	1400	SGA	No changes

Table 31: Prenatal predictors of SGA and placental T2 values linked to histology changes and birth outcome. Reference ranges (https://obgyn.onlinelibrary.wiley.com/doi/10.1002/uog.20157).*

T2 * and placental pathology

In this section, we have explored the trends and changes in T2* values with placental pathology data. Outliers including SGA cases that were delivered with normal weight have been converted into controls (sample 2 cases: SGA-3, controls+3 and DM groups) as these are no longer defined as SGA. DM+SGA cases (3 cases) were excluded as the group was too small for analysis.

The graph shows that in SGA, there has been a slight increase in T2* when the placental weight is trending small. Diabetics cases showed a rise in their T2* with the increase in placental weight. In controls, T2* increases with the decrease of the placental weight (Fig.71).

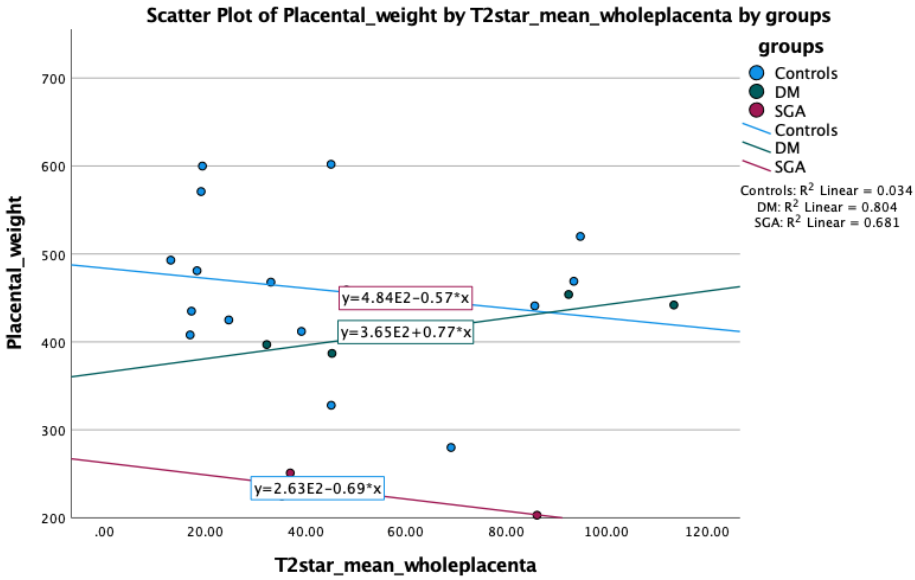

Figure 71: Placental weight (gm) and T2 whole placenta (ms) in 3 groups of participants.*

Both birth weight and birth centiles have no effect on T2* in controls where the T2* is relatively constant. In SGA, T2* has fallen with the increments of birth weight and centiles. Diabetics showed an increment in their T2* with the rise in birth centiles and a decrement with the increase of birth weight (Fig.72 and Fig.73).

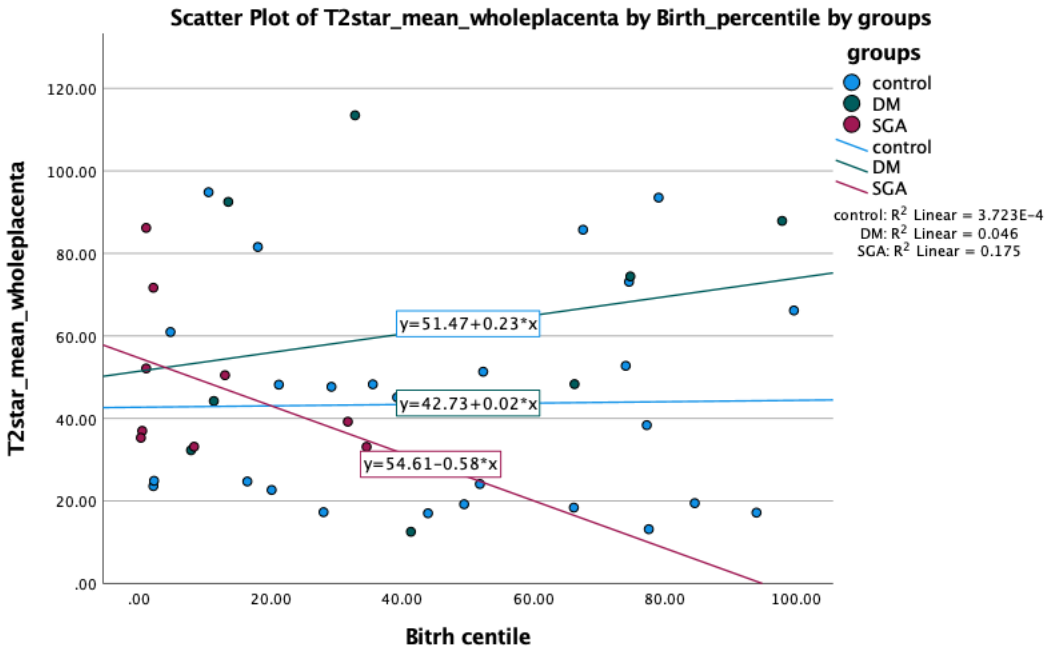

Figure 72: Placental T2 whole placenta (ms) and birth percentiles in 3 groups of participants.*

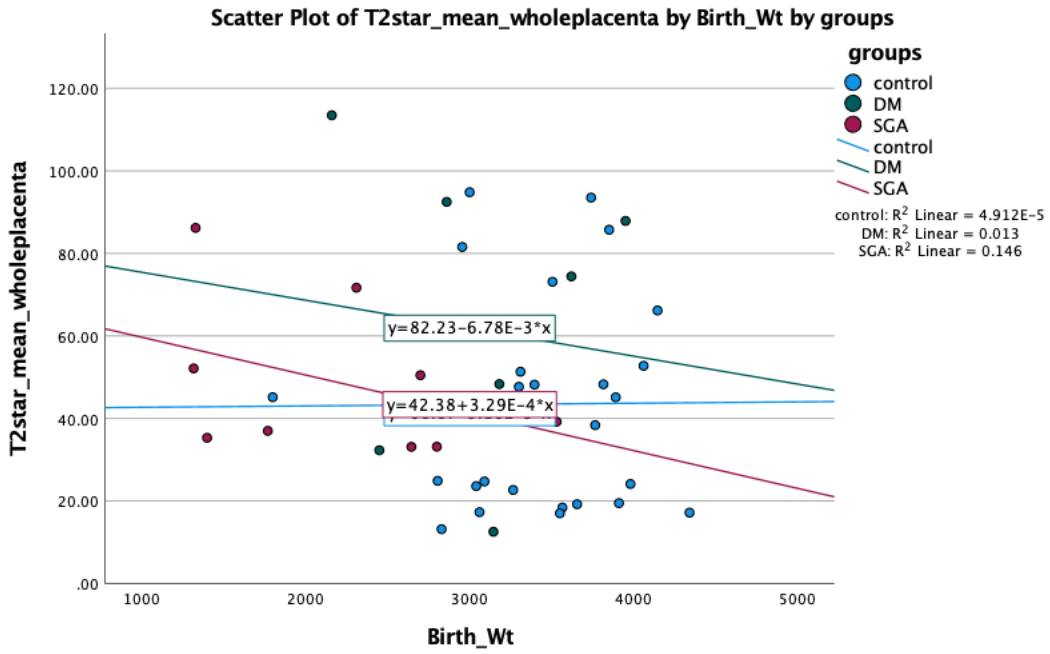

Figure 73: Placental T2 whole placenta (ms) and birth weight (gm) in 3 groups of participants.*

Comparing T2* with placental measurements from MRI and pathology

Data fitted well to the regression line. With smaller SA, T2* values were higher in SGA cases. Controls had a higher T2* values with larger SA. Diabetics T2* mean is increasing with the decrease in SA (Fig.74).

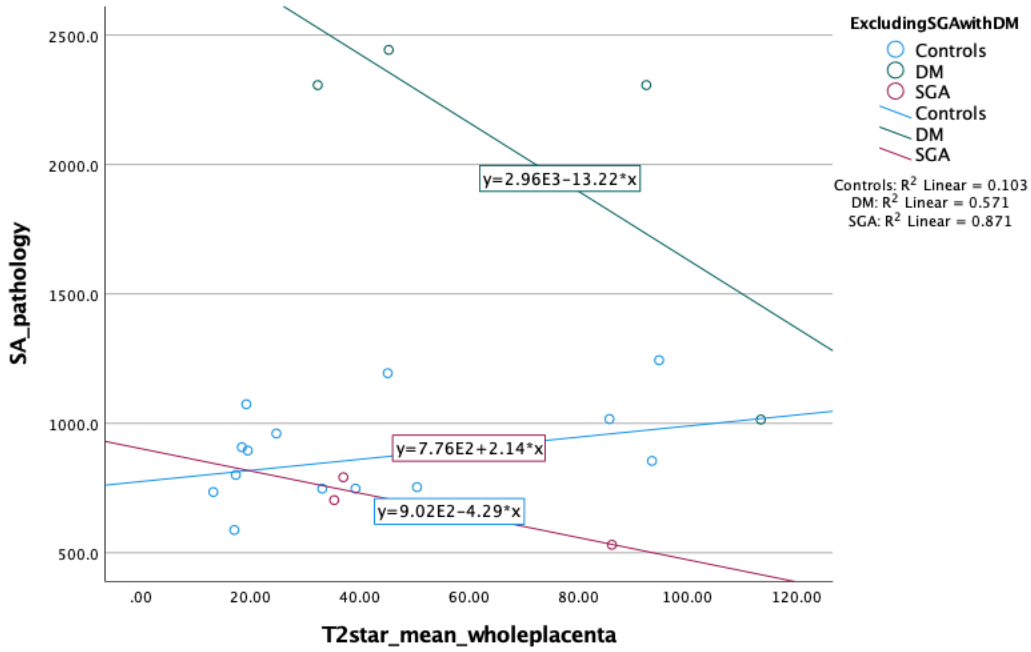

Figure 74: Placental SA by pathology (cm2) and T2 whole placenta (ms) in 3 groups of participants.*

A rise in the placental surface area resulted in an increase in placental T2* in controls and diabetics. SGA placentas had an increase of their T2* values with the decrease in SA (Fig.75).

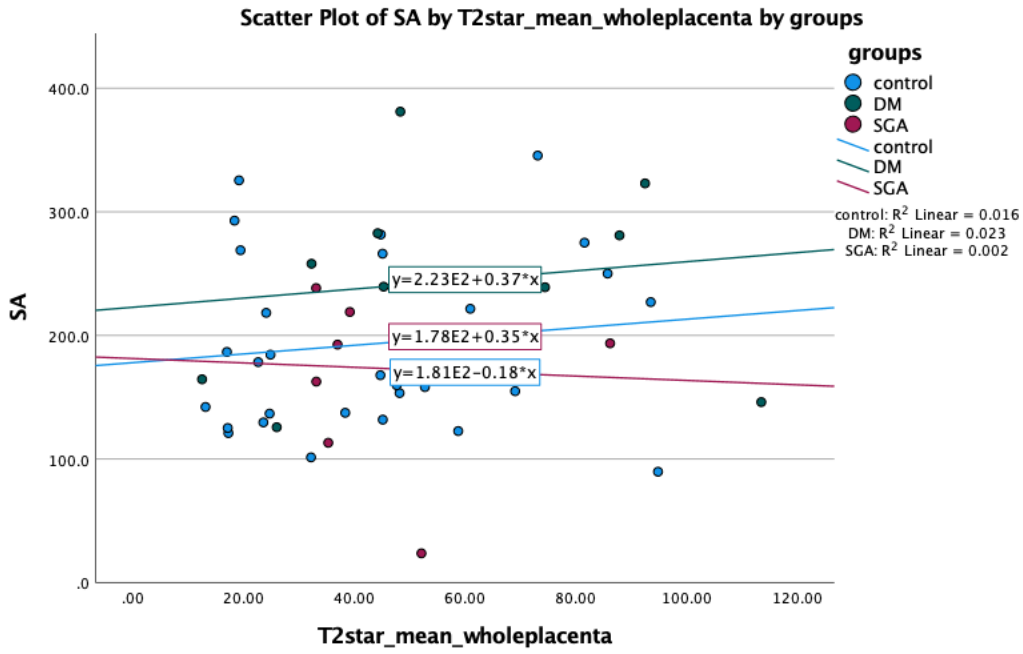

Figure 75: Placental SA by MRI (cm2) and T2 whole placenta (ms) in 3 groups of participants.*

Placental T2* was higher in smaller placenta volumes for both the SGA group and the diabetic group, whereas the controls had a negligible volume effect on T2*. (Fig.76).

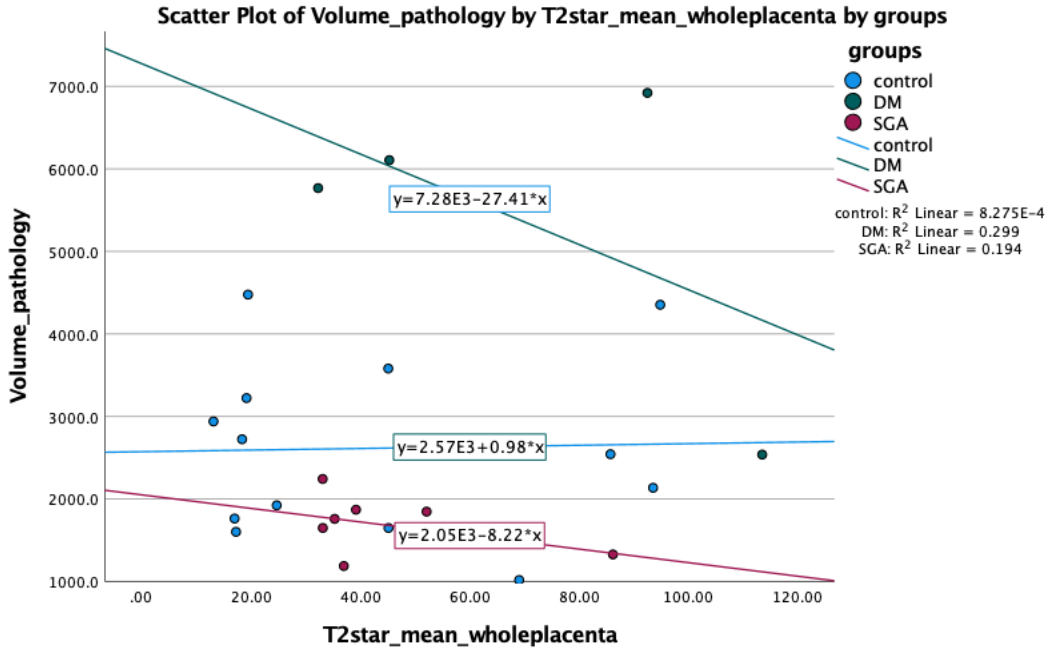

Figure 76: Placental volume by pathology (cm3) and T2 whole placenta (ms) in 3 groups of participants.*

Placental T2* was higher in SGA and diabetics cases with higher volume. Control cases had no change in their T2* with their growth (Fig.77).

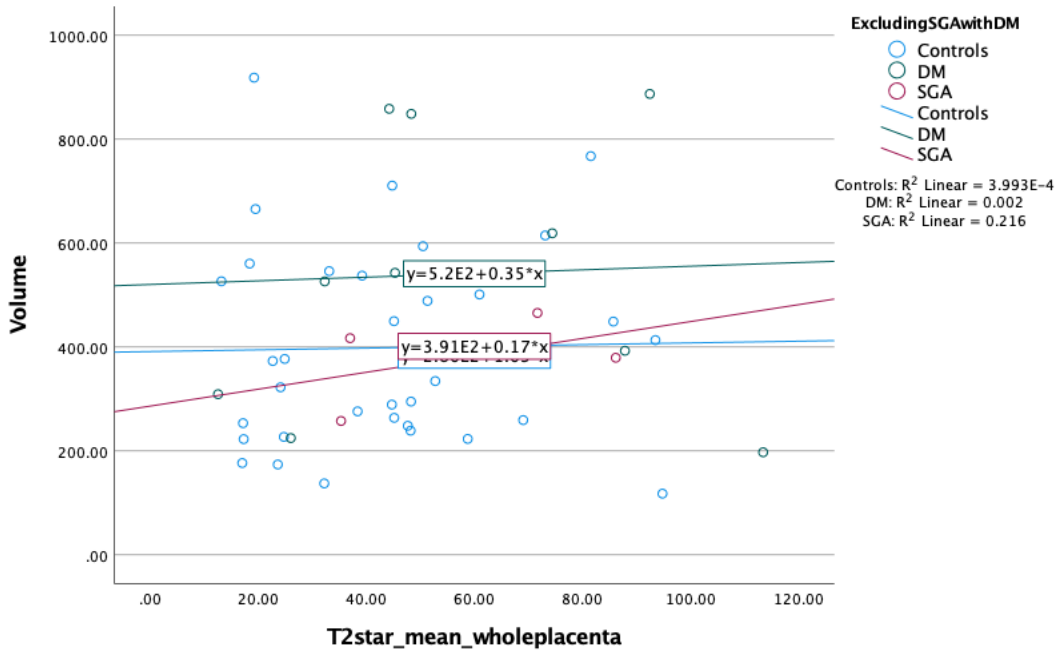

Figure 77: Placental volume by MRI (cm3) and T2 whole placenta (ms) in 3 groups of participants.*

Placental T2* was higher in controls when the thickness is in a downward trend. SGAs/diabetics T2* values were slightly increasing with the increase in thickness (Fig. 78).

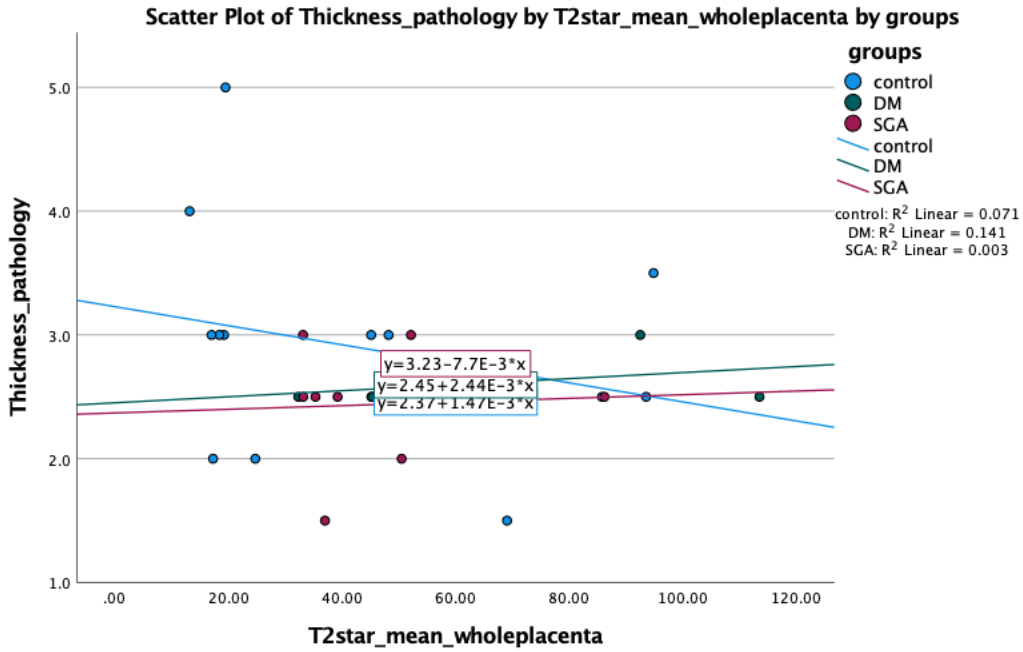

Figure 78: Placental thickness by pathology (cm) and T2 whole placenta (ms) in 3 groups of participants.*

When the placental thickness increases, T2* increases in SGA cases. The trend in controls and diabetics was decrease in thickness causing an increase in T2* (Fig.79).

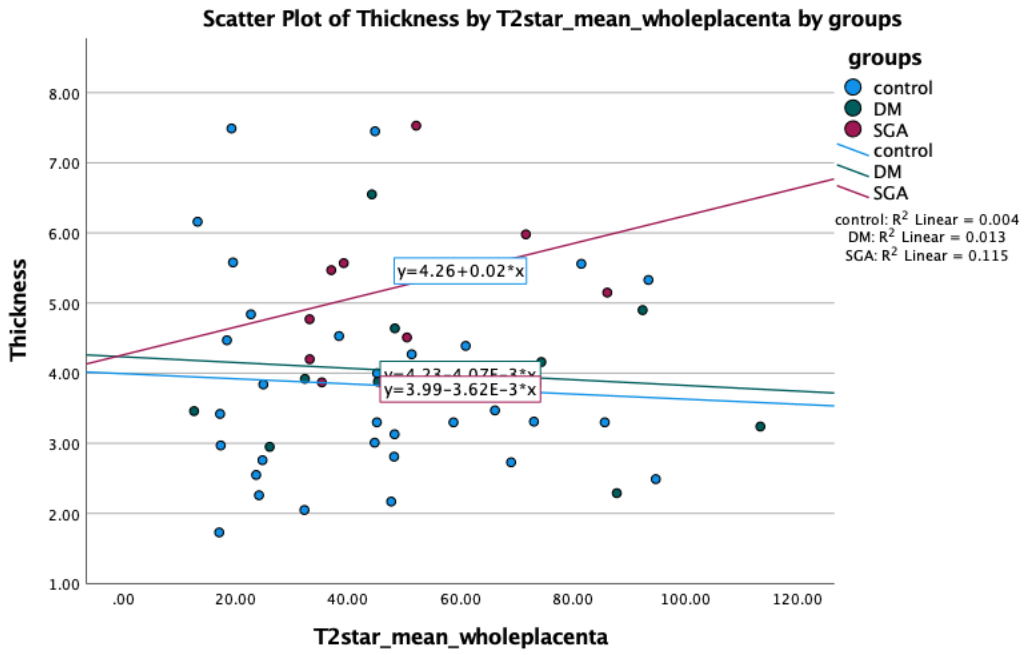

Figure 79: Placental thickness by MRI (cm) and T2 whole placenta (ms) in 3 groups of participants.*

F/P ratio and T2* had a similar trend in both SGA and diabetics groups. T2* values were increasing with the decrease in the ratio. Whereas in controls, there was a slight increase in the F/P ratio caused increase in T2* values (Fig.80).

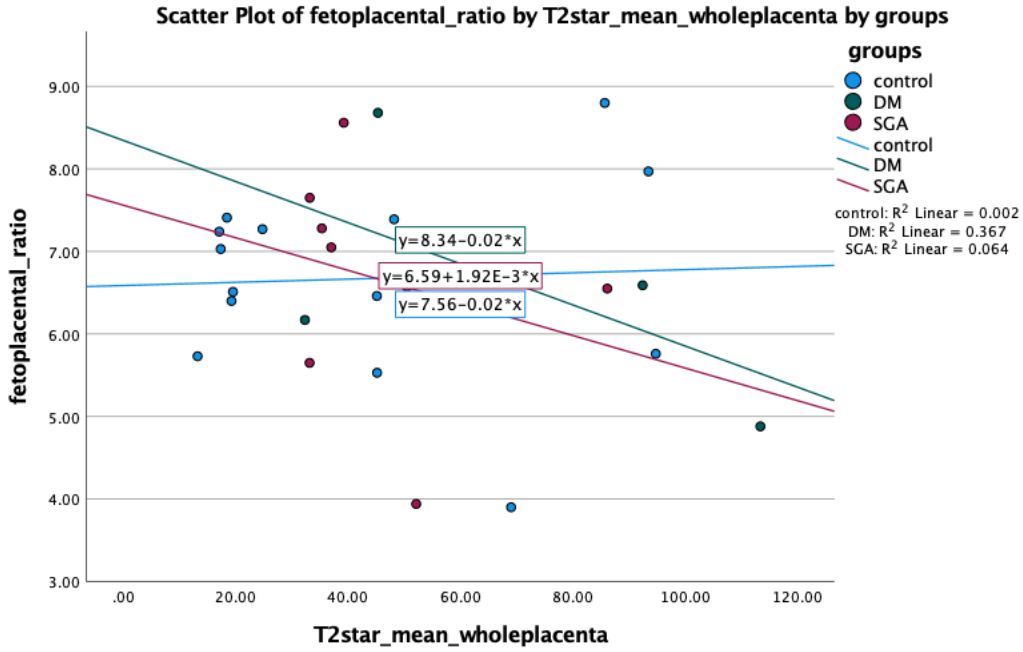

Figure 80: Feto-placental ratio and T2 whole placenta (ms) in 3 groups of participants.*

Discussion

Our data was supported with histopathology evidence. The results were correlated with antenatal findings with a link between MRI findings and histopathology. SGA placentas were significantly different in weight and MRI-derived midpoint thickness. Reduction in the functional unit of the placenta due to reduced placental weight may result in FGR (Sanin, López et al. 2001). Placental MRI- thickness showed a significant correlation with SGA histology changes (p=0.02). Although SA was also showing a difference, it was not significant (p=0.07). This could be assigned to the low number of histopathology reports of SGA (n=10) that resulted in that difference. Thickness was different between MRI and pathology as they were lower in case of histopathology. We hypothesize this could be due to pulling out the placenta after delivery or manipulation could result in aberration of histopathology results from MRI ones. The placenta is also examined flat after delivery whilst in utero it covers a curve due to the shape of the uterus resulting in apparent increase in thickness due to 'squashing' the placenta in the middle when 'curling' up the edge. Although placental shape was described as discoid in all cases, this naming is not accurate as placental dimensions infer.

Morphological changes

Morphology changes of the placenta specimens showed different trends in relation to changes on MR images.

- Volume took the same pattern in both MRI and pathology.
- Surface area took the same pattern in both.
- Placental weight was lower in diabetics in relation to GA while it was going upward in controls and SGAs with placenta growth.
- Placental volume in diabetics went upward on both MRI and pathology but weight went down with GA. The reason for this trend might be due to smaller thickness in these placentas as explained above. The placenta in pathological examination is flat while its squashed in vivo. Also, the small number effect (n=4) in this group makes it easier to have exaugurated effect of statistics.

Regarding T2* and placental pathology

- T2* was higher in SGA placentas when placental weight was smaller. As T2* reflects the oxygenation of the placenta and it detects deoxyhaemoglobin. T2* has therefore been reported to reflect placental hypoxia and could potentially be used as a measure for the severity of FGR. Furthermore, birth weight was not related to T2* in controls, but increased birth weight in SGA related to an increase in T2* whilst the opposite in DM cases. Sorensen at al. reported T2* reflected placental pathology and showed a better relationship with pathology than birth weight. This group also showed a low T2* in FGR cases and suggest that the T2* predicts placental malperfusion (Sinding, Sørensen et al. 2021).
- The surface attachment in controls and DM showed a positive association with T2* but SGA, a negative association so increasing surface attachment may reflect decrease in oxygenation (that is the T2* is higher so more deoxyhaemoglobin with the smaller SA so reduced perfusion potentially identified). Interestingly not the same at pathology and this may be related to the assumed discoid shape and calculation used for SA at pathology rather than the SA measured at MRI.
- Pathology control volume did not show any effect on T2*, both DM and SGA had negative effect so increased T2* with smaller volumes reflecting more deoxyhaemoglobin in the smaller placentas.
- When assessed with MRI volumes the relationship with T2* was different (higher T2* with higher volume), this could be due to the difference in volume measurement in pathology and MRI.
- Placental thickness on MRI showed similar trends in both MRI and pathology measurements in controls and SGA but not the case in diabetics (higher thickness with high T2* on pathology but lower T2* on MRI) (Fig. 78).

The above concerns mean that although T2* potentially gives us a way to assess the placenta in utero, the relationship to the morphology is not the same as it is at pathology. Care must therefore be taken before making any clinical assumptions and further research is needed to assess why these differences occur.

When assessed with the feto placenta ratio the T2* is unchanged in control cases and shows a negative relationship in both DM and SGA cases. This is similar to that seen in utero where the T2* was relatively constant whatever the GA in control cases but

had a positive relationship with GA in SGA suggesting that as the pregnancy progresses the placental perfusion is decreasing in these groups but interestingly a positive relationship in DM as if there is increased perfusion.

Ideally these trends will be evaluated in a larger group and also assessed alongside any changes seen on histological assessment that might suggest altered perfusion.

Limitations

This section was added into a separate part as an unfinished chapter. Unfortunately, due to COVID-19 pandemic, we could not have our samples reported as was planned. The department of histopathology in Sheffield was bombarded with reporting COVID placentas that were sent to them at the pandemic time which put our research in less priority. Samples took around 10 months to get them reported and as pregnancies delivered in different timepoints so we could not get much of them reported. We haven't also got the chance to discuss our findings with the histopathologist which could have improved the reporting and data analysis.

Conclusion

T2* trends were relatively constant in the control populations, while in other groups was showing variabilities. We are seeing differences in the morphology and T2* which reflect placental blood flow and fetal oxygenation, these may be reflected in placental morphology. If we can prove this link by repeating it with a bigger sample then we may be able to have a more robust findings and may bring it to USS and see if we can recognise things earlier.

Future work

There are many areas that could be potentially a base to work for future research. These may include:

- Joint work with histopathologists to link the MRI findings of the placenta in FGR with the histological changes noticed on the ex-vivo placentas.
- Work alongside experts in Ultrasound scan to try and replicate the findings on MRI in the second and third trimester and then repeat the work in the first trimester to assess if we can see the morphological differences in the placenta and predict SGA babies much earlier in pregnancy.
- More details are in need to assess in terms of different morphological features and if they could be picked up earlier using USS. Kimberly M Isakov et al. used USS measurements of the placenta to assess placental volume. This could be a good opportunity for collaboration (Isakov, Emerson et al. 2018).
- To assess if the addition of morphological changes improves the accuracy of detection of SGA fetuses. Even with small numbers of SGA our results showed trends that may be a potential for future work. Although the numbers of the groups need to be bigger as this might alter the results and give more powerful data. This will then open research into treatment of SGA in the future.

  T2* analysis is showing the difference in its values reflecting changes in blood flow. A larger group of cohorts is needed for assessment and link with pathology data that might give us a clue into altered placental perfusion in FGR placentas.
- Work with bioengineers to look at deep neuronal networks and texture work to assess if this aids the diagnosis of all placental abnormalities. This would bring opportunity for collaboration and exploration of artificial intelligence (AI) and machine learning.

Overall conclusion

Interest in the placenta is increasing, as we realise more and more the impact this has in the fetus and the different pathologies we are seeing in the placenta and there is more work to be done, but we hope that we have added to the contribution by confirming some pathologies and placental morphological changes (thickness, surface area and volume) that can be detected on the placenta during pregnancy. T2* differences can reflect perfusion and the texture work will help in the diagnosis of PAS.

Section 4

MRI features of perifibrinous deposits in the placenta due to COVID-19 : a case report

Summary

COVID-19 has been linked to pregnancy complications and loss (Baud, Greub et al. 2020). Infection during pregnancy is usually mild (Knight, Bunch et al. 2020). The risk is highest in the third trimester with increased hospital admission rates and maternal and fetal compromise (Yang, Mei et al. 2020). Post-COVID placentitis is uncommon but the effect on the placenta and the fetus is extensive (Linehan, O'Donoghue et al. 2021). We present a case correlating clinical, imaging, and pathological findings. **Case Report:** A 29-year-old para 2 gravida 1, with a normal fetal anomaly scan at 22 weeks gestational age (GA) contracted COVID at 24 weeks gestation. Fully recovered but reported reduced fetal movements at 27 weeks and 1 day. **Imaging:** US scan showed bright echoes within the brain, small lungs and oligohydramnios. MRI showed abnormal brain signals, small lungs and oligohydramnios but also a very abnormal placenta. Reduced and heterogeneous T2 signal and a marked reduction in the DWI signal intensity. The placental size was markedly reduced (volume 785.6 cm^3 expected for GA is 5604.8-5952.4 cm^3. The surface area of attachment was 3220 mm^2, expected 22180.4-29293.2 mm^2). **Pathology:** The placenta was small (5th centile) with massive perivillous fibrin deposition and multifocal chronic deciduitis. Histology revealed placental chorionic villi showing diffuse sclerotic changes surrounded by perivillous fibrin deposition in the intervillous space. The basal plate revealed multifocal chronic deciduitis. When imaging the fetus, it is important to examine the placenta and correlate any abnormalities. The placenta is a forgotten organ and should be routinely included and assessed to allow the detection of important abnormalities.

Introduction

COVID-19 has been linked to pregnancy complications and loss (Baud, Greub et al. 2020). Infection during pregnancy is usually mild (Knight, Bunch et al. 2020). The risk is highest in the third trimester with increased hospital admission rates and maternal and fetal compromise (Yang, Mei et al. 2020). Although post-COVID placentitis is uncommon, the effect on the placenta and the fetus is extensive (Linehan, O'Donoghue et al. 2021).

There is little evidence available describing the placenta in situ. Following the COVID-19 pandemic, several researchers reported placental pathology in COVID-infected pregnancies. Their pathological findings were significantly different than those of uninfected placentas but there are no consistent findings. Maternal-fetal disease transmission have also been described. A recent published report of 68 cases from 12 countries described the three most recognisable pathological features which were: chronic histiocytic intervillositis (CHI), increased fibrin deposition (IF), and trophoblast necrosis (TN) (Schwartz, Avvad-Portari et al. 2022). Syncytiotrophoblast cells are the target for the COVID-19 infection as they express ACE2 receptors which influence the viral infection (Schwartz, Avvad-Portari et al. 2022). There were some cases in which additional cell types were positive for the virus. In intrauterine fetal death (IUFD), placentas were extensively involved. Only one paper described any MRI findings, and these were obtained following an intrauterine fetal death (IUFD) (Marinho, da Cunha et al. 2021). Our case reports massive perivillous fibrin deposition (MPFD) and intervillous thrombi previously reported post-COVID-19 infection (Linehan, O'Donoghue et al. 2021, Marinho, da Cunha et al. 2021) but is the first report of detection by MRI in an ongoing pregnancy. We present the MRI findings and pathological correlation in the placenta in a case post-COVID-19 infection.

Clinical presentation

A pregnant woman was reviewed at 22 weeks gestation for abnormal fetal foot position. She was then discharged with reassurance of normality including fetal growth. Two weeks later she tested positive for COVID-19. Two weeks after the COVID-19 infection, she presented with itchy hands and feet, but no abnormality was noticed. Two days later, at 27 weeks and 1 day, she presented with reduced fetal movements. She was referred for a routine growth scan which showed a

growth-restricted baby. She had a previous normal vaginal delivery of an appropriately grown baby.

Investigations and imaging findings

Ultrasound Scans

A growth scan at 29 weeks and 4 days was performed, revealing a globally small fetus with all measurements below the third centile and oligohydramnios. The umbilical artery pulsatility index (PI) showed absent end-diastolic flow but the middle cerebral artery (MCA), ductus venosus and uterine artery dopplers were normal. The fetal brain images demonstrated a prominent third ventricle containing bright areas. The fetal chest appeared small.

Fetal MRI

An urgent fetal MRI showed a globally small fetus. There was poor differentiation between the white and grey matter, and abnormal DWI pattern, a bulky cavum septum pellucidum and the neuronal migration pattern was still evident (should no longer be present at 29 weeks GA) (Fig. 81).

The placenta was seen to be abnormal. There was very little signal on the diffusion-weighted images (Fig. 82a) which should be uniformly bright at this gestational age (Fig. 82b). On the T2- weighted images the placenta was of a lower signal intensity than expected and very heterogenous (Fig. 83) which was consistent with diffuse fibrin deposition.

Management and outcome

Cardiotocography was performed which showed reduced variability and reduced short-term variation (STV) of 3.9. The couple were counselled that although there was no definitive diagnosis at this stage there was a high risk of an abnormal outcome.

A watch and wait policy was offered, with a referral for a fetal echocardiogram, a repeat MRI two weeks later and a twice-weekly assessment of liquor and dopplers. The alternative of late termination of pregnancy with a feticide procedure and induction of labour was also given as an option. The couple opted for termination of pregnancy and a feticide procedure was performed. A stillborn male baby was delivered at 30 weeks and 2 days weighing 780 g (expected for 30 weeks is: 1115 ± 329 g).

A post-mortem examination was performed which confirmed growth restriction and showed placental fibrin deposition. All other postnatal investigations were normal including viral infection and thrombophilia screen.

The cause of intrauterine growth restriction was placentitis resulting in massive peri-villous fibrin deposition and chronic deciduitis, as confirmed by the histopathology report. COVID placentitis is the likely explanation since massive perivillous fibrin deposition is a well-recognised lesion in placentas affected with COVID, and in this case immunostaining for SARS-CoV2 was positive in the villous trophoblast (Schwartz, Avvad-Portari et al. 2022). Investigations excluded coagulation disorders and cytomegalovirus.

Postmortem and pathology report

A comprehensive post-mortem examination was performed. The results of the placenta and fetal examination revealed mildly macerated male fetus with no dysmorphic features with weights and measurements consistent with 28 weeks and an atrophic thymus. The placenta was small for the given gestational age (5^{th} centile) and consisted of massive perivillous fibrin deposition on the cut surface (Fig. 84a and 84b). Histological examination confirmed the widespread perivillous fibrin deposition and immunostaining for SARS-COV2 was strongly positive in the syncytiotrophoblast (Fig. 84c). An additional finding was numerous neurons with eosinophilic cytoplasm in the cerebellum and brainstem, indicating hypoxic changes, groups of calcified neurons in the periventricular area, which represent dead cells due to a previous hypoxic insult, as well as fresh and old subarachnoidal haemorrhage. Fetal demise was due to hypoxic-ischaemic changes induced by the abnormalities in the placenta.

MR images analysis results

Compared to normal reference values, placenta volume and surface attachment were smaller for the same gestation: Volume 786cm^3 (normal 5605-5952), surface area of attachment 3320 mm^2 (normal 22180-29293 mm^2). Visually the placenta was very abnormal.

The T2 weighted images demonstrated a heterogenous low signal whilst the DWI had a massively reduced signal (Fig.83).

Discussion

In this report, we have described a third trimester COVID-19 infection associated with placental insufficiency and intrauterine growth restriction. Antenatal MRI findings corresponded with the pathology results. The clinical background and histopathology results were consistent with COVID placentitis, confirmed with immunostaining for SARS-COV2.

The MRI findings were different to those in the one reported case in the literature (Marinho, da Cunha et al. 2021). The T2 weighted images were similar with increased heterogeneity and the increased dark areas most likely corresponding to the fibrin deposits. However, the DWI was higher than normal in the previous report but in that case the fetus had already demised. In our case, the DWI signal was unusually low.

Perivillous fibrin deposition is a rare entity, that accounts for (0.028% - 0.5%) of deliveries, the cause of which is still unknown, but mechanisms linked to maternal autoimmune and alloimmune have been suggested (Faye-Petersen and Ernst 2013). Increase fibrin deposition is the most common finding in post COVID placentitis, although it is normal for placentas to contain fibrin deposits to a certain extent. Placental perfusion is compromised when fibrin is superimposed on a damaged placenta. The most severe abnormalities are MPFD and maternal floor infarction.

The degree of placental damage in COVID placentitis is unrelated to the clinical features or severity of infection (Schwartz, Avvad-Portari et al. 2022). In a clinical statement published by the Royal College of Physicians of Ireland (RCPI), it was recommended that pregnancies complicated by COVID infection be assessed thoroughly when they present with reduced fetal movement (Fitzgerald, O'Donoghue et al. 2022). This followed a report of 6 stillborn and neonatal death cases from January to March 2022, all of which were caused by the new SARS-COV-2 alpha variant (B.1.1.7) related to most stillbirth cases caused by COVID placentitis (Fitzgerald, O'Donoghue et al. 2022). In November 2021 the US centres

for disease control and prevention confirmed most cases of stillbirth were associated with SARS-Cov-2 delta variant (B.1.617.2) (DeSisto, Wallace et al. 2021). The virus variant was not tested in this case; however, the case was diagnosed during the time period when delta was the dominant circulating strain.

Autopsies of 63% of cases revealed no fetal abnormalities. Intrauterine hypoxia was identified as the most common pathologic finding (Schwartz, Avvad-Portari et al. 2022). The key feature of post-mortem findings with COVID-19 is acute fetal hypoxia where maternal-fetal transmission of infection is uncommon. If damage does happen, it is usually confined to the placenta (Schwartz, Avvad-Portari et al. 2022). In most cases, doppler ultrasound has no benefit in the assessment of COVID placentitis. For that reason, MRI is recommended in the assessment of COVID placentitis (Schwartz, Avvad-Portari et al. 2022).
In this report, IUGR is most likely the result of placental damage and insufficient transfusion of oxygen and nutrient. Although IUGR features need some time to develop, accumulation of fibrin in the intervillous space could eventually obstruct placental blood flow, resulting in placental insufficiency and stillbirth. Maternal-fetal COVID transmission cannot be confirmed as placental damage could cause the resulted fetal compromise. Placental infection through vertical transmission is rare as the virus requires specific receptors, i.e., angiotensin-converting enzyme 2 (ACE2) to attach to, which are not abundant in placenta trophoblastic cells (Lü, Qiu et al. 2020).

Conclusion

Although it is uncommon, poor fetal outcome may be associated with post COVID placentitis. MRI appearances, including the DWI signal, volume, and surface attachment should be assessed in any pregnancy post COVID-19 where there are clinical concerns for the health of the fetus. We believe this is the first reported case of MRI detecting COVID-19 placentitis in the antenatal period.

Learning points

- Post COVID-19 placentitis is a rare entity but the severity of placental damage is unrelated to the severity of infection.

- MRI changes showed a heterogenous placenta with lower signal intensity of DWI and T2- weighted images.
- In our case, fibrin deposition and chronic deciduitis caused placental insufficiency, UGR and end organ damage which is consistent with other cases reported.

Figures

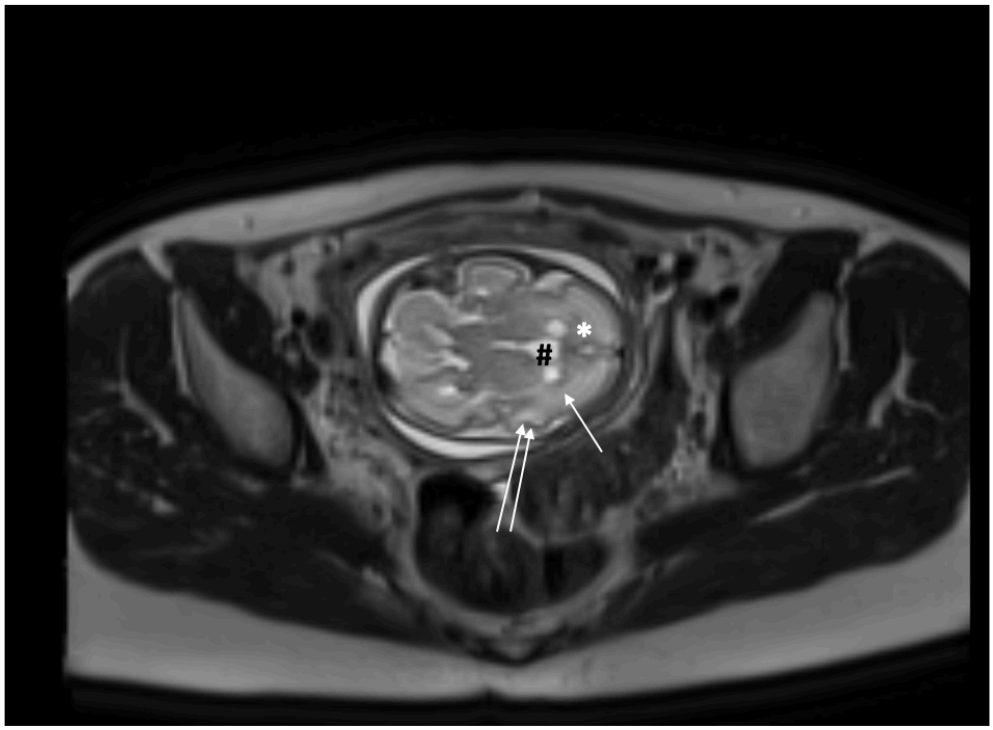

Figure 81 T2 haste axial section fetal MRI, the fetal brain shows abnormal changes (increased differentiation between the white (arrow) and grey matter (double arrow), bulky cavum septum pellucidum (#) and prominent neuronal migration pattern, seen as bands in the white matter of the frontal lobe (*)).

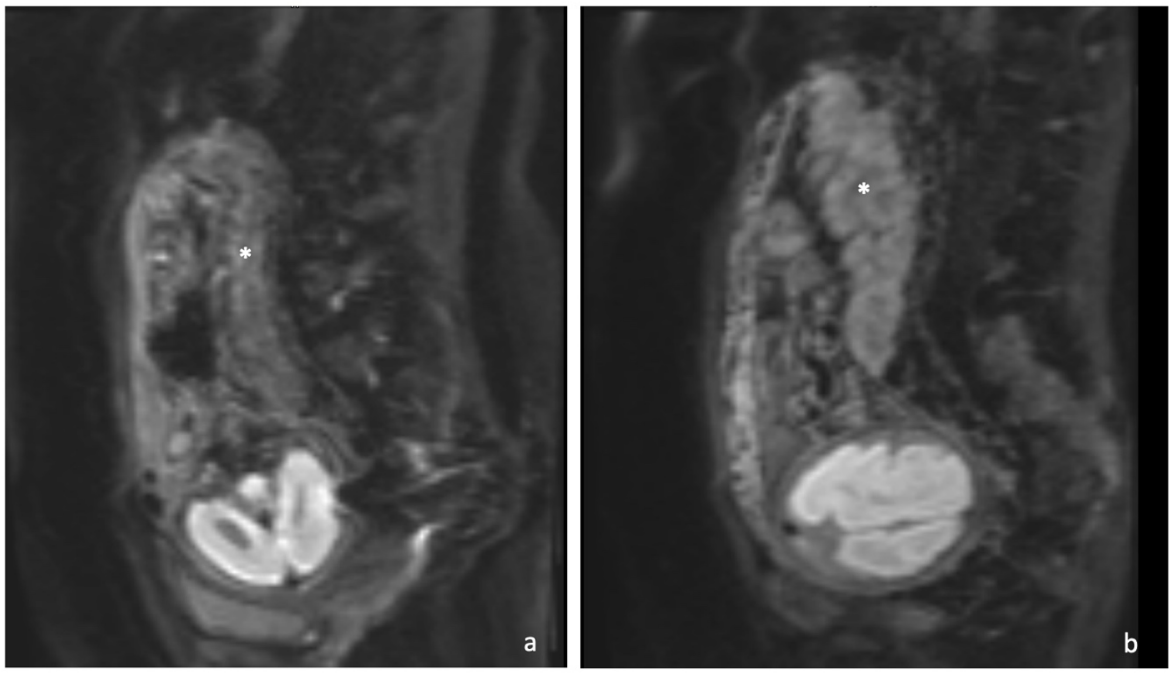

Figure 82 Sagittal DWI MRI showing reduced diffusion in the placenta (*), Figure 94b. DWI MRI of normal fetal MRI scan at 29 weeks gestation, the placenta is uniformly bright (*).

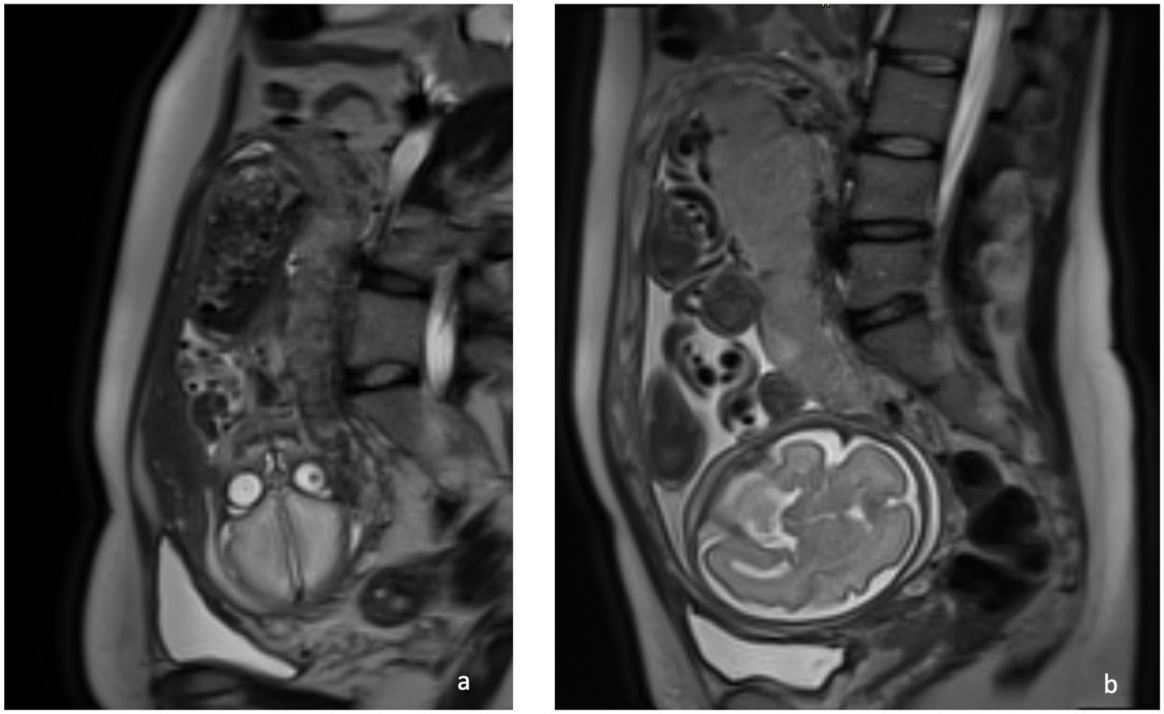

Figure 83a T2 weighted sagittal section MR image demonstrating heterogeneous placental signal and very low signal intensity consistent with the diffuse fibrin deposition.

Figure 83b. T2 weighted sagittal section MR images of a normal placenta at same gestation.

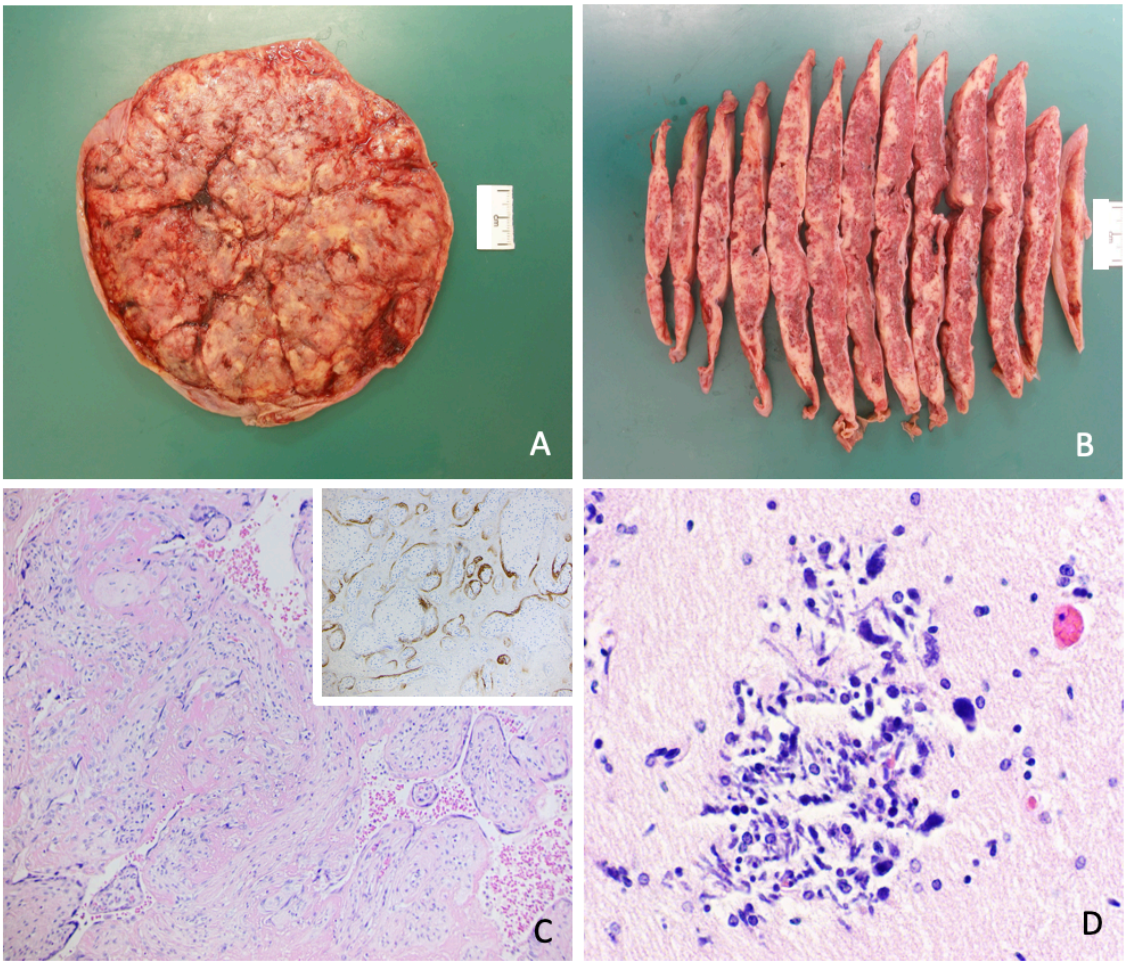

Figure 84 Macroscopic view of the maternal surface of the fixed placental sample showing widespread yellowish material (A), which on cut surface is represented by massive perivillous fibrin deposition, imparting a marbling effect (B). Histological examination of the placenta stained with haematoxylin and eosin confirmed the massive perivillous fibrin deposition, seen as a diffuse pinkish material surrounding chorionic villi and in the inset is the immunostaing for SARS-CoV2 showing positivity in the syncytiotrophoblast as a brown granular material (C, original magnification x10). The brain section shows a focus of calcified neurones, which represent longstanding hypoxic-ischaemic encephalopathy (D, original magnification x40).

Research dissemination

Published a paper entitled “MRI features of perifibrinous deposits in the placenta due to COVID-19” in the British Journal of Radiology-case reports, 12/01/2023.

The link of the paper is: https://doi.org/10.1259/bjrcr.20220132

This paper was featured on Aunt Minnie’s website and has been used as the case of the week for teaching purposes. The link to it is:

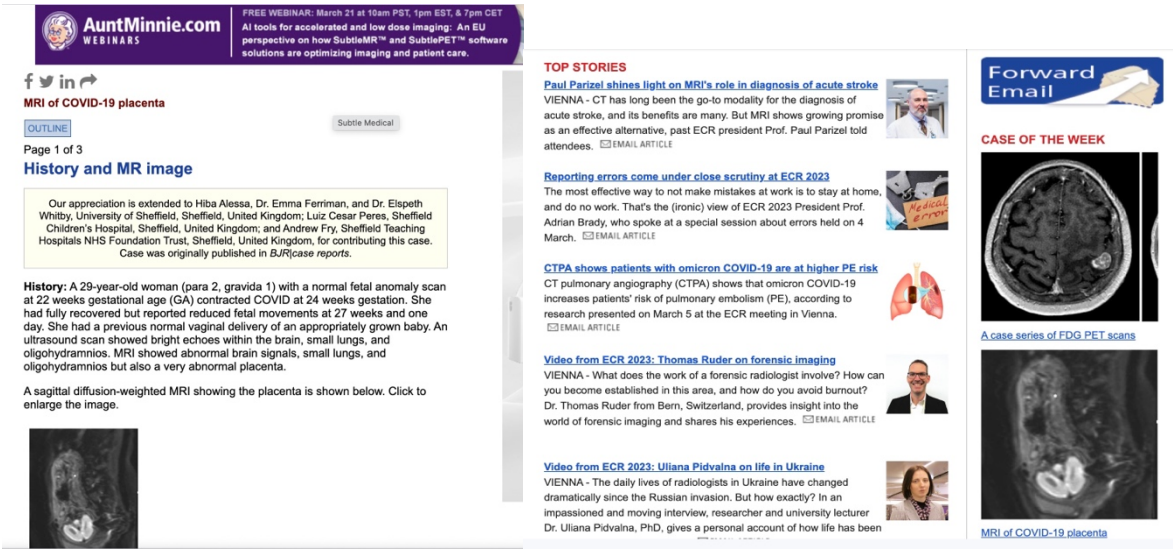

Conferences

1. ISUOG- (14th Feb 2019), attended online, titled (placental insufficiency from causes to consequences).
2. The perinatal pathology study day (2nd May 2019) which was about perinatal pathology of the placenta, IUGR cases and post-mortem MRI.
3. North of England Obstetrical and Gynaecological Society Sheffield Meeting (7th Jun 2019). Presentations and posters were related to fetal and woman health.
4. Research Meeting Day at the University of Sheffield on the 17th and 18th June 2019.

5. International Stillbirth Alliance's Annual Conference- Madrid (5th, 6th Oct 2019), attended online, which was on perinatal mortality and bereavement care. I attended online, presentations on fetal stillbirth caused by placental insufficiency.
6. Fetal Growth Conference- Berlin (8th-11th Oct 2019). Organized by the perinatal institute. The aim was to provide a forum to present and examine the latest evidence on fetal growth. The conference was headed by Prof Jason Gardosi from the UK as well as other organizing professors.
7. In-Utero MRI, 7th-10th Jan 2020, Oxford, UK. The program was endorsed by the International Society of Magnetic Resonance in Medicine (ISMRM).
8. UKIO 2020: attended online.
9. RSNA 2020: attended online.

Conferences presented posters

1. BIR, 4-6th November 2020:

Presented "ADC values as a biomarker for placenta accrete spectrum" as an electronic-poster presentation at the virtual BIR Annual Congress 2020.

2. UKIO 2021, presented a poster titled (Apparent Diffusion Coefficient and texture may help predict the severity of placental invasion).

This poster was featured on Aunt Minnie's website, the link to the post is:

https://www.auntminnieeurope.com/index.aspx?sec=ser&sub=def&pag=dis&ItemID=620251

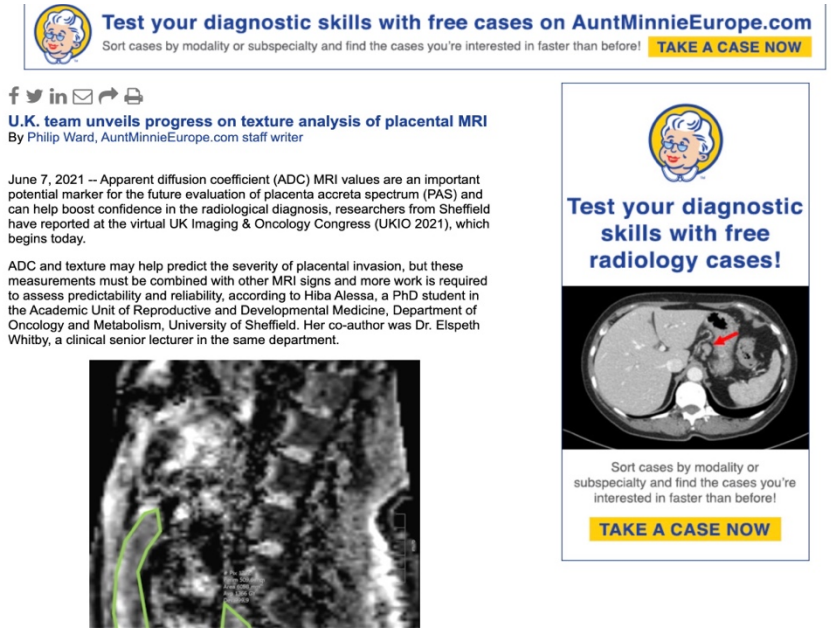

3. ISUOG, 6th October 2021

Presented an electronic poster titled “Combining apparent diffusion coefficient with other MRI measures may help predict the severity of placental invasion”.

4. UKIO July 2022, Liverpool, UK

Presented a poster titled “MRI features of perifibrinous deposits in the placenta due to COVID-19”.

Conferences oral presentations

1. AURDM, 6th March 2020

   The Academic Unit of reproduction and development), 9th symposium in Jessops wing. I participated in 3 minutes thesis competition, spoke about my project, and presented my results.

2. ISUOG, 6th October 2021

   Presented an oral presentation titled “Textural analysis has a role in the diagnosis of placenta accreta spectrum”.

3. BMFMS November 2022

Presented a short talk about my poster, the conference was held in Birmingham. The poster titled (Can placental MRI predicts fetal growth patterns? a prospective pilot study).

Doctoral Times Magazine

Published an article in the Doctoral Times Spring 2022 magazine, the issue was exploring the topic of research methodologies. The article title was “Research Methodology under the COVID-19 Pandemic. I have talked about clinical recruitment and how this was affected by the COVID-19 pandemic.

Research Methodology under the COVID-19 Pandemic

By **Hiba MA Alessa** - PhD Student, Department of Oncology and Metabolism

Research methodology under the COVID-19 pandemic:
As a clinical researcher, I faced many struggles during the pandemic, and I had to overcome them to get back into research. The effect of COVID was inevitable, and many methodological stages have been affected.

Delays in clinical recruitment: My area of research requires me to deal with patients, so when the pandemic started, we were not able to commence. It was very unfortunate that we were unable to start, especially when I had just finished my literature review. So as an alternative, my supervisor advised me to change the project subject and work on a different methodology plan. Through adaptation, I came up with another area that was still relevant and related to my research. A shift from stoppage of clinical recruitment and working out different methodologies on retrospective data eventually helped me to be more confident with the methods I have learned.

Participants were reluctant to be included in the research subject: Once the recruitment process began, COVID was on the rise. It was imperative when dealing with participants that they were not put at risk of catching the virus. I took precautions, for example, standing at a distance while speaking with them and making sure to sanitize. However, we cannot deny the fact that there was still a fear of contracting the infection.

Cancellation of appointments
On the day of their appointment some participants did not show up for many reasons related to COVID, like waiting for their PCR test, being or caring about someone who was sick.

COVID-infected pregnant women were eager to join the research, as they wanted to make sure that their babies' health was okay. So, this was part of the last-minute amendments we created to adapt to the change.

The Positive and Negative implications. We were able to include more patients. Some of our clients were more interested to be included in our research when they had a history of COVID infection, as the side effects of COVID were still being researched.

Research under COVID restrictions has had both positives and negatives. Although sometimes we cannot reach the goals that we have planned, a shift in plans can also lead to impressive project results.

My advice to Ph.D. students: Keep yourselves focused on the light at the end of the tunnel. Quite often there are times when you cannot keep your plans under control, and the only thing you can do is to keep yourself motivated and resilient. I would also recommend keeping yourself and your Ph.D. as the top priority.

1.) Stay away from distractions, use productivity apps that will help you to stay focused.

2.) Always have plans ahead of the week and document your daily goals to achieve them

3.) Following mini goals is much more helpful than looking at the whole project. For example, setting up a daily writing routine. Sometimes it's overwhelming to think about the whole project and how many things you have to achieve. When you make a very good plan to work on a daily basis, this reduces the amount of anxiety when thinking about your project and the bigger picture.

Appendix

Appendix I

MRI T2 HASTE Sagittal and axial sections showing crumpet placenta.

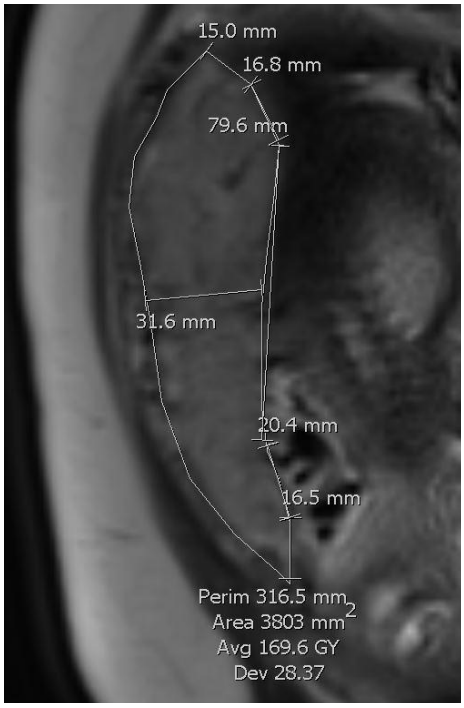

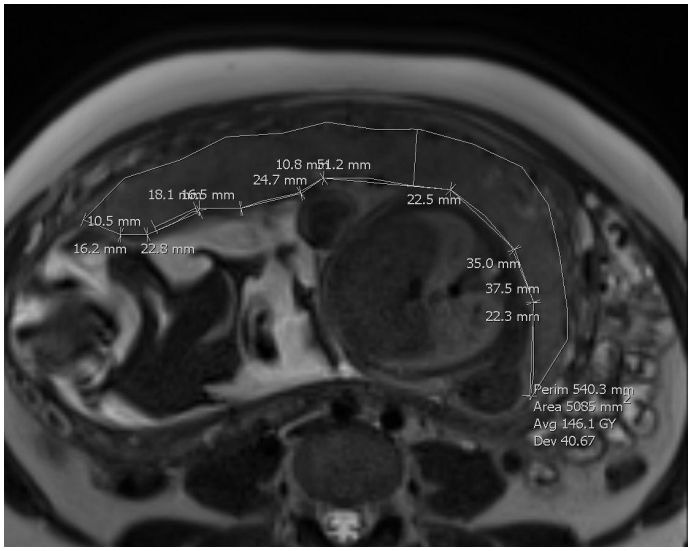

MRI T2 HASTE Axial section showing cupcake placenta.

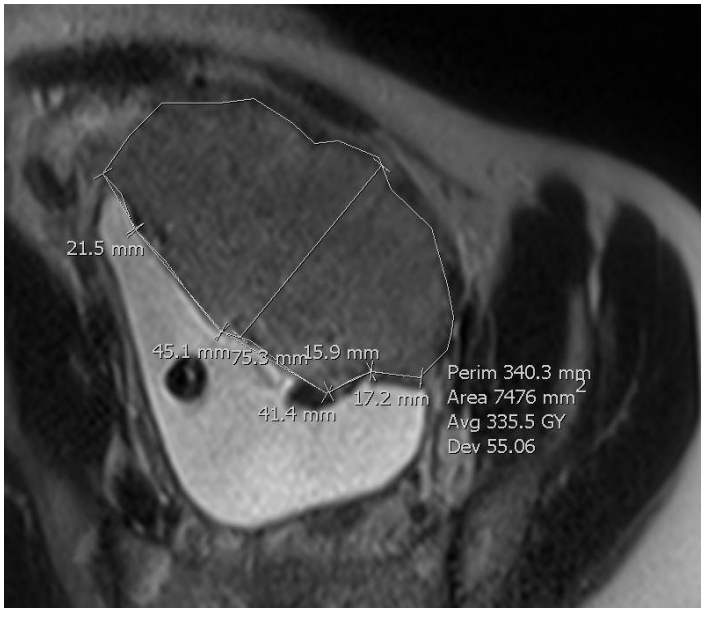

Appendix II

Ultrasound and MRI form

Ultrasound parameters	
Doppler US parameters	
1. Uterine Artery flow velocity/Peak index	
2. Fetal middle cerebral artery flow velocity	
3. Umbilical artery flow velocity /Peak index	
4. Umbilical artery Doppler index	
5. Umbilical Artery end-diastolic flow	
6. Increased nuchal translucency	
7. Placental volume	
8. Placental thickness	
9. Placental location	
10. Curve-linear length	
11. Vascularisation flow index	
12. Crown-rump length	
13. Abdominal circumference	
14. Head circumference	
15. Middle cerebral artery Doppler	
16. Femur length	
17. Estimated fetal weight (Accor to GA)	
18. Amniotic fluid index (deepest pocket)	
19. Hematoma	
20. Morphology	
21. US echogenicity	
22. Cord insertion	
23. Abnormal placental adherence	
24. Masses	
25. US elastosonography	
26. Fetal karyotype (if known)	

27. Other	

MRI Of the placenta and fetus	T 1	T1*	(SSFSE) T2	DWI	MRI spectroscopy
1. Placenta size					
2. Shape					
3. Surface attachment					
4. Volume					
5. PAD features					
6. Midpoint Thickness					
7. Umbilical cord insertion and number of vessels					
8. Fetal brain volume					
9. BPD					
10. FOD					
11. Placental grading (Grannum classification)					
12. Liver volume					
13. Foot length					
14. Other					

Appendix III

Pathology form

Patient name_____ Hospital number:_____

Date Cut up___/___/___ Pathologist/SpR_____BMS Cut up___ _____

General

The placenta is received ☐ Fresh ☐ Fixed

The placenta weight is _____g (_____percentile – normal range 10th-90th) and measures _____x____x___ cm.

The fetoplacental weight ratio is _____ (_____percentile – normal range 10th-90th).

The shape of the placenta is

☐ Discoid
☐ Irregular
☐ Bilobate
☐ Succenturiate

Peripheral membranes are

☐ Complete
☐ Incomplete
☐ Translucent
☐ Green
☐ Opaque
☐ The Insertion is marginal.
☐ The Insertion is circumvallate_____% circummarginate_____%

The umbilical cord measures _____x____cm.

☐ There are_____coils to the_____(UCI ____coils/cm – normal range 0.07-0.30 coils/cm). Indentations are____
☐ Central insertion
☐ Eccentric insertion
☐ Marginal insertion
☐ Velamentous insertion
☐ Number of vessels_____

☐There is a _____ knot.

Fetal surface

☐ Translucent

☐ Opaque

☐ Green

☐ Normal chorionic vessels

Maternal surface

☐ Intact

☐ Ragged

☐ Prominent calcification

☐ Normal color

Processor used:	HIS083 ☐ HIS093 ☐ HIS319 ☐
Embedded by/ date	/
Embedding Centre used:	HIS157 ☐ HIS092 ☐
Sectioned by/ date	/
Microtome used:	HIS076 ☐ HIS077 ☐ HIS078 ☐ HIS079 ☐ HIS080 ☐ HIS156 ☐

☐ Pale

☐ Attached blood clot

Cut surface shows

☐ No focal lesions.

☐ _____firm, white lesions, the largest measures _____x____cm

☐ _____haemorrhagic lesions, the largest measures _____x____cm

☐ Pale areas

☐ The lesions comprise altogether _____% of volume.

Pictures taken	☐	Microbiology Swabs	☐
Cytogenetics	☐	Virology	☐

B											
P											

Tick where applicable:

Water bath used:	HIS160 ☐ HIS175 ☐ HIS176 ☐ HIS177 ☐ HIS178 ☐ HIS179 ☐
H&E QC by /date	/
Draft to Path	
Edit to Sec	
Final to Path	
Date Sent out	

Appendix IV

Participant demographics data

Maternal characteristics					
Patient name					
Maternal age (years)					
Maternal height (cm)					
Maternal weight(kg)					
BMI					
Obesity (BMI>30)					
Level of education (less than High school?)					
Racial origin					
Parity					
Gravidity					
Inter pregnancy interval					
Blood pressure					
Gestational weight gain* (GWG)					
Prior or current Preeclampsia					
Prior essential hypertension					
Diabetic	DM1		1sttrimester Hb A1c(%)		GTT

	DM2		2nd trimester Hb A1c(%)		
	GDM		3rd trimester Hb A1c(%)		
Insulin use (%)					
Prior autoimmune disease					
Pre-existing vascular disease					
Pre-existing renal impairment					
Prior stillbirth					
Mode of conception					
Cigarette Smoking	Paternal:		Maternal:		
Alcohol > alcoholic beverage [12g]/d until pregnancy was known					
Recreational drugs					
Gestational age at birth (weeks)					
Use of ART *					
Heavy first-trimester vaginal bleeding					
Multiple pregnancy					

Medication	
Ultrasound parameters	
Doppler US	
Increased nuchal translucency	
Perinatal outcomes	
Gestational age (weeks)	
Birth weight(grams)	
Birth weight for GA (percentile)	
Caesarean section	
Fetal Gender	
Apgar score 5 min	
Malformation	
Prior fetal growth restriction or small baby	
Paternal or maternal SGA	
Others	
Notes :	

Appendix V

Patient information sheet (PIS): first page

Sheffield Teaching Hospitals NHS
NHS Foundation Trust

The University Of Sheffield.

Participant Information Sheet. V2.1

Dated 29th November 2021

STH STH20937
IRAS 260951
REC 19/LO/1656

MAGNETIC RESONANCE IMAGING OF THE PLACENTA and fetal growth

INFORMATION SHEET FOR PARTICIPANTS

Hiba Alessa
Elspeth Whitby
Mark Fenwick
Andrew Fry
Roobin Jokhi
Marta Cohen

Thank you for taking the time to read through this information sheet.

If you are interested in taking part in this study and would like further details you can phone 0114 2261081 or ask for more information when you next attend the hospital.

What is the purpose of the study?

The purpose of this study is to allow us to image the baby and placenta with Magnetic resonance imaging (MRI). We are looking at the baby and placenta in mothers where there is no problem with either (normal controls) or where the baby is small or where there is a history of diabetes (before or during pregnancy) or a previous history of pregnancy loss. This

The University Of Sheffield.

Sheffield Teaching Hospitals NHS
NHS Foundation Trust

V2.1 24/08/21

STH: STH20937

IRAS 260951
REC Reference:19/LO/1656

Magnetic Resonance Imaging of the placenta and fetal growth

Consent form

Name of researcher: Hiba Alessa, Elspeth Whitby, Mark Fenwick, Roobin Jokhi, Marta Cohen ,….

Please initial box

1. I agree that I have read and understood the information sheet dated 24/08/21for the project. ☐
2. I have had sufficient opportunities to ask questions about the project. ☐
3. I understand that it is up to me whether or not I take part and that I can stop at any time without needing to say why. ☐

☐

4. I understand that data collected from the study will be anonymised and kept for the duration of the study only.
5. I agree to take part in the study ☐
6. I am aware that my medical records and my child's medical records may be viewed for follow up information as to the health of my child. ☐
7. I am happy for my anonymised images to be used in publications and teaching. ☐

Please note that data may be available to the regulatory authorities and sponsor organisation.

Name of participating person	Date	Signature
Name of person taking consent	Date	Signature

Copies: One for each participating person, one for the researcher, one to be kept in the project site file.

Appendix VII

IRAS approval letter

NHS
Health Research Authority
London - Central Research Ethics Committee
3rd Floor, Barlow House
4 Minshull Street
Manchester
M1 3DZ

Telephone: 0207 1048 007

Please note: This is the favourable opinion of the REC only and does not allow you to start your study at NHS sites in England until you receive HRA Approval

15 November 2019

Dr Elspeth Whitby
University of Sheffield
Academic Unit of Reproductive and Developmental Medicine
Room 59 Level 4 Jessop Wing Hospital
Tree Root Walk
Sheffield
S10 2SF

Dear Dr Whitby

Study title:	**MRI of the placenta and its relationship to fetal growth and development.**
REC reference:	**19/LO/1656**
Protocol number:	**V1.0**
IRAS project ID:	**260951**

The Proportionate Review Sub-committee of the London - Central Research Ethics Committee reviewed the above application.

Ethical opinion

On behalf of the Committee, the sub-committee gave a favourable ethical opinion of the above research on the basis described in the application form, protocol and supporting documentation, subject to the conditions specified below.

Appendix VIII

Research advert

ARE YOU INTERESTED IN HELPING RESEARCH?

We are looking for volunteers to attend for 2 MRI scans of their baby and placenta whilst they are pregnant.

You will get to see images of your baby. This will take about 20 minutes and take place at the Royal Hallamshire Hospital.

PLEASE ASK FOR FURTHER DEATAILS

Phone number: 07943409644

Email: hmaalessa1@sheffield.ac.uk

STH: STH20937

IRAS 260951

REC Reference:

Magnetic Resonance Imaging of the placenta and fetal growth

25th September 2019

Appendix IX

Research flier

The University Of Sheffield.

MRI research to diagnose fetal growth abnormalities

NHS Sheffield Teaching Hospitals NHS Foundation Trust

We would like to do 2 MRI scans for pregnant ladies in their second and third trimesters.
The aim of the research is to study the placenta's features that may help to detect fetal growth abnormalities.
MRI scan is safe during pregnancy and can provide detailed clear images of your baby inside the womb.

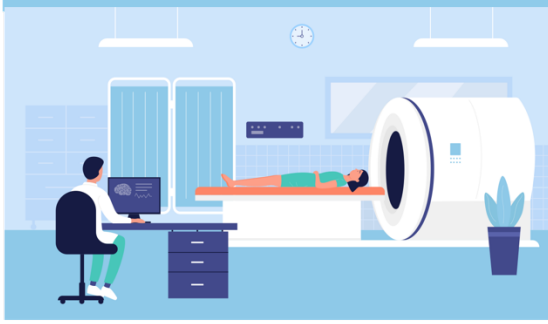

We are interested in 4 groups:
1. Normal pregnancy
2. Have a baby that is not growing as well as we expect.
3. Mum has a type of diabetes
4. Have or had COVID during you pregnancy.

If you would like more information please contact:

Hiba Alessa (PhD student)
07943409644
Elspeth Whitby (Consultant Radiologist)
07778660192
Or email:
hmaalessa1@sheffield.ac.uk
e.whitby@sheffield.ac.uk

Appendix X

Patient's positive feedback

1. **"Thank you so much! These are amazing and thank you to all of you that are conducting this research it's been an amazing experience and I feel very lucky to have gotten the chance to see my baby in such amazing detail".**

2. A tweet from a participant

   "Meanwhile I've been growing something else. Expected arrival early 2022. MRI image courtesy of an excellent research study at Sheffield Teaching Hospitals".

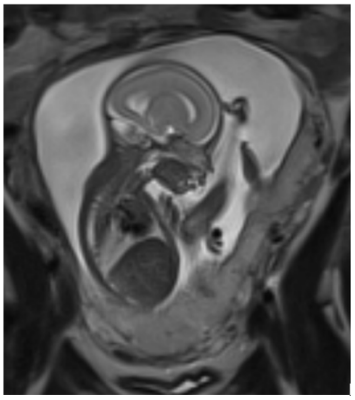

Appendix XI

BIR ADC poster

The University Of Sheffield.

ADC values as a biomarker for placenta accreta spectrum

Student- Hiba Alessa, Supervisor- Elspeth Whitby
Academic Unit of Reproductive and developmental Medicine, Department of Oncology and Metabolism, University of Sheffield

Introduction

Placenta accreta spectrum (PAS) is an obstetric emergency and a leading cause of life threatening bleeding.
Identifying invasion signs on MRI, such as heterogeneity and dark bands, are experts' dependent, and therefore developing an objective approach is warranted.
Effective antenatal diagnosis may significantly help in reducing maternal morbidity and mortality.

Objectives

The aim of this resaerch is to apply MRI apparent diffusion coefficient (ADC) to improve the aacuracy of antenatal PAS detection.

Method

A retrospective review of 153 cases. ADC values were obtained from two regions of interest (ROIs). The area above the bladder and the entire placenta on a midline sagittal image (Fig.1). Heterogeneity of the placenta and placental dark bands were also noted. Pathological diagnosis was obtained from medical records.

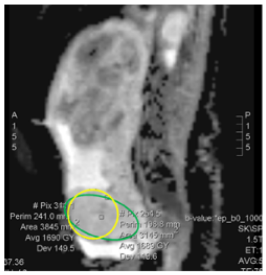

Fig.1: ADC MRI of a Sagittal section showing areas of whole placenta (green circle) and regional segmantation (yellow circle).

Conclusion

ADC MRI values are a potential marker for future evaluation of PAS to aid confidence in the imaging diagnosis. further studies are required.

Results

Mean ADC of invaded placentas were higher than of normal, equal to 1400 mm2/second in comparison to 1552 mm2/sec for invaded placentas.
Independent t-test showed significant correlation of regional ADC and pathology (p= 0.03).
ADC of a small region of invaded placenta showed higher accuracy than ADC of the whole placenta.
ADC was higher in invaded placentas when testing both ROIs, for whole and small placental region (Fig.2).

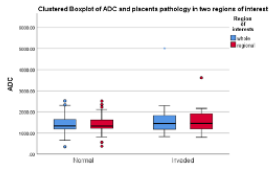

Fig.2: Boxplot comparing ADC in normal and invaded placentas.

Mean ADC of invaded placenta was significantly higher where there is local heterogeniety (red bar) which is one local dark area seen in MRI (Fig.3).

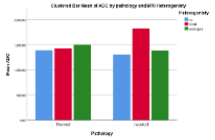

Fig.3: Bar chart comparing ADC in normal and invaded placentas with heterogenity.

Placentas with local heterogeniety showed higher ADC than of homogenous placentas (Fig.4).
Regional ADC has a signficant corrolation with placental heterogeniety (p=0.02).

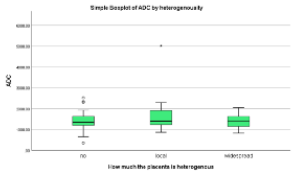

Fig.4: Boxplot of ADC mean and heterogeniety

The median ADC for the group having > 5 dark bands was 1590.70 mm2/sec compared to 1472.20 mm2/sec group having no dark bands (Fig.5).

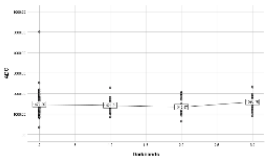

Fig.5: scatterplot of mean ADC and darkbands tested in whole placental region.

Aknowlegment
I would like to express my deep gratitude to Dr. Elspeth Whitby for her valuable and constructive suggestions during the development of this research work. Her willingness to give her time so generously has been very much appreciated.

Contact details:
hmaalessa1@Sheffield.ac.uk
Twitter: @AlessaHiba

Appendix XII

Data distribution

Histogram and Q-Q plots were used to test the normality of data, the data were abnormally distributed.

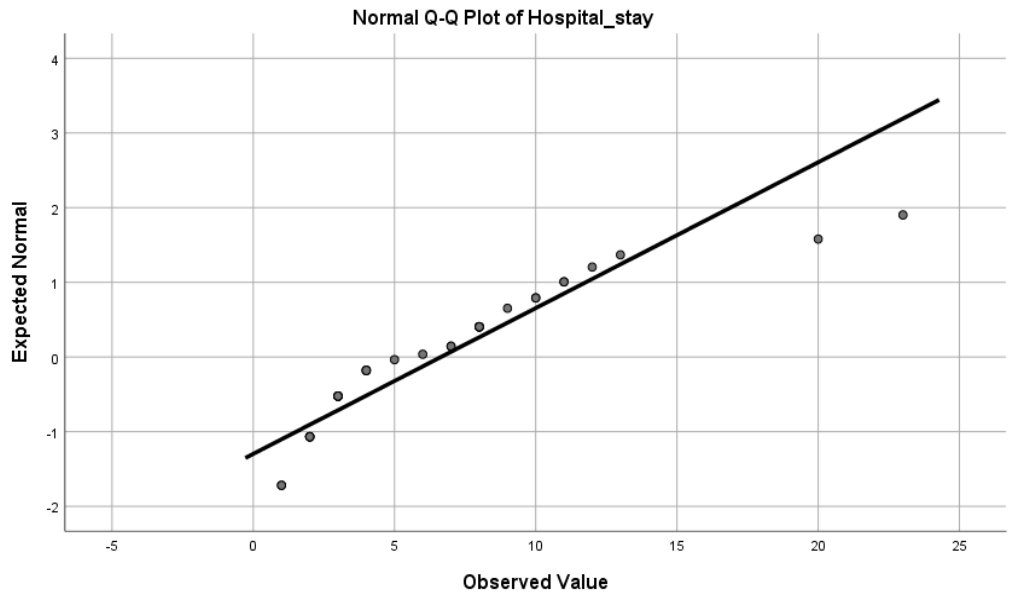
Normal Q-Q Plot of Hospital_stay
Expected Normal
Observed Value
4
3
2
1
0
-1
-2
-5
0
5
10
15
20
25

a.

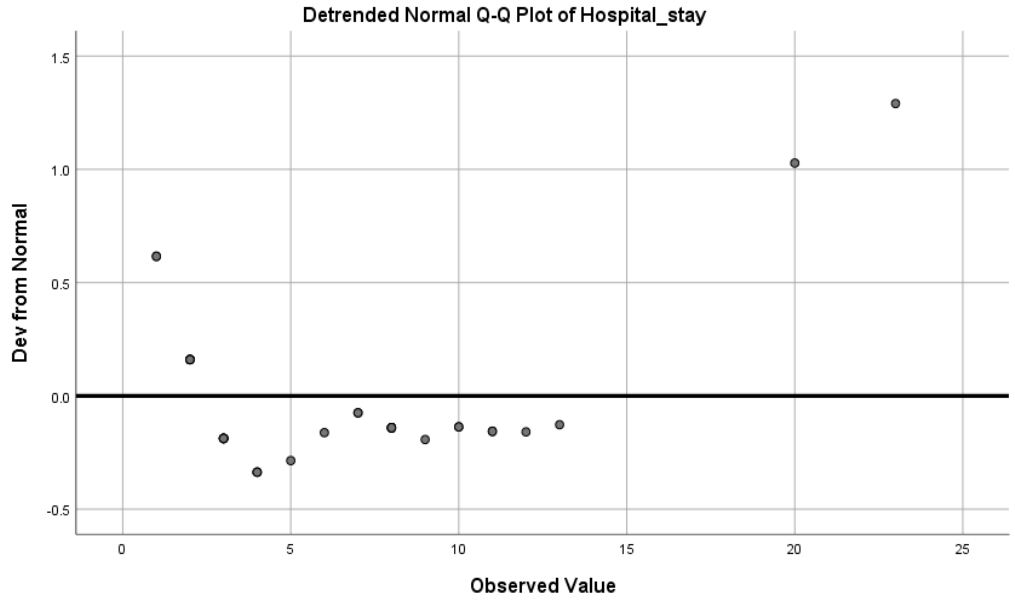
Detrended Normal Q-Q Plot of Hospital_stay
Dev from Normal
Observed Value
1.5
1.0
0.5
0.0
-0.5
0
5
10
15
20
25

b.

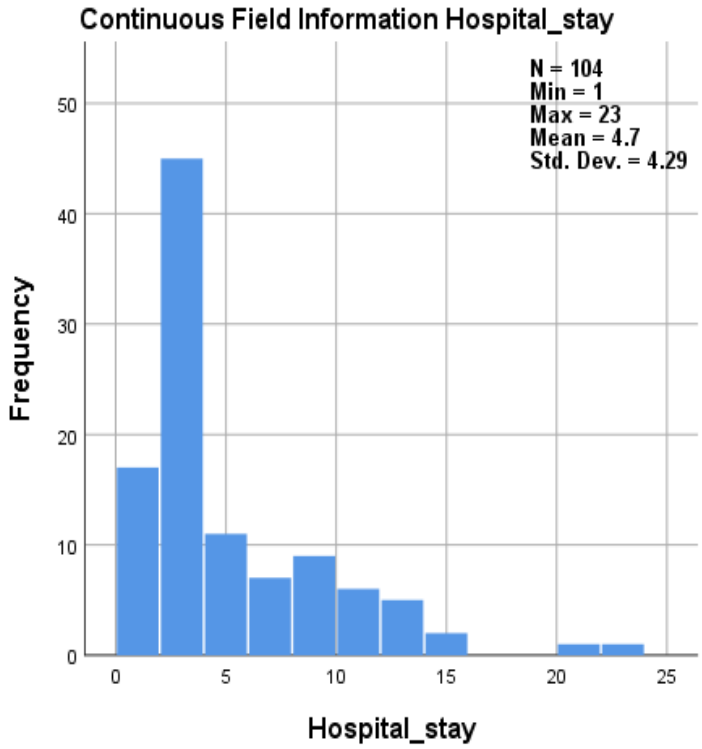

c.

Q-Q plots (a &b) and histogram; c, showing the distribution of data.

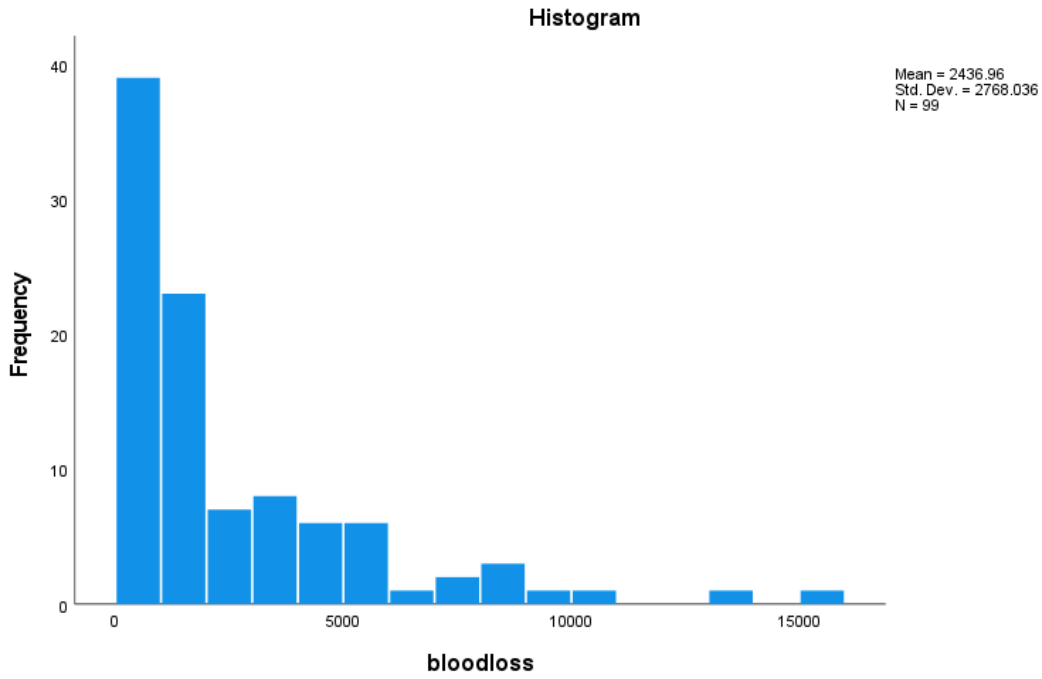

Histogram of the data distribution of the amount of blood loss in millilitres (mL).

As the data was not normally distributed, Kruskal-Wallis test was applied to assess for any correlation between blood loss and heterogeneity. Significance was assumed at $p<0.05$.

Data distribution

When analysing ADC with pathology data, data was normally distributed in normal and percreta but not in increta and accreta groups. This could be due to the low number of increta cases. For that reason, we combined increta and accreta into one group. Data after combining increta/ accreta cases were normal (n=77), accreta (n=28) and percreta (n=22)

Tests of normality of data:

Histograms and Q-Q plots were drawn to test the normality of the data. ADC data were tested in each group of PAS for normality. The data were normally distributed.

Whole placenta ADC

A. Normal

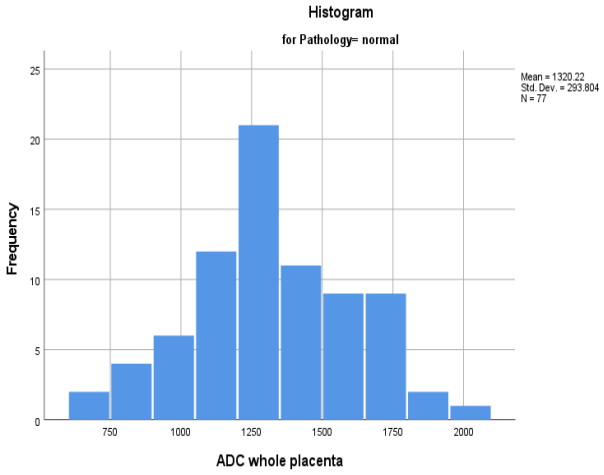

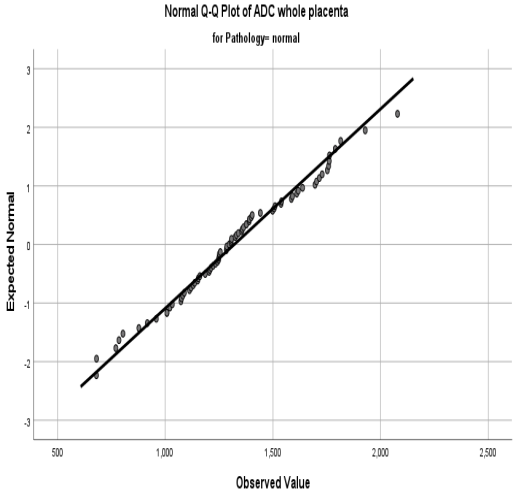

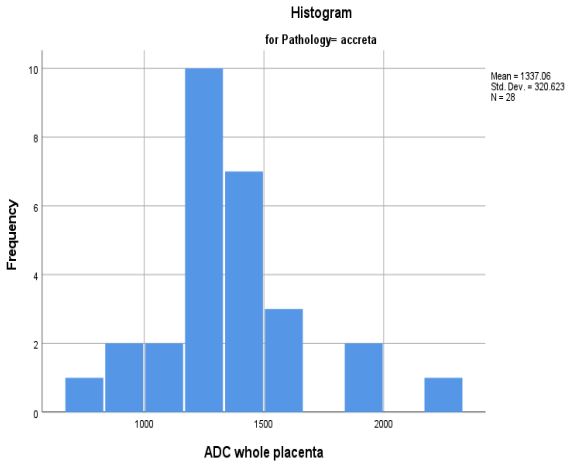

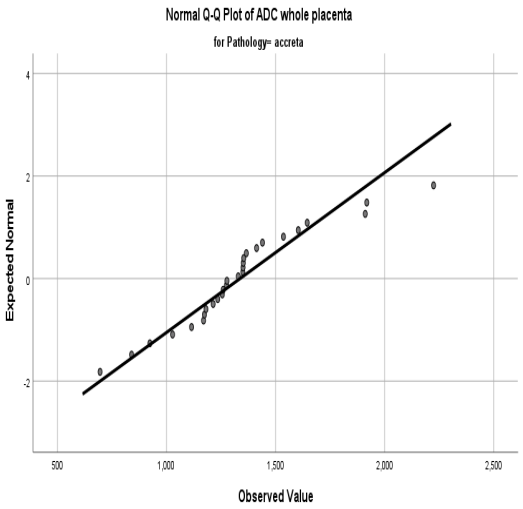

B. Accreta

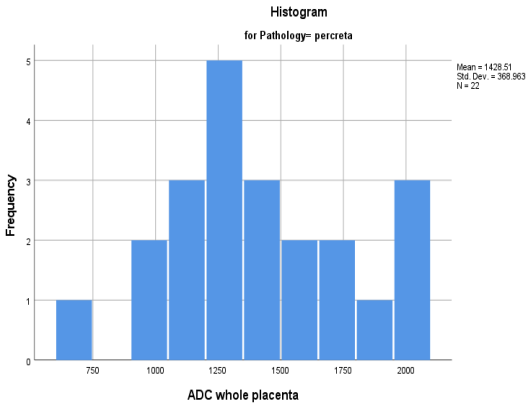

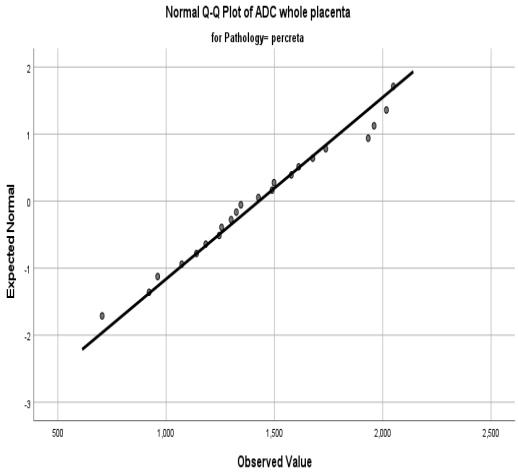

C. Percreta

Histograms and Q-Q plots of ADC whole placenta distribution in PAS groups.

Regional ADC:

A. Normal

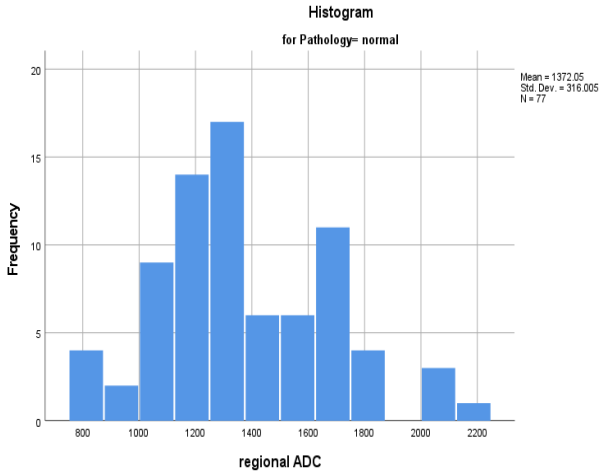

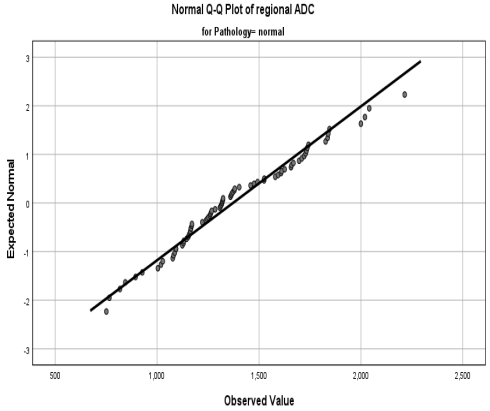

B. Accreta

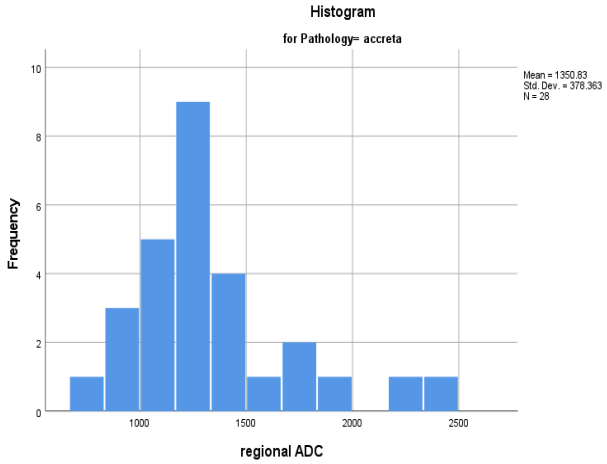

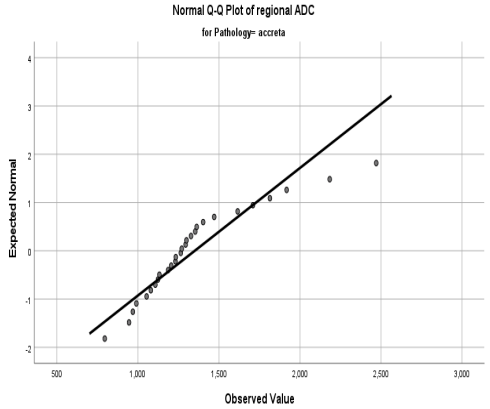

C. Percreta

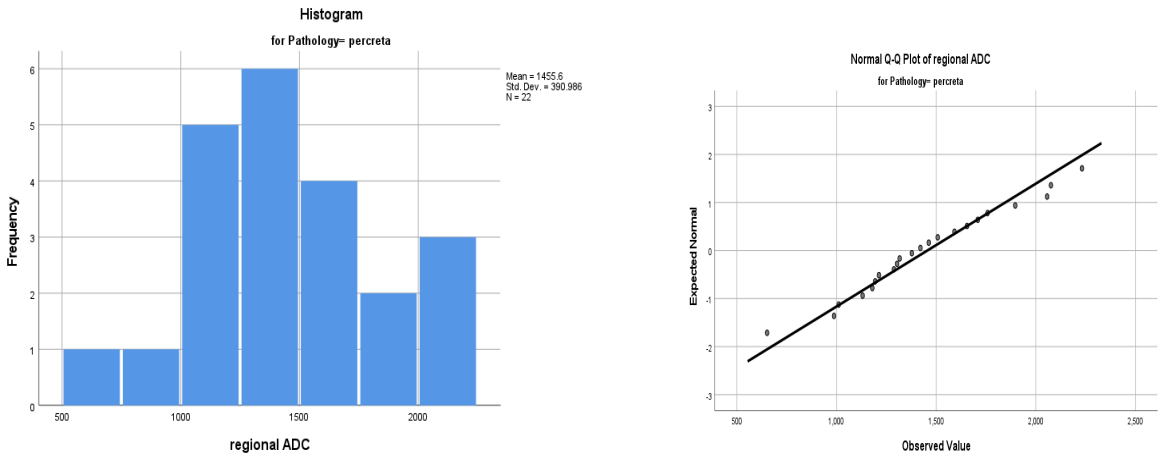

Histograms and Q-Q plots of ADC ROI distribution in PAS groups.

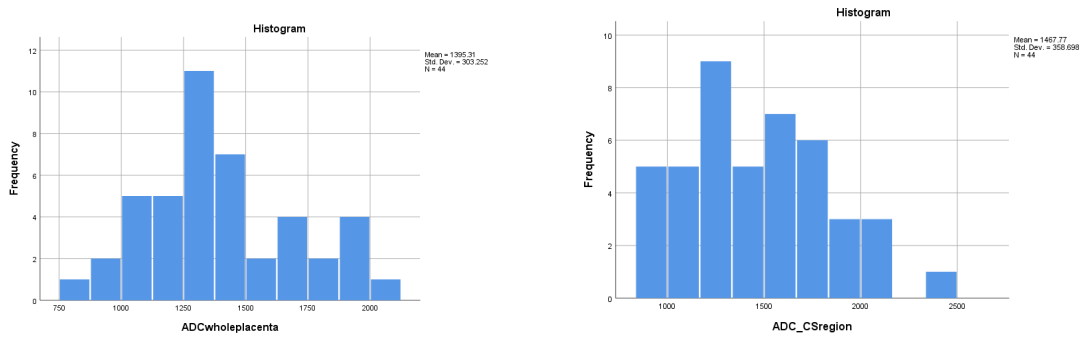

A. B.

Histograms of ADC whole placenta (A) and CS (B). Data was normally distributed.

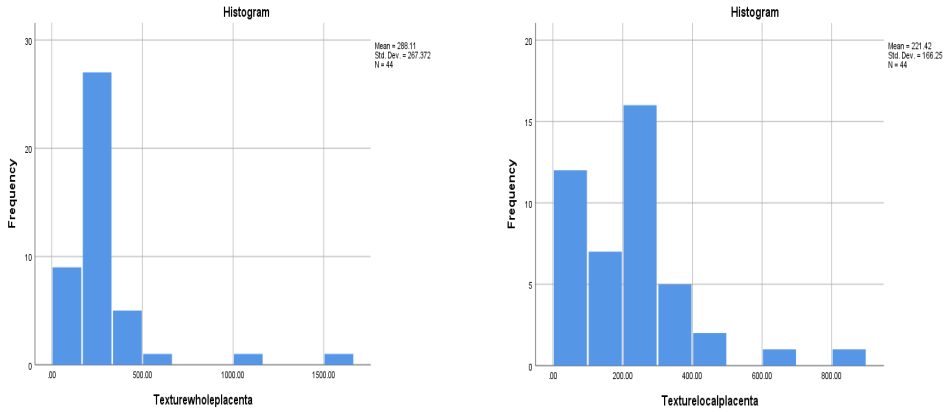

A. B.

Histograms of the mean texture of the whole placenta (A) and CA area (B). The data was abnormally distributed.

Appendix XIII

Texture tables

Whole placental texture	P value	ROC curve
CONVENTIONAL min	**0.002**	0.6
CONVENTIONAL mean	0.798	0.6
CONVENTIONAL std	0.596	0.5
CONVENTIONAL max	0.596	0.5
CONVENTIONAL Q1	0.421	0.6
CONVENTIONAL Q2	0.666	0.6
CONVENTIONAL Q3	0.984	0.6
CONVENTIONAL Skewness	0.444	0.5
CONVENTIONAL Kurtosis	0.126	0.5
CONVENTIONAL Excess Kurtosis	0.126	0.5
CONVENTIONAL peak Sphere 0.5mL discretized volume sought	1	0.5

CONVENTIONAL peak Sphere 0.5 mL value only for PET or NM	0.844	0.5
CONVENTIONAL peak Sphere 1mL discretized volume sought	1	0.5
CONVENTIONAL peak Sphere 1mL value only for PET or NM	0.991	0.5
CONVENTIONAL calcium Agatston Score only for CT	**0.000**	0.6
CONVENTIONAL_TLG mL only For PET or NM	0.164	0.7
DISCRETIZED mean	**0.000**	0.8
DISCRETIZED std	**0.000**	0.7
DISCRETIZED max	**0.000**	0.7
DISCRETIZED Q2	**0.000**	0.7
DISCRETIZED Skewness	0.308	0.5
DISCRETIZED Kurtosis	0.231	0.7
DISCRETIZED Excess Kurtosis	0.231	0.7
DISCRETIZED peak Sphere 0.5mL discretized volume sought	1	0.5
DISCRETIZED peak Sphere 0.5 mL value only for PET or NM	**0.000**	0.7
DISCRETIZED peak Sphere 1mL discretized volume sought	1	0.5
DISCRETIZED peak Sphere 1 mL value only for PET or NM	**0.000**	0.7
DISCRETIZED TLG mL only For PET or NM	**0.000**	0.8
DISCRETIZED HISTO_Entropy_log10	**0.000**	0.7
DISCRETIZED HISTO_Entropy_log2	**0.000**	0.7
DISCRETIZED HISTO Energy Uniformity	**0.000**	0.4
SHAPE Volume mL	**0.000**	0.6
SHAPE Volume vx	**0.000**	0.6
SHAPE Sphericity only For 3D ROI	**0.000**	0.6
SHAPE Surface mm 2 only For 3D ROI	**0.000**	0.5
SHAPE Compacity only For 3D ROI	**0.000**	0.6
PARAMS Bin Size	**0.001**	0.23

PARAMS YS partial Resampling	**0.000**	0.5
PARAMS XS partial Resampling	**0.000**	0.5
GLCM Homogeneity Inverse Difference	**0.000**	0.18
GLCM Energy Angular Second Moment	**0.000**	0.31
GLCM Contrast Variance	**0.000**	0.79
GLCM Correlation	0.034	0.50
GLCM Entropy log10	**0.000**	0.72
GLCM Entropy log2 Joint Entropy	**0.003**	0.72
GLCM Dissimilarity	**0.000**	0.80
GLRLM SRE	**0.000**	0.82
GLRLM LRE	**0.001**	0.22
GLRLM LGRE	**0.000**	0.1
GLRLM HGRE	**0.000**	0.76
GLRLM SRLGE	**0.000**	0.18
GLRLM SRHGE	**0.000**	0.75
GLRLM LRLGE	**0.000**	0.17
GLRLM LRHGE	**0.000**	0.75
NGLDM Coarseness	**0.000**	0.40
NGLDM Contrast	**0.002**	0.72
NGLDM Busyness	**0.000**	0.29
GLZLM SZE	**0.000**	0.88
GLZLM LZE	**0.002**	0.47
GLZLM LGZE	0**.000**	0.15
GLZLM HGZE	0.028	0.76
GLZLM SZLGE	**0.000**	0.25
GLZLM SZHGE	**0.000**	0.81
GLZLM LZLGE	0.367	0.34
GLZLM LZHGE	**0.003**	0.46
GLZLM GLNU	**0.000**	0.84
GLZLM ZP	0.465	0.81

Local placental texture	P value	ROC curve

CONVENTIONAL min	0.152	0.42
CONVENTIONAL mean	0.530	0.41
CONVENTIONAL std	0.404	0.49
CONVENTIONAL max	0.465	0.47
CONVENTIONAL Q1	0.781	0.39
CONVENTIONAL Q2	0.585	0.45
CONVENTIONAL Q3	0.571	0.42
CONVENTIONAL Skewness	0.926	0.58
CONVENTIONAL Kurtosis	0.585	0.52
CONVENTIONAL Excess Kurtosis	0.585	0.52
CONVENTIONAL peak Sphere 0.5mL discretized volume sought	1	0.5
CONVENTIONAL peak Sphere 0.5 mL value only for PET or NM	0.475	0.40
CONVENTIONAL peak Sphere 1mL discretized volume sought	1	0.5
CONVENTIONAL peak Sphere 1mL value only for PET or NM	0.209	0.4
CONVENTIONAL calcium Agatston Score only for CT	**0.026**	0.5
CONVENTIONAL_TLG mL only For PET or NM	0.468	0.41
DISCRETIZED mean	**0.000**	0.62
DISCRETIZED std	**0.003**	0.51
DISCRETIZED max	**0.002**	0.60
DISCRETIZED Q2	**0.001**	0.61
DISCRETIZED Skewness	0.198	0.54
DISCRETIZED Kurtosis	0.465	0.60
DISCRETIZED Excess Kurtosis	0.465	0.60
DISCRETIZED peak Sphere 0.5mL discretized volume sought	1	0.5
DISCRETIZED peak Sphere 0.5 mL value only for PET or NM	**0.007**	0.55
DISCRETIZED peak Sphere 1mL discretized volume sought	1	0.5

DISCRETIZED peak Sphere 1 mL value only for PET or NM	**0.039**	0.60
DISCRETIZED TLG mL only For PET or NM	**0.000**	0.65
DISCRETIZED HISTO Entropy log10	**0.000**	0.55
DISCRETIZED HISTO Entropy log2	**0.000**	0.55
DISCRETIZED HISTO Energy Uniformity	**0.000**	0.47
SHAPE Volume mL	**0.000**	0.52
SHAPE Volume vx	**0.001**	0.45
SHAPE Sphericity only For 3D ROI	**0.000**	0.44
SHAPE Surface mm 2 only For 3D ROI	**0.001**	0.45
SHAPE Compacity only For 3D ROI	**0.000**	0.44
PARAMS Bin Size	**0.002**	0.32
PARAMS YS partial Resampling	**0.000**	0.46
PARAMS XS partial Resampling	**0.000**	0.46
GLCM Homogeneity Inverse Difference	**0.078**	0.3
GLCM Energy Angular Second Moment	**0.000**	0.37
GLCM Contrast Variance	**0.002**	0.6
GLCM Correlation	0.171	0.47
GLCM Entropy log10	**0.000**	0.6
GLCM Entropy log2 Joint Entropy	**0.035**	0.6
GLCM Dissimilarity	**0.001**	0.6
GLRLM SRE	**0.000**	0.7
GLRLM LRE	**0.000**	0.30
GLRLM LGRE	**0.000**	0.42
GLRLM HGRE	**0.000**	0.61
GLRLM SRLGE	**0.000**	0.42
GLRLM SRHGE	**0.001**	0.63
GLRLM LRLGE	**0.000**	0.36
GLRLM LRHGE	**0.000**	0.57
NGLDM Coarseness	**0.000**	0.45
NGLDM Contrast	**0.000**	0.55
NGLDM Busyness	0.585	0.49
GLZLM SZE	**0.000**	0.66

GLZLM LZE	**0.000**	0.28
GLZLM LGZE	**0.000**	0.37
GLZLM HGZE	0.280	0.61
GLZLM SZLGE	**0.000**	0.44
GLZLM SZHGE	**0.001**	0.60
GLZLM LZLGE	0.530	0.32
GLZLM LZHGE	**0.001**	0.32
GLZLM GLNU	**0.000**	0.63
GLZLM ZP	1	0.69

Appendix XIV

Histograms of placental measurements, ADC and T2* showing data distribution.

Sample 1 test of normality

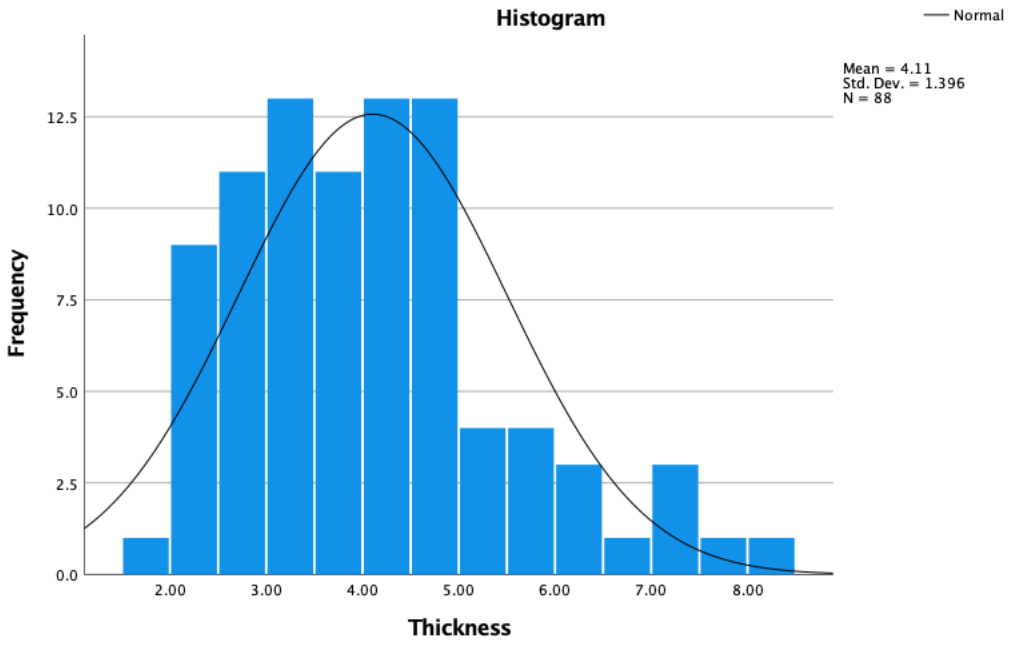

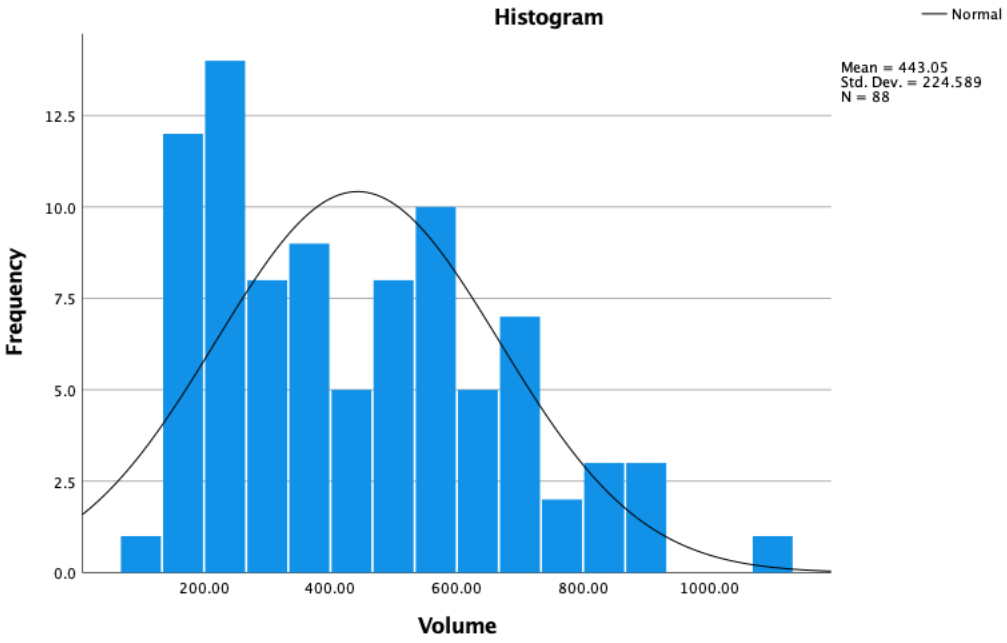
Histogram
Normal
Mean = 443.05
Std. Dev. = 224.589
N = 88
Frequency
12.5
10.0
7.5
5.0
2.5
0.0
200.00
400.00
600.00
800.00
1000.00
Volume

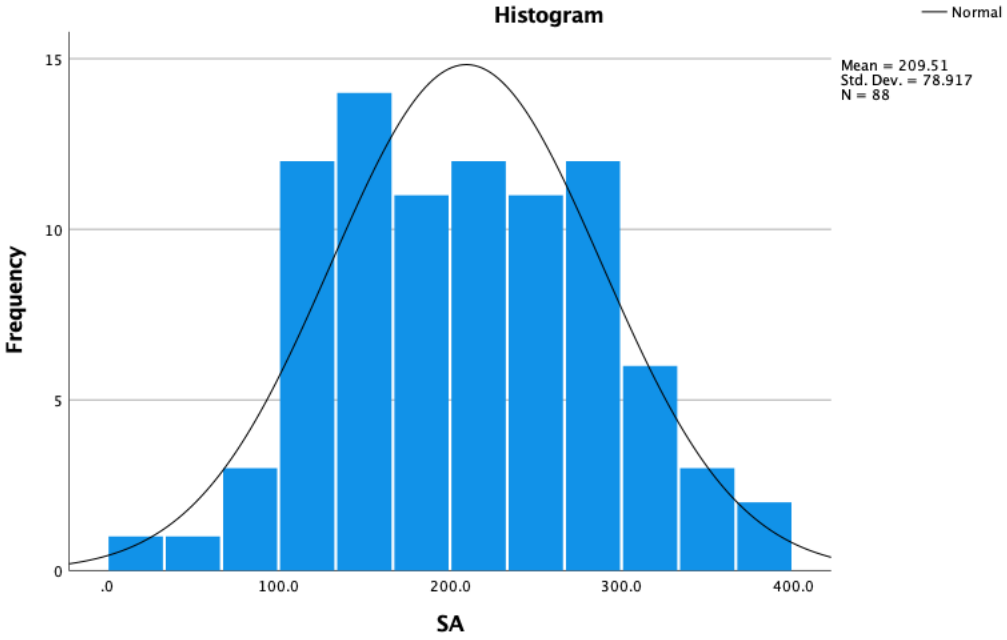
Histogram
Normal
Mean = 209.51
Std. Dev. = 78.917
N = 88
Frequency
15
10
5
0
.0
100.0
200.0
300.0
400.0
SA

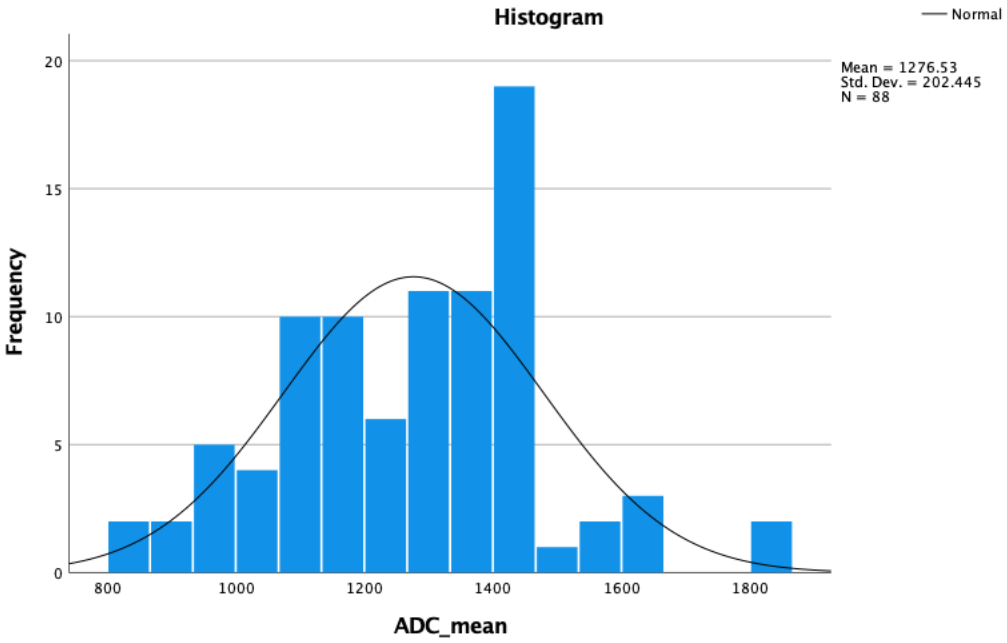
Histogram
Normal
Mean = 1276.53
Std. Dev. = 202.445
N = 88
Frequency
20
15
10
5
0
800
1000
1200
1400
1600
1800
ADC_mean

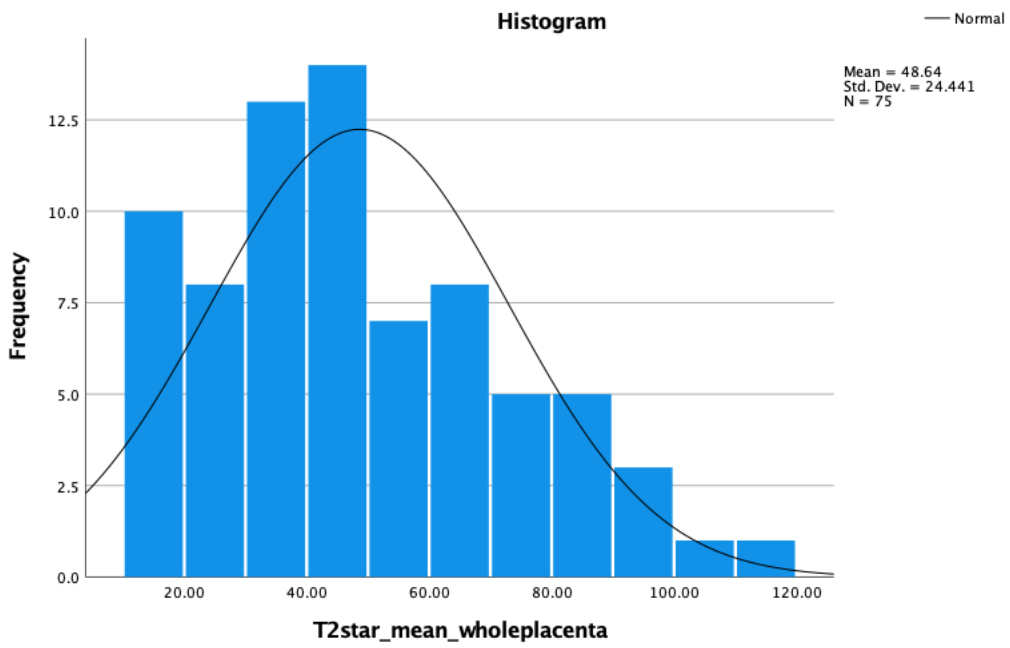

Sample 2 test of normality

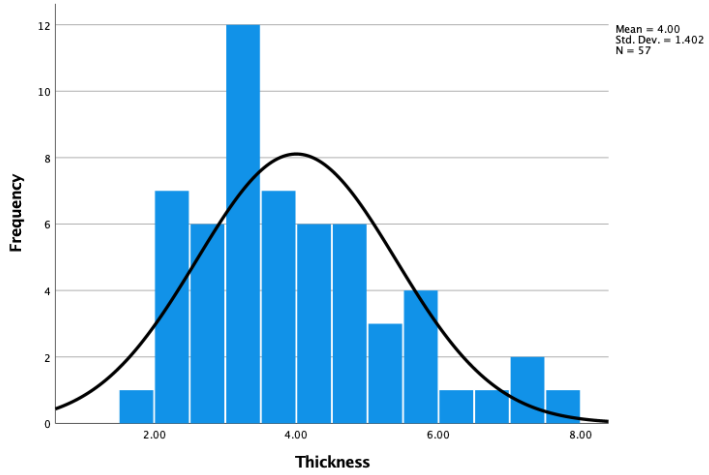

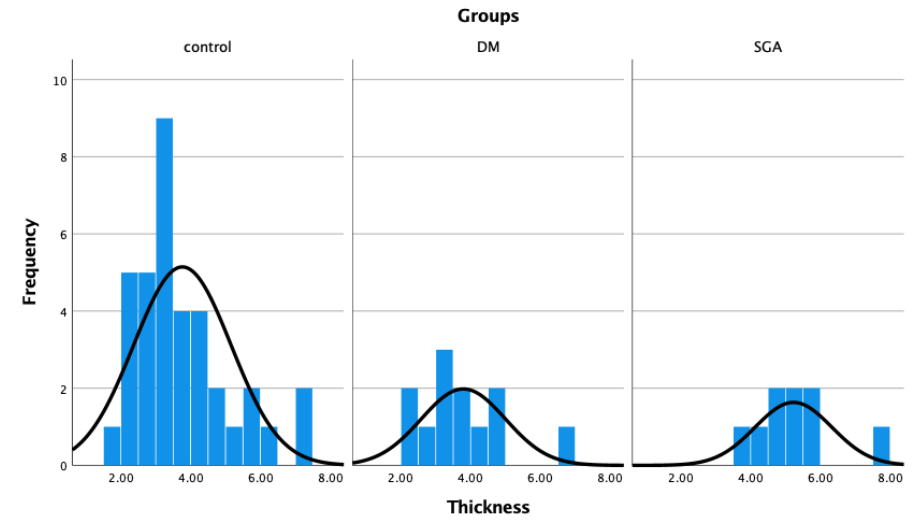
Groups
control
DM
SGA
Frequency
Thickness

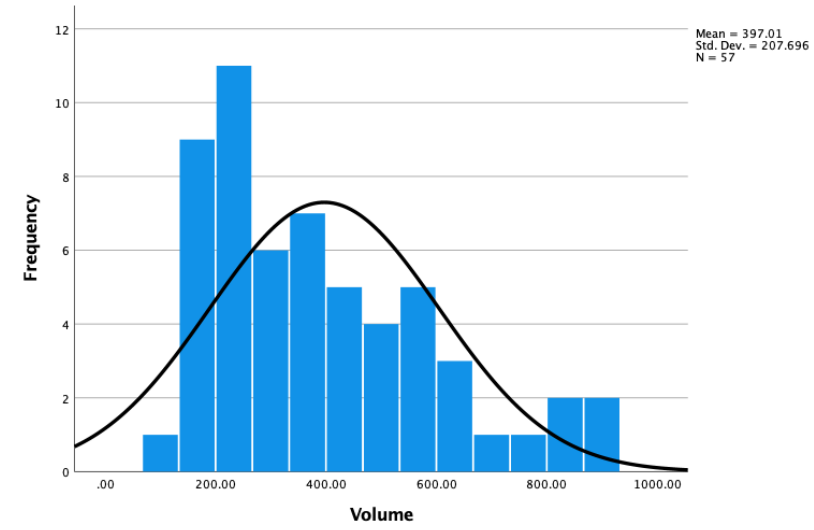
Mean = 397.01
Std. Dev. = 207.696
N = 57
Frequency
Volume

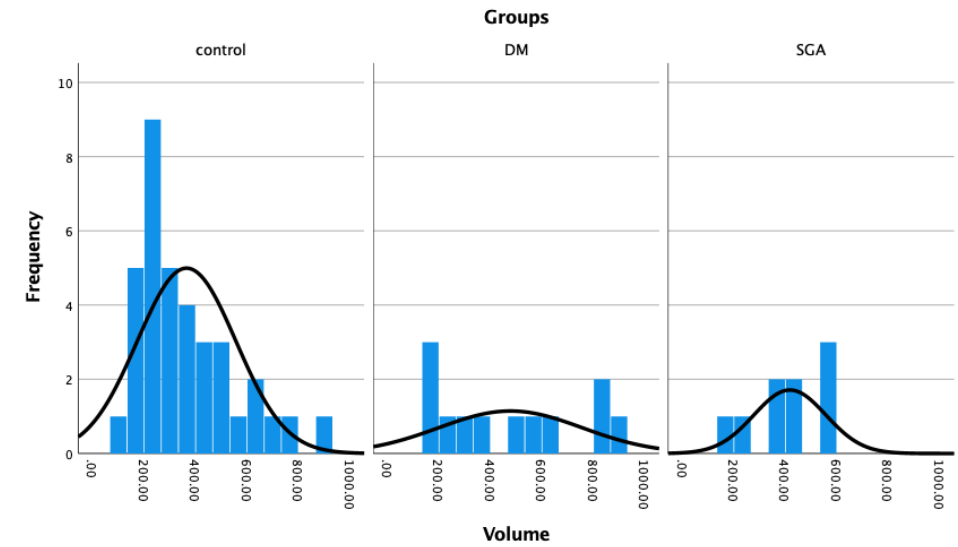
Groups
control
DM
SGA
Frequency
Volume

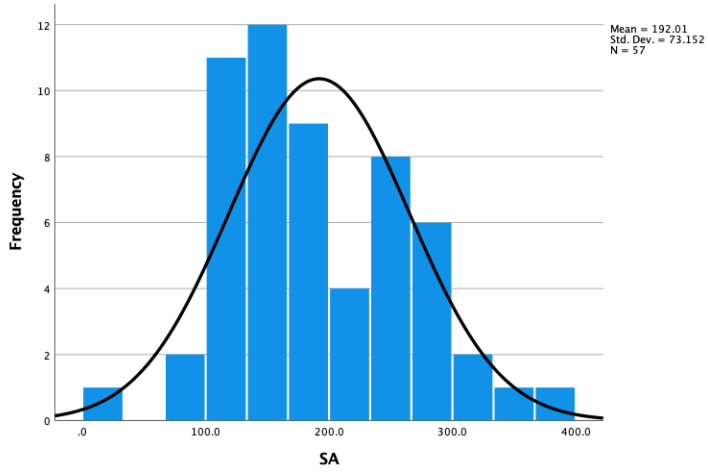
Mean = 192.01
Std. Dev. = 73.152
N = 57
Frequency
SA

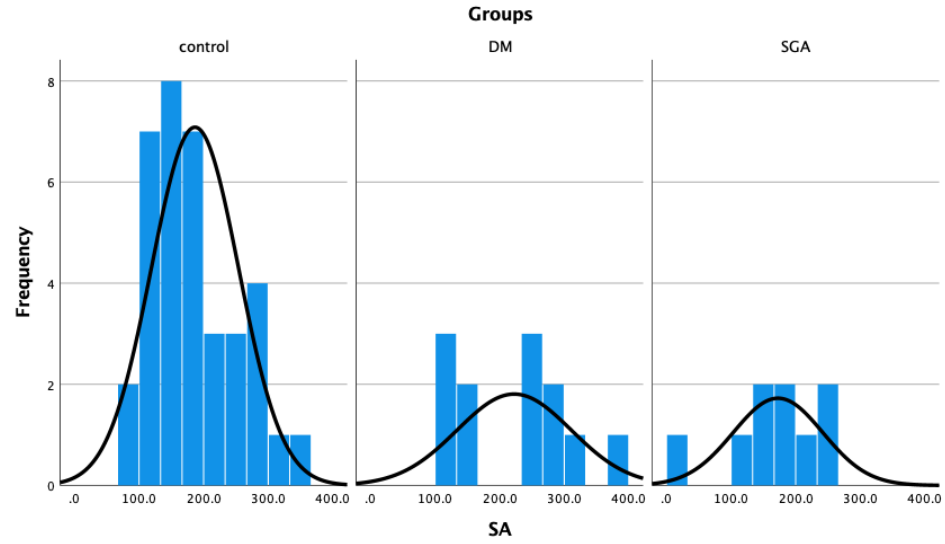
Groups
control
DM
SGA
Frequency
SA

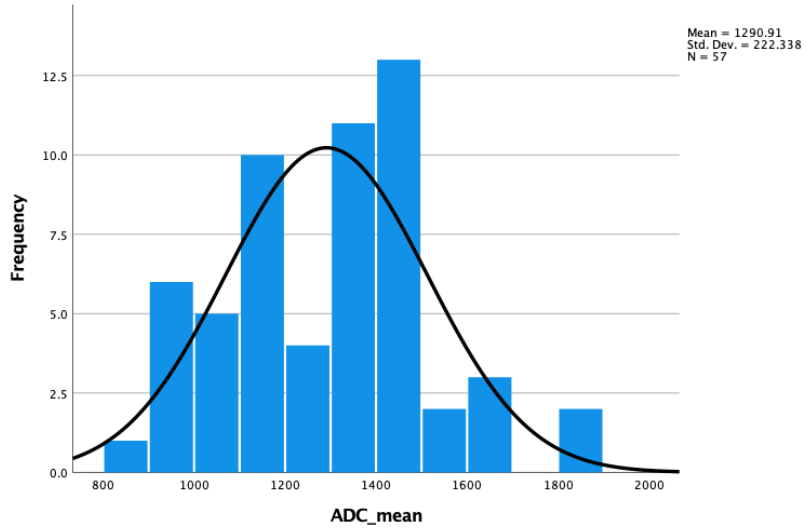
Mean = 1290.91
Std. Dev. = 222.338
N = 57
Frequency
ADC_mean

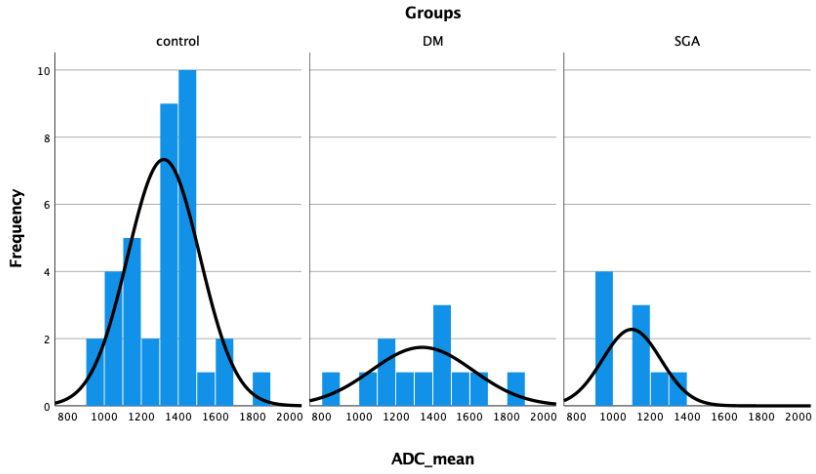
Groups
control
DM
SGA
Frequency
ADC_mean

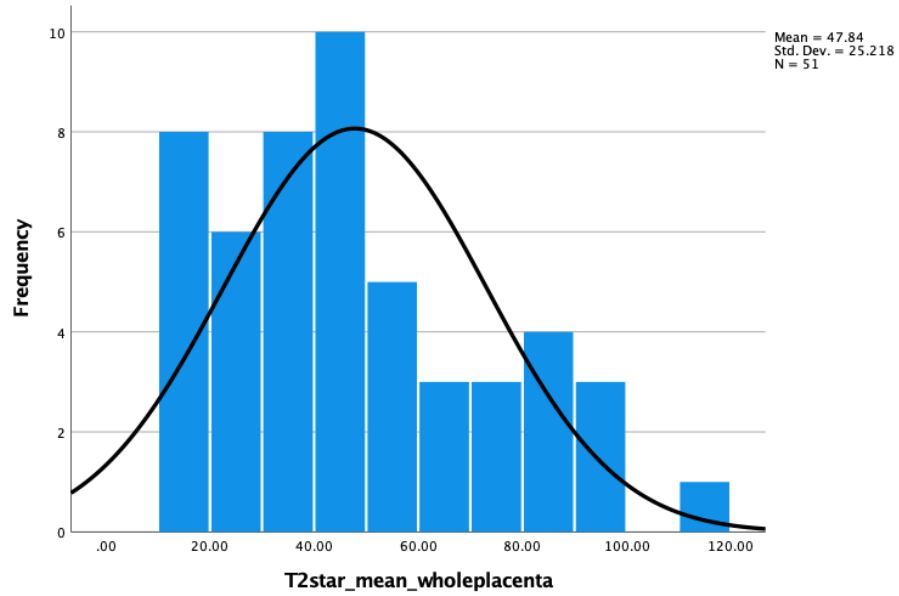
Mean = 47.84
Std. Dev. = 25.218
N = 51
Frequency
T2star_mean_wholeplacenta

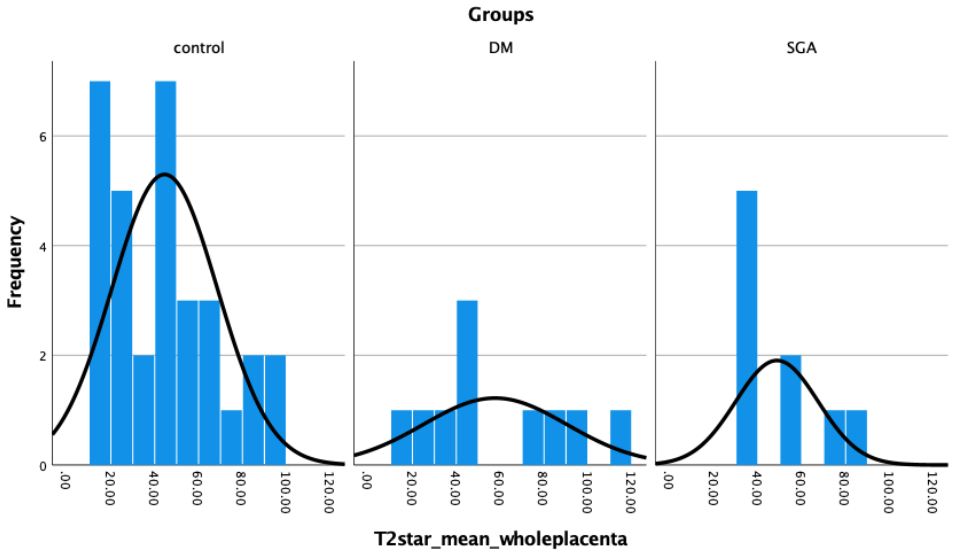

Appendix XV

Covariates	**Module 1** (B, standard error)	**Module 2** (B, standard error)
Intercept	0.28, 0.6	0.154, 0.647
GA	0.1, 0.02*	0.141, 0.023*
Diabetes with SGA	-	0.855, 0.795
COVID	-	-0.265, 0.334
Groups comparison		
SGA/Control	0.6, 0.4	0.382, 0.471
DM/Control	-0.3, 0.3	-0.308, 0.305
R^2	0.37	0.38
Observations numbers	Controls=60 SGA=10 DM=18	Controls=60 SGA=10 DM=18

Note: P< 0.05 noted as *

B= coefficients

Comparison of groups using ANCOVA and different covariates modules for assessment of thickness.

Covariates	**Module 1 (B, standard error)**	**Module 2 (B, standard error)**
Intercept	-424.6, 86*	-432.3, 87.6*
GA	31, 3*	31.4, 3.1*
Diabetes with SGA	-	35.2, 107.6
COVID	-	-23.6, 45.2
Groups comparison		
SGA/Control	-120.2, 52.9*	-128.2, 63.8*
DM/Controls	30.6, 40.8	32.9, 41.4
R^2	0.56	0.56
Observations numbers	Controls=60 SGA=10 DM=18	Controls=60 SGA=10 DM=18

Note: P< 0.05 noted as *

Comparison of groups using ANCOVA and different covariates modules for assessment of volume.

Covariates	**Module 1 (B, standard error)**	**Module 2 (B, standard error)**
Intercept	-49.9, 34.3	-49.9, 34.88
GA	9.3, 1.2*	9.4, 1.2*
Diabetes with SGA	-	-25.8, 42.8
COVID	-	-11.695,17.9
Groups comparison		
SGA/Control	-65.9, 21.1*	-56.4, 25.4*
DM/Control	19.1, 16.3	20.2, 16.5
R^2	0.43	0.438
Observations numbers	Controls=60 SGA=10 DM=18	Controls=60 SGA=10 DM=18

Note: P< 0.05 noted as *

Comparison of groups using ANCOVA and different covariates modules. For assessment of surface area.

Covariates	**Module 1 (B, standard error)**	**Module 2 (B, standard error)**
Intercept	-49.9, 34.3	-49.9, 34.88
GA	9.3, 1.2*	9.4, 1.2*
Diabetes with SGA	-	-25.8, 42.8
COVID	-	-11.695,17.9
Groups comparison		
SGA/Control	-65.9, 21.1*	-56.4, 25.4*
DM/Control	19.1, 16.3	20.2, 16.5
R^2	0.43	0.438
Observations numbers	Controls=60 SGA=10 DM=18	Controls=60 SGA=10 DM=18

Note: P< 0.05 noted as *

Comparison of groups using ANCOVA and different covariates modules. For assessment of surface area.

Covariates	**Module 1 (B, standard error)**	**Module 2 (B, standard error)**
Intercept	1486.6, 109.3*	1508.9, 110.2*
GA	-6.7, 3.8	-7.7, 3.9
Diabetes with SGA	-	-140, 135.3
COVID	-	51.7, 56.8
Groups comparison		
SGA/Control	-171.2, 67.3*	-133.9, 80.2
DM/Controls	-12.5, 51.8	-17.7, 52
R^2	0.125	0.149
Observations numbers	Controls=60 SGA=10	Controls=60 SGA=10

	DM=18	DM=18

Note: P< 0.05 noted as *

Comparison of groups using ANCOVA and different covariates modules for assessment of ADC.

Covariates	**Module 1 (B, standard error)**	**Module 2 (B, standard error)**
Intercept	31.1, 15.4*	32.4, 15.4*
GA	0.6, 0.5	0.5, 0.5
Diabetes with SGA	-	-12.3, 17.3
COVID	-	0.3, 7.8
Groups comparison		
SGA/Control	-2.7, 8.5	1, 10.3
DM/Controls	9.9, 7.8	9.9, 7.8
R^2	0.039	0.047
Observations numbers	Controls=54 SGA=10 DM=12	Controls=54 SGA=10 DM=12

Note: P< 0.05 noted as *

Comparison of groups using ANCOVA and different covariates modules for assessment of T2.*

Appendix XVI

Tables of placental pathology in controls, SGA and diabetics

prenatal dx	placenta weight	cental centiles	ntiles (ma	Thickness	SA (elipse)	Volume	feto/placental ratio	ratio centiels	shape	membranes	insertion	mblical cord measurments (cmmber of	of coi	coils index (UCI) (coils/cm)	insertion2	No of vessels	fetal surface	maternal surface	cut surface lesions	Delivery time	Histology findings	COVID status/placentitis	Conclusion
Normal	571	75	90	3	1074.4	3223.2	6.4	25-50	discoid	complete/ transluecent	marginal	32x1.7	11/ left	0.34	paracentral	3	semi-opaque, pale and slightly brown	intact, normal color	1 firm, white (1x0.9cm	term	focal delayed villous maturation, chorangiosis	negative	hypercoiled umblical cord plus histology changes.
Normal	600	75	90	5	895.4	4477	6.51	25-50	discoid	ow, semi opaque with fil	marginal	32x1.2	10/left	0.31	eccentric	3	disrupted 9x5 cm	ragged and pale/incomplete	2 hemorrhagic legions,	term/third trimester	recent intervillous thrombi	negative	slighthy hypercoiled umblical cord
Normal	481	25	50	3	907.9	2724	7.41	50-75	discoid	ıe, thickened and coverec	NA	39x1.4	6/left	0.15	central	3	multiple white	intact and slightly pale	no focal lesions	term/thrid trimester	decidual arteriopathy (maternal	positive/ no placentitis	term placenta with sign histological changes
Normal	469	25	50	2.5	854.5	2136	7.97	75-90	discoid	translucent with fibrous	marginal	36x0.9	6/left	0.16	paracentral	3	translucent with normal chorionic vessels	intact and pale	2 hemorrhagic legions,	term/third trimester	villous infarcts, patchy increase in syncytial knot formation.	negative	maternal vascular(arterial) perfusion abnormality. Mild and generalised delay in villous maturation.
	602	75	90	3	1193.8	3581	6.46	75-90	discoid	te, translucent, greenish	marginal	48x2	ɜft, with pseudc	0.31	paracentral	3	translucent, pale with normal chorionic vessels	intact with calicification, 50% is pale	no focal lesions	term	no changes	negative	hypercoiled umblical cord plus histology changes.
Normal	425	10	25	2	961.3	1923	7.27	50-75	discoid	plete, translucent and sli	NA	20x1	ɜft with 1 peudı	0.5	central	3	translucent with normal color	normal	no focal lesions	term	no changes	negative	markedly hypercoiled umblical cord.
Normal	459	25	50	3	895.4	2686	7.39	50-75	discoid	complete, translucent, pale and slimy.	marginal	41x1	3/left	0.07	paracentral	3	translucent with normal chorionic vessels	normal	one firm focal lesion o	term	focal remote villous infarction with focal recent hematoma in the intervillous space	negative	focal remote villous infarction with focal recent hematoma in the intervillous space
Normal	408	25	50	3	587.5	1763	7.24	50-75	irregular	complete, semi opaque, thickened	marginal	26x1	with 2 pseudo	0.15	paracentral	3	translucent with normal chorionic vessels, subamniotic blood covering 50% of surface	intact, normal color	1 hemorrhagic legions,	term	The chorionic villi are of immature appearance for gestational age. The villi are larger than expected and are round and simplified in outline. In many villi, the fetal capillaries are abnormally located within the centre of the stroma leading to reduction in vasculo-syncytial membrane formation, and elsewhere the villi appear hyper-vascular with multiple small vascular structures. There is focal marked villous oedema affecting some of the larger stem villi and intermediate villi. There is patchy perivillous fibrin deposition	negative	Distal villous maldevelopment: delayed villous maturation, variable vascularity, villous oedema.
Normal	520	50	75	3.5	1244.1	4354	5.76	10--25	discoid	complete, translucent	marginal	20x1	ɒnots and defec	0.3	central	3	translucent and	intact, normal color with	no focal lesions	term	no changes	negative	UCI is at upper limit.
Normal	435	25	50	2	801.1	1602	7.03	50-75	discoid	complete and	marginal	30x1.5	7/left	0.23	paracentral	3	translucent with	normal	1 firm peripheral white	term	laminar necrosis of peipheral	negative	no abnormality
Normal	417	10	25	2.5	753.9	1885	6.19	25-50	discoid	complete and	marginal	21x1	4/left	0.19	paracentral	3	translucent with	normal	no focal lesions	term	no changes	negative	no abnormality
Normal	441	10	25	2.5	1017.1	2543	8.8	90-95	discoid	complete and translucent.	marginal	33x 1.3	8/left	0.24	paracentral	3	translucent and greenish with normal chorionic vessels	normal	no focal lesions	term	diffuse acute chorioamionitis, phlebitis, arteritis, multifocal chorangiotic changes, acute vasculitis, intramural fibrin deposition, acute subchorionitis.	negative	normal size, term placenta with high fetoplacental ratio showing acute chorioamionitis (maternal stage 2 grade 2, fetal stage 2, grade 1).
Normal+CO	280	10	15	1.5	678.6	1017.9+113	3.9	<3rd	ɔorionic diam	ragged and green	marginal	26x0.8	8/left	0.3	central	3	full thickness sampling defect 2.5 x 3cm and is yellow stained.	ragged and very disrupted,	no focal lesions	preterm	peripheral membranes shows reactive amniotic epithelium (meconium induced) and laminar necrosis. The basal plate shows adherent myometrium.	postive/ no placentits	This is a monochorionic diamniotic twin placenta. Twin A placenta and B both show hypercoiling of the cord. Twin placenta B also shows a velamentous cord insertion. There are reactive changes to the amnion and twin placenta B shows extensive regressive changes consistent with previous
Normal	328	50	75	2.5	659.7	1649	5.53	50-75	discoid	complete and translucent.	marginal	30x 1.5	10/left	0.33	marginal	3	translucent with normal chorionic vessels	intact, normal color	no focal lesions	preterm	Villi show accelated maturation with small hypermature villi for age. Intervillous space shows recent multifocal villous hematoma	negative	preterm placenta with normal wight and F/P ratio. There is hypercoiling of the umblical cord with sign. histlogical changes
normal	493	50	75	4	735.1	2940	5.73	10--25	discoid	incomplete, ragged	nmarginal in	26x 0.9	ɜft with 1 peudı	0.38	central	3	scanty chorionic vessels	ragged and incomplete	no focal lesions	preterm	no changes	negative	noraml weight and F/P ratio, preterm, hypercoiling of umblical cord.

Controls placental pathology is shown in details.

prenatal dx	placenta weight	placental centiles min	centile max	THICKNESS	SA (elipse)	Volume	feto/placental ratio	ratio centiels	shape	membranes	insertion	measurments (cm)	no of coils	(UCI) (coils/cm)	cord insersion	No of vessels	fetal surface	maternal surface	cut surf
SGA	416	10	25	2	754	1508	6.57	25-50	discoid	incomplete, translucent.	marginal	20x0.9	7/left	0.35	central	3	translucent with normal chorionic vessels	normal	no focal
SGA	203	3	5	2.5	531	1328	6.55	50-75	discoid	complete and translucent.	marginal	32x1	13/left	0.4	central	3	translucent with normal chorionic vessels	normal	no focal
SGA	412	10	25	2.5	748	1870	8.56	75-90	discoid	translucent and green.	marginal	30x0.8	4/left	0.13	paracentral	3	normal chorionic vessels	normal	2 hemor largest 0
SGA	251	5	10	1.5	792	1188	7.05	50-75	discoid	friable, complete, pale and translucent.	marginal	14x 0.7	6/left	0.42	eccentric	3	pale with normal chorionic vessels and subaminiotic blood	incomplete, ragged and normal color	ragged a lesions
SGA	468	50	75	3	747.7	2243	5.65	10--25	discoid	complete and	marginal	60x 1.3	9/left	0.15	paracentral	3	translucent with	normal	no focal
SGA	281	3	5	2.5	678.6	1697	6.97	50-75	discoid	complete and translucent.	marginal	28x 0.7	16/left	0.57	eccentric	3	translucent with normal chorionic vessels	normal	no focal
SGA+GDM	334	50	75	3	615.8	1847	3.94	3-5th	discoid	plete and transluc	circummarginal	55x 1.3	31/right	0.56	central	3	translucent with normal chorionic vessels	ragged and incomplete	no focal
SGA +GDM	366	10	25	2.5	659.7	1649	7.65	75-90	discoid	complete and translucent.	circummarginal in 80%	53x 1	34/left	0.64	eccentric	3	translucent with normal chorionic vessels	normal	4 hemor the large compros
SGA	157	5	10	2.5	253.7	634	7.51	95-97	discoid	complete and translucent.	circummarginate 50%.	11 x 0.9cm	5/left	0.45	paracentral	3	translucent with normal chorionic vessels and white plaques.	normal	no focal
SGA	225	0	3	2.5	703.7	1759	7.28	50-75	discoid	complete and translucent.	marginal	38x 1.3	13/left	0.34	paracentral	3	translucent with normal chorionic vessels	focally ragged with a peripheral thinned area measuring 8x5x0.4cm	no focal

SGA placental pathology is shown in details.

prenatal dx	placenta weight	placental centiles min	centiels max	Thickness	SA	Volume	feto/placental ratio	ratio centiels	shape	membranes	insertion	umblical cord measurments (cm)	no of coils	coils index (UCI) (coils/cm)	insertion2	No of vessels	fetal surface	maternal surface	cut surface lesions	Delivery time	Histology findings	COVID status/placentitis	Conclusion
DM	397	10	25	2.5	2307	5768	6.17	25-50	discoid	complete/ translucent	marginal	36x1	6/left	0.16	central	3	translucent with normal chorionic vessels and white plaques.	intact, normal color	1 firm sub chorionic laminated lesion of 2x 0.4 cm	term	focal chorangiotic changes, old sub-chorionic and intervillous hematomas.	negative	focal chorangiotic changes, old sub-chorionic and intervillous hematomas.
DM	442	75	90	2.5	1015	2538	4.88	10--25	discoid	complete and translucent.	marginal	30x 1.4	6/left	0.2	central	3	translucent with normal chorionic vessels	ragged and pale	no focal lesions	preterm	acute chorioamionitis (maternal: stage1, grade 1 ,fetal: stage 2, grade 1). Accelerated villous maturation with small hypermature villi for age.	negative	preterm, normal macroscopic features and acute chorioamionitis (maternal: stage1, grade 1 ,fetal: stage 2, grade 1). Accelerated villous maturation with small hypermature villi for age.
DM	454	50	75	3	2307.2	6922	6.59	25-50	discoid	complete and translucent.	NA	49x 1.5	20/ left	0.4	eccentric	2	translucent with normal chorionic vessels	normal	no focal lesions	preterm	laminar necrossis of the periphral membranes	negative	normal weight and volume, preterm placenta with umblical cord hypercoiling, single umblical artery.
DM	387	10	25	2.5	2442.9	6107	8.68	90-95	discoid	complete,slimy and brownish	circummarginal in 30%	41x 1.1	20/ left	0.48	eccentric	3	12x 3 cm lacking vessels on one peripherally, pale and slimy with white plaques	normal with periphrally attached blood clot of 10x 2 cm	no focal lesions	term	acute chorioamionitis (maternal: stage1, grade 1 ,no fetal). Apropriate villous maturation.	negative	term, normal weight and increased F/P ratio (>90th centile) refecting small placenta. Umblical cord hypercoiling and acute chorioamionitis.

DM placental pathology is shown in details.

Appendix XVII

Microstructural features (histopathology)

Histopathology features identified:

COVID status:

There was no evidence of COVID placentitis.

Pathology correlation to clinical presentation

Maternal vasculature

- Decidual arteriopathy (maternal perfusion abnormality), peripheral cord insertion), vascular malperfusion/ insufficiency, patchy perivillous and intramural fibrin deposition.

- Obstruction: focal remote villous infarction, patchy increase in syncytial knots formation.

Fetal vasculature

- Vascular maldevelopment: chorangiosis, delayed and accelerated villous maturation, distal villous maldevelopment, focal and multifocal chorangiotic changes.
- Obstruction: intervillous thrombi.
- Loss of integrity: villous, sub-chorionic and intervillous hematomas.
- Inflammatory: acute chorioamnionitis (infection), phlebitis, arteritis, acute vasculitis, acute subchorionitis.

Histological changes

The findings in each group assessed for histopathology and their link to placental insufficiency are described:

Controls placentas

- Hypercoiling was present in (7/15) of normal placentas.
- 2/15 of normal placentas were preterm.
- Twins' placenta (1/15). This was a monochorionic diamniotic twin placenta with demise of one fetus (twin B), twin A placenta and B both showed hypercoiling of the cord. Twin placenta B also showed a velamentous cord insertion. There were reactive changes to the amnion and twin placenta B showed extensive regressive changes consistent with previous demise.
- Cut surface lesions: (6/15) of different sizes and number (see appendix).

Histology changes:

Five placentas showed no abnormal histological changes.

Thrombi (2/15)

- Recent intervillous thrombi (1/15), small recent subchorionic thrombus (1/15)
- Maternal perfusion abnormality (5/15)
- Decidual arteriopathy (1/15).
- Infarction: focal remote villous infarction (3/15).
- Hematoma: focal recent hematoma in the intervillous space (2/15). Recent multifocal villous hematoma in the intervillous space (1/15).

Abnormal villous development: (3/15)

The chorionic villi were of immature appearance for gestational age. The villi were larger than expected and were round and simplified in outline. In many villi, the fetal capillaries were abnormally located within the centre of the stroma leading to reduction in vasculo-syncytial membrane formation, and elsewhere the villi appear hyper-vascular with multiple small vascular structures. There was a focal marked villous oedema affecting some of the larger stem villi and intermediate villi (1/15).

Focal delayed villous maturation (1/15).

Villi showed accelerated maturation with small hypermature villi for age (1/15).

Inflammation

Diffuse acute chorioamionitis, phlebitis, arteritis, acute vasculitis, intramural fibrin deposition, acute subchorionitis (1/15).

Other changes:

- Chorangiosis (1/15), multifocal chorangiotic changes (1/15).
- Laminar necrosis of peripheral membranes (2/15).

- Patchy perivillous fibrin deposition within normal limits (1/15).
- Peripheral membranes showed reactive amniotic epithelium (meconium induced). The basal plate showed adherent myometrium (1/15).
- Patchy, single cell immunohistochemical expression of SARS-COV2 (1/15).
- Patchy increase in syncytial knot formation (1/15).

SGA placentas

- Three placentas showed no abnormal changes (3/10).
- Umbilical cord hyper coiling and increased UCI ratio was present in all SGA cases except two (including one normal placenta with a normal birth weight baby), those cord changes were usually accompanied with other histological changes.
- 5/10 of SGA placentas were preterm.
- Low fetoplacental weight ratio, circummargination of the membranes (1/10).
- Cut surface lesions: 2/10 placentas showed haemorrhagic lesions. The first had 2 lesions the largest was 0.5x0.5xm and the second had 4 lesions with the largest measured 1x1cm.

Histology changes:

Maternal vascular malperfusion/ insufficiency (1/10).

Abnormal villous development (8/10)

- Accelerated villous maturation (2/10).
- Focal delayed villous maturation (2/10).
- Distal villous maldevelopment and abnormal villi of the chorionic villi (2/10).
- Diffuse delayed villous maturation with monotonous villi showing centrally placed capillaries (1/10).

- There was also frequent villous agglutination (1/10).

Inflammation (2/10)

- Isolated cord phlebitis, acute chorioamnionitis and meconium induced changes, acute subchorionitis, acute vasculitis (1/10).
- Prominent chronic histiocytic intervillositis and chronic deciduitis (1/10).

Thrombi

- Multiple mural thrombosis (1/10).
- Hematoma
- Multifocal recent intervillous haematoma in the intervillous space (1/10).
- Other changes:
- laminar necrosis in the peripheral membranes (1/10).
- Hemosiderin laden macrophages deposition in the basal plate (1/10).
- Some excess of perivillous fibrin deposition (1/10).
- Increased syncytial knot formation (1/10).
- The peripheral membranes showed reactive amniotic epithelium (1/10).

Diabetics placentas

- Hypercoiling of the umbilical cord was present (2/4) of diabetics' placentas.
- Preterm (2/4).

- Single umbilical artery (1/4).
- Increased F/P ratio reflecting small placenta but with normal weight (1/4).
- Cut surface lesions: (1/4) firm subchorionic laminated lesion 2x0.4 cm.
- Abnormal fetal surface (1/4), 12x3 cm lacking vessels on one periphery, pale with white plaques.
- Maternal surface: peripherally attached blood clots (1/4).

Histology changes:

- Focal chorangiotic changes and old sub-chorionic and intervillous hematomas (1/4).
- Accelerated villous maturation with small hypermature villi for age (1/4).
- Laminar necrosis of the peripheral membranes (1/4).
- Acute chorioamnionitis: (2/4) one with (maternal: stage 1, grade 1, no fetal) and the other with (maternal: stage1, grade 1, fetal: stage 2, grade 1).

Tables of detailed placental pathology are listed in appendix. 3/10 showed SGA histopathological changes. Multiple combined or widespread pathological changes usually happened together and resulted in IUGR changes.

There were few histological changes in the placentas of controls group (27%), but these changes were either focal, mild or not accompanied with other changes.

One diabetic placenta had accelerated villous maturation (AM), but this was not associated with a reduced size in either the fetus or the placenta (table 32).

SGA pathology changes	Controls (n=15)	SGA (n=10)	DM (n=4)
Infarction/ maternal and fetal vascular malperfusion	3/15 (Focal infarction)	2/10	-
Accelerated maturation (AM)	1/15	2/10	1/4
Decidual villopathy (DV)	-	1/10	-
Excess perivillous fibrin deposition (EPFD)	-	1/10	-
Total pathology	N= 4/15 (27%)	N= 6/10(60%)	N=1/4(25%)

Table 32: SGA histopathology changes in placentas of our cohort.

References

(2010). "ACR manual on contrast media, version 7.0." American College of Radiology.

(2018). "Obstetric Care Consensus No. 7: Placenta Accreta Spectrum." Obstet Gynecol **132**(6): e259-e275.

Abuhamad, A. (2013). "Morbidly adherent placenta." Semin Perinatol **37**(5): 359-364.

ACR (2014). "ACR practice parameter for performing and interpreting magnetic resonance imaging (MRI)." American College of Radiology.

Allen, B. C. and J. R. Leyendecker (2013). "Placental evaluation with magnetic resonance." Radiol Clin North Am **51**(6): 955-966.

Andescavage, N., S. Dahdouh, M. Jacobs, S. Yewale, D. Bulas, S. Iqbal, A. Baschat and C. Limperopoulos (2019). "In vivo textural and morphometric analysis of placental development in healthy & growth-restricted pregnancies using magnetic resonance imaging." Pediatr Res.

Andescavage, N., A. duPlessis, M. Metzler, D. Bulas, G. Vezina, M. Jacobs, S. N. Iqbal, A. Baschat and C. Limperopoulos (2017). "In vivo assessment of placental and brain volumes in growth-restricted fetuses with and without fetal Doppler changes using quantitative 3D MRI." J Perinatol **37**(12): 1278-1284.

Andescavage, N., A. Yarish, M. Donofrio, D. Bulas, I. Evangelou, G. Vezina, R. McCarter, A. duPlessis and C. Limperopoulos (2015). "3-D volumetric MRI evaluation of the placenta in fetuses with complex congenital heart disease." Placenta **36**(9): 1024-1030.

Andescavage, N. N., A. du Plessis and C. Limperopoulos (2015). "Advanced MR imaging of the placenta: Exploring the in utero placenta-brain connection." Semin Perinatol **39**(2): 113-123.

Arany, E. and D. J. Hill (1998). "Fibroblast growth factor-2 and fibroblast growth factor receptor-1 mRNA expression and peptide localization in placentae from normal and diabetic pregnancies." Placenta **19**(2-3): 133-142.

Avni, R., M. Neeman and J. R. Garbow (2015). "Functional MRI of the placenta--From rodents to humans." Placenta **36**(6): 615-622.

Bailit, J. L., W. A. Grobman, M. M. Rice, U. M. Reddy, R. J. Wapner, M. W. Varner, K. J. Leveno, J. D. Iams, A. T. N. Tita, G. Saade, D. J. Rouse and S. C. Blackwell (2015).

"Morbidly adherent placenta treatments and outcomes." Obstet Gynecol **125**(3): 683-689.

Baker, P. N., I. R. Johnson, P. A. Gowland, J. Hykin, P. R. Harvey, A. Freeman, V. Adams, B. S. Worthington and P. Mansfield (1994). "Fetal weight estimation by echo-planar magnetic resonance imaging." Lancet **343**(8898): 644-645.

Baker, P. N., I. R. Johnson, P. R. Harvey, P. A. Gowland and P. Mansfield (1994). "A three-year follow-up of children imaged in utero with echo-planar magnetic resonance." Am J Obstet Gynecol **170**(1 Pt 1): 32-33.

Bao, Y., Y. Pang, Z. Sun, Q. Li, D. Tang and L. Xia (2021). "Functional diagnosis of placenta accreta by intravoxel incoherent motion model diffusion-weighted imaging." Eur Radiol **31**(2): 740-748.

Barker, D. J., K. L. Thornburg, C. Osmond, E. Kajantie and J. G. Eriksson (2010). "The surface area of the placenta and hypertension in the offspring in later life." Int J Dev Biol **54**(0): 525-530.

Barkhof, F., R. J. Heijboer and P. R. Algra (1992). "Inadvertent i.v. administration of gadopentetate dimeglumine during early pregnancy." AJR Am J Roentgenol **158**(5): 1171.

Baughman, W. C., J. E. Corteville and R. R. Shah (2008). "Placenta accreta: spectrum of US and MR imaging findings." Radiographics **28**(7): 1905-1916.

Benirschke, K., & Driscoll, S. G. (1967). "The pathology of the human placenta " Springer Berlin Heidelberg: 97-571.

Berger, A. (2002). "Magnetic resonance imaging." Bmj **324**(7328): 35.

Berkley, E. M. and A. Z. Abuhamad (2013). "Prenatal diagnosis of placenta accreta: is sonography all we need?" J Ultrasound Med **32**(8): 1345-1350.

Blackburn, S. T. (2012). Maternal, fetal, and neonatal Physiology: a clinical perspective. Maternal, fetal, and neonatal physiology: a clinical perspective, Maryland Heights, MO ; London : Elsvier/Saunders.

Bonel, H. M., B. Stolz, L. Diedrichsen, K. Frei, B. Saar, B. Tutschek, L. Raio, D. Surbek, S. Srivastav, M. Nelle, J. Slotboom and R. Wiest (2010). "Diffusion-weighted MR imaging of the placenta in fetuses with placental insufficiency." Radiology **257**(3): 810-819.

Bourgioti, C., K. Zafeiropoulou, S. Fotopoulos, M. E. Nikolaidou, A. Antoniou, C. Tzavara and L. A. Moulopoulos (2018). "MRI Features Predictive of Invasive Placenta

With Extrauterine Spread in High-Risk Gravid Patients: A Prospective Evaluation." AJR Am J Roentgenol **211**(3): 701-711.

Bouyssi-Kobar, M., A. J. du Plessis, R. L. Robertson and C. Limperopoulos (2015). "Fetal magnetic resonance imaging: exposure times and functional outcomes at preschool age." Pediatr Radiol **45**(12): 1823-1830.

Brunelli, R., G. Masselli, T. Parasassi, M. De Spirito, M. Papi, G. Perrone, E. Pittaluga, G. Gualdi, E. Pollettini, A. Pittalis and M. M. Anceschi (2010). "Intervillous circulation in intra-uterine growth restriction. Correlation to fetal well being." Placenta **31**(12): 1051-1056.

Bulas, D. and A. Egloff (2013). "Benefits and risks of MRI in pregnancy." Semin Perinatol **37**(5): 301-304.

Burton, G. J. and E. Jauniaux (2004). "Placental oxidative stress: from miscarriage to preeclampsia." J Soc Gynecol Investig **11**(6): 342-352.

Burton, G. J. and E. Jauniaux (2018). "Pathophysiology of placental-derived fetal growth restriction." Am J Obstet Gynecol **218**(2s): S745-s761.

Carr, M. W. and M. L. Grey (2002). "Magnetic resonance imaging." Am J Nurs **102**(12): 26-33.

Castellano, G., L. Bonilha, L. M. Li and F. Cendes (2004). "Texture analysis of medical images." Clin Radiol **59**(12): 1061-1069.

Chantraine, F., S. Blacher, S. Berndt, J. Palacios-Jaraquemada, N. Sarioglu, M. Nisolle, T. Braun, C. Munaut and J. M. Foidart (2012). "Abnormal vascular architecture at the placental-maternal interface in placenta increta." Am J Obstet Gynecol **207**(3): 188.e181-189.

Chavhan, G. B., P. S. Babyn, B. Thomas, M. M. Shroff and E. M. Haacke (2009). Principles, Techniques, and Applications of T2*-based MR Imaging and Its Special Applications1. Radiographics. **29:** 1433-1449.

Chen, E., W. A. Mar, J. M. Horowitz, A. Allen, P. Jha, D. R. Cantrell and K. Cai (2019). "Texture analysis of placental MRI: can it aid in the prenatal diagnosis of placenta accreta spectrum?" Abdominal radiology (New York) **44**(9): 3175-3184.

Chen, E., W. A. Mar, J. M. Horowitz, A. Allen, P. Jha, D. R. Cantrell and K. Cai (2019). "Texture analysis of placental MRI: can it aid in the prenatal diagnosis of placenta accreta spectrum?" Abdominal Radiology **44**(9): 3175-3184.

Chou, M. M. and E. S. Ho (1997). "Prenatal diagnosis of placenta previa accreta with power amplitude ultrasonic angiography." Am J Obstet Gynecol **177**(6): 1523-1525.

Chou, M. M., E. S. Ho, F. Lu and Y. H. Lee (1992). "Prenatal diagnosis of placenta previa/accreta with color Doppler ultrasound." Ultrasound Obstet Gynecol **2**(4): 293-296.

Clausen, C., J. Stensballe, C. K. Albrechtsen, M. A. Hansen, L. Lönn and J. Langhoff-Roos (2013). "Balloon occlusion of the internal iliac arteries in the multidisciplinary management of placenta percreta." Acta Obstet Gynecol Scand **92**(4): 386-391.

Clements, H., K. R. Duncan, K. Fielding, P. A. Gowland, I. R. Johnson and P. N. Baker (2000). "Infants exposed to MRI in utero have a normal paediatric assessment at 9 months of age." Br J Radiol **73**(866): 190-194.

Collins, S. L., G. N. Stevenson, A. Al-Khan, N. P. Illsley, L. Impey, L. Pappas and S. Zamudio (2015). "Three-Dimensional Power Doppler Ultrasonography for Diagnosing Abnormally Invasive Placenta and Quantifying the Risk." Obstet Gynecol **126**(3): 645-653.

Comstock, C. H., J. J. Love, Jr., R. A. Bronsteen, W. Lee, I. M. Vettraino, R. R. Huang and R. P. Lorenz (2004). "Sonographic detection of placenta accreta in the second and third trimesters of pregnancy." Am J Obstet Gynecol **190**(4): 1135-1140.

Cook, R. O., T. Konishi, A. N. Salt, C. W. Hamm, E. H. Lebetkin and J. Koo (1982). "Brainstem-evoked responses of guinea pigs exposed to high noise levels in utero." Dev Psychobiol **15**(2): 95-104.

Cramer, S. F. and D. S. Heller (2016). "Placenta Accreta and Placenta Increta: An Approach to Pathogenesis Based on the Trophoblastic Differentiation Pathway." Pediatr Dev Pathol **19**(4): 320-333.

Cuthbert, F., M. Teixidor Vinas and E. Whitby (2016). "The MRI features of placental adhesion disorder-a pictorial review." Br J Radiol **89**(1065): 20160284.

D'Antonio, F., C. Iacovella and A. Bhide (2013). "Prenatal identification of invasive placentation using ultrasound: systematic review and meta-analysis." Ultrasound Obstet Gynecol **42**(5): 509-517.

D'Antonio, F., C. Iacovella, J. Palacios-Jaraquemada, C. H. Bruno, L. Manzoli and A. Bhide (2014). "Prenatal identification of invasive placentation using magnetic resonance imaging: systematic review and meta-analysis." Ultrasound Obstet Gynecol **44**(1): 8-16.

Dahdouh, S., N. Andescavage, S. Yewale, A. Yarish, D. Lanham, D. Bulas, A. J. du Plessis and C. Limperopoulos (2018). "In vivo placental MRI shape and textural

features predict fetal growth restriction and postnatal outcome." J Magn Reson Imaging **47**(2): 449-458.

Damodaram, M., L. Story, E. Eixarch, A. Patel, A. McGuinness, J. Allsop, J. Wyatt-Ashmead, S. Kumar and M. Rutherford (2010). "Placental MRI in intrauterine fetal growth restriction." Placenta **31**(6): 491-498.

Daskalakis, G., S. Marinopoulos, V. Krielesi, A. Papapanagiotou, N. Papantoniou, S. Mesogitis and A. Antsaklis (2008). "Placental pathology in women with gestational diabetes." Acta Obstet Gynecol Scand **87**(4): 403-407.

De Santis, M., G. Straface, A. F. Cavaliere, B. Carducci and A. Caruso (2007). "Gadolinium periconceptional exposure: pregnancy and neonatal outcome." Acta Obstet Gynecol Scand **86**(1): 99-101.

Dean, P. B., P. Niemi, L. Kivisaari and M. Kormano (1988). "Comparative pharmacokinetics of gadolinium DTPA and gadolinium chloride." Invest Radiol **23 Suppl 1**: S258-260.

Derman, A. Y., V. Nikac, S. Haberman, N. Zelenko, O. Opsha and M. Flyer (2011). "MRI of Placenta Accreta: A New Imaging Perspective." American Journal of Roentgenology **197**(6): 1514-1521.

Derwig, I., D. J. Lythgoe, G. J. Barker, L. Poon, P. Gowland, R. Yeung, F. Zelaya and K. Nicolaides (2013). "Association of placental perfusion, as assessed by magnetic resonance imaging and uterine artery Doppler ultrasound, and its relationship to pregnancy outcome." Placenta **34**(10): 885-891.

Derwig, I. E., R. Akolekar, F. O. Zelaya, P. A. Gowland, G. J. Barker and K. H. Nicolaides (2011). "Association of Placental Volume Measured by MRI and Birth Weight Percentile." Journal of Magnetic Resonance Imaging **34**(5): 1125-1130.

Desoye, G. and S. Hauguel-de Mouzon (2007). "The human placenta in gestational diabetes mellitus. The insulin and cytokine network." Diabetes Care **30 Suppl 2**: S120-126.

Dimbylow, P. (2006). "Development of pregnant female, hybrid voxel-mathematical models and their application to the dosimetry of applied magnetic and electric fields at 50 Hz." Phys Med Biol **51**(10): 2383-2394.

Do, Q. N., M. A. Lewis, A. J. Madhuranthakam, Y. Xi, A. A. Bailey, R. E. Lenkinski and D. M. Twickler (2019). "Texture analysis of magnetic resonance images of the human placenta throughout gestation: A feasibility study." Plos One **14**(1): 11.

Do, Q. N., M. A. Lewis, Y. Xi, A. J. Madhuranthakam, S. K. Happe, J. S. Dashe, R. E. Lenkinski, A. Khan and D. M. Twickler (2020). "MRI of the Placenta Accreta Spectrum (PAS) Disorder: Radiomics Analysis Correlates With Surgical and Pathological Outcome." Journal of magnetic resonance imaging : JMRI **51**(3): 936-946.

Dubova, E. A., K. A. Pavlov, R. M. Yesayan, M. N. Nagovitsyna, O. N. Tkacheva, M. V. Shestakova and A. I. Shchegolev (2011). "Morphometric characteristics of placental villi in pregnant women with diabetes." Bulletin of experimental biology and medicine **151**(5): 650-654.

Edu, A., C. Teodorescu, C. G. Dobjanschi, Z. Z. Socol, V. Teodorescu, A. Matei, D. F. Albu and G. Radulian (2016). "Placenta changes in pregnancy with gestational diabetes." Romanian Journal of Morphology and Embryology **57**(2): 507-512.

Elchalal, U., Y. Ezra, Y. Levi, B. Bar-Oz, N. Yanai, O. Intrator and M. Nadjari (2000). "Sonographically thick placenta: a marker for increased perinatal risk--a prospective cross-sectional study." Placenta **21**(2-3): 268-272.

Elhawary, T. M., N. L. Dabees and M. A. Youssef (2013). "Diagnostic value of ultrasonography and magnetic resonance imaging in pregnant women at risk for placenta accreta." The journal of maternal-fetal & neonatal medicine. **26**(14): 1443-1449.

Eller, A. G., M. A. Bennett, M. Sharshiner, C. Masheter, A. P. Soisson, M. Dodson and R. M. Silver (2011). "Maternal morbidity in cases of placenta accreta managed by a multidisciplinary care team compared with standard obstetric care." Obstet Gynecol **117**(2 Pt 1): 331-337.

Elsayes, K. M., A. T. Trout, A. M. Friedkin, P. S. Liu, R. O. Bude, J. F. Platt and C. O. Menias (2009). "Imaging of the placenta: a multimodality pictorial review." Radiographics **29**(5): 1371-1391.

Fadl, S., M. Moshiri, C. L. Fligner, D. S. Katz and M. Dighe (2017). "Placental imaging: normal appearance with review of pathologic findings." Radiographics **37**(3): 979-998.

FDA., F. a. D. A. C. f. D. a. R. H. (Feb.1997). "primer on medical device interactions with magnetic resonance imaging systems [draft]." Office of the Federal Register, National Archives and Records Administration **62**(99).

Fejgin, M. D., D. J. Rosen, I. Ben-Nun, S. B. Goldberger and Y. Beyth (1993). "Ultrasonic and magnetic resonance imaging diagnosis of placenta accreta managed conservatively." J Perinat Med **21**(2): 165-168.

Ferrazzi, E., M. Bozzo, S. Rigano, M. Bellotti, A. Morabito, G. Pardi, F. C. Battaglia and H. L. Galan (2002). "Temporal sequence of abnormal Doppler changes in the peripheral and central circulatory systems of the severely growth-restricted fetus." Ultrasound Obstet Gynecol **19**(2): 140-146.

Ferré, J. C., E. Bannier, H. Raoult, G. Mineur, B. Carsin-Nicol and J. Y. Gauvrit (2013). "Arterial spin labeling (ASL) perfusion: techniques and clinical use." Diagn Interv Imaging **94**(12): 1211-1223.

Figueras, F., J. Caradeux, F. Crispi, E. Eixarch, A. Peguero and E. Gratacos (2018). "Diagnosis and surveillance of late-onset fetal growth restriction." Am J Obstet Gynecol **218**(2s): S790-S802.e791.

Finberg, H. J. and J. W. Williams (1992). "Placenta accreta: prospective sonographic diagnosis in patients with placenta previa and prior cesarean section." J Ultrasound Med **11**(7): 333-343.

Fitzpatrick, K. E., S. Sellers, P. Spark, J. J. Kurinczuk, P. Brocklehurst and M. Knight (2014). "The management and outcomes of placenta accreta, increta, and percreta in the UK: a population-based descriptive study." Bjog **121**(1): 62-70; discussion 70-61.

Flenady, V., A. M. Wojcieszek, P. Middleton, D. Ellwood, J. J. Erwich, M. Coory, T. Y. Khong, R. M. Silver, G. C. S. Smith, F. M. Boyle, J. E. Lawn, H. Blencowe, S. H. Leisher, M. M. Gross, D. Horey, L. Farrales, F. Bloomfield, L. McCowan, S. J. Brown, K. S. Joseph, J. Zeitlin, H. E. Reinebrant, J. Cacciatore, C. Ravaldi, A. Vannacci, J. Cassidy, P. Cassidy, C. Farquhar, E. Wallace, D. Siassakos, A. E. P. Heazell, C. Storey, L. Sadler, S. Petersen, J. F. Frøen and R. L. Goldenberg (2016). "Stillbirths: recall to action in high-income countries." Lancet **387**(10019): 691-702.

Frank, H. G. (2000). "Nonvillous parts and trophoblast invasion." Pathology of the Human Placenta, Edited by K Bernischke, P Kaufmann.: 171-272.

Gardosi, J. and A. Francis (1999). "Controlled trial of fundal height measurement plotted on customised antenatal growth charts." Br J Obstet Gynaecol **106**(4): 309-317.

Gardosi, J., S. Giddings, S. Buller, M. Southam and M. Williams (2014). "Preventing stillbirths through improved antenatal recognition of pregnancies at risk due to fetal growth restriction." Public Health **128**(8): 698-702.

Gardosi, J., S. M. Kady, P. McGeown, A. Francis and A. Tonks (2005). "Classification of stillbirth by relevant condition at death (ReCoDe): population based cohort study." Bmj **331**(7525): 1113-1117.

Gardosi, J., V. Madurasinghe, M. Williams, A. Malik and A. Francis (2013). "Maternal and fetal risk factors for stillbirth: population based study."

Gerhardt, K. J., L. L. Pierson, X. Huang, R. M. Abrams and K. E. Rarey (1999). "Effects of intense noise exposure on fetal sheep auditory brain stem response and inner ear histology." Ear Hear **20**(1): 21-32.

Glover, P., J. Hykin, P. Gowland, J. Wright, I. Johnson and P. Mansfield (1995). "An assessment of the intrauterine sound intensity level during obstetric echo-planar magnetic resonance imaging." Br J Radiol **68**(814): 1090-1094.

Gollub, R. L., & Shellock, F. G. (2000). "Claustrophobia, Anxiety, and Emotional Distress in the Magnetic Resonance Environment." Magnetic resonance procedures: health effects and safety: 197.

Gonzalez-Gonzalez, N. L., E. Gonzalez-Davila, L. G. Marrero, E. Padron, J. R. Conde and W. Plasencia (2017). "Value of placental volume and vascular flow indices as predictors of intrauterine growth retardation." European Journal of Obstetrics & Gynecology and Reproductive Biology **212**: 13-19.

Gordijn, S. J., I. M. Beune and W. Ganzevoort (2018). "Building consensus and standards in fetal growth restriction studies." Best Practice & Research Clinical Obstetrics & Gynaecology **49**: 117-126.

Gordon, Y., S. Partovi, M. Müller-Eschner, E. Amarteifio, T. Bäuerle, M. A. Weber, H. U. Kauczor and F. Rengier (2014). "Dynamic contrast-enhanced magnetic resonance imaging: fundamentals and application to the evaluation of the peripheral perfusion." Cardiovasc Diagn Ther **4**(2): 147-164.

Gowland, P. A., S. T. Francis, K. R. Duncan, A. J. Freeman, B. Issa, R. J. Moore, R. W. Bowtell, P. N. Baker, I. R. Johnson and B. S. Worthington (1998). "In vivo perfusion measurements in the human placenta using echo planar imaging at 0.5 T." Magn Reson Med **40**(3): 467-473.

Grannum, P. A., R. L. Berkowitz and J. C. Hobbins (1979). "The ultrasonic changes in the maturing placenta and their relation to fetal pulmonic maturity." Am J Obstet Gynecol **133**(8): 915-922.

Griffiths, S. K., L. L. Pierson, K. J. Gerhardt, R. M. Abrams and A. J. Peters (1994). "Noise induced hearing loss in fetal sheep." Hear Res **74**(1-2): 221-230.

Grigsby, P. L. (2016). "Animal Models to Study Placental Development and Function throughout Normal and Dysfunctional Human Pregnancy." Semin Reprod Med **34**(1): 11-16.

Gude, N. M., C. T. Roberts, B. Kalionis and R. G. King (2004). "Growth and function of the normal human placenta." Thromb Res **114**(5-6): 397-407.

Guttmacher, A. E., Y. T. Maddox and C. Y. Spong (2014). "The Human Placenta Project: placental structure, development, and function in real time." Placenta **35**(5): 303-304.

Hafner, E., M. Metzenbauer, B. Dillinger-Paller, D. Hoefinger, K. Schuchter, H. Sommer-Wagner and K. Philipp (2001). "Correlation of first trimester placental volume and second trimester uterine artery Doppler flow." Placenta **22**(8-9): 729-734.

Hafner, E., M. Metzenbauer, D. Hofinger, F. Stonek, K. Schuchter, T. Waldhor and K. Philipp (2006). "Comparison between three-dimensional placental volume at 12 weeks and uterine artery impedance/notching at 22 weeks in screening for pregnancy-induced hypertension, pre-eclampsia and fetal growth restriction in a low-risk population." Ultrasound in Obstetrics & Gynecology **27**(6): 652-657.

Hafner, E., T. Philipp, K. Schuchter, B. Dillinger-Paller, K. Philipp and P. Bauer (1998). "Second-trimester measurements of placental volume by three-dimensional ultrasound to predict small-for-gestational-age infants." Ultrasound Obstet Gynecol **12**(2): 97-102.

Hamada, S., J. Hasegawa, M. Nakamura, R. Matsuoka, K. Ichizuka, A. Sekizawa and T. Okai (2011). "Ultrasonographic findings of placenta lacunae and a lack of a clear zone in cases with placenta previa and normal placenta." Prenat Diagn **31**(11): 1062-1065.

Hand, J. W., Y. Li and J. V. Hajnal (2010). "Numerical study of RF exposure and the resulting temperature rise in the foetus during a magnetic resonance procedure." Phys Med Biol **55**: 913-930.

Hansch, E., U. Chitkara, J. McAlpine, Y. El-Sayed, M. D. Dake and M. K. Razavi (1999). "Pelvic arterial embolization for control of obstetric hemorrhage: a five-year experience." Am J Obstet Gynecol **180**(6 Pt 1): 1454-1460.

Haralick, R. M., K. Shanmugam and I. Dinstein (1973). "Textural Features for Image Classification." IEEE Transactions on Systems, Man, and Cybernetics **SMC-3**(6): 610-621.

Hayward, C. E., S. Lean, C. P. Sibley, R. L. Jones, M. Wareing, S. L. Greenwood and M. R. Dilworth (2016). "Placental Adaptation: What Can We Learn from Birthweight:Placental Weight Ratio?" Front Physiol **7**: 28.

Hecht, J. L., R. Baergen, L. M. Ernst, P. J. Katzman, S. M. Jacques, E. Jauniaux, T. Y. Khong, L. A. Metlay, L. Poder, F. Qureshi, J. T. Rabban, 3rd, D. J. Roberts, S. Shainker and D. S. Heller (2020). "Classification and reporting guidelines for the pathology diagnosis of placenta accreta spectrum (PAS) disorders: recommendations from an expert panel." Mod Pathol **33**(12): 2382-2396.

Heinrichs, W. L., P. Fong, M. Flannery, S. C. Heinrichs, L. E. Crooks, A. Spindle and R. A. Pedersen (1988). "Midgestational exposure of pregnant BALB/c mice to magnetic resonance imaging conditions." Magn Reson Imaging **6**(3): 305-313.

Heismann, B., M. Ott and D. Grodzki (2015). "Sequence-based acoustic noise reduction of clinical MRI scans." Magn Reson Med **73**(3): 1104-1109.

Hershey, D. W. (2014). "Fetal imaging: executive summary of a joint Eunice Kennedy Shriver National Institute of Child Health and Human Development,Society for Maternal-fetal Medicine, American Institute of Ultrasound in Medicine, American College of Obstetricians and Gynecologists, American College of Radiology, Society for Pediatric Radiology, and Society of Radiologists in Ultrasound Fetal Imaging Workshop." J Ultrasound Med **33**(10): 1876.

Hill, D. J., G. J. Tevaarwerk, C. Caddell, E. Arany, D. Kilkenny and M. Gregory (1995). "Fibroblast growth factor 2 is elevated in term maternal and cord serum and amniotic fluid in pregnancies complicated by diabetes: relationship to fetal and placental size." J Clin Endocrinol Metab **80**(9): 2626-2632.

Hoffman-Tretin, J. C., M. Koenigsberg, A. Rabin and A. Anyaegbunam (1992). "Placenta accreta. Additional sonographic observations." J Ultrasound Med **11**(1): 29-34.

Hutter, J., L. Jackson, A. Ho, M. Pietsch, L. Story, L. C. Chappell, J. V. Hajnal and M. Rutherford (2019). "T2* relaxometry to characterize normal placental development over gestation." Wellcome Open Research 2019 4:166 **4**(166).

Irving, F., & Hertig, AT. (1937). "A study of placenta accreta." Surgery, Gynecology and Obstetrics. **64**: 178–200.

Japaraj, R. P., T. S. Mimin and K. Mukudan (2007). "Antenatal diagnosis of placenta previa accreta in patients with previous cesarean scar." J Obstet Gynaecol Res **33**(4): 431-437.

Jauniaux E1, A.-d.-C. D., Langhoff-Roos J3, Fox KA4, Collins S5,6 and F. P. A. D. a. M. E. C. Panel. (2020). "FIGO classification for the clinical diagnosis of placenta accreta spectrum disorders. - PubMed - NCBI."

Jauniaux, E. and D. Ayres-de-Campos (2018). "FIGO consensus guidelines on placenta accreta spectrum disorders: Introduction." Int J Gynaecol Obstet **140**(3): 261-264.

Jauniaux, E., C. Bunce, L. Grønbeck and J. Langhoff-Roos (2019). "Prevalence and main outcomes of placenta accreta spectrum: a systematic review and meta-analysis." Am J Obstet Gynecol **221**(3): 208-218.

Jauniaux, E., F. Chantraine, R. M. Silver and J. Langhoff-Roos (2018). "FIGO consensus guidelines on placenta accreta spectrum disorders: Epidemiology." Int J Gynaecol Obstet **140**(3): 265-273.

Jauniaux, E., S. Collins and G. J. Burton (2018). "Placenta accreta spectrum: pathophysiology and evidence-based anatomy for prenatal ultrasound imaging." American journal of obstetrics and gynecology. **218**(1): 75-87.

Jauniaux, E., S. L. Collins, D. Jurkovic and G. J. Burton (2016). "Accreta placentation: a systematic review of prenatal ultrasound imaging and grading of villous invasiveness." Am J Obstet Gynecol **215**(6): 712-721.

Jauniaux, E., L. Grønbeck, C. Bunce, J. Langhoff-Roos and S. L. Collins (2019). "Epidemiology of placenta previa accreta: a systematic review and meta-analysis." BMJ Open **9**(11): e031193.

Jauniaux, E., A. M. Hussein, K. A. Fox and S. L. Collins (2019). "New evidence-based diagnostic and management strategies for placenta accreta spectrum disorders." Best Pract Res Clin Obstet Gynaecol **61**: 75-88.

Jauniaux, E. and D. Jurkovic (2012). "Placenta accreta: pathogenesis of a 20th century iatrogenic uterine disease." Placenta **33**(4): 244-251.

Kanal, E., A. J. Barkovich, C. Bell, J. P. Borgstede, W. G. Bradley, Jr., J. W. Froelich, J. R. Gimbel, J. W. Gosbee, E. Kuhni-Kaminski, P. A. Larson, J. W. Lester, Jr., J. Nyenhuis, D. J. Schaefer, E. A. Sebek, J. Weinreb, B. L. Wilkoff, T. O. Woods, L. Lucey and D. Hernandez (2013). "ACR guidance document on MR safe practices: 2013." J Magn Reson Imaging **37**(3): 501-530.

Kanal, E., J. Gillen, J. A. Evans, D. A. Savitz and F. G. Shellock (1993). "Survey of reproductive health among female MR workers." Radiology **187**(2): 395-399.

Kc, K., S. Shakya and H. Zhang (2015). "Gestational diabetes mellitus and macrosomia: a literature review." Ann Nutr Metab **66 Suppl 2**: 14-20.

Kerr de Mendonça, L. (1988). "Sonographic diagnosis of placenta accreta. Presentation of six cases." J Ultrasound Med **7**(4): 211-215.

Khong, T. Y. (2004). "Placental vascular development and neonatal outcome." Semin Neonatol **9**(4): 255-263.

Khong, T. Y., E. E. Mooney, I. Ariel, N. C. Balmus, T. K. Boyd, M. A. Brundler, H. Derricott, M. J. Evans, O. M. Faye-Petersen, J. E. Gillan, A. E. Heazell, D. S. Heller, S. M. Jacques, S. Keating, P. Kelehan, A. Maes, E. M. McKay, T. K. Morgan, P. G. Nikkels, W. T. Parks, R. W. Redline, I. Scheimberg, M. H. Schoots, N. J. Sebire, A. Timmer, G. Turowski, J. P. van der Voorn, I. van Lijnschoten and S. J. Gordijn (2016). "Sampling and Definitions of Placental Lesions: Amsterdam Placental Workshop Group Consensus Statement." Arch Pathol Lab Med **140**(7): 698-713.

Khong, T. Y. and W. B. Robertson (1987). "Placenta creta and placenta praevia creta." Placenta **8**(4): 399-409.

Kingdom, J. C., M. C. Audette, S. R. Hobson, R. C. Windrim and E. Morgen (2018). "A placenta clinic approach to the diagnosis and management of fetal growth restriction." Am J Obstet Gynecol **218**(2S): S803-S817.

Klucznik, R. P., D. A. Carrier, R. Pyka and R. W. Haid (1993). "Placement of a ferromagnetic intracerebral aneurysm clip in a magnetic field with a fatal outcome." Radiology **187**(3): 855-856.

Kok, R. D., M. M. de Vries, A. Heerschap and P. P. van den Berg (2004). "Absence of harmful effects of magnetic resonance exposure at 1.5 T in utero during the third trimester of pregnancy: a follow-up study." Magn Reson Imaging **22**(6): 851-854.

Kreidstein, M. L., D. Giguere and A. Freiberg (1997). "MRI interaction with tattoo pigments: case report, pathophysiology, and management." Plast Reconstr Surg **99**(6): 1717-1720.

Lam, G., J. Kuller and M. McMahon (2002). "Use of magnetic resonance imaging and ultrasound in the antenatal diagnosis of placenta accreta." J Soc Gynecol Investig **9**(1): 37-40.

Langhoff, L., L. Gronbeck, S. von Huth, A. Axelsson, C. Jorgensen, C. Thomsen and N. Vejlstrup (2017). "Placental Growth during Normal Pregnancy - A Magnetic Resonance Imaging Study." Gynecologic and Obstetric Investigation **82**(5): 462-467.

Larroza, A., Bodí, V., & Moratal, D. (2016). "Texture Analysis in Magnetic Resonance Imaging: Review and Considerations for Future Applications. Assessment of cellular and organ function and dysfunction using direct and derived MRI methodologies." 75-106.

Lausman, A., J. Kingdom, R. Gagnon, M. Basso, H. Bos, J. Crane, G. Davies, M.-F. Delisle, L. Hudon, S. Menticoglou, W. Mundle, A. Ouellet, T. Pressey, C. Pylypjuk, A. Roggensack and F. Sanderson (2013). "Intrauterine Growth Restriction: Screening, Diagnosis, and Management." Journal of Obstetrics and Gynaecology Canada **35**(8): 741-748.

Lax, A., M. R. Prince, K. W. Mennitt, J. R. Schwebach and N. E. Budorick (2007). "The value of specific MRI features in the evaluation of suspected placental invasion." Magn Reson Imaging **25**(1): 87-93.

LeBihan, D. (1990). "IVIM method measures diffusion and perfusion." Diagn Imaging (San Franc) **12**(6): 133, 136.

Leon, R. L., K. T. Li and B. P. Brown (2018). "A retrospective segmentation analysis of placental volume by magnetic resonance imaging from first trimester to term gestation." Pediatric Radiology **48**(13): 1936-1944.

Levine, D., C. A. Hulka, J. Ludmir, W. Li and R. R. Edelman (1997). "Placenta accreta: evaluation with color Doppler US, power Doppler US, and MR imaging." Radiology **205**(3): 773-776.

Levine, D., C. Zuo, C. B. Faro and Q. Chen (2001). "Potential heating effect in the gravid uterus during MR HASTE imaging." J Magn Reson Imaging **13**(6): 856-861.

Linduska, N., S. Dekan, A. Messerschmidt, G. Kasprian, P. C. Brugger, K. Chalubinski, M. Weber and D. Prayer (2009). "Placental Pathologies in Fetal MRI with Pathohistological Correlation." Placenta **30**(6): 555-559.

Linduska, N., A. Messerschmidt, S. Dekan, P. C. Brugger, M. Weber, A. Pollak and D. Prayer (2012). "Placental magnetic resonance imaging in monochorionic twin pregnancies." Journal of Maternal-Fetal & Neonatal Medicine **25**(8): 1419-1422.

Lu, T., M. Li, Y. Wang, H. Li, M. Wu and G. Wang (2023). "Standard diffusion-weighted, diffusion kurtosis and intravoxel incoherent motion in differentiating invasive placentas." Arch Gynecol Obstet.

Lu, T., Y. Wang, Y. Deng, C. Wu, X. Li and G. Wang (2022). "Diffusion and perfusion MRI parameters in the evaluation of placenta accreta spectrum disorders in patients with placenta previa." Magma **35**(6): 1009-1020.

Lubner, M. G., A. D. Smith, K. Sandrasegaran, D. V. Sahani and P. J. Pickhardt (2017). "CT Texture Analysis: Definitions, Applications, Biologic Correlates, and Challenges." Radiographics **37**(5): 1483-1503.

Macara, L., J. C. P. Kingdom, P. Kaufmann, G. Kohnen, J. Hair, I. A. R. More, F. Lyall and I. A. Greer (1996). "Structural analysis of placental terminal villi from growth-restricted pregnancies with abnormal umbilical artery Doppler waveforms." Placenta **17**(1): 37-48.

Maldjian, C., R. Adam, M. Pelosi, M. Pelosi, 3rd, R. D. Rudelli and J. Maldjian (1999). "MRI appearance of placenta percreta and placenta accreta." Magn Reson Imaging **17**(7): 965-971.

Marcos, H. B., R. C. Semelka and S. Worawattanakul (1997). "Normal placenta: Gadolinium-enhanced, dynamic MR imaging." Radiology **205**(2): 493-496.

Martyn, C. N. and S. E. Greenwald (1997). "Impaired synthesis of elastin in walls of aorta and large conduit arteries during early development as an initiating event in pathogenesis of systemic hypertension." Lancet **350**(9082): 953-955.

Matsuo, K., C. L. Conturie and R. H. Lee (2014). "Snowman sign: a possible predictor of catastrophic abnormal placentation." Eur J Obstet Gynecol Reprod Biol **181**: 341-342.

Maurea, S., V. Romeo, P. P. Mainenti, M. I. Ginocchio, G. Frauenfelder, F. Verde, R. Liuzzi, M. D'Armiento, L. Sarno, M. Morlando, M. Petretta, P. Martinelli and A. Brunetti (2018). "Diagnostic accuracy of magnetic resonance imaging in assessing placental adhesion disorder in patients with placenta previa: Correlation with histological findings." Eur J Radiol **106**: 77-84.

McKelvey, S. S. and H. H. Kay (2007). "Magnetic resonance spectroscopy of the placenta." Placenta **28**(5-6): 369-377.

Meng, X., L. Xie and W. Song (2013). "Comparing the diagnostic value of ultrasound and magnetic resonance imaging for placenta accreta: a systematic review and meta-analysis." Ultrasound Med Biol **39**(11): 1958-1965.

Metzenbauer, M., E. Hafner, D. Hoefinger, K. Schuchter, G. Stangl, E. Ogris and K. Philipp (2001). "Three-dimensional ultrasound measurement of the placental volume in early pregnancy: Method and correlation with biochemical placenta parameters." Placenta **22**(6): 602-605.

Mevissen, M., S. Buntenkötter and W. Löscher (1994). "Effects of static and time-varying (50-Hz) magnetic fields on reproduction and fetal development in rats." Teratology **50**(3): 229-237.

Mifsud, W. and N. J. Sebire (2014). "Placental pathology in early-onset and late-onset fetal growth restriction." Fetal Diagn Ther **36**(2): 117-128.

Millischer, A. E., B. Deloison, S. Silvera, Y. Ville, N. Boddaert, D. Balvay, N. Siauve, C. A. Cuenod, V. Tsatsaris, L. Sentilhes and L. J. Salomon (2017). "Dynamic contrast enhanced MRI of the placenta: A tool for prenatal diagnosis of placenta accreta?" Placenta **53**: 40-47.

Millischer, A. E., P. Sonigo, Y. Ville, F. Brunelle, N. Boddaert and L. J. Salomon (2013). "Standardized fetal anatomical examination using magnetic resonance imaging: a feasibility study." Ultrasound Obstet Gynecol **42**(5): 553-559.

Monier, I., B. Blondel, A. Ego, M. Kaminiski, F. Goffinet and J. Zeitlin (2015). "Poor effectiveness of antenatal detection of fetal growth restriction and consequences for obstetric management and neonatal outcomes: a French national study." Bjog **122**(4): 518-527.

Monier, I., B. Blondel, A. Ego, M. Kaminski, F. Goffinet and J. Zeitlin (2016). "Does the Presence of Risk Factors for Fetal Growth Restriction Increase the Probability of Antenatal Detection? A French National Study." Paediatr Perinat Epidemiol **30**(1): 46-55.

Moore, R. J., B. Issa, P. Tokarczuk, K. R. Duncan, P. Boulby, P. N. Baker, R. W. Bowtell, B. S. Worthington, I. R. Johnson and P. A. Gowland (2000). "In vivo intravoxel incoherent motion measurements in the human placenta using echo-planar imaging at 0.5 T." Magn Reson Med **43**(2): 295-302.

Moore, R. J., B. K. Strachan, D. J. Tyler, K. R. Duncan, P. N. Baker, B. S. Worthington, I. R. Johnson and P. A. Gowland (2000). "In utero perfusing fraction maps in normal and growth restricted pregnancy measured using IVIM echo-planar MRI." Placenta **21**(7): 726-732.

Mühler, M. R., O. Clément, L. J. Salomon, D. Balvay, G. Autret, C. Vayssettes, C. A. Cuénod and N. Siauve (2011). "Maternofetal pharmacokinetics of a gadolinium chelate contrast agent in mice." Radiology **258**(2): 455-460.

Myers, C., K. R. Duncan, P. A. Gowland, I. R. Johnson and P. N. Baker (1998). "Failure to detect intrauterine growth restriction following in utero exposure to MRI." Br J Radiol **71**(845): 549-551.

Myers, C., K. R. Duncan, P. A. Gowland, I. R. Johnson and P. N. Baker (1998). "Failure to detect intrauterine growth restriction following in utero exposure to MRI." Br J Radiol **71**: 549-551.

Nardozza, L. M., A. C. Caetano, A. C. Zamarian, J. B. Mazzola, C. P. Silva, V. M. Marcal, T. F. Lobo, A. B. Peixoto and E. Araujo Junior (2017). "Fetal growth restriction: current knowledge." Arch Gynecol Obstet **295**(5): 1061-1077.

Ness, R. B. and B. M. Sibai (2006). "Shared and disparate components of the pathophysiologies of fetal growth restriction and preeclampsia." American Journal of Obstetrics and Gynecology **195**(1): 40-49.

NICE (2011). "Caesarean Section, in CG132; ." CG132.

Novak, Z., A. S. Thurmond, P. L. Ross, M. K. Jones, K. L. Thornburg and R. W. Katzberg (1993). "Gadolinium-DTPA transplacental transfer and distribution in fetal tissue in rabbits." Invest Radiol **28**(9): 828-830.

Ohgiya, Y., H. Nobusawa, N. Seino, O. Miyagami, N. Yagi, S. Hiroto, J. Munechika, M. Hirose, N. Takeyama, N. Ohike, R. Matsuoka, A. Sekizawa and T. Gokan (2016). "MR Imaging of Fetuses to Evaluate Placental Insufficiency." Magn Reson Med Sci **15**(2): 212-219.

Okazaki, O., N. Murayama, N. Masubuchi, H. Nomura and H. Hakusui (1996). "Placental transfer and milk secretion of gadodiamide injection in rats." Arzneimittelforschung **46**(1): 83-86.

Oyelese, Y. and J. C. Smulian (2006). "Placenta previa, placenta accreta, and vasa previa." Obstet Gynecol **107**(4): 927-941.

Pala, H. G., B. Artunc-Ulkumen, F. M. Koyuncu and Y. Bulbul-Baytur (2015). "Three-dimensional ultrasonographic placental volume in gestational diabetes mellitus." http://dx.doi.org/10.3109/14767058.2015.1012066.

Palacios Jaraquemada, J. M. and C. Bruno (2000). "Gadolinium-enhanced MR imaging in the differential diagnosis of placenta accreta and placenta percreta." Radiology **216**(2): 610-611.

Panici, P. B., M. Anceschi, M. L. Borgia, L. Bresadola, G. Masselli, T. Parasassi, G. Perrone and R. Brunelli (2012). "Intraoperative aorta balloon occlusion: fertility preservation in patients with placenta previa accreta/increta." J Matern Fetal Neonatal Med **25**(12): 2512-2516.

Panigel, M., G. Wolf and A. Zeleznick (1988). "Magnetic resonance imaging of the placenta in rhesus monkeys, Macaca mulatta." J Med Primatol **17**(1): 3-18.

Papageorghiou, A. T., E. O. Ohuma, D. G. Altman, T. Todros, L. C. Ismail, A. Lambert, Y. A. Jaffer, E. Bertino, M. G. Gravett, M. Purwar, J. A. Noble, R. Pang, C. G. Victora, F. C. Barros, M. Carvalho, L. J. Salomon, Z. A. Bhutta, S. H. Kennedy and J. Villar

(2014). "International standards for fetal growth based on serial ultrasound measurements: the Fetal Growth Longitudinal Study of the INTERGROWTH-21st Project." The Lancet **384**(9946): 869-879.

Patil, V., G. Srinivas, S. Ms, S. Kiran Das, R. Hiremath and N. Shabadi (2019). "Diagnostic Significance of Ultrasonographic Markers and Score in Detection of Gestational Diabetes Mellitus in the Indian Subcontinent." Ultrasound Q.

Pedersen, J. (1955). "WEIGHT AND LENGTH AT BIRTH OF INFANTS OF DIABETIC MOTHERS." Acta Endocrinologica **18**(4): 553-554.

Persson, B., M. Stangenberg, N. O. Lunell, U. Brodin, N. G. Holmberg and V. Vaclavinkova (1986). "Prediction of size of infants at birth by measurement of symphysis fundus height." Br J Obstet Gynaecol **93**(3): 206-211.

Pijnenborg, R., L. Vercruysse and A. Hanssens (2006). "The uterine spiral arteries in human pregnancy: Facts and controversies." Placenta **27**(9-10): 939-958.

Rahaim, N. S. and E. H. Whitby (2015). "The MRI features of placental adhesion disorder and their diagnostic significance: systematic review." Clin Radiol **70**(9): 917-925.

Rais, R., R. Starikov, W. Robert, P. Has and M. He (2019). "Clinicopathological correlation of large-for-gestational age placenta in pregnancies with pregestational diabetes." Pathol Res Pract **215**(3): 405-409.

Ray, J. G., M. J. Vermeulen, A. Bharatha, W. J. Montanera and A. L. Park (2016). "Association Between MRI Exposure During Pregnancy and Fetal and Childhood Outcomes." Jama **316**(9): 952-961.

RCOG, G.-t. G. N. (2011). "Placenta Praevia, Placenta Praevia Accreta and Vasa Praevia: Diagnosis and Management." Internet; ; 4.6.

RCOG, G.-t. G. N. (2013). "The Investigation and Management of the Small–for–Gestational–Age Fetus." February 2013.

Reeves, M. J., M. Brandreth, E. H. Whitby, A. R. Hart, M. N. Paley, P. D. Griffiths and J. C. Stevens (2010). "Neonatal cochlear function: measurement after exposure to acoustic noise during in utero MR imaging." Radiology **257**(3): 802-809.

Rofsky, N. M., D. J. Pizzarello, J. C. Weinreb, M. M. Ambrosino and C. Rosenberg (1994). "Effect on fetal mouse development of exposure to MR imaging and gadopentetate dimeglumine." J Magn Reson Imaging **4**(6): 805-807.

Romeo, V. and S. Maurea (2020). "The new era of advanced placental tissue characterization using MRI texture analysis: Clinical implications." Ebiomedicine **51**.

Romeo, V., C. Ricciardi, R. Cuocolo, A. Stanzione, F. Verde, L. Sarno, G. Improta, P. P. Mainenti, M. D'Armiento, A. Brunetti and S. Maurea (2019). "Machine learning analysis of MRI-derived texture features to predict placenta accreta spectrum in patients with placenta previa." Magn Reson Imaging **64**: 71-76.

Rozenfeld, M. N. and D. J. Podberesky (2018). "Gadolinium-based contrast agents in children." Pediatr Radiol **48**(9): 1188-1196.

RSNA (2022). "Statement on safety of the developing fetus in medical imaging during pregnancy."

Sadovsky, E., Z. Palti, W. Z. Polishuk and E. Robinson (1967). "Atypical placentography in placenta accreta." Obstet Gynecol **29**(6): 784-787.

Salomon, L. J., N. Siauve, F. Taillieu, D. Balvay, C. Vayssettes, G. Frija, Y. Ville, C. A. Cuénod and O. Clément (2006). "In vivo dynamic MRI measurement of the noradrenaline-induced reduction in placental blood flow in mice." Placenta **27**(9-10): 1007-1013.

Sarioglu, F. C., O. Sarioglu, H. Guleryuz, E. Ozer, D. Ince and H. N. Olgun (2020). "MRI-based texture analysis for differentiating pediatric craniofacial rhabdomyosarcoma from infantile hemangioma." European radiology.

Saunders, R. (2005). "Static magnetic fields: animal studies." Prog Biophys Mol Biol **87**: 225-239.

Sefidbakht, S., B. Zeinali-Rafsanjani, M. Safari, F. Zarei, B. Bijan, R. Jalli, M. Kasraeian, H. Vafaei-Cisakht and N. Asadi (2019). "Correlating Placental ADC Values with Gestational Age and Grannum Class in Normal Placentas." Iranian Journal of Radiology **16**(1).

Sehgal, A., J. E. Dahlstrom, Y. Chan, B. J. Allison, S. L. Miller and G. R. Polglase (2019). "Placental histopathology in preterm fetal growth restriction." Journal of Paediatrics and Child Health **55**(5): 582-587.

Selander, J., M. Albin, U. Rosenhall, L. Rylander, M. Lewné and P. Gustavsson (2016). "Maternal Occupational Exposure to Noise during Pregnancy and Hearing Dysfunction in Children: A Nationwide Prospective Cohort Study in Sweden." Environ Health Perspect **124**(6): 855-860.

Shamshirsaz, A. A., K. A. Fox, B. Salmanian, C. R. Diaz-Arrastia, W. Lee, B. W. Baker, J. Ballas, Q. Chen, T. R. Van Veen, P. Javadian, H. Sangi-Haghpeykar, N. Zacharias, S. Welty, C. I. Cassady, A. Moaddab, E. J. Popek, S. K. Hui, J. Teruya, V. Bandi, M. Coburn, T. Cunningham, S. R. Martin and M. A. Belfort (2015). "Maternal morbidity in

patients with morbidly adherent placenta treated with and without a standardized multidisciplinary approach." Am J Obstet Gynecol **212**(2): 218.e211-219.

Shapira-Zaltsberg, G., D. Grynspan, M. V. Quintana, P. C. Dominguez, D. Reddy, J. H. Davila and E. Miller (2018). "MRI features of the placenta in fetuses with and without CNS abnormalities." Clinical Radiology **73**(9).

Sharma, D., S. Shastri and P. Sharma (2016). "Intrauterine Growth Restriction: Antenatal and Postnatal Aspects." Clin Med Insights Pediatr **10**: 67-83.

Shellock, F. G. (2002). "Magnetic resonance safety update 2002: implants and devices." J Magn Reson Imaging **16**(5): 485-496.

Shellock, F. G. and J. V. Crues (1988). "High-field-strength MR imaging and metallic biomedical implants: an ex vivo evaluation of deflection forces." AJR Am J Roentgenol **151**(2): 389-392.

Shellock, F. G. a. S.-G., A.M. (2001). "The magnetic resonance environment and implants, devices, and materials. Magnetic resonance procedures: health effects and safety. ." CRC Press, Boca Raton.

Shih, J. C., J. M. Palacios Jaraquemada, Y. N. Su, M. K. Shyu, C. H. Lin, S. Y. Lin and C. N. Lee (2009). "Role of three-dimensional power Doppler in the antenatal diagnosis of placenta accreta: comparison with gray-scale and color Doppler techniques." Ultrasound Obstet Gynecol **33**(2): 193-203.

Siauve, N. (2019). How and why should the radiologist look at the placenta? Eur Radiol. Germany.

Siauve, N., G. E. Chalouhi, B. Deloison, M. Alison, O. Clement, Y. Ville and L. J. Salomon (2015). "Functional imaging of the human placenta with magnetic resonance." Am J Obstet Gynecol **213**(4 Suppl): S103-114.

Silver, R. M., M. B. Landon, D. J. Rouse, K. J. Leveno, C. Y. Spong, E. A. Thom, A. H. Moawad, S. N. Caritis, M. Harper, R. J. Wapner, Y. Sorokin, M. Miodovnik, M. Carpenter, A. M. Peaceman, M. J. O'Sullivan, B. Sibai, O. Langer, J. M. Thorp, S. M. Ramin and B. M. Mercer (2006). "Maternal morbidity associated with multiple repeat cesarean deliveries." Obstet Gynecol **107**(6): 1226-1232.

Sivan, E., M. Spira, R. Achiron, U. Rimon, G. Golan, S. Mazaki-Tovi and E. Schiff (2010). "Prophylactic pelvic artery catheterization and embolization in women with placenta accreta: can it prevent cesarean hysterectomy?" Am J Perinatol **27**(6): 455-461.

Smith, F. W., A. H. Adam and W. D. Phillips (1983). "NMR imaging in pregnancy." Lancet **1**(8314-5): 61-62.

So Young Park, M. Y. K., Yee Jeong Kim, Yi Kyeong Chun, Hye Sun Kim, Hee Soo Kim, Sung Ran Hong (2019). "Placental Pathology in Intrauterine Growth Retardation.".

Soltys, R. A. (1992). "Summary of preclinical safety evaluation of gadoteridol injection." Invest Radiol **27 Suppl 1**: S7-11.

Soongsatitanon, A. and V. Phupong (2018). "First trimester 3D ultrasound placental volume for predicting preeclampsia and/or intrauterine growth restriction." https://doi.org/10.1080/01443615.2018.1529152.

Sorensen, A., J. Hutter, M. Seed, P. E. Grant and P. Gowland (2019). "T2* weighted placental MRI: basic research tool or an emerging clinical test of placental dysfunction?" Ultrasound Obstet Gynecol.

Sovio, U., I. R. White, A. Dacey, D. Pasupathy and G. C. S. Smith (2015). "Screening for fetal growth restriction with universal third trimester ultrasonography in nulliparous women in the Pregnancy Outcome Prediction (POP) study: a prospective cohort study." The Lancet **386**(10008): 2089-2097.

Stables D, R. J. (2010). "Physiology in childbearing: with anatomy and related biosciences. ." Baillière Tindall.

Starikov, R., K. Inman, K. Chen, V. Lopes, E. Coviello, H. Pinar and M. He (2014). "Comparison of placental findings in type 1 and type 2 diabetic pregnancies." Placenta **35**(12): 1001-1006.

Strizek, B., J. C. Jani, E. Mucyo, F. De Keyzer, I. Pauwels, S. Ziane, A. L. Mansbach, P. Deltenre, T. Cos and M. M. Cannie (2015). "Safety of MR Imaging at 1.5 T in Fetuses: A Retrospective Case-Control Study of Birth Weights and the Effects of Acoustic Noise." Radiology **275**(2): 530-537.

Sun, H., H. Qu, L. Chen, W. Wang, Y. Liao, L. Zou, Z. Zhou, X. Wang and S. Zhou (2019). "Identification of suspicious invasive placentation based on clinical MRI data using textural features and automated machine learning." European Radiology **29**(11): 6152-6162.

Tabsh, K. M., C. R. Brinkman, 3rd and W. King (1982). "Ultrasound diagnosis of placenta increta." J Clin Ultrasound **10**(6): 288-290.

Tanaka, K., K. Yamada, M. Matsushima, T. Izawa, S. Furukawa, Y. Kobayashi and M. Iwashita (2018). "Increased maternal insulin resistance promotes placental growth and

decreases placental efficiency in pregnancies with obesity and gestational diabetes mellitus." J Obstet Gynaecol Res **44**(1): 74-80.

Tanaka, Y. O., S. Sohda, S. Shigemitsu, M. Niitsu and Y. Itai (2001). "High temporal resolution dynamic contrast MRI in a high risk group for placenta accreta." Magn Reson Imaging **19**(5): 635-642.

Teitelbaum, G. P., W. G. Bradley, Jr. and B. D. Klein (1988). "MR imaging artifacts, ferromagnetism, and magnetic torque of intravascular filters, stents, and coils." Radiology **166**(3): 657-664.

Teixidor Viñas, M., E. Chandraharan, M. V. Moneta and A. M. Belli (2014). "The role of interventional radiology in reducing haemorrhage and hysterectomy following caesarean section for morbidly adherent placenta." Clin Radiol **69**(8): e345-351.

Teo, T. H., Y. M. Law, K. H. Tay, B. S. Tan and F. K. Cheah (2009). "Use of magnetic resonance imaging in evaluation of placental invasion." Clin Radiol **64**(5): 511-516.

Thorp, J. M., Jr., R. B. Councell, D. A. Sandridge and H. H. Wiest (1992). "Antepartum diagnosis of placenta previa percreta by magnetic resonance imaging." Obstet Gynecol **80**(3 Pt 2): 506-508.

Thurn, L., P. G. Lindqvist, M. Jakobsson, L. B. Colmorn, K. Klungsoyr, R. I. Bjarnadóttir, A. M. Tapper, P. E. Børdahl, K. Gottvall, K. B. Petersen, L. Krebs, M. Gissler, J. Langhoff-Roos and K. Källen (2016). "Abnormally invasive placenta-prevalence, risk factors and antenatal suspicion: results from a large population-based pregnancy cohort study in the Nordic countries." Bjog **123**(8): 1348-1355.

Twickler, D. M., M. J. Lucas, A. B. Balis, R. Santos-Ramos, L. Martin, S. Malone and B. Rogers (2000). "Color flow mapping for myometrial invasion in women with a prior cesarean delivery." J Matern Fetal Med **9**(6): 330-335.

Tyndall, D. A. and K. K. Sulik (1991). "Effects of magnetic resonance imaging on eye development in the C57BL/6J mouse." Teratology **43**(3): 263-275.

Valentini, A. L., B. Gui, V. Ninivaggi, M. Miccò, M. Giuliani, L. Russo, M. G. Marini, M. Tintoni, A. F. Cavaliere and L. Bonomo (2017). "The morbidly adherent placenta: when and what association of signs can improve MRI diagnosis? Our experience." Diagn Interv Radiol **23**(3): 180-186.

Veerbeek, J. H., P. G. Nikkels, H. L. Torrance, J. Gravesteijn, E. D. Post Uiterweer, J. B. Derks, S. V. Koenen, G. H. Visser, B. B. Van Rijn and A. Franx (2014). "Placental pathology in early intrauterine growth restriction associated with maternal hypertension." Placenta **35**(9): 696-701.

Victoria, T., A. M. Johnson, S. S. Kramer, B. Coleman, M. Bebbington and M. Epelman (2011). "Extrafetal findings at fetal MR: evaluation of the normal placenta and correlation with ultrasound." Clin Imaging **35**(5): 371-377.

Wallace, J. M., S. Bhattacharya and G. W. Horgan (2013). "Gestational age, gender and parity specific centile charts for placental weight for singleton deliveries in Aberdeen, UK." Placenta **34**(3): 269-274.

Wang, P. I., S. T. Chong, A. Z. Kielar, A. M. Kelly, U. D. Knoepp, M. B. Mazza and M. M. Goodsitt (2012). "Imaging of pregnant and lactating patients: part 2, evidence-based review and recommendations." AJR Am J Roentgenol **198**(4): 785-792.

Wong, E. C. (2014). "An introduction to ASL labeling techniques." J Magn Reson Imaging **40**(1): 1-10.

Wong, H. S., Y. K. Cheung, J. Zuccollo, J. Tait and K. C. Pringle (2008). "Evaluation of sonographic diagnostic criteria for placenta accreta." J Clin Ultrasound **36**(9): 551-559.

Wright, C., D. M. Morris, P. N. Baker, I. P. Crocker, P. A. Gowland, G. J. Parker and C. P. Sibley (2011). "Magnetic resonance imaging relaxation time measurements of the placenta at 1.5 T." Placenta **32**(12): 1010-1015.

Yip, Y. P., C. Capriotti, S. L. Talagala and J. W. Yip (1994). "Effects of MR exposure at 1.5 T on early embryonic development of the chick." J Magn Reson Imaging **4**: 742-748.

Yip, Y. P., C. Capriotti and J. W. Yip (1995). "Effects of MR exposure on axonal outgrowth in the sympathetic nervous system of the chick." J Magn Reson Imaging **5**: 457-462.

Zhang, J., H. Xu, Y. Xin, C. Zhang, Z. Liu, X. Han, Q. Liu, Y. Li and Z. Huang (2020). "Assessment of the massive hemorrhage in placenta accreta spectrum with magnetic resonance imaging."